SYNTHESIS AND COMPUTATIONAL STUDIES OF 1-4-η-CYCLOHEXA-1,3-DIENE DERIVATIVES OF IRONTRICARBONYL COMPLEXES

OLAWALE FOLORUNSO AKINYELE

April, 2015

SYNTHESIS AND COMPUTATIONAL STUDIES OF1-4-η-CYCLOHEXA-1,3-DIENEDERIVATIVES OF IRONTRICARBONYL COMPLEXES

BY

OlawaleFolorunsoAKINYELE

B.Sc (Hons), M.ScIbadan.

Matriculation Number 38303

A Thesis in the Department of Chemistry,

Submitted to the Faculty of Science

in partial fulfilment of the requirements for Degree of

DOCTOR OF PHILOSOPHY

of the

UNIVERSITY OF IBADAN

April, 2015.

ABSTRACT

Metal complexes have interesting properties and varied applications in light emitting diodes. A number of substituted pyridine metal (Rhenium, Ruthenium and Iridium) complexes have been synthesised and characterised. However, the synthesis and characterisation of substituted pyridine iron complexes such as Tricarbonyl (1-4-η-pyridino-cyclohexa-1,3-diene) iron complexes for its light emitting property remain scanty. Therefore, this research was designed to synthesise, characterise and calculate the electronic properties of Tricarbonyl (1-4-η-5-exo-N-pyridino-2-cyclohexa-1,3-diene) iron complexes.

TwelveTricarbonyl (1-4-η-5-exo-N-pyridino-cyclohexa-1,3-diene) iron complexeswere synthesised by the addition of pyridines to the dienyl ring of Tricarbonyl-1-5- η-cyclohexadienyl irontetrafluoroborate at room temperature, in solutions of acetonitrile. They were characterised using elemental analysis, infra-red (IR) and proton-nuclear magnetic resonance (^{1}H NMR) spectroscopy. Their theoretical studies were carried out using Molecular Mechanics Force Field (MMFF), semi-empirical Parameterization Method three (PM3), Density Functional Theory (DFT) and Time Dependent Density Functional Theory (TDDFT) with Becke three, Lee, Yang and Parr at 6-31G* level. The MMFF was used to obtain the stable conformer before subjecting each complex to geometry calculations. The geometrical and thermodynamic properties were obtained from PM3 while the electronic energy [Highest Occupied Molecular Orbital (HOMO) and Lowest Unoccupied Molecular Orbital (LUMO)], chemical potential, chemical hardness and electrophilicity index were obtained from DFT. The calculation of electronic-excited state was carried out using TDDFT.

The calculated elemental compositions of the synthesised complexes were in agreement with the observed values. All the complexes had very sharp IR peaks at 1980 and 2055 cm^{-1} corresponding to the stretching vibrations of carbonyl bond attached to the metal. The ^{1}H NMR spectra displayed well separated overlapping multiplets which are characteristic of the outer diene protons H_1 and H_4 at 3.2 ppm while the inner protons H_2 and H_3 appeared at 4.7 and 5.3 ppm respectively. The geometrical parameters ranged from 1.374 to 1.795 Å (bond lengths), 105.1 to 128.8 ^{o} (bond angles) and -8.9 to 128.5 ^{o} (dihedral angles). These properties were functions of the substituents on the rings. The thermodynamic parameters were: free energy change (-412.6 to -188.5 $kJmol^{-1}$), enthalpy change (-237.3 to +4.7 $kJmol^{-1}$) and entropy change (+595.2 to +697.3 $Jmol^{-1}K^{-1}$) indicating that the formation of these complexes was spontaneous. The electronic

properties were within the range of -9.8 to -9.1 eV and -6.1 to -4.8 eV (HOMO and LUMO energies) respectively, 3.3 to 4.5 eV (energy band gap), -6.9 to -7.9 eV (chemical potential), 1.6 to 2.2 eV (chemical hardness), 11.4 to 18.1 eV (electrophilicity index). These values were indicative of reactivities of these molecules. The electronic-excited state of methyl and dimethyl substituted complexes were triplets having 3.46, 3.42 and 3.40 eV excitation energies with 0.022, 0.039 and 0.019 oscillator strength. The amino substituted complexes were singlets with 4.34 eV excitation energy and 0.024 oscillator strength indicating their light emitting ability.

The electronic-excited state of synthesised methyl, dimethyl, and amino substituted Tricarbonyl (1-4-η-pyridino-cyclohexa-1,3-diene) iron complexes are capable of emitting light via phosphorescence and fluorescence, and may be useful in light emitting diodes.

Keywords: Molecular characterisation, Geometry optimisation, Quantum mechanical calculation, Electronic parameters.

Word count: 489

ACKNOWLEDGEMENTS

To God be the glory, great things He had done. Being a Ph D student in the University of Ibadan has been the most exciting part of my life. During my studentship, I had the fulfilment of working with a few talented individuals, who filled me with the valued knowledge, hard-work and good company. Firstly, I am grateful to the Department of Chemistry and the Postgraduate School for enrolling me for the graduate programme. My sincere thanks and gratitude go to Professor T. I. Odiaka and Dr I. A. Adejoro for their endless efforts and enthusiasm in administering and giving me the opportunity to learn and discover my intellectual ability. My special thanks go to Dr Semire who taught me how to use the Spartan programme. It is my pleasant duty to express my gratitude to all whose support and encouragement made my task much easier.

I am short of words to thank, admire and appreciate the following people for their contribution towards making this dream a reality. They are Drs, A.J. Odola (of blessed memory), A.O. Bosede, I. A. Oladosu, N. O. Obi-Egbedi, OlufemiAdewuyi, Prof. M. O. Faborode and Mr Rufus Olasunkanmi. I wish to express my thanks to my colleagues at Adeyemi College of Education, Ondo for their most friendly cooperation and support in the needy hours, among whom are Adebayo Adesuyi, NiyiOmodara, OluwaseunFehintola, OlumuyiwaObijole and NiyiFamobuwa. Anthony Izuagie deserves a special mention.

I express my profound thanks to the Head of Department of Chemistry, Professor A. AAdesomoju and other members of Staff of Chemistry Department, University of Ibadan.

Finally I want to express my gratitude to my wife, Makanjuola for her intimate love and sacrifices that have brought and will continue to bring happiness into my life and the lives of our children, Damilola, Olamide and Moyosore. My appreciation goes to my junior brother Bimbola for his contribution and encouragement. To my parents, for their many years of love, support and expectations, I say a big thank you.

CERTIFICATION

This is to certify that Mr OlawaleFolorunsoAkinyelecarried out this research work in the Department of Chemistry, University of Ibadan, Ibadan Nigeria, under the supervision of Professor T.I. Odiaka and Dr I.A. Adejoro.

---------- ----------Timothy I.Odiaka.

(Professor) Dr I. A. Adejoro,

B.Sc, Ph.D (Wales), C.Chem. M.R.S.C. (London) B.Sc, M.Sc, Ph.D (Ibadan)

Professor in Inorganic/Organometallic Chemistry Senior Lecturer in Physical

Department of Chemistry ChemistryUniversity of

Ibadan Department of Chemistry

Ibadan, Nigeria. University of Ibadan

Ibadan, Nigeria.

DEDICATION

This research work is dedicated to my lovely wife Mrs M. A. Akinyele andthechildren, Damilola, Olamide and Moyosore for their understanding.

TABLE OF CONTENTS

LIST OF FIGURES

LIST OF PLATES

LIST OF TABLES

LIST OF ABBREVIATIONS

ACPF	Averaged coupled pair functional
AM1	Austin Model 1
AO	Atomic orbitals
B3LYP	Becke three Lee Yang Parr
BP	Becke and Perdew
CGF	Contracted Gaussian Functions
DFT	Density functional theory
DIIS	Direct inversion iteration substrate
ECP	Effective Core Potential
FT-IR	Fourier transform Infra-red
GCA	Generalized gradient approximation
GTO	Gaussian type orbitals
HF	Hartree Fock
HOMO	Highest occupied molecular orbital
INDO	Intermediate Neglect of Differential Overlap
IR	Infrared
LCAO	Linear Combination of Atomic Orbitals
LDA	Local density approximation
LUMO	Lowest unoccupied molecular orbital
MMFF	Molecular mechanics force fields
MNDO	Modified Neglect pf diatomic overlap
MP	Moller Plesset model
MTAP	Magnetic Stetraazaporphyrin
NDDO	Neglect of Diatomic Differential Overlap
NMR	Nuclear Magnetic Resonance

OLED	Organic Light Emitting Diodes
PBE	Perdew and Becke Exchange
PPM	Parts Per Million
PM3	Semi empirical Parameterization Method three
PW	Parr and Wardew
QM/MM	Quantum mechanics/ Molecular mechanics
RHF	Restricted Hartree Fock
SCF	Self consistent field
STO	Slatter type orbitals
TDDFT	Time dependent density functional theory
UV	Ultra-violet
VCD	Vibrational circular dichroism
WFT	Wavefunction theory
XAS	X-ray absorption spectra
ZINDO	Zerner's Intermediate neglect of differential Overlapp
ZORA	Zeroth-order regular approximation
Exo	Addition of nucleophile from above the ring
Endo	Addition of nucleophile from below the ring

SYMBOLS

υ	Frequency of absorption
Py	Pyridine
MeO	methoxy group
CO	carbonyl group
BF^-_4	Tetrafluoroborate ion
λ	Wavelength
η	Hapticity (Eta) of the organic group
I	Ionization energy
E	Electron Affinity
eV	electron volt
μ	Chemical potential
ω	Electrophilicity index
χ	Electronegativity
η	Global chemical hardness

Å	Angstrom unit
K	kelvin

CHAPTER ONE

INTRODUCTION

1.1 Introduction to Organometallic Chemistry

Metals or Metal ions co-ordinate to organic molecules to form organic derivatives of such metals. Metals generally form complexes with a wide variety of uncharged molecules such as carbon monoxide and unsaturated π-hydrocarbon. In many of these complexes, the metal atoms are in low-positive, zero or negative formal oxidation states. Transition metals form numerous compounds in which there is a sigma bond to carbon, but in most cases there is bonding to unsaturated π- hydrocarbons. Organometallic chemistry as the name implies can be referred to as the chemistry of carbon containing compounds in which the carbon atoms of the organics are linked directly to the metal. This aspect of chemistry covers a wide range of interests for a large number of chemists. It is an important domain of the science which represents a convergence of inorganic, organic and physical chemistry, where the respective disciplines can benefit by interaction with each other.

1.2 Historical background

The development of organometallics dates back to 1827, when Ziese discovered that the reaction of ethylene with potassiumtetrachloroplatinate II in water yielded an orange solid. This is shown stoichiometrically in equation 1.1 (Ziese, 1827).

$$C_2H_4 + K_2PtCl_4 + H_2O \rightarrow [KPtCl_3(C_2H_4)]\,H_2O + KCl \quad \text{----------} \quad 1.1$$

This discovery was closely followed by the discovery of Zink alkyl in 1848 by Frankland, Nickel tetracarbonyl,Iron pentacarbonyl by Mond *et al.,* in 1890, 1891, diironnonacarbonyl, crystal structure of which was observed in 1910 (Whitaker and Jeffery, 1967), dicobaltoctacarbonyl and molybdenum hexacarbonyl in 1910 by Mond

et al.,1910, chromium hexacarbonyl,ruthenium pentacarbonyl, (Job and Cassal, 1926), Iridium metal cluster $Ir_4(CO)_{12}$,(Manchot *et al.*,1940), dirhenium decacarbonyl, (Hieber *et al.*,1943). However, the present upsurge of interest in organometallic must be attributed to the discovery of Ferrocene by Keally and Pauson in 1951 followed by structural elucidation.Ferrocenewasone of the first organo-transition metal complexes to be isolated and fully characterized, its structure clearly revealing the direct bonding of the metal atom to the carbon atoms of the organic substrate. An enormous number of metal carbonyls. (Wilkinson *et al.,* 1952) and organo-transition metal carbonyls have been reported in the last few decades and their synthesis, structure and reactivities have been thoroughly reviewed (Abel, 1963and Hileman, 1965).The study of the reactions of these organo-transition metal carbonyls (especially where M = Fe, Ru, Os, Cr, Mo W) has received considerable attention in recent years (Fisher and Werner, 1966; McCleverty, 1976; Keally *et al.*, 1951).

1.3 Nature of bonding in Transition metal π-hydrocarbon complexes

Bonding in most organometallic compounds is generally described by the σ- and π-bonding scheme outlined by Dewar and Chatt, (Chatt and Duncanson, 1953)model of metal - olefin bonding. The overall effect is the movement of electron density from the olefin π-bonding orbital into its antibonding orbital, thus weakening the C – C bond of the coordinated olefin. This model is supported by numerous infra-red studies showing a general decrease in the olefin stretching frequency upon metal co-ordination. Related bonding schemes are believed to operate for other organics bonded to the transition metal centres. The relative importance of σ- and π- bonding effects depend very strongly on the nature of the metal as well as on the nature of the co-ordinated organic moiety.

1.4 The Concept of Effective Atomic Number Rule

The effective atomic number rule, otherwise known as the eighteen electron rule was first proposed by Sidgwick and Bailey, and this was the first generalization about the electronic structure of transition metal complexes (Chatt, 1974). It states that "all stable organometallics should have eighteen electrons in their metal valence shell." The orbitals involved in this bonding are 1ns,3np and 5(n-1)d orbitals, where 1, 3 and 5 represent the orientation in space of orbitals. For transition metal, n must be less or

equal to 4. The metals carbonyls together with organometallic compounds of transition metal are remarkable for the way in which most of them obey the rule. A few of such complexes e.g. Vanadium hexacarbonyl (17 electron species) which do not are stored in an inert atmosphere. If the numbers of electrons are less than eighteen, a low- lying molecular into which electrons can be promoted to initiate thermal decomposition is generated. However, in compounds having more than eighteen electrons, the excess electrons reside in the antibonding orbital and interact with the bonding orbital electrons leading to instability of the complex and its consequent decomposition. It should be noted however, that, in applying this rule to these compounds, the number of electrons in the valence shell of the uncomplexed metal is added to the number of electrons donated by the ligands, followed by the addition of electrons (if negative) or subtraction of electrons (if positive) in accordance with the overall charge on the complex.

1.5 Introduction to Computational Organometallic Chemistry

Computational chemistry is a field of science which deals with the theoretical aspect of molecules. Many theories and models were developed from quantum molecular chemistry (QMC) as a sequel to the quest of theoretical chemists to provide supplementary or alternative data to the experimental results. Some of these theories have developed into software and coupled with recent advances in computer hardware, it is now easy for theoretical chemists to calculate quantities of interest (Young, 2001;Hinchlife, 1989 and Cundari, 2001). It has been considered as a very important topic for chemical and inorganic research. It helps to pave the way towards understanding the physical and chemical properties of compounds. It has recentlyimproved reaction field theory and is now more useful in visualizing molecular shapes (Cramer, 2002; Parr *et al.*, 1989). Theoretical organometallic chemistry is interesting field in its own right, it is undergoing rapid development of recent. The interest arises from the fact that many novel compounds are being recently discovered and previously inaccessible organic compounds are now being synthesized (Pearson and Rees, 1994; Pearson, 1994; Hegedus, 1994) many organometallic compounds are catalyst for a number of reactions. This has led to the synthesis of various organic compounds. Various theoretical studies have been carried out on a number of compounds using different theoretical models; in fact a lot of progress has been made

in the area of accurate quantum chemical treatment of systems containing Transition metals. This has been much faster during the past few years than expected. Semi-empirical, abinitio and density functional theory (DFT) studies on the structures and the stabilities of organometallic compounds have been reported (Maseras, 1999; Gorling *et al*., 1999; Barckholtz and Bursten, 2000; Schultz *et al*., 2005). Computer modeling of organometallic compounds is now a mature subject with the structures and properties of pure and defective materials being routinely calculated (Jensen and Ryde, 2003; Morschel *et al*., 2008). A wide variety of procedures have been developed to calculate the molecular structures, energetic and other properties (Huang *et al*., 2007; Hu and Boyd, 2000; Praetorius *et al*., 2008). These are broken down into two categories, quantum chemical models and molecular mechanics models. These models are being used in calculating the physical and chemical properties of so many compounds, and a number of these theories have been used in different reactions ranging from kinetics, mechanisms, synthesis and energies involved in various reactions (Lewars, 2003; Cundari, 2001; Crabtree, 2005).

1.6 Organometallic complexes and luminescence

Organometallic complexes are low molecular weight special class of compounds which consist of organic π-conjugated ligand bonded to a metal ion. An important advantage of these complexes is their high luminescence efficiency arising from electrical excitation. Luminescence is a process by which an excited material emits light in a process that does not involve an increase in temperature, the excitation in this case is achieved using ultraviolet radiation.

Organic and organometallic complexes through absorption of photons give rise to photoluminescence which are either fluorescence (emission of light as a result of singlet to singlet electronic relaxation typically of lifetime of the order 10^{-9} seconds) or phosphorescence which results from the relaxation of electron(s) from the triplet excited state to ground state singlet usually of lifetime of between milliseconds and hours.

Within the last two decades, there have been an upsurge of interest due to their wide applicability in organic light emitting diodes (OLEDs) as phosphorescent emitters (Thompson, 2007).

1.7 Aim of the research

Metal pyridine complexesremain a subject of research interest and the current investigations into these complexes are not unconnected with their very interesting propertiesand varied applications.

Literature reports showed that Rhenium, Ruthenium and Iridium pyridine complexes have been studied but not much information was found on Iron pyridine complexes

The aim of this research is to syntheise pyridino-1-4-η-cyclohexa-1,3-diene derivatives of irontricarbonyl complexes by reacting $[FeCO)_3$-1-5-η-dienyl]BF_4. (Dienyl= C_6H_7 and 2-$MeOC_6H_6$) with selected pyridines as shown in the chemical equation below.

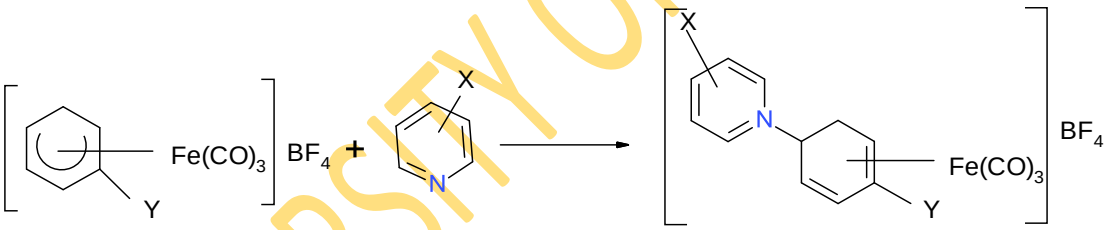

X = H, CH_3 , NH_2, $NH(CH_3)$, $N(CH_3)_2$

Y = H, OCH_3 .....1.1

The specific objectives of the study will include the following:

- Characterisation of the complexes by microanalysis, imfrared, proton neutron magnetic resonance and ultraviolet-visible spectroscopy.
- Predict the gas-phase thermodynamic and electronic properties of the attached ligand and its metal complexes.
- Contribute to the existing database of thermodynamic and electronic parameters of organometallic complexes.

- As the first set of electronic and thermodynamic data for the novel organometallic systems, the results will serve as a good source of theoretical information for both theoretical and experimental chemists.

CHAPTER TWO

THEORETICAL BACKGROUND

2.1 Theoretical Models

There are many approaches of Computational chemistry that are popular in molecular modeling. These approaches can be subdivided into two broad parts, empirical approach and quantum approach. Empirical approach uses simple models of harmonic potential, electrostatic interaction and dispersion forces for basic comparisons of energetics and geometric optimization (Hyperchem, 2003; Warren, 2003). The Quantum mechanical approach is divided into semi-empirical methods and non-empirical (ab-initio) methods. Approach to quantum mechanics postulates the fundamental principles and then uses these postulates to deduce experimental results. The state of a system in quantum mechanics is a function of the coordinates of particles called the wavefunction Ψ. This state changes with time. Thus for one particle, one-dimensional system, we have $\Psi = \Psi_{(x,\ t),}$ thus, the wavefunction contains all possible information about the system. Suppose we have a single particle of an electron of mass, m, moving in field of space under the influence of a potential, V, to find the future state of a system from the knowledge of its first state, we need an equation that tells us how the wavefunction changes with time. This particle is described by a wavefunction $\Psi_{(x,\ t),}$ that satisfies the Schrödinger's time dependent equation (2.1).

$$-\frac{\hbar}{2m}\frac{\delta^2\Psi_{(x,t)}}{\delta x^2} + V_{(x)}\Psi_{(x.t)} = i\hbar\frac{\delta\Psi_{(x,t)}}{\delta t} \quad \text{..... (2.1)}$$

Where $\hbar = \frac{h}{2\pi}$; h is Planck's constant.

Although, the time dependent Schrödinger's equation might look very difficult, many applications of quantum mechanics to chemistry derive their model from simpler Schrödinger's time-independent equation (2.2).

$$-\frac{\hbar^2}{2m}\frac{\delta^2\Psi_{(x)}}{\delta x^2} + V_{(x)}\Psi_{(x)} = E\Psi_{(x)} \quad \text{..... (2.2)}$$

Where E, is the electronic energy.

2.2 The Schrödinger's Wave Equation

Quantum mechanics describes molecules in terms of interaction among nuclei and electrons and molecular geometry in terms of minimum energy arrangements of nuclei. All quantum mechanical methods can be traced back to the Schrödinger's equation, which for the special case of hydrogen atom (a single particle in three dimensions) may be solved exactly as given in equation (2.3).

$$\left[-\frac{1}{2}\nabla^2 - \frac{\mathrm{Ze}}{\mathrm{r}}\right]\Psi_{(r)} = E\Psi_{(r)} \quad \text{..... (2.3)}$$

The quantity in square bracket represent the kinetic and potential energy of an electron at a distance, r, from a nucleus of charge, Z, (1 for hydrogen). E is the electronic energy in atomic units and Ψ, is a function of the electron coordinates; r is a wavefunction describing the motion of the electrons as fully as possible. The wavefunction for the hydrogen atom are the familiar s, p, d..... atomic orbitals. The square of the wavefunction multiplied by a small volume gives the probability of finding the electron inside this volume. This is called the electron density. The generalized Schrödinger's equation for a multinuclear and multielectron system is a simple looking expression shown in equation (2.4).

$$\mathrm{H}\,\Psi = \mathrm{E}\,\Psi \quad \text{..... (2.4)}$$

H is called the "Hamiltonian operator" which describes both kinetic energies of the nuclei and electrons that make up the molecules, as well as the electrostatic interactions felt between the nuclei and electrons. The nuclei are positively charged and the electrons are negatively charged, both attracting each other. The quantity, E, in

equation (2.4) is the energy of the system, and Ψ is termed the wavefunction. The "Hamiltonian Operator", H, is given by equation (2.5).

$$H = \frac{1}{2}\sum_i^{es}\nabla_i^2 - \frac{1}{2}\sum_A^{nu}\frac{1}{M_A}\nabla_i^2 - \sum_i^{es}\sum_A^{nu}\frac{Z_A}{r_{iA}} + \sum_i^{e}<\sum_j^{e}\frac{1}{r_{ij}} + \sum_A^{n}<\sum_B^{n}\frac{Z_A Z_B}{R_{AB}} \quad \text{..... (2.5)}$$

Z is the nuclear charge, M_A is the ratio of mass of nucleus A to the ratio of mass of an electron, R_{AB} is the distance between nuclei A and B, r_{ij} is the distance between electron i and nucleus A.

The many electrons Schrödinger equation cannot be solved exactly for a simple two-electron system such as helium atom or hydrogen molecule. So, approximations are introduced to provide practical methods. These approximations include;

2.3 Born-Oppenheimer Approximation

The wavefunctions are functions of the position of both the nuclei and the electrons of the system. However, since a nucleus is much heavier than an electron (approximately 1840 times more), its movements compared to the electrons are negligible. In this case, they can be considered to be frozen and their kinetic energy set at zero but they still contribute to the potential energy of the system.

One way of simplifying the Schrödinger's equation for molecular systems is to assume that, the motion of nuclei is slow compared to the speed at which electrons move (the speed of light). This lead to an electronic Schrödinger's expression given in (2.6), where the Hamiltonian operator collapses to equation (2.7).

$$H^{ei}\Psi^{ei} = E^{ei}\Psi^{ei} \quad \text{..... (2.6)}$$

$$H^{ei} = -\frac{1}{2}\sum_i^{e}\nabla_i^2 - \sum_i^{e}\sum_A^{n}\frac{Z_A}{r_{iA}} + \sum_i^{e}<\sum_j^{e}\frac{1}{r_{ij}} \quad \text{..... (2.7)}$$

Equation 2.5 describes the nuclear kinetic energy which is missing in equation 2.7 or given as zero, and the nuclear coulumbic term in equation 2.5 is a constant. The latter

needs be added to the electronic energy, E^{ei}, to yield the total energy, E, for the system (equation 2.8).

$$E = E^{ei} + \sum_{A}^{nu} < \sum_{B}^{nu} \frac{Z_A Z_B}{R_{AB}} \qquad \text{..... (2.8)}$$

2.4 Hartree – Fock Approximation

Much of the difficulty of solving the Schrödinger equation stems from the need to simultaneously determine the energy of each electron in the presence of all other electrons. In the Hartree-Fock (HF) method, this is avoided by calculating the energy of each electron in the averaged static field of the others. Initially, a guess is made of the electron energies. The energy of each electron is then calculated in the field of the initial electron configuration.

The electronic Schrödinger's equation (2.7) is still difficult and needs further approximations. We first assume that electrons move independently of each other, individual electrons are confined to functions termed molecular orbitals, each of which is determined by assuming that the electron is moving with the average field of all electrons. The total wavefunction is written in form of a single determinant (Slater determinant) which means that, it is antisymmetric upon interchange of electron coordinates. The total wavefunction is given in equation (2.9)

$$\Psi = \frac{1}{\sqrt{N!}} \begin{vmatrix} X_{1(1)} & \cdots & X_{2(1)} & \cdots & X_{n(1)} \\ X_{1(2)} & \cdots & X_{2(2)} & \cdots & X_{n(2)} \\ X_{1(n)} & \cdots & X_{3(n)} & \cdots & X_{n(n)} \end{vmatrix} \qquad \text{..... (2.9)}$$

The term X_i is called a spin orbital and is the product of a spatial function or molecular orbital, Ψ, and a spin function, α and β. The set of molecular orbitals leading to the lowest energy are obtained by a process referred to as "Self-Consistent Field" or SCF procedure. This is Hartree-Fock procedure, but SCF methods also include density functional procedures. All SCF procedures lead to equations of the form (2.10).

$$f_i X_{\chi_i} = \sum X_{\chi_i} \quad \text{..... (2.10)}$$

The Fock operator f_i is given by the expression (2.11).

$$f_{(i)} = \frac{1}{2}\nabla_i^2 + V^{eff} \quad \text{..... (2.11)}$$

X= spin and spatial co-ordinates of the electron, i and χ are the spin orbitals while V^{eff} is the effective potential "seen" by the electron, i.

2.5 Linear Combination of Atomic Orbitals (LCAO) Approximation

This approximation takes advantage of the motion thatone electron solutions for many-electron atoms and molecules will closely resemble the one electron solutions for the hydrogen atom. In practice, the molecular orbitals are expected as linear combinations of a finite set of one electron functions known as basis function Φ. The LCAO Approximation is given in equation (2.12).

$$\Psi_i = \sum_{\mu=1}^{Basisfuncti\ on} C_{\mu,i}\,\phi_\mu \quad \text{..... (2.12)}$$

where c is the molecular orbital coefficient, often simply called molecular orbital, because the Φ is usually centred at the nuclear positions, and is generally called atomic orbitals.

Hartree-Fock models differ in the number and kind of atomic basis functions, and their computational cost increases as the fourth power of the number of basis function.

2.6 Correlated Models

The Hartree-Fock models treat the motions of individual electrons as independent of one another in that they replace "instantaneous interactions" between individual electrons by interactions between electrons and the average field created by all other electrons. As a consequence, electrons "get in each other's way" to a greater extent than they should. This leads to overestimation of the electron-electron repulsion energy and to a total energy that is too high. Electron correlation accounts for coupling of electron motions and leads to reduction of electron-electron repulsion energy and to a lowering of the total energy. The correlation energy is defined as the difference

between the Hartree-Fock energy and the experimental energy, although many correlated models have been introduced. We shall concern ourselves with only three classes. Density functional models introduced an approximate correlation term in an explicit manner. They offer the advantage of not being significantly more costly than Hartree-Fock models in terms of computational time. The quality of density functional model depends on the choice of this term, although it is not apparent how an improvement can be made on a particular choice. Moller-Plesset models extend the flexibility of Hartree-Fock models by mixing ground-state and excited-state wavefunctions. They are significantly more costly than both Hartree-Fock and Density functional models, but offer the advantage over the latter of a clear path to improvement. It leads to the "exact result" although in practice the limit is not obtainable. The B3LYP/6-31G* density functional model and the MP2/6-31G* Moller-Plesset models are among the most popular correlated models. They are effective in addressing the deficiencies of the Hartree-Fock models but are still simple enough for routine use. B3LYP/6-311 + G** and MP2/6-311 +G** models are not practical for routine use except for very small molecules(Hyperchem, 2003; Hehre, 2003).

2.7 Semi- Empirical Molecular Orbital Models

Hartree-Fock and Correlated models are costly in terms of Computational time, a disadvantage that informed the introduction of additional approximations to significantly reduce the computational time while still retaining the underlying quantum mechanical formalism. This model follows directly from Hartree-Fock models by introducing the following approximations:

1 Elimination of overlap between functions on different atoms ("NDDO approximation"). This implies that atoms do not see each other 'This is drastic but reduces computation by more than an order of magnitude over Hartree-Fock models.

2 Restriction to a "minimal valence basis set" of atomic functions. This means that inner shells (core) functions are removed, thus significantly reducing the cost/time of doing calculations.

3 Introduction of parameters to reproduce specific experimental data, e.g equilibrium geometries and heat of formation. The PM3 model is the most widely parameterized semi-empirical model.

2.8 The PM 3 method

A new method for obtaining parameters for semi-empirical methods has been developed and applied to the modified neglect of diatomic overlap (MNDO) method. The method uses derivatives of calculated values for properties with respect to adjustable parameters to obtain the optimized values of parameters. The large increase in speed is a result of using a simple series expression for calculated values of properties rather than employing full semi-empirical calculations. With this optimization procedure, the rate-determining steps for parameterized elements change from the mechanics of parameterization to assembling of experimental reference data. The power of semi-empirical method lies not in the theoretical rigour but in the fact that the adjustable parameters within the method are optimized to reproduce important chemical properties. Any semi-empirical method is composed of a theoretical frame work and a set of parameters (Stewart, 1989).

2.9 Density Functional Theory (DFT)

This describes the electronic states of atoms, molecules and compounds in terms of the three dimensional electronic density of the system. This is a great simplification over the wavefunction Theory (WFT) which involves a 3N-dimensional antisymmetric wavefunction for a system with N-electrons. The electron density unlike the wave function is a physically observable quantity. This theory was developed in the mid 1960s by Hohenberg, Kohn and Sham (Jensen, 2007; Szabo and Ostlund, 1982) and states that "The energy, E, of a system can be expressed as a functional of the electron density $\rho_{(r)}$ of the system.

$$E = F\left[\rho_{(r)}\right] \quad \ldots\ldots \quad (2.13)$$

The theory further states that the functional is exact and universal which implies that it is applicable to any molecular system. This can be written as the sum of the following energy terms:

$$E = E_T + E_V + E_J + E_{XC} \quad (2.14)$$

E_T is the kinetic energy of non-interacting electrons, E_V is the classical electron repulsion, E_J is the electron-nucleus interaction and E_{XC} is the quantum mechanical contributions to the potential energy (self-interaction correction, exchange and correlation and the part of the kinetic energy that is not included in the E_T). The exact form of the exchange –correlation functional, E_{XC}, is unknown and all attempts to determine the total energy of the system rely on the approximations to this term.

Except for E_T, all the components depend on the total electron density $\rho_{(r)}$,(equation 2.15).

$$\rho_r = 2\sum_i^{orbital} |\Psi_{i\,(r)}|^2 \quad (2.15)$$

where Ψ_i is called Kohn-Sham orbitals and the summation is carried out over pairs of electrons.

Density Functional theories are classified according to the type of approximations that are made to the Exc, hence the approximation with the lowest level of complexity is the Local density approximation (LDA) where the functional form of Exc depends solely on the electron density, ρ(r) at each point in space. The next level of development is the generalized gradient approximation (GGA) where the functional form of Exc depends on the electron density ρ(r) and the gradient of the electron density $\nabla\rho(r)$, at each point in space. This includes B, P86, PW91, B95, PBE and LYP. From the previous GGA functionals, there are combinations between exchange and correlation functional. These are made in order to describe the systemcompletely. Some of the most common combinations being BLYP, BP86 and BPW91, the exchange correlation functional, Exc, include the exchange energy. The Hartree-Fock theory provides the exchange energy and including a part of the Hartree-Fock exchange energy in Exc has been done to improve the functionals by minimizing/eliminating the artificial self-exchange of the GGA functionals. Functionals which include portion of the Hartree-Fock exchange energy are referred to as hybrid functionals e.g. B3LYP (McQuarrie, 1983; Lowe, 1978; Christoffersen, 1989; Hohenberg and Kohn, 1964) which is the only functional used in this thesis. This is an example of a hybrid-GGA functional. The meta-GGA which includes the

spin kinetic energy in the Exc in addition to the laplacian of the electron density and the gradient, by including the kinetic energy density, the self-correlation is eliminated. Examples of this include M06-L and M06. Density Functional theory has now become the preferred method for evaluating the electronic structure of complex chemical systems, because its cost scales more favourably with system size and competes well in accuracy except for very small systems. The theory is employed in the treatment of compounds containing metals/Transition metals because of the additional advantage of static electron correlation.

2.10 Hybrid Functionals

The previous functional types present a problem because the exchange part is poorly described due to the problem of electronic self-interaction. Since the exchange part is exactly defined in Hartree-Fock, an alternative approach would be to mix HF, GGA and LSDA functionals to describe the exact exchange and correlation part of the hybrid functional. A famous example of the exchange and correlation combination is the most often used hybrid functional; B3LYP (Becke, 1993; Lee *et al.,* 1988; Hehre *et al.,* 1986). This functional is a mix between LDA and GGA functionals taken from the DFT and HF methods to a certain extent. It is shown in equation (2.16).

$$E_{XC}^{BLYP} = E_{XC}^{LDA} + \alpha_0(E_{XC}^{HF} - E_{XC}^{LDA}) + \alpha_X(E_X^{GGA} - E_X^{LDA}) + \alpha_C(E_C^{GGA} - E_C^{LDA}) \quad \text{..... (2.16)}$$

where $\alpha_o = 0.20$, $\alpha_x = 0.72$, and $\alpha_c = 0.81$. These are empirical parameters determined by fitting the predicted values to a set of atomization energies, proton affinities, and total atomic energies.

2.11 Basis sets

Basis functions are used to create the atomic orbitals (AO) or molecular orbitals and are usually expanded as a linear combination of such functions with the coefficients to be determined. These basis functions can be classified into two main types:

- Slater-type orbitals, also called STOs, have the exponential dependence:$e^{-\zeta r}$and are very close in their mathematical expression to the real AO:

$$\eta_{abc}^{STO}(x,y,z) = Nx^a y^b z^c e^{-\zeta r} \quad \text{.....} \quad (2.17)$$

N,is a factor of normalisation, ζ is the exponent, r, is a spherical coordinate, and a, b and c are the angular momentum part, L = a+b+c. ζ(zeta) controls the width of orbital (large ζ gives tight function, small ζgives diffuse function for H-like atom at least for 1s, however they lack radial nodes and not pure spherical harmonics

- Gaussian-type orbitals, also known as GTOs, have the exponential dependence:$e^{-\zeta r^2}$

$$\eta_{abc}^{GTO}(x,y,z) = Nx^a y^b z^c e^{-\zeta r^2} \quad \text{.....} \quad (2.18)$$

whereN is a normalisation factor and x, y and z are Cartesian coordinates.

The STOs describe very closely the behaviour of hydrogen atomic orbitals because they feature a cusp at r=0 and a good exponential decay for bigger values, of r. The GTOs, in contrast, do not show a cusp at r=0 and decrease too rapidly for large values of r. Despite these problems, the GTOs are a better compromise due to the fact that the product of two GTOs centered on two different atoms is a third one situated between them. This is not the case for STOs, which are therefore very difficult to handle computationally because the four-centre-two-electron integrals are very time consuming. A number of GTOs can be combined to approximate an STO, and this often proves to be more efficient than using the STO itself. The degree of complexity, and thus precision of a basis set is defined by the number of contracted functions (CGF) employed to represent each atomic orbital, the minimum being one contracted function to describe a basis function. For example the STO-3G basis set (where G indicates a combination of contracted Gaussian functions) is formed by a linear combination of three CGF for each basis function so as to resemble an STO. For more precision and better description of the system, two or more functions can be used to describe each type of orbital. Usually double-zeta and triple-zeta basis sets give a good precision.

The valence electrons are the ones that change most in chemical reactions, so it is most important to have a flexible description of these electrons. Such basis sets, where the

core and valence orbitals are treated differently, are called split valence basis sets. The most used example of a split valence basis set is the 6-31G basis set. The nomenclature of this type of basis set: X-YZG is:

- X represents the number of primitives GTOs used to describe one single contracted Gaussian function of the core.

- Y and Z (more can be added for a better precision) represent the number of primitive GTOs describing the valence orbitals. In the case of 6-31G, it is composed of two functions, one containing three primitives and the other only one.

Additions can be made to the basis sets using polarization functions and/or diffuse functions. Bonding between atoms induces a deformation of the electronic cloud around each atom, called polarization. To allow this, functions with higher angular momentum are added to the basis set. For example, the addition of a p function to H allows polarization. In the same way a d-function can be added to a basis set containing p valence orbitals, f-functions for d-valence orbitals. For more precise results, the polarization functions included can be defined better: for example for a hydrogen atom with 6-31G basis set, p and d polarization functions can be added, the basis set becoming 6-31G(pd). The diffuse functions, represented by a "+" (for example 6-31+G or 6-31++G), describe the part of atomic orbitals distant from the nuclei that can have a very important role when considering anions or diffuse electronic clouds in second or third row transition metals. Another fact to note is that for transition metals, the inner core of these atoms is very large and so the number of basis functions used to describe it would be very big. To resolve this problem, those basis functions can be replaced by an Effective Core Potential (ECP). The ECP will model the effects of the nucleus and the electrons from the inner shell on the valence electrons as an average effect. This allows not only the reduction of big computational calculations, but can include some relativistic effects on the system studied because these basis functions are generated from relativistic atomic calculations. The Pople basis sets used in this work have a straight forward nomenclature scheme (Pople and Nesbet, 1954). The notation 6-31G means that 6 primitive gaussians are used for each core orbital and two functions containing three and one primitives are used for each of the valence orbitals. In similar fashion 6-311G means that 6 primitive gaussians are

used for each core orbital and three functions containing three, one and one primitives are used for each of the valence orbitals. Most Pople basis sets start with 6-31G or 6-311G and then extend them by adding diffuse (+) and/or polarization functions.

2.12 Band Energy

In solid state physics, the electronic structure of a solid describes the ranges of energy that an electron is forbidden or allowed to have. This is due to the diffraction of the quantum mechanical electron waves in the periodic crystal lattice. The band structure of any material or compound determines its properties especially the optical and electronic properties(Walter, 1989). The electron of a single isolated atom occupies atomic orbitals, which form a discrete set of energy levels. If several atoms are brought together to form compounds, the atomic orbitals produce a number of molecular orbitals which is proportional to the number of atoms. When a large number of atoms are brought together to form a solid, the number of orbitals becomes exceedingly large, and the difference in energy in between them becomes very small. These levels may form continuous bands of energy rather than discrete energy levels of the atoms in an isolated state. However, some intervals of energy contain no orbitals, no matter how many atoms are aggregated, forming band gaps. Within an energy band, energy levels are so numerous as to be a near continuum. Firstly, the separation between energy levels in a solid is comparable with the energy that electrons constantly exchange with phonons (atomic vibrations). Secondly, it is comparable with the energy uncertainty due to the Heisenberg uncertainty principle, for reasonably long intervals of time. As a result, the separation between energy levels is of no consequence. Any solid has a large number of bands. In theory, it can be said to have infinitely many bands. Bands of are different widths, due to the properties of the atomic orbital from which they are formed; they may also overlap to form a single band. The electrical properties of a material are determined by its electronic structure. In a metal, the orbitals of the atoms overlap with the equivalent orbitals of their neighbouring atoms in all directions to form molecular orbitals similar to those of isolated molecules. With N interacting atomic orbitals, we will have N molecular orbitals. In metals however, or any continuous solid structure, N will be a very large number (typically $10^{22}$for a $1cm^3$ metal piece). With so many molecular orbitals spaced together in a given range of energies, they form an apparently continuous band of energies. In a metal atom, in

contrast to say an inert gas, the valence orbitals are not filled, thus the band of N molecular orbitals will not be filled either, but at certain energy level, all molecular orbitals above this level will be empty. The energy spacing between the highest occupied and the lowest unoccupied band is called the 'Band gap'. The lowest unoccupied band is called the Conduction band and the highest occupied band is called the Valence band (Neamen, 2006). The conductivity of a metal is due either to only partly filled valence or conduction bands, or to the band gap being near zero, so that with even a weak electric field the electrons easily redistribute; electron at higher energy and holes at lower energy. The situation is ideal for rapid transport of charge. The difference between insulators and semiconductors is only that the forbidden band gap between the valence band and conduction band is large in an insulator, so fewer electrons are found there and the electrical conductivity is lower.

Theoretically, a simple free electron molecular orbital model provides the minimum elements needed for describing quantitatively a conductor, semiconductor or an insulator built up on a linear chain of atoms. According to the quantum-mechanical model for free particle in a one dimensional box (potential zero inside the box and infinity outside) the wavefunction correspond to a ladder of eigen values. Experimentally, the band gap is related to the wavelength of the first absorption band in the electronic spectrum of the substance. Thus a photon with wavelength λ can excite an electron from HOMO level to LUMO level if the condition is fulfilled.

$\Delta E = E_{LUMO} - E_{HOMO}$ ……,.. (2.19)

$\Delta E = h\upsilon = h\frac{c}{\lambda}$……...……..…….. (2.20) Where h is Planck's constant, c is the speed of light and λ is the wavelength.

This band gap is one of the most useful aspects of the band structure, as it strongly influences the electrical and optical properties of materials (Houscroft and Sharpe, 2008).

2.13 Quantum mechanical foundation for determination of geometry and energy

Theoretical chemistry is concerned with inter-atomic interactions and inter-electronic interactions. An electron can behave as a particle and also as a wave. In quantum mechanics, electron behaves as a wave as well as particle; hence the following equations may therefore be applied.

$$\frac{\delta^2\Psi}{\delta x^2} = -\frac{4\pi^2\Psi}{\lambda^2} \quad \text{..... (2.21)}$$

where, $\lambda = \frac{h}{p}$

$E = h\upsilon = T+V$ and $T = \frac{1}{2}mv^2 = \frac{p^2}{2m}$

In these equations, ψ is the wavefunction, x is the coordinate axis, λ is the wavelength, E is the total energy of the electron, υ, is the wave frequency, T is the kinetic energy of the electron, p is the momentum of the electron treated as a particle of mass m, V is potential energy of the electron and h is Planck's constant.

$$Therefore, \quad \frac{\delta^2\Psi}{\delta x^2} = -\frac{4\pi^2 p^2}{h^2}\Psi$$

$$since\ E = T + V\ and\ T = \frac{p^2}{2m}$$

$$Then, \quad E - V = T = \frac{p^2}{2m}$$

$$But \quad p^2 = 2m(E - V)$$

$$Therefore, \frac{\delta^2\Psi}{\delta x^2} = -\frac{8\pi^2 m}{h^2}(E - V)$$

This is a generalized equation for 1-dimension, i. e,x-direction only.

$$\nabla^2\Psi + \frac{8\pi^2 m}{h^2}(E - V) = 0 \quad \text{..... (2.22)}$$

which can be re-written as:

$\left(-\frac{h^2\nabla^2}{8\pi^2 m} + V\right)\Psi = E\Psi$ ..... (2.23)

Or

$H\Psi = E\Psi$ ..... (2.24)

The expression, denoted by H, inside the brackets is called Hamiltonia operator and the Ψis an eigen function of the operator.

2.14 Reactivity indices

Within the concept framework of DFT, the chemical potential, μ, is a measure of the escaping tendency of an electron from equilibrium as defined by Parr *et al*., 1978.The electronegativity, χ could be written as the partial derivative of the system's energy with respect to the number of electrons, N, at the fixed external potential $v_{(r)}$:

$$\mu = \left(\frac{\partial E}{\partial N}\right)_{v_{(r)}} = -\chi \quad \text{..... (2.25)}$$

Where χ is the electronegativity.

The global hardness, η, can be seen as the resistance to charge transfer;

$$\eta = \frac{1}{2}\left(\frac{\delta^2 E}{\delta N^2}\right)_{v_{(r)}} \quad \text{..... (2.26)}$$

According to Mulliken, one has;

$$\mu = \chi = -\frac{1}{2}(I + A). \quad \text{..... (2.27)}$$

And

$$\eta = \frac{1}{2}(I - A). \quad \text{..... (2.28)}$$

Where E and$v_{(r)}$ are electronic energy and external potential of an N-electron system,

Using a finite difference approximation and Koopman's theorem,the above (Geerling *et al*., 1996; De Proft *et al*., 1996a, 1996b)can be written as:

$$\mu \approx -\frac{1}{2}(I + A) \approx \frac{1}{2}(E_L + E_H) \quad \text{..... (2.29)}$$

$$\eta \approx \frac{1}{2}(I - A) \approx \frac{1}{2}(E_L - E_H) \quad \text{..... (2.30)}$$

Parr *et al*., 1999 proposed a new DFT concept called the electrophilicity index, ω, in terms of the above two global activity indices, μ and η, (equation 2.31).

$$\omega = \frac{\mu^2}{2\eta} = \frac{(I + A)^2}{2(I + A)} = \frac{(E_L + E_H)^2}{2(E_L + E_H)} \quad \text{..... (2.31)}$$

where E_H and E_L are the energies of the highest occupied and the lowest unoccupied molecular orbital, I and A are the first ionization potential and electron affinity respectively. .

2.15 Electrophilicity index

This is the property of being electrophilic (Parthasarathi *et al*., 2004).It is the relative reactivity of an electrophile. An electrophile is attracted to electrons that participated in a chemical reaction by accepting electrons to form bond to a nucleophiles (Ingold, 1933, 1934), andbecause electrophiles accept electrons, they are Lewis acidsaccording to the general acid-base theory of Bronsted and Lowry, 1923. Most electrophiles are positively charged, having an atom which carries a partial positive charge or not have an octect of electrons. The concept of electrophilicity index was quantitatively introduced by Parr, Szentpaly and Shubin in 1999and it is referred to as the stabilization energy when atoms and molecules in their ground states acquire additional electronic charge from the environment. The electrophilicity index, ω, represents the stabilization energy of the system when it gets saturated by electrons coming from the surrounding: The above formulae are working tools for us to calculate the chemical potential, hardness, and electrophilicity index. All the calculated reactivity parameters are based on the values of the chemical potential, μ, and the

global chemical hardness, η. They were calculated using finite difference and the frozen orbital approximations, which yields them in terms of the highest occupied molecular orbital energy, E_H, and the lowest unoccupied molecular orbital energy, E_L.

2.16 Dipole moment

The molecular dipole moment is the measure of distribution of charge in a molecule. The accuracy of the overall distribution of electrons in a molecule is difficult to quantify since it involves all the multipoles. The result for the dipole moment and polarizability may provide an insight into the solubility and chemical reactivities of the complexes and their potential application in the synthesis of new derivatives.

2.17 Polarizability

This is the ability of these molecules to acquire a dipole moment, p, in an electric field; E. The appearance of p is due to the displacement of electric charges in atomic systems under the influence of E.The moment, p, thus disappears when no electric field is present. The concept of polarizability is generally not applied to particles having permanent dipole moment such as polar molecules.

$p = \alpha E$ Where α is a quantitative measure of polarizability, which is called molecular polarizability for some molecules. The value of α may depend on the direction of E: this is known as anisotropic polarizability. It is calculated as the average of the polarizability tensor, α, which is $\alpha = \frac{1}{3}(\alpha_{xx} + \alpha_{yy} + \alpha_{zz})$.

2.18 Koopman's Theorem

The theorem states that, in a closed-shell Hartree-Fock theory, the first ionization energy of a molecular system is equal to the negative of the orbital energy of the highest occupied molecular orbital (HOMO) (Koopmans, 1934; Politzer, 1998). This theory is exact in the context of restricted Hartree-Fock theory and it is assumed that the orbitals of the ions are identical to those of the neutral molecule. Ionization energies obtained from this procedure are in qualitative agreement with experimental ionization energies; hence the validity of the theorem is tied to the accuracy of the underlying Hartree-Fock wavefunctions. However, there are two main sources of error and these are orbital relaxation, which refer to changes in the Fock-operator and

Hartree-Fock orbitals when changing the number of electrons in the system, and electron correlation, which refers to the validity of representing the entire many-body wavefunction using Hartree-Fock wavefunction (Bingham *et al*., 1975).

Similar theorem exists in density functional theorem (DFT) for relating the exact first ionization energy and electron affinity to the HOMO and LUMO energies, although both the derivation and the precise statement differs from Koopman's theorem, with errors larger than 2eV depending on the exchange-correlation approximation employed. Although, the Koopman's original paper never made any claim regarding the significance of eigen values of the Fock-operator other than that of HOMO.

2.19 Survey of synthetic methods

Introduction

Three major synthetic methods have so far been identified as synthetic routes to organometallics. These are thermolysis, room temperature synthesis or below room temperatureand photolysis.

2.19.1 Thermolysis

This is a method involving the use of heat and refluxing of the reactant solutions at the temperature of the solvent(Leigh and Fisher, 1965) to give product. They synthesized 1,5-dicyclo- octadiene metal carbonyl, (Metal = Molybdenum and Tungsten) by heating molybdenum hexacarbonyl and 1,3-cyclooctadiene together in dioxane on a bath maintained at 120 ºC for 17 hours. The reaction mixture was cooled down to room temperature and then filtered, after which the residue was washed on the filter with hexane and the volatiles removed from the filtrate by distilling them in vacuo into a trap cooled with liquid nitrogen. The residue was sublimed twice in vacuo at 50 ºC to give the product. The analogous Tungsten complex was synthesized by mixing Tungsten hexacarbonyl and 1,3-dicyclooctadiene in di- n-butylether and refluxing at the solvent temperature for 30 hours. The reacting mixture was cooled, decanted and the resulting product was washed with hexane until the washing became colourless. The volatiles were removed from the solution by distillation in vacuo into a trap cooled

with liquid nitrogen. The product was sublimed in vacuo and the sublimate re-sublimed in vacuo at 70 ºC and again at 50 ºC to give the pure compound as a brownish product. A mixture of η^5-$C_5H_5V(CO)_4$, glacial acetic acid and acetic anhydride was refluxed for 16 hours under nitrogen with constant stirring and cooled to room temperature to give a greyish precipitate which was filtered, washed with five portions of diethylether and dried under pressure. This greyish precipitate was identified as cyclopentadienyl vanadiumdiacetate (King, 1966). Refluxing of $\eta^5C_5H_5Rh(CO)_3$ in benzene for 80 hours has led to the synthesis of $\eta^5(C_5H_5)_2Rh_2(CO)_3$ while N-methylene bis-(carbonyl-η^5-cyclopentadieyl rhodium has similarly been prepared by refluxing a solution of μ-CO-η^5-$C_5H_5Rh(CO)_2$ and N-methyl-N-nitrosourea in benzene for 25 hours. The product was recrystallized from n-pentane at -78 ºC to give $\eta^5C_5H_5Rh(CO)_2$-μ-$CH(CH_3)_2$(Woffgang *et al*., 1977). Heating under reflux of a mixture of 2,3-diphenylindenone and $Fe_3(CO)_{12}$ in benzene-toluene mixture of boiling point 85 ºC for 2 hours yielded a brown powder chromatographed on silica gel. Unreacted indenone was eluted with mixture of benzene-dichloromethane and the red band on the column was taken up in ether and the fraction evaporated in vacuo. The residue was crystallized from ethanol-light petroleum to give brownish red crystals of the product characterized as tricarbonyl(2,3-diphenylindenone iron) (Emile and Walter, 1965). Benzyloxy carbonylamino cyclopentadienyl manganesetricarbonyl was synthesized by refluxing Azidoformyl cyclopentadienyl manganesetricarbonyl in benzyl alcohol for 3 hours in an oil bath at 140 ºC followed by the removal of the solvent in vacuo and extraction of the residue with hot benzene/chloroform. Thermolysis of the extract solution with carbon black followed by filtration and evaporation of the solvent afforded a residue which was chromatographed over basic alumina. Elution with benzene/chloroform yielded yellow needles which on recystallization from petroleum ether yielded analytical samples of the product (Michael and Narkis, 1965). Pauson *et al*. 1967, synthesized tricarbonyltripyridine chromium from chromium hexacarbonyl and excess pyridine under reflux for 40 hours in aromatic free ligroin (boiling point, 80-100 ºC). On cooling to 0 ºC, the red-needle-like product separated out and was filtered, washed with ligroin, dried and stored under nitrogen at 0 ºC. The synthesis and characterization of some organometallic homo- and copolymers carrying diethynylated n-complexes were reported (Uwe, 1996). As

monomers, the diethynylated derivatives of cymantrene and cyclopentadienyl(1,3-istrimethylsilylcyclobutadiene)cobalt were utilized.

Jeffrey and Steven, 2001, also reported that metal alkoxides are precursors of interfacial species which can be used to enhance interactions between dissimilar components of a composite. Metal alkoxides react with surface hydroxyl groups of metal oxides or oxidized metals to give covalently bound surface alkoxide species through protolytic loss of one or several alkoxide groups (Jeffrey and Steven, 2001). Monodisperse chromium nanoparticles from the thermolysis of a Fischer carbene complex were successfully synthesized (Seung *et al*., 2004). The development of uniform nanometer-sized particles has been a major research focus because of their many technological and fundamental properties. Various nanoparticles of transition metals and their oxides have been synthesized, and their magnetic and catalytic properties characterized. In the synthesis of transition metal nanoparticles, the thermolysis of metal carbonyl compounds, such as $Co_2(CO)_8$, $Fe(CO)_5$, and $W(CO)_6$, were used.

A new 1,3,4-oxadiazole containing rhenium(I) complex, was synthesized and characterized by elemental analysis, IR, ^1H NMR, UV-vis and luminescence spectroscopy (Yan Ping *et al*., 2007). Nitrile-functionalized NCN-pincer complexes of type [MBr(N,,C-$C_6H_2(CH_2NMe_2$]. The structures of (M=Pd and Pt) in solid state were reported(Stefan*et al*., 2008) who showed that d^8- configurated transition metal ions Pd^{+2} and Pt^{+2} possess a somewhat distorted square planar. In a related synthesis by Wanli et' al. The complexes were synthesized and structurally characterized by means of elemental analysis, vibrational, ^1H NMR and FT-IR spectroscopy. The crystal structures of all the complexes were determined by X-ray crystallography (Wanli *et al*., 2009).

2.19.2 Room temperature and below

A large number of organometallics have been synthesized either at room temperature or below. The reactants may be of equal concentrations (equimolar) or the nucleophiles may be in excess relative to the organometallics being attacked. Reactions that proceed to completion at room temperature or below are usually very fast and give good yields of products. Tricarbonyl (1-4-η-toluidino cyclohexa-1,3-diene was obtained by

reacting acetonitrile solutions of η^5-$C_6H_7Fe(CO)_3BF_4$ and toluidine (Odiaka and Williams, 1981). Pyridines have been shown to add to the dienyl ring of tricarbonyl-1-5-η-cyclohexadienyl irontetrafluoroborate at room temperature in solutions of acetonitrile to give the 1,3-diene derivatives (Odiaka and Kane-Maguire, 1981).

Brian*et al.*, 1976, prepared carbonyl (η^5- cyclohepta-1,4-diene) iron by dissolving sodium tetrahydridofluoride in deoxygenated water with cold (0 ºC) stirred oxygen free mixture of carbonyl (1-5-η-cycloheptadienyl) 7-cyclohexa-1,3-diene) iron tetrafluoro- borate. A mixture of cis 3,4-dichlorobutene, ironpentacarbonyl, ether and lithium amalgam at room temperature gave cyclobutadiene irontricarbonyl (Illie *et al.*, 1977). X-substituted anilines and cyclohexylamine add to the tropylium ring of the cation $[(\eta^5C_7H_7W(CO)_3]^+$ to give the corresponding ring adducts of tricarbonyl (cyclohepta-1,3,5-triene) tungsten (Odiaka and Kane-Maguire, 1985). $[(\eta^5C_7H_7W(CO)_3]BF_4$ also reacts with excess triphenylphosphine to give the pale yellow crystalline solid (Odiaka, 1985). 1-4-η-(N-2,6-dimethylanilino derivatives of cyclohexa-1,3-diene and cyclohepta1,3-diene have also appeared in literature (Odiaka, 1987, 1988a, 1988b). Annie *et al.*, 2001, used the addition–β-elimination mechanism to report the first transformation of enol ethers into the corresponding vinyl zirconium derivatives. Moreover, the in situ formation of Ti(II) and subsequent reaction with halogeno alkynes offers a new route for the preparation of functionalized alkynyl titanium and trismetalated olefin derivatives. $[Cp^*RuIVCl_2(S_2CR)]$, (R = NMe_2, NEt_2, and OiPr) were synthesized by the reaction of $[Cp^*RuIIICl_2]_2$ with $[RC(S)S]_2$. One-electron electrochemical oxidation of $[Cp^*RuCl_2(S_2CR)]$ produces paramagnetic $[Cp^*RuCl_2(S_2CR)]^+$, which are stable in CH_2Cl_2solution for at least several hours at 233 K. EPR experiments performed at 293 K show isotropic signals (g =-2.035) with clearly defined hyperfine coupling to ^{99}Ru and ^{101}Ru of 25 G and with peak-to-peak line widths of 15 G. At temperatures below 153 K, axial-shaped EPR spectra were obtained with g-values close to 2 (2.050-2.008) and narrow peak-to-peak line widths (15 G). Results from DFT calculations indicate that approximately 70% of the spin density in $[Cp^*RuCl_2(S_2CNMe_2)]^+$ is located on the ruthenium, although there is an increase of only 0.06 in the positive charge of the metal ion as a result of the oxidation. The high spin density on Ruthenium supports the assignment of a formalRu(V) oxidation state, which is unprecedented in organometallic chemistry. Chemical

oxidation of $Cp^*RuIVCl_2(S_2CNMe_2)$ with $NO(PF_6)$ in CH_3CN resulted in the isolationof $[Cp^*RuIV(MeCN)_2(S_2CNMe_2)]^{+2}$, while oxidation with $[(4\text{-}Br\text{-}C_6H_4)_3N](SbCl_6)$ in dichloromethane (CH_2Cl_2) resulted in the formation of chloro-bridged dimeric $[Cp^*RuIVCl(S_2CNMe_2)]_2^{+2}$. When $[Cp^*RuIVCl(S_2CNMe_2)]_2^{+2}$is dissolved in $CD_3\text{-}CN/CH_3CN$, it immediately converted to $[Cp^*RuIV(MeCN)_2(S_2CNMe_2)]^{+2}$. Cyclic voltametric experiments confirmed that in both solvents the chemical oxidation process occurred through the $[Cp^*RuVCl_2(S_2CNMe_2)]^+$ intermediate (Sheng *et al.*, 2005, Seah *et al.*, 2006).The synthesis, characterization, and electrochemical properties of the first $(CH)_{10}$-bridged bimetallic complexes was also reported (Eun *et al*., 2006).

New group 15 organometallic compounds, M(phenanthrenyl)$_3$ (M = P (1), Sb (2), Bi (3)) were prepared from the reactions of 9-phenanthrenyllithium with MCl_3. A reaction of 9-(diphenylphosphino)phenanthrene with 2,6-diisopropylphenyl azide led to the formation of (phenanthrenyl)$(Ph)_2P{=}N\text{-}(2,6\text{-}iPr_2C_6H_3)$ (4). The crystal structures of 2 and 4 were determined by single-crystal X-ray diffractions, both of which crystallize with two independent molecules in the asymmetric unit. Microwave irradiation (MW) as a "non-conventional reaction condition" has been applied in various areas of chemistry and technology to produce or destroy diverse materials and chemical compounds, as well as to accelerate chemical processes (Oxana *et al*., 2011). Jose and Maria, 1999, showed the synthetic utility of acetylacetonatogold complexes as reagents for preparing gold(III) complexes with C, N and O donor ligands and gold(I) complexes with phosphorus ylide, methanide, methanediide, sulfur ylide, amino, amido, nitrido alkyl, phosphido, thiolato, hydrosulfido, trithiocarbonato, dithiocarbamato, 1,1 dithiolato and alkynyl (including ethynyl) ligands.

2.19.3 Photolysis

Certain organometallics have been prepared using photolysis as the basis of synthesis. Photolysis in this case is referred to as the use of ultra-violet or visible irradiation in the synthesis of organometallics. Irradiation of iron pentacarbonyl at or below room temperature using ultraviolet irradiation affords diiron nonacarbonyl (King and Bisnette, 1964). The synthesis of (1,3-allyl-cyclohepta-4,6-diene) cobalt from cobalt octacarbonyl and cycloheptatriene involves the irradiation in toluene for 16 hours

under nitrogen using a 1000 watts mercury ultraviolet lamp (Chaudhari and Pauson, 1966). Ultraviolet irradiations of equimolar amounts of various metal carbonyls and triphenylphosphines in benzene for 18 hours have resulted in the isolation of various triphenylphosphine metal derivatives (Strohmeier and Bigorgne, 1965; Lewis *et al*., 1963; King, 1967). Cyclopentadienyl metal nitrosyl derivatives of manganese and iron have been synthesized by photolysis of aqeous solution of sodium nitrite and $C_5H_5Mn(CO)_2(PF_6)_2$ for 16 hours, the resulting former requiring addition in drop wise manner (King and Bisnette, 1967). $(CH_3)_5C_5Co(CO)_2$ was prepared by irradiation of a mixture of dicobalt octacarbonyl, toluene, pentamethyl cyclopentadiene and hexane for 18 hours using a 450 watts mercury ultraviolet lamp. Removal of the solvent at 25 ºC gave a residue which was extracted with pentane filtered and the pentane extract was cooled overnight to -78 ºC to give black crystals. The red-brown filtrate obtained was air sensitive and evaporation afforded dark-red brownish crystals which on sublimation gave the red sublimate of $(CH_3)_5C_5Co(CO)_2$(Craid *et al*., 1980). Photolytic studies of the reaction of η5-$C_5H_5Mo(CO)_3$ in tetrahydrofuran under carbonmonoxide and in the presence of liquid sulphurdioxide afforded a brown precipitate after two hours. The sulphurdioxode was allowed to evaporate and tetrahydrofuran was removed by rotary evaporation to give a residue which was extracted with tetrachloromethane, and the extract chromatographed on fluorisil. Elution with trichloromethane removed a purple band of unreacted η5-$C_5H_5Mo(CO)_3$ while with acetone, an orange band was characterized as η^5-$C_5H_5Mo(CO)_2S(O)_2$(Laura *et al*., 2007).Reaction of (PNP)Li with TaF_5 produces pentagonalbipyramidal (PNP)TaF_4). Alkylationwith MeMgBr allows for the isolation of (PNP)$TaMe_4$). (PNP)$TaMe_4$ evolves thermally and/or photochemically into a bis(methylidene) complex (PNP)Ta$(dCH_2)_2$. The identity of the latter has been established by X-ray structural, NMR spectroscopic,and DFT computational studies (Louis, 1990). Several new synthetic approaches to functionalized chromium amino- carbene complexes were developed (Thomas and Javier, 2004) making a wide array of complexes, including those containing optically active auxiliaries, available. Photolysis of these optically active carbene complexes in the presence of imines produces optically active p-lactams in high chemical and optical yield. Procedures for removal of the optically active auxiliary to produce the optically active free aminop-lactams have been developed (Amanda *et al*., 2001).The photochemistry of five diruthenium hexacarbonyl tetrahedrane compounds,

$Ru_2(CO)_6(l\text{-}S_2C_6H_4)$, $Ru_2(CO)_6(l\text{-}S_2C_2H_4)$, $Ru_2(CO)_6(l\text{-}S_2C_3H_6)$, $Ru_2(CO)_6(l\text{-}SCH_2CH_3)_2$, and $Ru_2(CO)_6(l\text{-dmpz})_2$, where dmpz¼3,5-dimethylpyrazolate, were examined in frozen Nujol glasses at ca. 90 K. These compounds were found to lose CO upon UV photolysis to form two isomeric photoproducts.Three ruthenium sulfide clusters with labile CH_3CN ligands have been photochemically synthesized. Irradiation of $[(cymene)_3Ru_3S_2](PF_6)_2$ in CH_3CN gives $[(cym)_2(CH_3CN)_3Ru_3S_2](PF_6)_2$, which were characterized by ^1H NMR spectroscopy, ESI mass spectrometry, and chemical reactivity (Thomas *et al*., 1996). The synthesis and characterization of new ferrocene derivatives of the type $Fe_2(CO)_6S_2Fc_2$ (Fc=Ferrocenyl) was reported (Abdulhamid, 2007). These compounds have been prepared by the reaction of the $Fe_2(CO)_9$ complex with a stoichiometric amount of the diferrocenyl disulphur compounds in a near refluxing THF solvent. Furthermore, the consequent mono–and di– trimethylphosphine derivatives were synthesized by photolysis or thermolysis of the $Fe_2(CO)_6S_2Fc_2$ complex in the presence of the phosphine ligands Also, the compounds: $Fe_2(CO)_6S_2Fc_2$.$Fe_2(CO)_5PMe_3S_2Fc_2$, and $Fe_2(CO)_4(PMe_3)_2S_2Fc_2$have been fully characterized by IR,^1H, ^{13}C, and ^{13}P NMR spectroscopy. $Fe_2(CO)_6S_2Fc_2$ crystal structure determinations confirm that the two ferrocenyl groups are trans to each other (Abdulhamid, 2007).

2.20 Literature review of theoretical methods

Molecular modeling has emerged as a viable and powerful approach to Chemistry. Molecular mechanics calculations coupled with computer graphics are now widely used in lieu of “tactile models” to visualize molecular shape and quality steric demands. Computational (Theoretical) Chemists continue to play an ever increasing role in chemical research and teaching (Dearing, 1988).

Software tools for computational Chemistry are based on empirical information. To use these, one needs to understand how the technique is implemented and the nature of the database used to parameterize the method (Gund *et al.*, 1988).These guidelines wereproposed for reporting molecular modeling resultsand to encourage computational Chemists /researchers to provide certain information so that others can reproduce and analyse their results (Craig, 2001).

Molecular modeling has become a vital technique in chemical research, and there are some unique challenges on the modeling of d- and f-block complexes (Gloria *et al*., 2002). Theoretical rationalization of the interaction between a Cobalt phthalocyanine (CoPc) and 2-mercaptoethanol (2ME) at PM3(tm) Semi empirical level of calculation was performed (Atay *et al*., 2002). The interaction energy profile (IEP) was obtained along the $r_{Co..s}$ reaction coordinate which allows the identification of the relevant species involved in the interaction, i.e. the A structure of $r_{Co..s}$ is 2.2Å, the transition state (TS) at $r_{Co..s}$ is 3.3Å and B structure at $r_{Co..s}$ 3.9Å. Reactivity descriptors such as Frontier molecular orbital (FMO), Fukui functions and local hardness are applied to the three species in order to identify the reactivity sites and to explain the interaction between CoPc and 2ME (Atay *et al*., 2002).Modeling of the metal ion/ligands complexation reaction between divalent metal cations(M^{2+}) and hydrophilic tridentate ligands murexide (Mu^{-}), in water, water + glycerol, and in glycerol, was carried out. Kinetic studies showed that the rate of the reaction is very dependent on the metal ion, with Zn^{2+}> Ni^{2+}, but, reactions are slower in dispersed glycerol than in water. Theoretical calculations, which have shown metal ion dependence, were consistent with experimental observations. The entropy values calculated in all solvents were negative and were similar in value, indicating that these spontaneous reactions are enthalpy driven.Diego *et al*., 2002 discovered that a folded envelope geometry was encountered in structurally characterized high valent early transition metal compounds containing a substituted 1,4-diaza-1,3-butadiene ligand. In these cases the diazabutadiene ligand can be regarded as a dianionicene- diamido ligand and the folded five member ring can be divided as a metallocyclo-2,5-diazapent-3-ene. A comparable metallocyclopent-3-ene description is attributed to η^4-butadiene complexes of early transition metals in which the ligand exhibits a σ^2, π-character. For this reason a parallel description was initially adopted by several authors for the enediamido ligands and the origin of the folding of the five member ring was attributed to the situation of the metal centre through the C=C double bond. A DFT study of the model complex $[CpTaCl_2(HNCHCHNH)]^1$ and Compound $[CpTaCl_2(\eta^4\text{-butadiene})]^2$ were carried out. The differences in the bonding description of theseligands coordinated to the identical $[CpTaCl_2]$ moiety are discussed through the examination of the HOMOs of 1 and 2 on the basis of FMO analysis (Diego and Augustin, 2002). However, it waspredicted that many reactions of transition metal compounds involve a change in

spin. These reactions may proceed faster, slower or at the same rate as otherwise equivalent processes in which spin is conserved. For example ligand substitution in $[CpMo(Cl)_2(PR_3)_2]$ is faster than expected, whereas addition of dinitrogen to $[Cp^*Mo(Cl)(PMe_3)_2]$ is slow. Spin-forbidden oxidative addition of ethylene to $[Cp^*Ir(PMe_3)_2]$ occurs competitively with ligands association. To explain these observations, the researchers discussed the shape of the different potential energy surfaces (PESs) involved, and the energy of the minimum energy crossing points (MECPs) between them. This computational approach is of great help in understanding the mechanisms of spin-forbidden reactions, provided that accurate calculations can be made to predict the relevant PESs. Density functional theory, especially using gradient-corrected and hybrid functional, performs reasonably well for difficult problem of predicting the energy splitting between different spin states of transition metal complexes, although careful calibration is needed (Rinaldo and Jeremy, 2003).Transition metal fragments are proposed to overcome the unfavourable interaction arising from the splayed out π-orbitals of the five- and six-member rings of C_{60} and C_{70} in complex formation. Computations carried out at Semi empirical PM3(tm) level on a series of $C_{60}MC_nH_n$ and $C_{70}MC_nH_n$ complexes suggest that it is possible to stabilize η^6 complexes of C_{60} and C_{70} using appropriate transition metal fragments (Eluvathigal *et al*., 2000).Molecular modeling and assignment of electronic absorption spectra of mononuclear $[Fe(S_2\text{-o-xyl})_2]^{2-}$ and two binuclear $[Fe_2(S_2\text{-o-xyl})_3]^{2-}$isomers were performed by Semi empirical calculations. The comparisons with available experimental data confirmed the reliability of the Semi empirical ZINDO/ S method in predicting the electronic absorption properties of these synthetic model complexes. Calculations with ZINDO/1 have also shown that the syc- binuclear ion is more stable than the anti-$Fe(S_2\text{-o-xyl})_3]^{2-}$ ion (Mehmet, 2006). In coordination chemistry, many reactions involve several electronic states, in particular states of different spin. This phenomenon of 'Multiple-State Reactivity' has been recognised for some time, both in gas-phase reactions of 'bare' metal ions, and for transition metal complexes in solution. Until recently, however, much of the discussion of these systems has remained qualitative, because standard computational methods do not allow the location of the critical points for these processes and the Minimum Energy Points (MECPs) between states of different spin. Increased computational resources and new algorithms now enable MECPs to be located for large, realistic transition

metal containing systems, yielding important reactions such as oxidative addition of C-H bonds to metal centres and ligands association/dissociation processes. Several examples are presented for inorganic, organometallic and bioinorganic reactions (Harvey *et al*., 2003). The density functional theoretical results of Structural, electronic, and optical properties of ligands free Zn_mSe_n clusters as a function of size of the cluster were reported.The results include the radial distribution of atoms and of Mulliken populations, the electronic energy level (in particular the HOMO and LUMO), the band gap and the stability as a function of size and composition (Goswan *et al*., 2006),The aromatic properties were investigated using the ground state geometry and electronic structure of M^{2-}_4 cluster (M = B, Al, Ga). The calculations were performed by employing the Density Functional Theory (DFT) method. It was found that all these three clusters adopted square planar M^{2-}dianion and exhibits characteristics of multifold aromaticity with two localized π-electrons. In spite of the unstable nature of these dianionic clusters in the gas phase, their interaction with the sodium atoms forms very stable bipyramidal M_4Na_2 complexes while maintaining their square planar structure and aromaticity (Sandeep *et al*., 2006). Theoretical study on a class of organometallic complexes containing the all-metal aromatic unit Ga_3 on the basis of density functional theory calculations on a series of model sandwich-like compounds $[DM(Ga_3)]^{3-}$, as well as those of the saturated compounds, $[DM_n(Ga_3)]$, [D = Ga^-_3, Cp^- ($C_5H_5^-$); M = Li, Na, K, Be, Mg, Ca] and extended compounds $(Cp^-)_m$ $(Li^+)_n$ $(Ga_3^-)_o$ (m, n and o are integers). For the six metals, the all-metal aromatic Ga^-_3 can only be assembled and stabilized in the ‘’heterodecked sandwich’’ scheme. The results revealed that the electronic, structural and aromatic properties of the all-metal Ga^-_3 could be well retained during the assembly, which is vindicative of ‘building block’ character (Li-ming *et al*., 2008). The combined use of theoretical and mathematical methods in the analysis of electron paramagnetic resonance data has greatly increased the ability to interpret even the most complex spectra reported for doublet state inorganic main group radicals. The account summarises the theoretical basis of such an approach and provides an in-depth discussion of some recent illustrative examples of the utilization of this methodology in practical applications. The emphasis is on displaying the enormous potential embodied within the approach (Heikki *et al*., 2007).Computer modeling of mixed metal fluorides for optical applications describe a new computational method for predicting the optical behaviour

of doped inorganic materials. There is considerable interest in using inorganic materials in photonic devices, and in many cases, the optical properties of these materials depend on doping by ions such as those from rare earth series. Among the inorganic materials of interest are mixed metal fluorides (e.g. $BaLiF_3$, BaY_2F_8, $YLiF_4$, $LiCaAlF_6$, $LiSrAlF_6$), doped with trivalent rare earth ions. The paper described the use of Mott-Littleton calculations to determine the optimum location for dopant ions, followed by crystal field calculations which make direct use of the output of Mott-Littleton calculations to calculate the optical properties of the dopant ion taking into account its symmetry and the positions of the surrounding ions, including any vacancies or interstitial ions present by virtue of charge compensation. It is then possible to predict whether a given dopant ion at particular site in a material will have favourable optical properties (Robert *et al*., 2004).

Electronic spectroscopic Studies: The primary method forcomputing transition energies to electronically excited stateswithin the framework of DFT is to employ a time-dependentformalism (Rung and Gross, 1984; Bauernschmitt and Ahlrichs, 1996)and the strengths, limitations of that model wereshown and discussed (Van Leeuwen, 2001; Burke *et al*., 2002; Marques and Gross, 2004). With respect totransition-metal complexes, a particularly troublesome feature of TD-DFT is the tendency of many functionals to significantlyunderestimate the energies of excited states characterized by highdegrees of non-local charge transfer, although in principle, thisproblem may be addressed by replacing the DFT exchangefunctional by 100% Hartree–Fock exchange (Dreuw and Head-Gordon, 2005) byusing certain range-separated functionals, as in a recentapplication to charge transfer excitation in pyridine complexeswith Ag_2O (Arcisauskaite *et al*., 2009), or by going beyond first-order response. Nevertheless, linear-response TD-DFT with various functionalscontinues to be an especially useful one-electron model forunderstanding the optical spectra of transition-metal complexes.

The TD-B3LYP was used to study the singletand triplet excited states of Ruthenium(II)polypyridine complexes andto explain their photodissociation behaviours on the basis of theexcited-state potential energy surfaces (Salassa *et al*., 2008). A number of earlierTD-DFT studies of Ruthenium and Osmiumpolypyridyl complexes havebeen reported with the goal of rationalizing their absorption and

emissionspectra in the gas and condensed phases (Guillemoles *et al*., 2002; Laine *et al*., 2005; Nazeeruddin *et al*., 2005; Laine *et al*., 2006; Charlot and Aukauloo, 2007; Marcacco*et al*., 2008; Abrahamsson *et al*., 2008). Jackson*et al*.,2008, have employed TD-DFT to characterize the intensenear UV absorptions in axially ligated FeIVQO complexes asligand to FeQO charge transfer transitions and therebyrationalize the strong resonance enhancement of the FeQOstretching mode upon excitation of these transitions. Hutinet*et al*., 2007, characterized the unusual mixed valence excited stateof a binuclear copper helicate with TD-B3LYP and TD-BP86and further computed its circular dichroism in order to assignits absolute chirality which derived from an interesting selfsortingprocess during crystallization. This was later shown in a related work by Schultz *et al*., 2008,whoshowed that this mixed valence behaviour extends over all four copper atoms in a helicate dimer, thereby rationalizingexperimental cyclic voltametry data and indicating a potentialmeans to construct a wrapped molecular copper wire. Ina related work, Bar-Nahum*et al*., 2009, found TD-B98 to be highly helpful in explaining an unusual long wavelength metal toligand charge-transfer transition occurring in a mixed valencetrinuclear copper disulphide.A recent review provides an overview of DFT and TD-DFTapplications to electronicspectroscopy and excited-stateproperties of d^6 metal carbonyls, strongly phosphorescentcyclometallated complexes, RuII photosensitizers (as used, for example, in solar cells and light switches), and isonitrilecomplexes of Re(I) and Ru(II) (Fan *et al*., 2008). They used spin-unrestricted TD-DFT with the BP86density functional, a continuum solvation model, and empiricalcorrections to calculate circular dichroism spectra of a number of trigonal dihedral Cr(III) d^3 complexes and compared this to earlierrelated work.

Peralta*et al*., 2008, used TD-DFT and magnetically perturbedTD-DFT with statistical averaging of orbital potentials tocalculate ultraviolet and magnetic circular dichroism spectraof MTAP (M = Ni, Zn) and ZnPc where TAP denotestetraazaporphyrin.Another particularly useful application of TD-DFT is forthe interpretation of the optical spectra of intermediates tooreactive to be readily isolated (Schipper *et al*., 2000). Thus, Kunishita*et al*., 2007,inferred the creation of a reactive Cu(II) 2-hydroxy-2-hydroperoxypropaneintermediate upon addition of hydrogenperoxide to a solution of a supported Cu(I) complex in acetonebased on a comparison of measured UV spectral data tothose computed at the TD-B98 level, thereby rationalizingsubsequent reactivity

of this complex.In the area of larger inorganic clusters,Stener*et al*., 2007, havesuccessfully reproduced and rationalized the blue shift in theoptical spectra of gold nanoparticles with decreasing clustersize using scalar relativistic TD-DFT applied to clusters of146, 44, and 6 gold atoms. Stener *et al*., 2008a also examinedthe optical spectroscopy of the WAu_{12} and $MoAu_{12}$ clusters atthe TD-DFT level, noting that while spin–orbit couplingmerely shifts the energies of the lowerexcitations in the formercompound, it gives rise to more complex splittings in many ofthe excitations for the latter compound. In another related work byStener*et al*., 2008b,reported their results forthe anionic dodecahedral clusters, VAu_{12}, $NbAu_{12}$, and$TaAu_{12}$.It is important to note that medium effects on opticalspectra (solvatochromism) can be large for polar transitionmetalcompounds, and the inclusion of such effects in theTD-DFT model is typically most efficient when the surroundingmedium is modeled as a dielectric continuum. Thus, forexample, Charlot and Aukauloo, 2007, have assessed aqueoussolvatochromic effects on the spectra of Ru(II)polypyridinecomplexes using the non-equilibrium polarized continuummodel (PCM) (Caricato *et al*., 2006; Scalmani *et al*., 2006).Casarin *et al*., 2007 showed good utility in the predictionof relative transition energies, and this has been applied to assessthe covalency of metal-chloride bonds in metallocenedichlorides,both with (Casarin *et al*., 2007) and without (Kozimor *et al*., 2008) accounting for relativisticspin–orbit effects. The inclusion of spin–orbit effects usingthe two-component zeroth-order regular approximation(ZORA) leads to significant improvements in predictedabsolute excitation energies for heavy transition metals (Fronzoni *et al*., 2005).

A particularly interesting application of this method is to studybenzenedithiolate complexes of Ni, Pd, Pt, Cu, Co, and Auoffered insights into those factors affecting the innocence ornon-innocence of the benzodithiolenes (Ray *et al*., 2007). Other recent studieshave provided insights into the nature of relativistic andsolvation effects on K-edge XAS spectra for Fe(II) and Fe(III) species (DeedBeer *et al*., 2008), as well as for ‘‘superoxidized’’ Fe(V) and Fe(VI) complexes (Berry *et al*., 2008; Sarangi *et al*., 2008).They used both ground-state DFT andvalence and near-edge TD-DFT to compare changes in bonding,UV spectra, and pre-edge XAS spectra between the wild-typeblue copper active site of azurin and a mutant- substitutingselenocysteine for cysteine. These authors found that changesin Cu–S vs. Cu–Se bond distances led to

very similarcovalencies in the two copper–chalcogen bonds, so thatspectra were minimally affected in spite of the 0.2A° variationin bond lengths.As an alternative method to computing electronic excitation energies, (Cheng *et al*., 2008; Gilbert *et al*., 2008), have bothrecently described an approach called excited-state DFT(eDFT) or the maximum overlap method (MOM), where ineach instance, the Kohn–Sham procedure is modified so thatthe total energy is minimized, subject to a constraint that thefinal density has maximal overlap with a target density. In thisway, densities that correspond to systems with one or moreholes in low energy orbitals may in principle, be constructedand their Kohn–Sham energies determined directly(as opposed to using TD-DFT). In the case of a system ofnon-interacting electrons, selection of a target density istrivially accomplished by swapping one or more virtualorbitals with occupied orbitals. By turning on the adiabaticcoupling in small steps, Cheng *et al*., 2008, found that they wereable to achieve self-consistent eDFT solutions even forRydberg states and Gilbert *et al*., 2008 showed the utility of MOMfor charge-transfer excited states. The work may betoo preliminary tohave its application extended to any transition-metal containing systems, butit has the potential to sidestep known problems with TD-DFT insuch complexes.An interesting question in the spectroscopy and optics ofmetal clusters is the quenching of spin–orbit coupling as afunction of geometry. This was studied using PBE for goldclusters by Castro *et al*., 2008.One key application where it is important to predict thecorrect spin-state splitting is multi-state reactivity. Yang*et al*., 2006 used B3LYP calculations to study the gas-phasespin-forbidden addition reactions of Y^+, Zr^+, Nb^+, Mo^+,Pd^+, and Ag^+ with N_2O to form $MONN^+$, where M denotesthe metal atom; the location of the crossing scheme is sensitiveto the spin-state splitting. Additional examples are foundin the two-state reactivity examples studied by Shaik *et al*., 2007,and in the two-state triplet–singlet mechanism for olefinepoxidation and oxidation reactions.The computation ofvibrational frequencies is nearly always undertaken in modernpractice in order to verify the nature of optimized stationarypoints. One study focusing morespecifically on an information provided by the vibrationalspectrum has been described(Hebben *et al*., 2007). In order tocritically assess a prior suggestion that homoaromatic interactionsbetween ethylene ligands causes the geometry of$Ni(C_2H_4)_3$ to have all of its heavy atoms in a common plane, they used BP86 calculations to assign in detailedmeasured IR and Raman spectra for $Ni(C_2H_4)_3$, $Pd(C_2H_4)_3$,and $Pt(C_2H_4)_3$. From analysis of the interfragment

forceconstants, they concluded that homoaromaticity plays no rolein the structures of these species: the Ni and Pd cases are welldescribed as Dewar–Chatt–Duncanson complexes; the Pt caseincludes some metallocyclopropane character. A prior studynoted the high accuracy of hybrid functionals with respect topredicting the vibrational spectra of $Ni(C_2H_4)$ and $Ni(C_2H_4)^+$ (Alexander and Dines, 2004).Vibrational spectroscopy can be useful in assigning chiralityin transition metal complexes, typically from comparison ofexperimental and computed vibrational circular dichroism(VCD) or Raman optical activity (ROA) spectra. Some recent examples in this area include prediction of VCD and ROA (Sato *et al*., 2006), spectra for some chiral tris(acetylacetonato)metal complexes.Coupling optical and vibrational spectroscopies, resonanceRaman and off-resonance Raman spectroscopies also play keyroles in the characterization of transition-metal containingsystems (Petrenco *et al*., 2006). Recent advances in the direct computation ofresonance Raman intensities have been reported (Johnsonand Peticolas, 1976) and applications have included examination of the first photoexcitationstep in a tetranuclear (Ru_2Pd_2) light-harvestingcomplex (Herrmann *et al*., 2007) and the determination that benzenedithiolateligands need not be innocent in complexes of group 8, 9, and10 metals (Petrenko *et al*., 2006).Another interesting use of computed vibrational frequencies is for the construction of molecular partition functions fromwhich equilibrium or kinetic isotope effects (EIEs and KIEs,respectively) may be computed so as to gain improved insightinto electronic structure or mechanism. Popp *et al*., 2007, reported a computed $^{18}O/^{16}O$ KIE in good agreement with experiment for theformation of a PdO_2 adduct. They found that the ratedeterminingstep involved an end-on to side-on isomerizationof the O_2 unit, which was contrary to an earlier proposal that the measured KIE was consistent with a concerted2-electron oxidation and direct side-on binding of the O_2.(Lanci and Ruth, 2006; Lanci *et al*., 2007; Roth and Cramer, 2008), have also been quite active in comparingexperimental and DFT-derived KIEs in transition-metalcontaining systems (Lanci and Ruth, 2006; Lanci *et al*., 2007).Carbonniere *et al*., 2006 studied theharmonic effects on thevibrational spectra of d^0 transition-metal peroxides and foundB3LYP and PBE0 to offer good comparison with experiment, while BP86, OLYP, and TPSS did less well. Applications ofTD-DFT are carried out using the linear-response formalismin which the applied electromagnetic field is weak; this issufficient for single-photon spectroscopy.

Nonlinear optics and two-photon spectroscopy (Rubio-Pons *et al*., 2006) require high-order treatmentsor a combination of TD-DFT with a sum over states.

Due to their tremendousimportance in biology and their possible extension to bioinspiredcatalytic systems, the chemistry of heme- andnon-heme-supported iron–oxo species had been subject ofextensive theoretical attention (Yoshizawa *et al*., 1977; Solomon *et al*., 2000; Ghosh *et al*., 2004; Abu-Omar *et al*., 2005; Kryatov *et al*., 2005; Bassan *et al*., 2006; Park *et al*., 2006; Brown *et al*., 2007; Harman *et al*., 2007; Nam, 2007; Neidig *et al*., 2007; Pau *et al*., 2007; Que, 2007; Bell *et al*., 2008). For example, DFT-B3LYP calculations were instrumental in establishing thatbis(a-diimine) complexes of single iron atoms hitherto commonlydescribed as high-spin FeO complexes are properlydescribed as antiferromagnetically coupled bis(a-diiminate)-Fe(II) species, the non-innocent ligands each having acceptedone electron from iron into a low-energy p orbital. In adetailed study, the ability of various functionals to predict thebinding energy of CO, NO, and O_2 to heme-supported ironwas studied by Radon and Pierloot, 2008, used severalfunctionals and also the CASPT2 model. These authors foundthat CASPT2 provided the best agreement withexperimentand that the OLYP functional was similarly accurate.Theperformance of this functional in the prediction of stateenergy splitting in supported iron compounds is good, but the BP86 predicted severe overbinding whileB3LYP and PBEO predicted severe underbinding. A study byStrickland and Harvey, 2007, focused on the same binding processes(and also considered binding of H_2O) and emphasized thecontribution of a spin-crossoverrequirement to the kineticbarrier associated with CO binding with metals. (Shaik*etal*., 2007; Altun*et al*., 2007; Derat *et al*., 2007; Hazan *et al*., 2007; Li *et al*., 2007; Wang *et al*., 2007; Chen *et al*., 2008a; Chen *et al*., 2008b; Cho *et al*., 2008; Hirao *et al*., 2008; Shaik *et al*., 2008; Wang *et al*., 2008; Cho *et al*., 2009; Klinker *et al*., 2009),were prominent in characterizing the single- and two-statereactivities of various supported iron compounds, particularlyfor cases relevant to metalloenzymes like cytochrome P450,hemeoxygenase, horseradish peroxidase and nitric oxidesynthase, have provided additional recent insights intomechanistic details through DFT calculations, primarily makinguse of the B3LYP functional. The most recent exampleinvolves triplet and quintet reactivity in non-hemeoxo-iron(IV),which was modeled in B3LYP calculations.In the case of polynuclear iron compounds, Reilly *et*

al., 2007, employed PBE to study the ground state geometries and spinmultiplicities of cationic iron oxide clusters containing one ortwo iron atoms and up to five oxygen atoms. They comparedcomputed reaction paths for the oxidation of CO with massspectrometric data to assess the relative facility of CO oxidationvs. oxygen atom replacement by CO and found good correlationbetween computed barriers and observed reaction channels. Gold/iron oxide composite nanoparticles have a number ofpotential biological applications, based on binding magneticnanoparticles to various substances, and there are many questionsabout the binding strengths. Sun *et al*., 2007, showed that the PW91functionals applied to $Au_6Fe_{13}O_8$ clusters can explain thedifferential binding ability of various amino acids to these nanoparticles.They also studied magnetic moments, bond distances,and gold coating energies in clusters up to size $Au_5Fe_{13}O_8$considering biologically relevant multinuclear iron complexes,Schwarz *et al*., 2008, employed BP86 to correlate predicted d-orbital energy splittings with those determined from magneticcircular dichroism (MCD) for the two non-equivalent ironatoms in the active site of toluene-4-monooxygenase (T4MO)which is strongly similar to that of soluble methane monooxygenase(sMMO). Based on their calculations, which alsoaddressed the energetics of different active site geometriesformed from the two iron centres and anchored amino acidside chains acting as ligands, they concluded that a watermolecule found to be axially bound to one of the iron centresin several sMMO X-ray crystal structures is unlikely to remainbound when the oxygenases are complexed with theirrespective effector proteins, T4moD and MmoB.They furtherconcluded that complexation by these effector proteins is likely to change the orientation of a terminal glutamate ligand onone iron, thereby possibly facilitating formation of a Fe_2O_2reactive intermediate and rationalizing the 1000-fold increasein catalytic activity of sMMO when complexed with MmoB.Rinaldo*et al*., 2007, examined the catalyticcycle of sMMO by employing a QM/MM method in which aQM subsystem is treated with the B3LYP functional, and suggested that the protein stabilizes a peroxo intermediatehaving a m-Z2:Z2 coordination geometry and also adjuststhe overall thermochemistry so as to favour products overreactants, thus emphasizing the importance ofincluding the full protein environment in the modeling ofmetalloenzymes.An additional spectroscopic technique that can be useful forcharacterizing the electron structure of iron compounds isMossbauer spectroscopy. Han and Noodleman, 2008a, have reported goodagreement

between experimental isomer shifts for 61 differentiron sites and those computed at the PW91 level after applyinga linearcorrection. (Han and Noodleman, 2008b), subsequentlyevaluated the performance of a number of other functional for computed Mossbauer isomer shifts and found similarlygood performance from OPBE and OLYP. Basedon computed isomer shifts, geometries, pKa values, spinpopulations, predicted ground states, and quadrupolesplittings,Han and Noodleman assigned a cis-m-1,2 peroxo bridging structureto intermediate state P of MMO, a bis(m-oxo) structureto intermediate Q, and a cis to trans isomerizationpathway connecting P to Q, that is, coupled to specific ligandrearrangements.A different binuclear iron site of substantial biologicalinterest was found in ribonucleotidereductase, where therehave been substantial controversy with respect to the geometry and electronic structure of intermediate X in the catalyticcycleincluding antiferromagnetically coupledhigh-spin Fe(III) and Fe(IV) centres (Solomon *et al*., 2000; Kryatov *et al*., 2005). Mitic*et al*., 2007, have compared d-orbital energies computed for various hypotheticalgeometries at the BP86 level to splittings determined from MCD and predicted transition energies from TD-DFT and DSCF calculations for the same geometries to electronicspectroscopic data; based on their calculations, it was concludedthat the best model for intermediate, X, involves one bridging-m-oxo group and one bridging-m-hydroxo group. This predictionstands in contrast to a prior suggestion of a bis-(m-oxo) corebased on a similar analysis (Han *et al*., 2006), illustrating the somewhat subtlespectral differences predicted for different model geometries.However, Mitic*et al*., 2007, emphasized that the use of grouptheory to predict spectral intensities can offer helpfuladditional information for use in resolving spectral differences. Turning to polyiron clusters involving sulphide bridges inplace of oxo bridges, which have been extensively studied byDFT and indeed have served as a testing and validationground for broken-symmetry techniques over several years (Shoji *et al*., 2007). In an effort to understand the widespread distribution ofFe_4S_4 clusters in biology, Jensen *et al*., 2008, have carried outBP86 calculations for MFe_3S_4 and $M_2Fe_2S_4$ clusters whereM = Cr, Mn, Fe, Co, Ni, Cu, Zn, and Pd. They observed goodagreement for structures and spin states in cases that areknown experimentally, and noted that the structures andreduction potentials of the cubic clusters are surprisinglyinsensitive to substitution of other transition metals, suggestingthat this may be an evolutionary advantage.They also noted that the modified clusters havealternative spin states that lie closer in energy

to one anotherthan those for the all-iron case, so that spin crossover may bemore facile in the mixed-metal clusters.Li *et al*., 2008, found that MR-CI calculations agreed withexperiment that FeO_2 is linear, but nine of the ten tested densityfunctionals predicted it to be bent, with only BH&HLYP givinga linear ground state. However, BH&HLYP predicts qualitativelyincorrect results for other states.The prediction of one-electron reduction (or oxidation)potentials for molecules containing transition-metals has beenextensively explored in recent past (Baik *et al*., 2002; Uudsemaa and Tamm, 2003; Blumberger *et al*., 2004; Tateyama *et al*., 2005; Chiorescu *et al*., 2008), building on thegood success of DFT-based models applied to predict thisproperty in organic systems(Patterson *et al*., 2001; Fontanesi *et al*., 2002; Bhattacharyya *et al*., 2007; Hodgson *et al*., 2007; Moeris *et al*., 2008). Recent efforts in this areainclude a study by examining the aqueous$Ru^{3+}|Ru^{2+}$ couple with 37 density functionals and five basissets and further considering the effects of one or two explicitshells of solvent water (six or 18 water molecules, respectively)about the bare Ru ion in addition to continuum solvation. They concluded that at least, two shells of explicit waterwere necessary to approach quantitative agreement withexperiment and that an important issue is a substantialdegree of positive charge transfer from the metal ion to theouter-shell waters in microsolvated clusters. For two explicit solvent shells,the difference in solvation energy of Ru^{3+} and Ru^{2+} variesfrom 6.83 to 7.45 eV, depending on the choice ofdensity functional and basis set, showing that one must becautious about qualitative values of calculated reductionpotentials especially in articles where the sensitivity to thefunctional is not explored. A QM/MM calculations on both Ru^{2+} and Ru^{3+} inaqueous solution carried out. Although the QM region was treated byHartree–Fock theory (not DFT), the simulations providevaluable insight into the solvated structures presented in thesolution. For example, for Ru^{3+} the second coordinationshell contains only ten water molecules (Kritayakornupong, 2007). Three-bodycorrections to a purely MM calculation were insufficient toreproduce the hydration structure of Ru,$^{3+}$. The structureof the hydration shell of Fe^{3+}(aq) was studied(Amira *et al*., 2005), and the hydrolysis of Fe^{3+} was studied(De Abreu et al., 2006).The relative stability of hydrated oxo vs. hydroxy structureshas been examined by experiments and calculations forcompounds with the formula MO_2H_2+, where M = Fe, Co,or Ni. For M = Ni, the $(H_2O)MO^+$ structure is favoured,whereas for M = Fe, the $M(OH)_2$+ structure is favoured; forM = Co, the isomers are energetically similar (Schroder *et al*., 2009).In

another work, focus was on a large number of supported Rucomplexes due to their anticancer therapeuticproperties. Chiorescu*et al*., 2008, benchmarked various continuumsolvation models in conjunction with the B3LYP functionalfor 80 reduction potentials in four solvents. Comparison withexperimental data indicated that errors were minimized whensolute cavities were constructed from Bondi's set of atomicradii. The default choices in some electronic structureprograms were found to lead to errors in the region70 to 140 mV.In another work aimed at predicting aqueous one-electron reductionpotentials for the most common aqueous couple of allof the first-row transition metals(Moeris*et al*., 2008; Moens *et al*., 2007), foundthat the global value of the electrophilicity was a good predictor of reductionpotentials when computed for clusters including two salvation shells about the central metal ion. Uudsemaa and Tamm, 2003,had previously studied these series, computing the reductionpotentials directly from DFT and continuum solvation freeenergies, and had come to similar conclusions with respect tothe importance of two solvation shells (Leib *et al*., 2007).DFT work has been done to rationalize the influence thatvarious factors may have on the activity of the supportedruthenium complexes (Correa and Cavallo, 2006; Webster, 2007; Mathew *et al*., 2008; Zhao and Truhlar, 2009).Thus, for instance, Mathewet al., 2008, have used DFT to study five different self-deactivationpathways, all based on intramolecular C–H bond activation,and suggested that increased rigidity in NHC substituentsmight be expected to improve catalyst stability. They used B3LYP and M06 to demonstrate thatthroughout the metathesis process, the olefin remains''bottom-bound'' to the $(H_2IMes)(Cl)_2Ru$ catalyst and thechlorides remained trans to one another, such that efforts to designdiastereo- and enantioselective catalysts should be undertakenwithin this coordination environment. In another work, Benitez*et al*., 2009, used the M06 functional to calculate the dissociationenergy of the Ru bond to tricyclohexylphosphine (PCy3)in a Grubbs catalyst and found excellent agreement withexperiment. They found that the M06 functional leads toimproved accuracy over B3LYP (by 0.5kcalmol^{-1}) forrelative energies of various stable intermediates and muchimproved accuracy (by 23kcalmol^{-1}) for PCy3, andtherefore concluded that their calculations settle a longstandingcontroversy. Zhao and Truhlar, 2009, then repeated the calculations with the Ruand Cl atoms removed to find the contribution of non-covalentinteractions of the bulky ligands. For B3LYP, this non-covalentinteraction is repulsive, but for M06-L it is attractive, and in fact it is 4.5kcal mol^{-1} stronger for the

Grubbs I precatalyst than for the Grubbs II precatalyst. Thus the difference in thebond dissociation energies is essentially completely accountedfor by non-covalent attractive interactions. This is an importantqualitative finding because the catalyst design literature isalmost entirely focused on the electron donating ability ofthe ligands and their potential coordinate covalent bondingstrength, with some consideration given to steric crowding,but there has been essentially no consideration of attractivenoncovalent interactions.M06-L gives a bond dissociation energy of 39–40kcalmol^{-1}for the Grubbs II precatalyst, whereas MPW1B95 gives 30kcalmol^{-1}, and B3LYP, TPSS, BP86, PBE, andPBE0 give values in the range 14-23kcalmol^{-1}(Benitez *et al*., 2009). The value inferred from the experiment (Sanford *et al*., 2001) in toluene is 27kcalmol^{-1}.After the 40 kcalmol^{-1} value was published (Zhao and Truhlar, 2009), a gas-phaseexperiment was published (Torker *et al*., 2008),yielding the same 40kcalmol^{-1}.This not only confirmed the M06-L calculation, but it showedthat the older density functionals give much worse results forthe large, real molecules than for the smaller model catalysts.This effect of size has also been noted in main-groupchemistry and is attributed to an accumulation ofmedium-range correlation energy in large, complex systems,with smaller effects in extended chains. In more recentwork, Stewart *et al*., 2009, reported that B3LYP predictsgeometries for Ru-metathesis-relevant complexes moreaccurately than M06-L.In another related work Pandian*et al*., 2009, had successfully applied theM06 functional to the Ru-catalyzed ring closing metathesis of1,6-heptadiene, while Sieffert and Buhl, 2009,studied the binding enthalpyof a triphenylphosphine ligand in Ru(CO)Cl(PPh_3)$_3$(CHQCHPh)with BP86, B3LYP, and the M05 and M06 families, as well aswith density functionals to which an empirical MM dispersionis added. They found that BP86, B3LYP, and M05 do notreproduce the experimental results whereas all four membersof the M06 family and the empirically corrected functional M05-2X was found to be intermediate. They agreed withthe conclusion of Zhao and Truhlar, 2009,that non-covalentinteractions make a very large contribution to the totalbinding enthalpy. The success of new density functionals forthese non-covalent interactions allowed them to define acomputationally efficient protocol for studying catalyticreactions.In another work on ruthenium, Caramori and Frenking, 2007,carried out energy decomposition analysis to characterizethe bonding of NO to ground and excited-state rutheniumtetraamine complexes. Krapp *et al*., 2007, have used BP86 andCCSD(T) calculations to clarify details of the electronicstructures

of supported iron and ruthenium complexescoordinating naked carbon, e.g., $(CO)_2(PMe_3)_2Ru(C)$. The Becke Three Lee Yang and Parr (B3LYP) calculations were used to assess mechanistic details associatedwith oxygen formation in water catalyzed by supporteddiruthenium complexes, an area that continues to generateintense interest to the experimental and theoretical chemists (Betley *et al*., 2008; Cape and Hurst, 2008; Ketterer *et al*., 2008; Liu *et al*., 2008a; 2008b: Muckerman *et al*., 2008; Glossman, 2009; Cramer and Thrular, 2009).

CHAPTER THREE

SYNTHESIS, MODELING AND COMPUTATIONAL DETAILS

3.1 Synthetic method

The organometallic compound $[(1\text{-}5\text{-}\eta\text{-}C_6H_7)Fe(CO)_3]BF_4$ was synthesized using standard procedure acquired (Birch *et al*., 1968)and recrystallized from hot water. The pyridines were purchased (BDH or Aldrich) in the purest grade available and the liquid samples were freshly distilled before use. Acetonitrile was distilled in bulk and magnesium sulphate added to remove traces of water before use.

3.2 Addition of pyridines to Tricarbonyl (1-5-η -cyclohexadienyl) irontetrafluoroborate$[Fe(CO)_3(1\text{-}5\text{-}\eta\text{-}C_6H_7)]BF_4$

3.2.1 Synthesis and characterization of Tricarbonyl (1-4-η-5-exo-N-pyridino-cyclohexa-1,3-diene) irontetrafluoroborate (I)

Solutions of $[(1\text{-}5\text{-}\eta\text{-}C_6H_7)Fe(CO)_3]BF_4$; (0.046 g ; 0.15 mmol) in acetonitrile (5 ml) and pyridine (0.1185 g ; 1.5 mmol) in 5 ml of acetonitrile were mixed in a 50 ml of beaker and the mixture was allowed to stand at room temperature for 10minutes. Rotary evaporation of the mixture at 35 ºC and at reduced pressure produced a light brown solid which was shaken with 20 mlof light petroleum spirit (60-80 ºC) and filtered. The resulting product was washed several times with petroleum ether to remove excess pyridine, and dried to give a pale yellow solid in 58% yield. Infra-red υ_{CO} and υ_{BF4} in potassium bromide disc is given in Table 4.1.

3.2.2 Synthesis and characterization of Tricarbonyl (1-4-η-5-exo-N-2-methyl pyridino-cyclohexa-1,3-diene) irontetrafluoroborate (II)

An analogous reaction $[(1\text{-}5\text{-}\eta\text{-}C_6H_7)Fe(CO)_3]BF_4$; (0.046 g ; 0.15 mmol) in acetonitrile (5 ml) and 2-methylpyridine (0.1545 g ; 1.5 mmol) in 5 ml of acetonitrile followed by a similar work-up to that of product (1) above produced product (II) as a brown oil of 60% yield. Its infra-red υco and υ_{BF4} bands together with elemental analytical data are given in Table 4.1

3.2.3 Synthesis and characterization of Tricarbonyl (1-4-η-5-exo-N-3-methyl-pyridino-cyclohexa-1,3-diene) irontetrafluoroborate (III)

An analogous reaction of $[(1\text{-}5\text{-}\eta\text{-}C_6H_7)Fe(CO)_3]BF_4$; (0.046 g; 0.15 mmol) in acetonitrile (5 ml) and 3-methylpyridine (0.1545 g; 1.5 mmol) in 5ml of acetonitrile followed by a similar work-up to that of product (1) above produced product (III) as a brown oil of 63% yield. Details of its infra-red spectrum in acetonitrile and υ_{BF4} bands in potassium bromide disc together with elemental analysis are provided in Table 4.1.

3.2.4 Synthesis and characterization of Tricarbonyl (1-4-η-5-exo-N-4-methyl-pyridino-cyclohexa-1,3-diene) irontetrafluoroborate (IV)

An analogous reaction of $[(1\text{-}5\text{-}\eta\text{-}C_6H_7)Fe(CO)_3]BF_4$; (0.046 g ; 0.15 mmol) in acetonitrile (5 ml) and 4-methylpyridine (0.1545 g; 1.5 mmol) in 5 ml of acetonitrile followed by a similar work-up to that of product (1) above produced product (IV) as a brown solid of 63% yield. Details of its infra-red spectrum in acetonitrile and υ_{BF4} bands in potassium bromide disc together with elemental analysis are provided in Table 4.1.

3.2.5 Synthesis and characterization of Tricarbonyl (1-4-η-5-exo-N-4-amino pyridino-cyclohexa-1,3-diene) irontetrafluoroborate (V)

An analogous reaction of $[(1\text{-}5\text{-}\eta\text{-}C_6H_7)Fe(CO)_3]BF_4$; (0.046 g ; 0.15 mmol) in acetonitrile (5 ml) and 4-aminopyridine (0.141 g; 1.5 mmol) in 5 ml of acetonitrile followed by a similar work-up to that of product (1) above produced product (V) as a brown solid of 63% yield. Details of its infra-red spectrum in acetonitrile andυ_{BF4}

bands in potassium bromide disc together with elemental analysis are provided in Table 4.1.

3.2.6 Synthesis and characterization of Tricarbonyl (1-4-η-5-exo-N-4-N-dimethylaminopyridino- cyclohexa-1,3-diene) irontetrafluoroborate (VI)

Similar preparative route to that described for product (I) above using [(1-5-η-C_6H_7)$Fe(CO)_3$]BF_4 ; (0.046 g ; 0.15 mmol) in acetonitrile (5 ml) and 4-N-dimethyl-aminopyridine (0.183 g; 1.5 mmol) in 5cm^3 of acetonitrile gave the product (V1) as a brown solid of 64% yield. Details of its infra-red spectrum in acetonitrile and υ_{BF4} bands in potassium bromide disc together with elemental analysis are provided in Table 4.1.

3.3 Addition of pyridines to Tricarbonyl (1-5-η-2-methoxycyclohexadienyl) irontetrafluoroborate[$Fe(CO)_3$(1-5-η-2-$MeOC_6H_6$)]BF_4

3.3.1 Synthesis and characterization of Tricarbonyl (1-4-η-5-exo-N-pyridino-2-methoxycyclohexa-1,3-diene) iron tetrafluoroborate (VII)

Solutions of Tricarbonyl (1-5-η-2-methoxycyclohexadienyl) iron tetrafluoroborate [$Fe(CO)_3$(1-5-η-2-$MeOC_6H_6$)]BF_4, (0.0504 g: 0.15 mmol.) in 5 ml of acetonitrile and pyridine (0.1185 g: 1.5mmol.) in 5 ml of acetonitrile were mixed in 50 ml beaker and the mixture was allowed to stand at room temperature for 10minutes. Rotary evaporation of the mixture at 35 ºC and at reduced pressure produced a light brown solid which was shaken with 20 ml of light petroleum spirit (60-80 ºC) and filtered. The resulting product was washed several times with petroleum ether to remove excess pyridine and dried to give product (VII) as a pale yellow solid in 64 % yield.

3.3.2 Synthesis and characterization ofTricarbonyl (1-4-η-5-exo-N-2-methyl pyridino-2-methoxycyclohexa-1,3-diene) iron tetrafluoroborate (VIII)

An analogous reaction of [$Fe(CO)_3$(1-5-η-2-$MeOC_6H_6$)]BF_4, (0.0504 g: 0.15 mmol.) in 5 ml of acetonitrile and 2-methylpyridine (0.1545 g: 1.5mmol.) in 5 ml of acetonitrile followed by similar work-up to that of product I above gave the product VIII as a light yellow solid in 60 % yield. This product turned dark brown on exposure to air indicating the decomposition due to attack by air. It also gave poor microanalysis and

showed the absence of nitrogen which suggests the loss of the 2-methylpyridino substituent in the decomposition process. The IRυ_{CO} in acetonitrile was 2055 cm^{-1} and 1980 cm^{-1} while the IRυ_{BF4} in nujol mull: ca 1060 cm^{-1}(broad).

3.3.3 Synthesis and characterization of Tricarbonyl (1-4-η-5-exo-N-3-methyl pyridino-2-methoxycyclohexa-1,3-diene) iron tetrafluoroborate (IX)

An analogous reaction of $[Fe(CO)_3(1\text{-}5\text{-}\eta\text{-}2\text{-}MeOC_6H_6)]BF_4$, (0.0504 g: 0.15 mmol.) in 5 ml of acetonitrile and 3-methylpyridine (0.1545 g: 1.5mmol.) in 5 ml of acetonitrile followed by similar work-up to that of product I above gave the product IX as an air-sensitive brown-oil. This product turned black on exposure to air indicating attack by oxygen and consequent decomposition. The IRυ_{CO} in acetonitrile was 2055 cm^{-1} and 1980 cm^{-1} while the IRυ_{BF4} in nujol mull: ca 1060 cm^{-1}(broad).

3.3.4 Synthesis and characterization of Tricarbonyl (1-4-η-5-exo-N-4-methyl pyridino-2-methoxycyclohexa-1,3-diene) iron tetrafluoroborate (X)

An analogous reaction of $[Fe(CO)_3(1\text{-}5\text{-}\eta\text{-}2\text{-}MeOC_6H_6)]BF_4$, (0.0504 g: 0.15 mmol.) in 5 ml of acetonitrile and 4-methylpyridine (0.1545 g: 1.5mmol.) in 5 ml of acetonitrile followed by similar procedure to that of product I above gave the product X as a yellow solid. IRυ_{CO} in acetonitrile, 2055 cm^{-1} and 1980 cm^{-1}. IRυ_{BF4} in nujol mull: ca 1060 cm^{-1}(broad). An in "situ" ^{1}H N.M.R spectrum of product (X) in d_3-acetonitrile is given in Table 4.4.

3.3.5 Synthesis and characterization of Tricarbonyl (1-4-η-5-exo-N-4-amino pyridino-2-methoxycyclohexa-1,3-diene) iron tetrafluoroborate (XI)

An analogous reaction of $[Fe(CO)_3(1\text{-}5\text{-}\eta\text{-}2\text{-}MeOC_6H_6)]BF_4$, (0.0504 g: 0.15 mmol.) in 5 ml of acetonitrile and 4-aminopyridine (0.141 g: 1.5mmol.) in 5 ml of acetonitrile followed by similar work-up to that described for product I above gave product XI as a light brown solid in 67 % yield. IRυ_{CO} in acetonitrile, 2055 cm^{-1} and 1980 cm^{-1}. Efforts to obtain a good ^{1}H N.M.R spectrum for this product in both d_6-acetone and d_3-actonitrile proved abortive. It thus requires be synthesizing and storing under dinitrogen atmosphere to keep it pure and stable.

3.3.6 Synthesis and characterization of Tricarbonyl (1-4-η-5-exo-N-4-N-dimethylpyridino-2-methoxycyclohexa-1,3-diene) iron tetrafluoroborate (XII)

An analogous reaction of $[Fe(CO)_3(1\text{-}5\text{-}\eta\text{-}2\text{-}MeOC_6H_6)]BF_4$, (0.0504 g: 0.15 mmol.) in 5 ml of acetonitrile and 4-N-dimethylaminopyridine (0.183 g: 1.5mmol.) in 5 ml of acetonitrile followed by similar work-up to that of product I above gave the product XII as an air-sensitive brown solid after the procedure. IRυ_{CO} in acetonitrile, 2055 cm^{-1} and 1980 cm^{-1}. IRυ_{BF4} in nujol mull: ca 1060 cm^{-1}(broad). Product (XII) gave poor ^1H N.M.R spectrum in d_6-acetone indicating attack by oxygen to form unknown species during the ^1H N.M.R study.

Modeling and Computational details

3.4 Methodology and software

Most applications of Semi empirical and DFT in chemistry are carried out using large electronic structure packages, and one way to understand the available methodology is to review the capabilities of these packages. Many of these packages are updated frequently, and many of them have web pages where new versions and added capabilities can be monitored. Specific implementations include SPARTAN, HYPERCHEM, QCHEM, GAUSSIAN and GAMESS. In this thesis we explored the SPARTAN molecular software package for our calculations (Spartan '10VI.1.0, 2010).

3.5 General description of Spartan

Spartan is a general, multipurpose scientific soft-ware package for the study of solid state molecular structures and reactions. The soft-ware package describes molecular mechanics models using the SYBYL and MMFF force fields, with aqueous energy correction available for the latter and quantum chemical models such as semi-empirical, ab-initio, density functional and Moller Plesset models. Molecular calculations in this thesis are carried out by implementing the Semi empirical PM3 and

Density Functional theory (DFT), Hartree-Fock (HF), and Time-dependent density functional theory (TDDFT) within the Spartan software package.

3.6 Computational methodology

Spartan ’10 V1.1.0 molecular software package was used for all the calculations and computations, all calculations and computations were done on isolated gaseous system at Temperature of 298.15K and a pressure of 1atmosphere. The structures of the organometallic complexes are presented in Figures 3.1 to 3.12. The computational methods used comprised of Semi empirical parameterization method PM3, Hartree-Fock HF, Density functional theory DFT, and Time-dependent density functional theory TDDFT. The PM3 was used in predicting geometrical parameters, dipole moment, thermodynamic stability, electronic states and vibrational frequencies. The density functional theory was used for the prediction of reactivity indices and molecular characterization of the complexes through infra-red, ultraviolet-visible, ^{1}H and ^{13}C neutron magnetic resonance spectroscopy. The Hartree-Fock procedure was used for predicting electronic states of these complexes and comparing the ionization energies and electron affinities with what is obtainable in DFT while the treatment of excited states was carried out by employing time-dependent density functional theory.

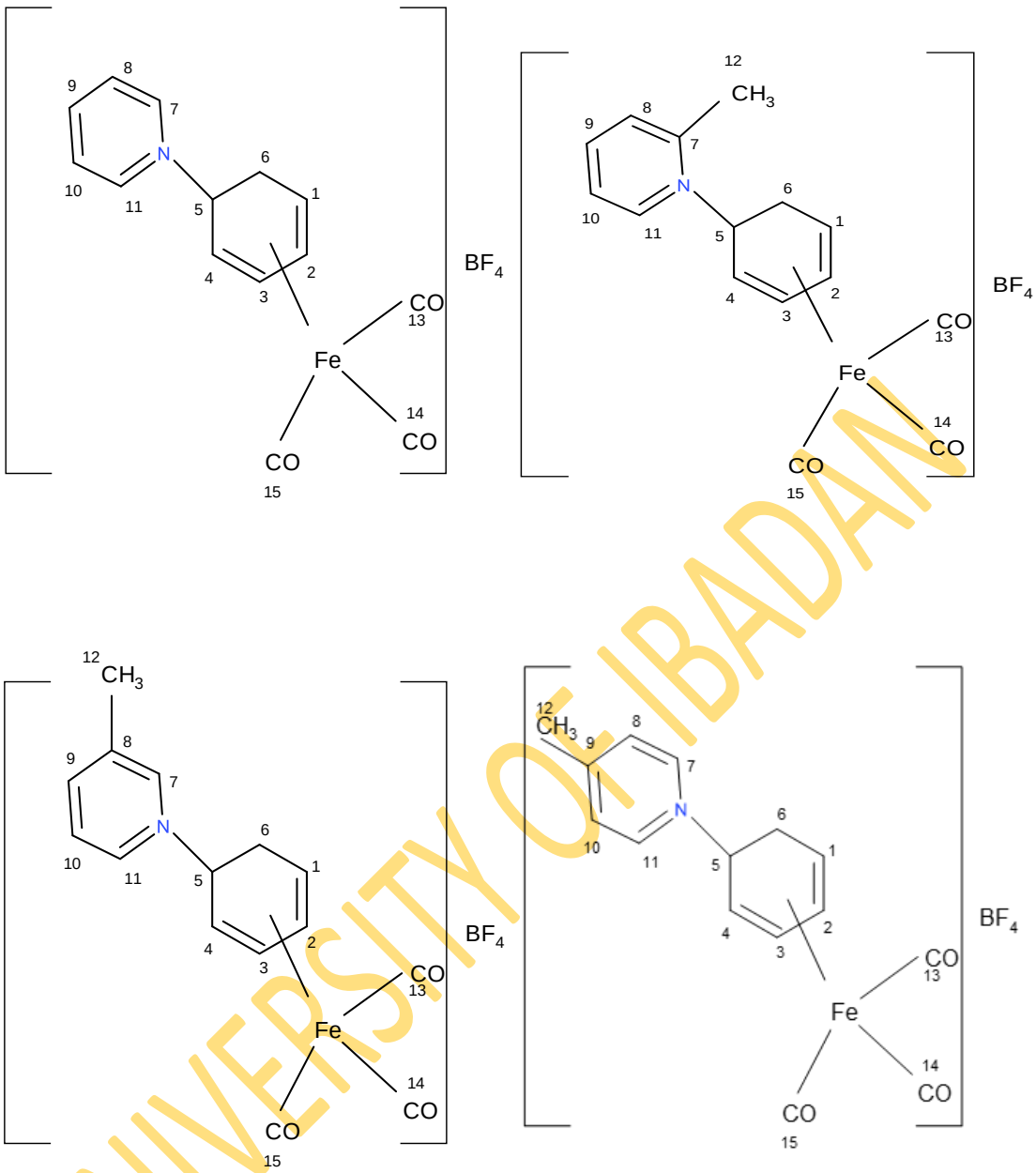

Figure 3.1: Structure of Tricarbonyl (1-4-η-5-exo-N-pyridino-cyclohexa-1,3-diene) iron tetrafluoroboratecomplexes

3.7 Computation of Tricarbonyl (1-4-η-5-exo-N-X-pyridino-cyclohexa-1,3-diene) iron tetrafluoroborate complexes

Semi-empirical PM3 Molecular orbital calculations were carried out on all the species involved in the study using Spartan '10. The method employed include semi empirical PM3 which is common and had been adjudged to be the best and most suitable for Transition metals and organometallic complexes, and all structures were fully optimized using their ground state geometries. The structures are presented in Figure 3.1 while the optimized geometries are shown in Plate 3.1.

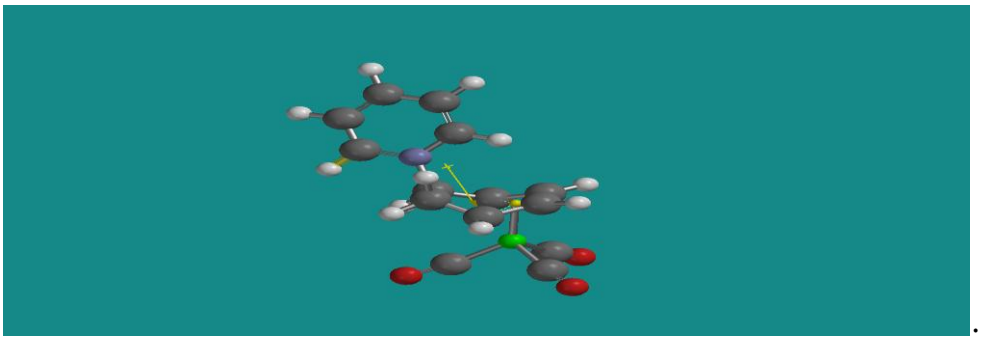

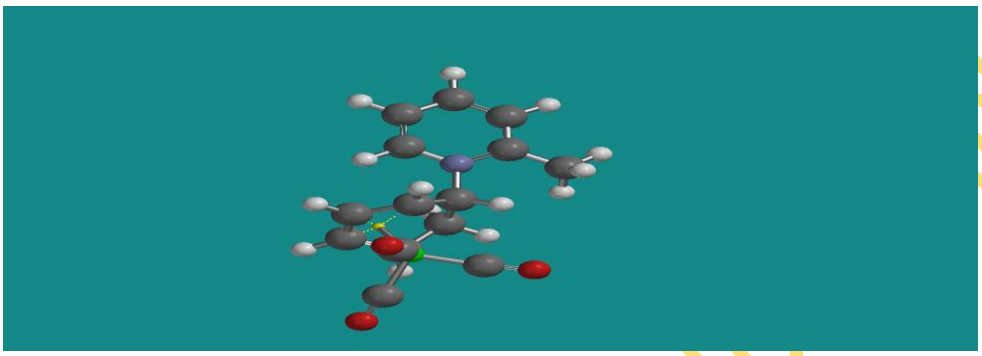

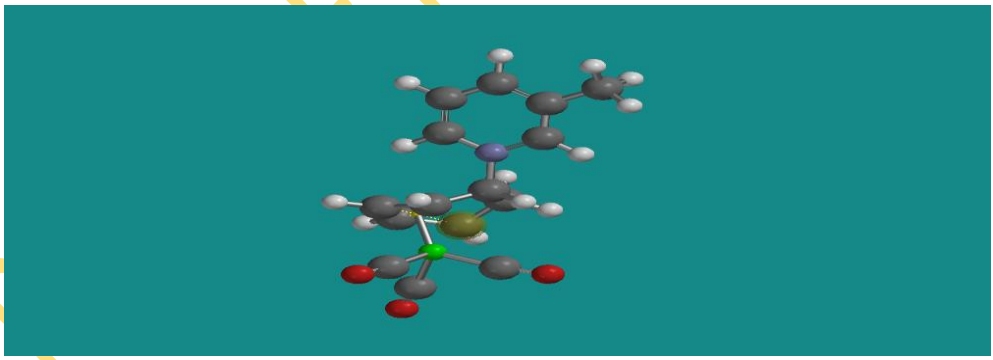

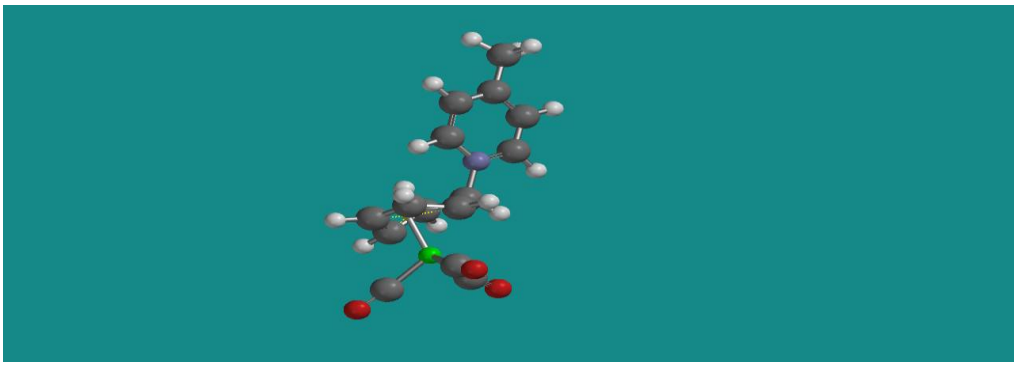

Platee 3.1: Optimized structures ofTricarbonyl (1-4-η-5-exo-N-X-pyridino-cyclohexa-1,3-diene) iron tetrafluoroboratecomplexes (BF_4 is excluded for clarity)

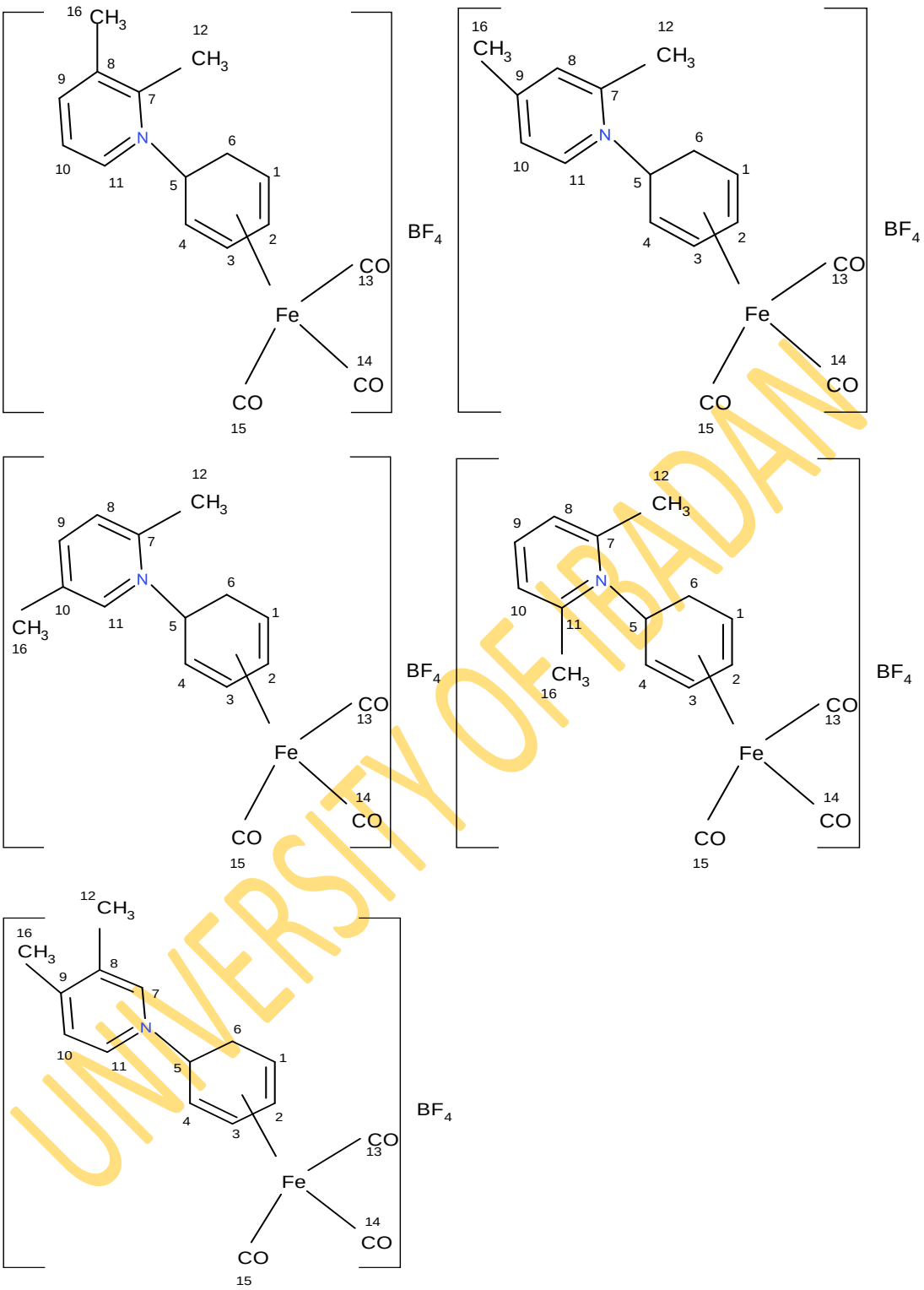

Figure 3.2: Structure of Tricarbonyl (1-4-η-5-exo-N-X, X-dimethylpyridino-cyclohexa-1,3-diene) iron tetrafluoroborate complexes

3.8 Computation of Tricarbonyl (1-4-η-5-exo-N-X, X-dimethylpyridino-cyclo-hexa-1,3-diene) iron tetrafluoroborate complexes

All the X,X-dimethylpyridino-1-4-η-cyclohexa-1,3-diene irontricarbonyl complexes simulated as well as the molecular orbital calculations on ground state equilibrium geometries were carried out using Spartan '10. The method employed throughout was Semi-empirical PM3 which had been adjudged the best and most suitable for Transition metals and organometallic compounds. The structures of these simulated compounds are presented in Figure 3.2 while the optimized structures are presented in Plate 3.2.

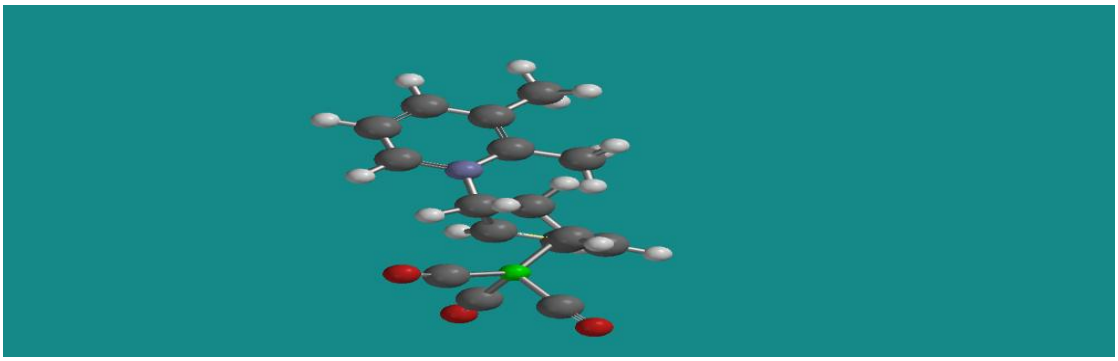

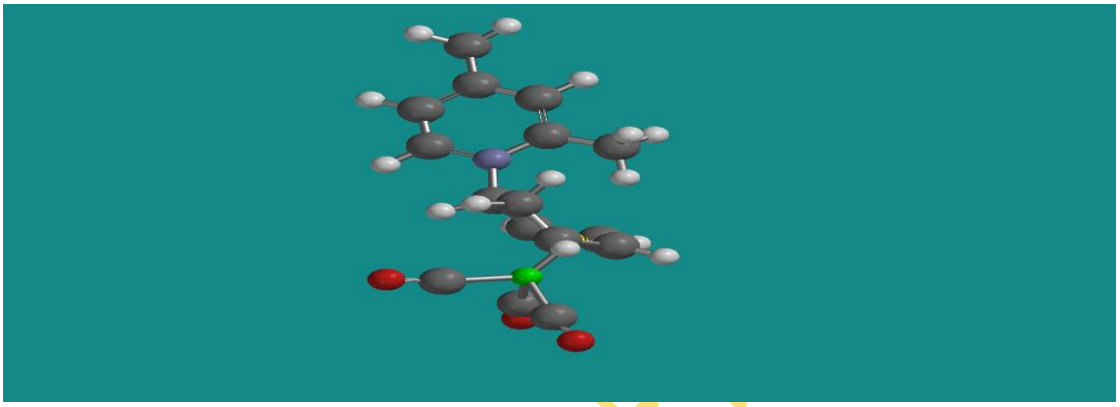

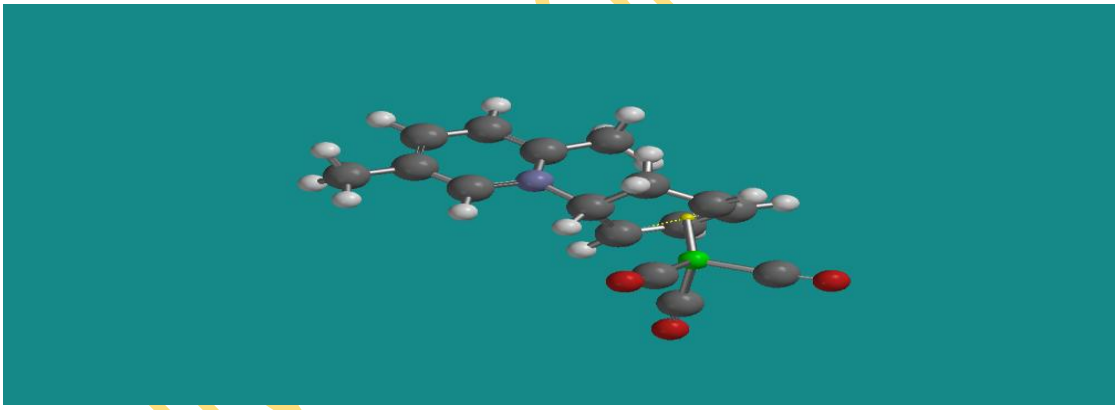

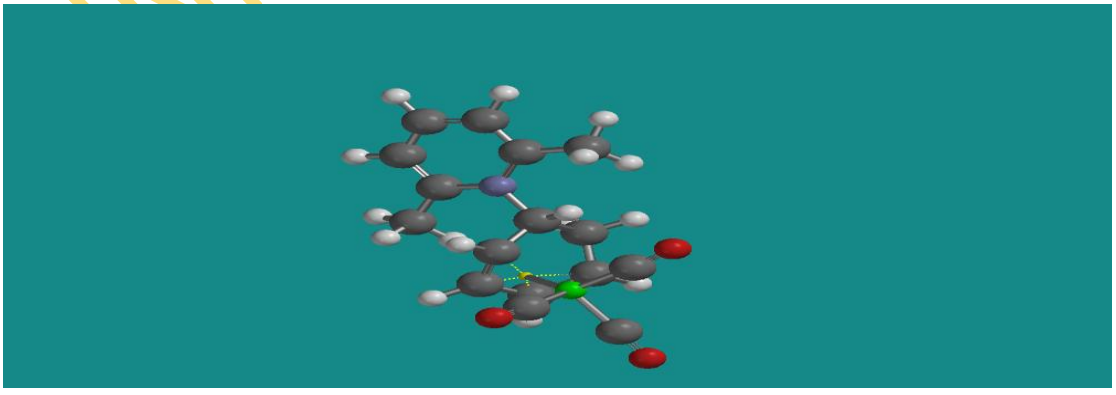

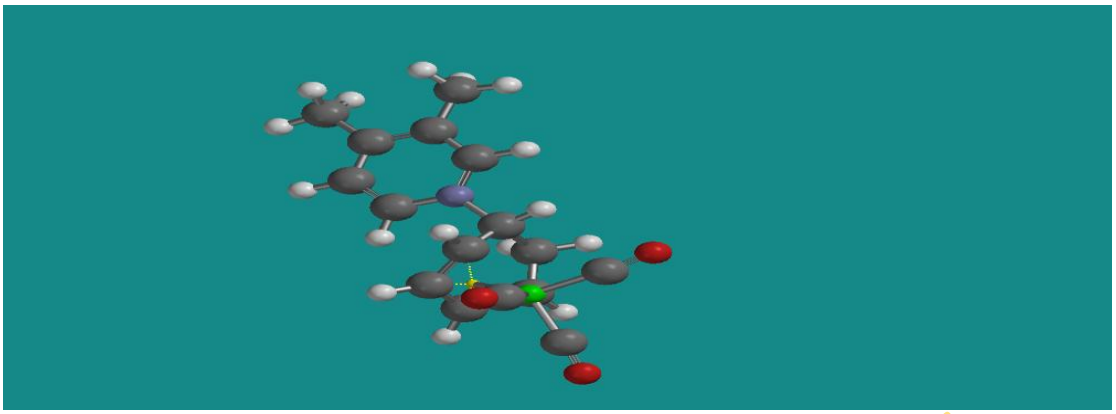

Plate 3.2: Optimized structures of Tricarbonyl (1-4-η-5-exo-N-X, X-dimethyl-pyridino-cyclohexa-1,3-diene) irontetrafluoroborate(BF_4 is excluded for clarity)

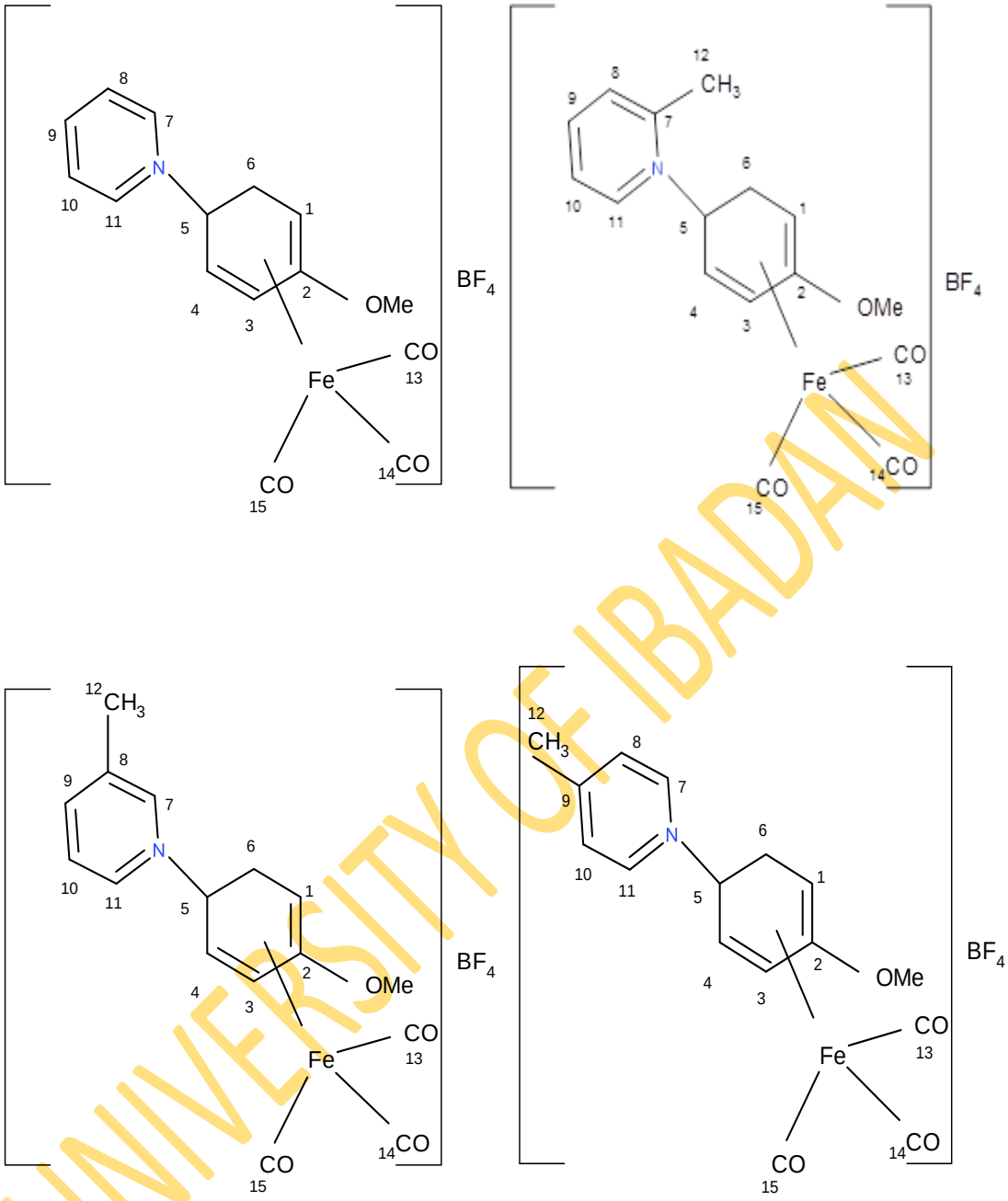

Figure 3.3: Structure of Tricarbonyl (1-4-η-5-exo-N-X-pyridino-2-methoxy-cyclohexa-1,3-diene) iron tetrafluoroborate complexes

3.9 Computation of Tricarbonyl (1-4-η-5-exo-N-X-pyridino-2-methoxy-cyclohexa-1,3-diene) iron tetrafluoroborate complexes

All the pyridino-1-4-η-2-methoxycyclohexa-1,3-diene irontricarbonyl complexes were modeled. Initial geometries were fully optimized using Semi-empirical method at PM3 level. The calculations were carried out to evaluate the geometries, electronic structure, dipole moment, thermodynamic parameters and vibrational frequencies using Spartan '10 running on Intel processor 1.60 GHz computers. The structure of these complexes are displayed in Figure 3.3 while the optimized geometries of the new pyridino derivatives of 1-4-η-2-methoxycyclohexa-1,3-diene irontricarbonyl complexes are shown in Plate 3.3.

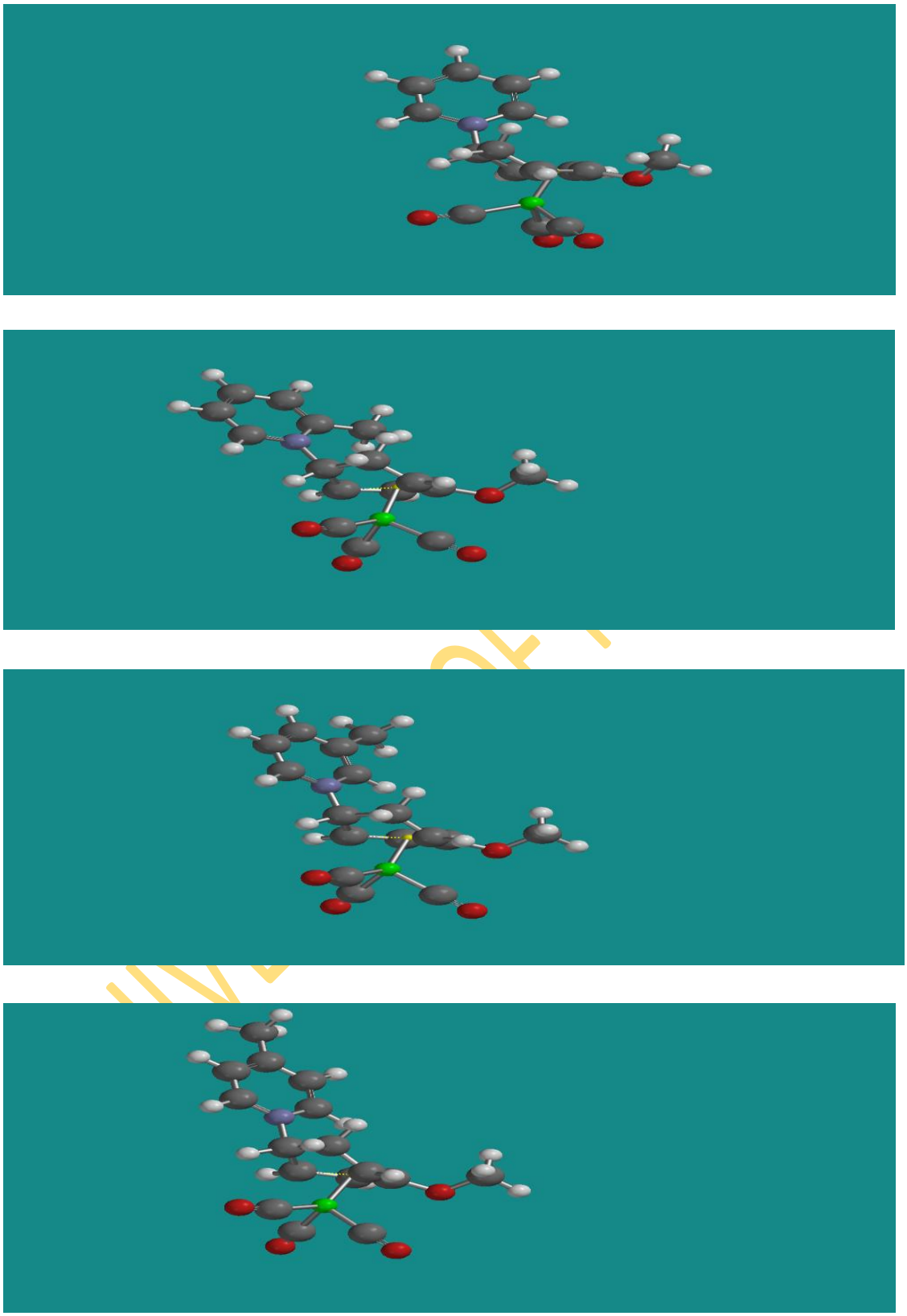

Plate 3.3: Optimized Structures ofTricarbonyl (1-4-η-5-exo-N-X-pyridino-2-methoxycyclohexa-1,3-diene) iron tetrafluoroborate complexes. (BF_4 ion is excluded for clarity)

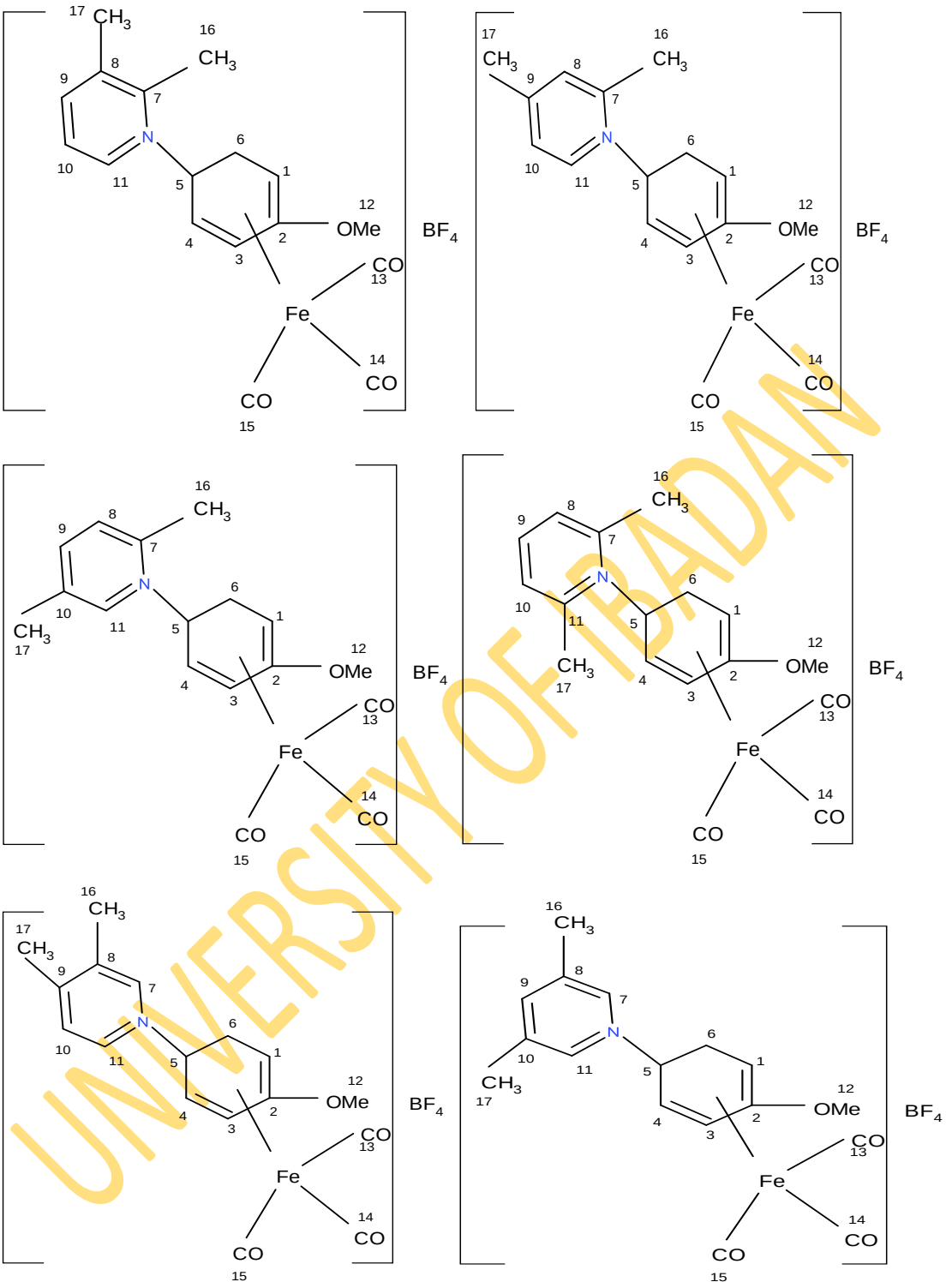

Figure 3.4: Structures of Tricarbonyl (1-4-η-5-exo-N-X,X-dimethylpyridino-2-methoxycyclohexa-1,3-diene) irontetrafluoroborate complexes

3.10 Computation ofTricarbonyl (1-4-η-5-exo-N-X, X-dimethylpyridino-2-methoxycyclohexa-1,3-diene) iron tetrafluoroborate complexes

All the complexes were modeled using Spartan ’10. Semi-empirical molecular orbital calculations were carried out on all species involved. The PM3 method that had been adjudged to be suitable for Transition metal complexes and organometallic compounds was employed throughout the study. All structures were fully optimized. The theoretical ground state geometries, electronic structure, thermodynamic parameters and vibrational frequencies of these modeled compounds were all investigated using the Semi-empirical PM3 and the results are discussed. The structures of these complexes are shown in Figure 3.4 while the optimized geometries of these X,X-dimethylpyridino-1-4-η-2- methoxycyclohexa-1,3-diene irontricarbonyl complexes are presented in Plate 3.4.

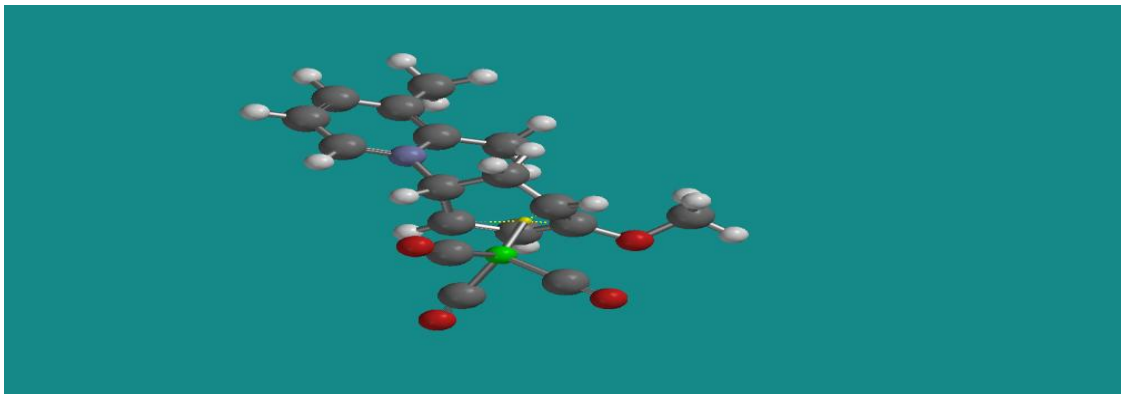

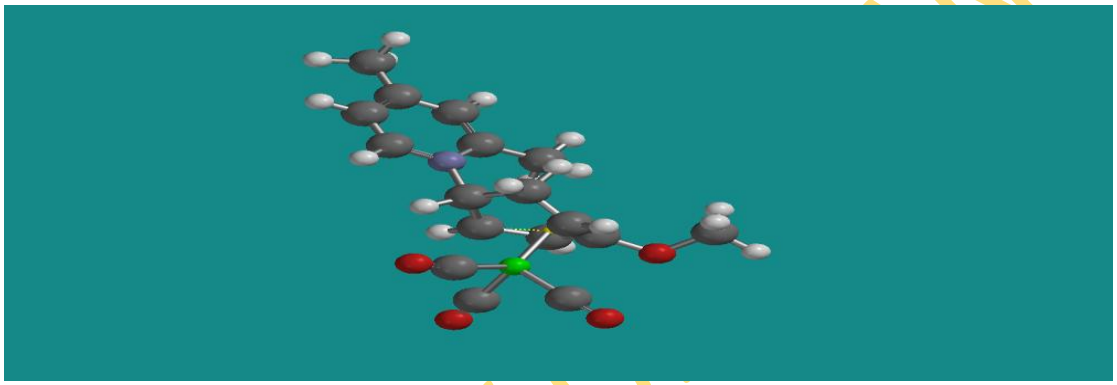

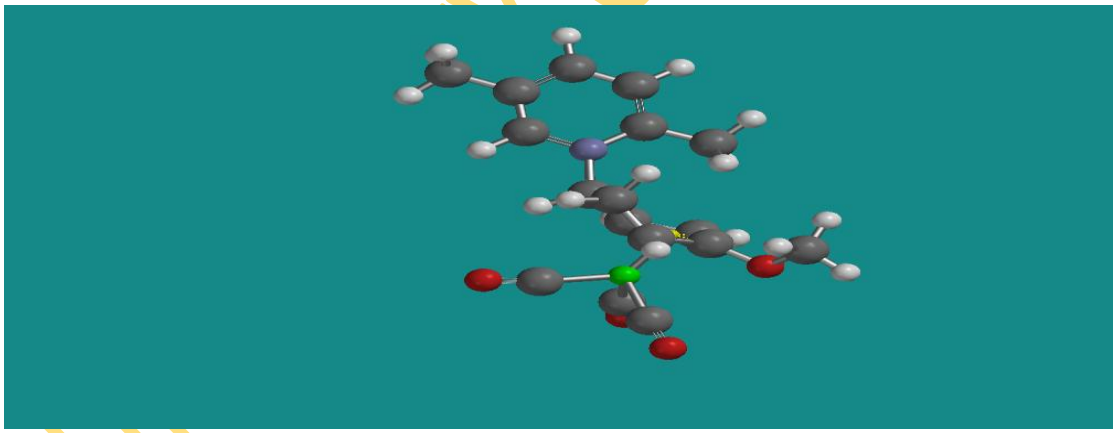

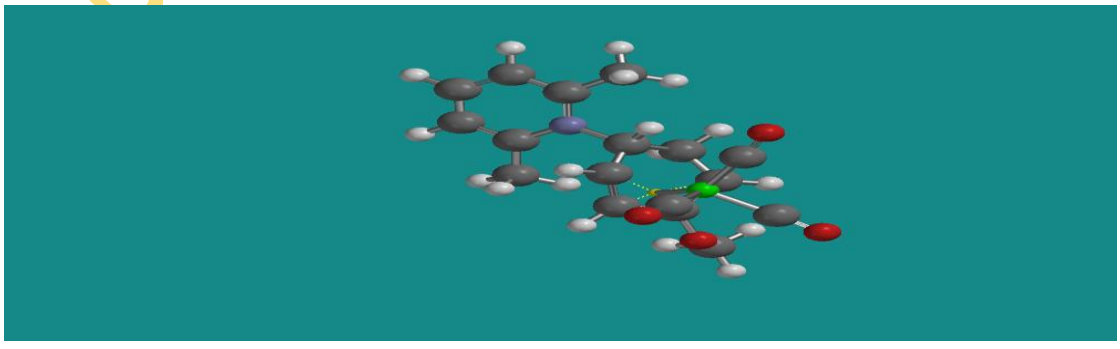

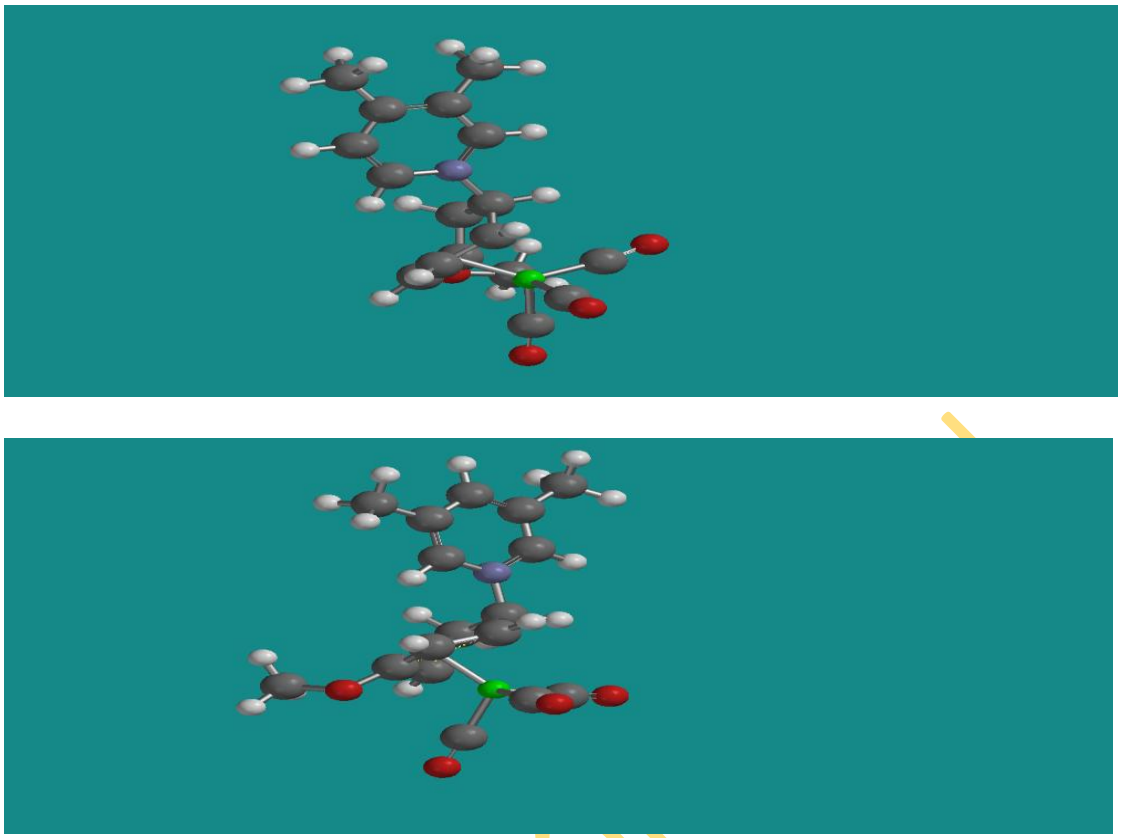

Plate 3.4: Optimized Structures of Tricarbonyl (1-4-η-5-exo-N-X, X-dimethyl pyridino-2-methoxycyclohexa-1,3-diene) iron tetrafluoroborate complexes. (BF_4 is excluded for clarity)

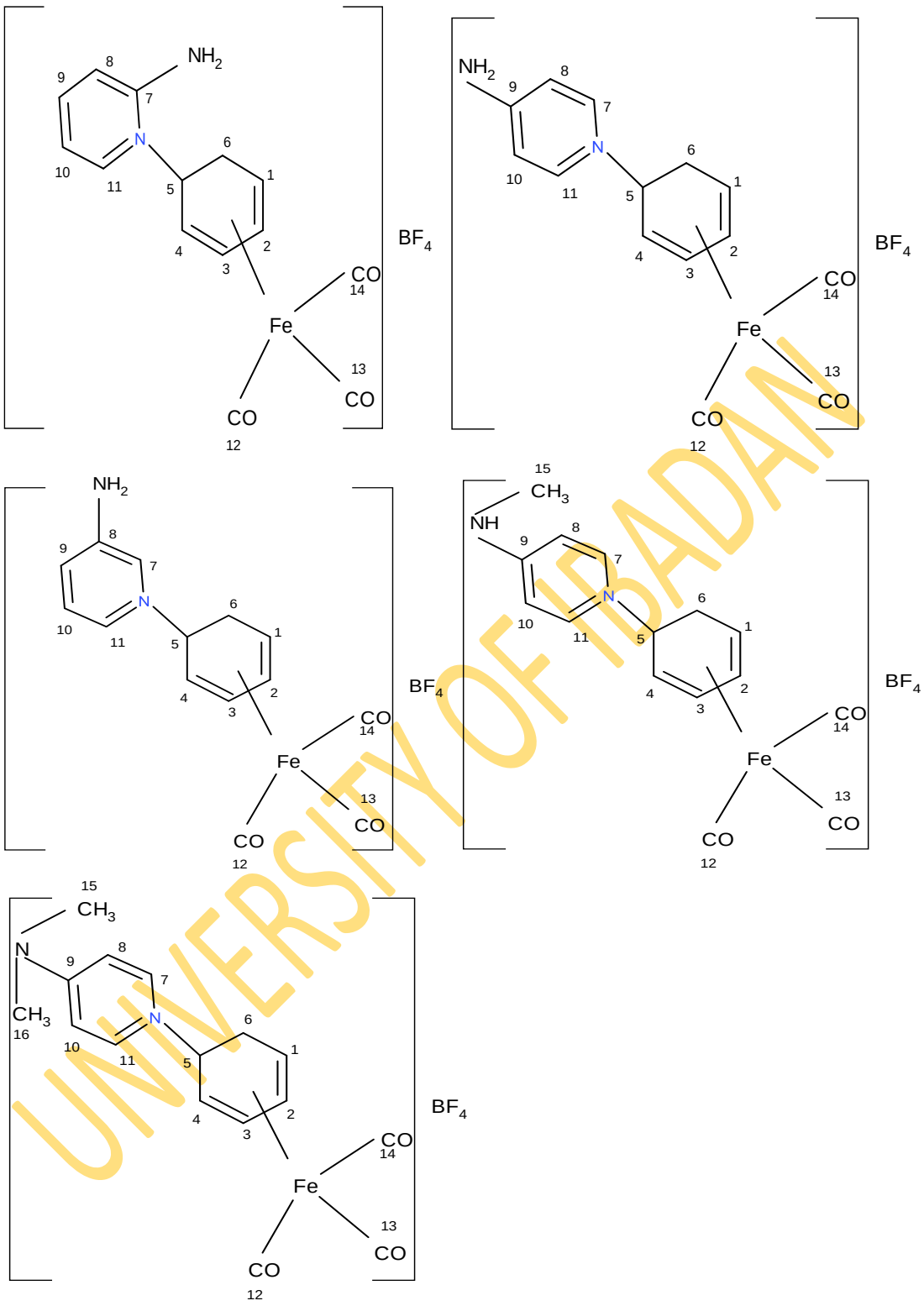

Figure 3.5: Structures of Tricarbonyl (1-4-η-5-exo-N-X-aminopyridino-cyclohexa-1,3- diene) irontetrafluoroborate complexes

3.11 Computation of Tricarbonyl (1-4-η-5-exo-N-X-aminopyridino-cyclohexa-1,3-diene) irontetrafluoroboratecomplexes

All the complexes were modeled using Spartan ’10. Semi-empirical molecular orbital calculations were carried out on all species involved. The PM3 had been adjudged to be suitable for Transition metal complexes and organometallic compounds was employed throughout the study. All structures were fully optimized. The theoretical ground state geometries, electronic structure, thermodynamic parameters and vibrational frequencies of these modeled compounds were all investigated using the Semi-empirical PM3 results are discussed. The structures of these complexes are shown in Figure 3.5 while the optimized geometries of these Tricarbonyl (1-4-η-5-exo-N-amino pyridino-cyclohexa-1,3-diene) iron complexesare displayed in Plate 3.5.

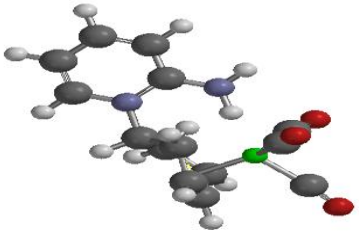

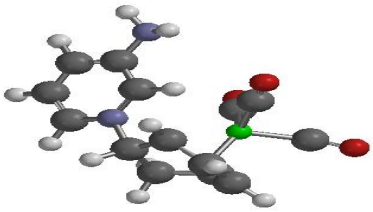

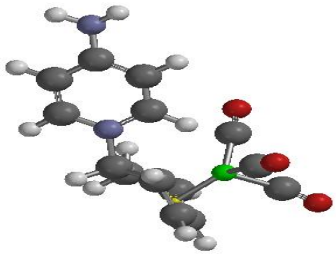

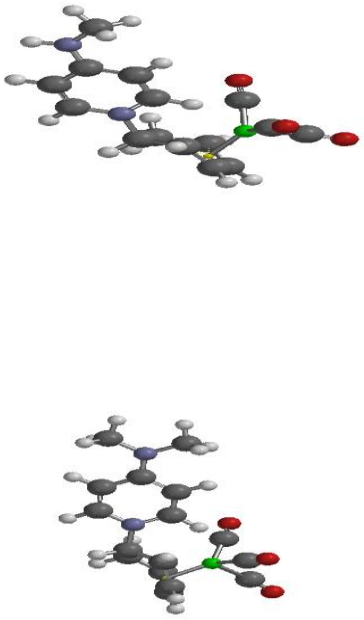

Plate 3.5: Optimized structures of Tricarbonyl (1-4-η-5-exo-N-X-aminopyridino-cyclohexa-1,3-diene) iron tetrafluoroboratecomplexes(The BF_4 is excluded for clarity)

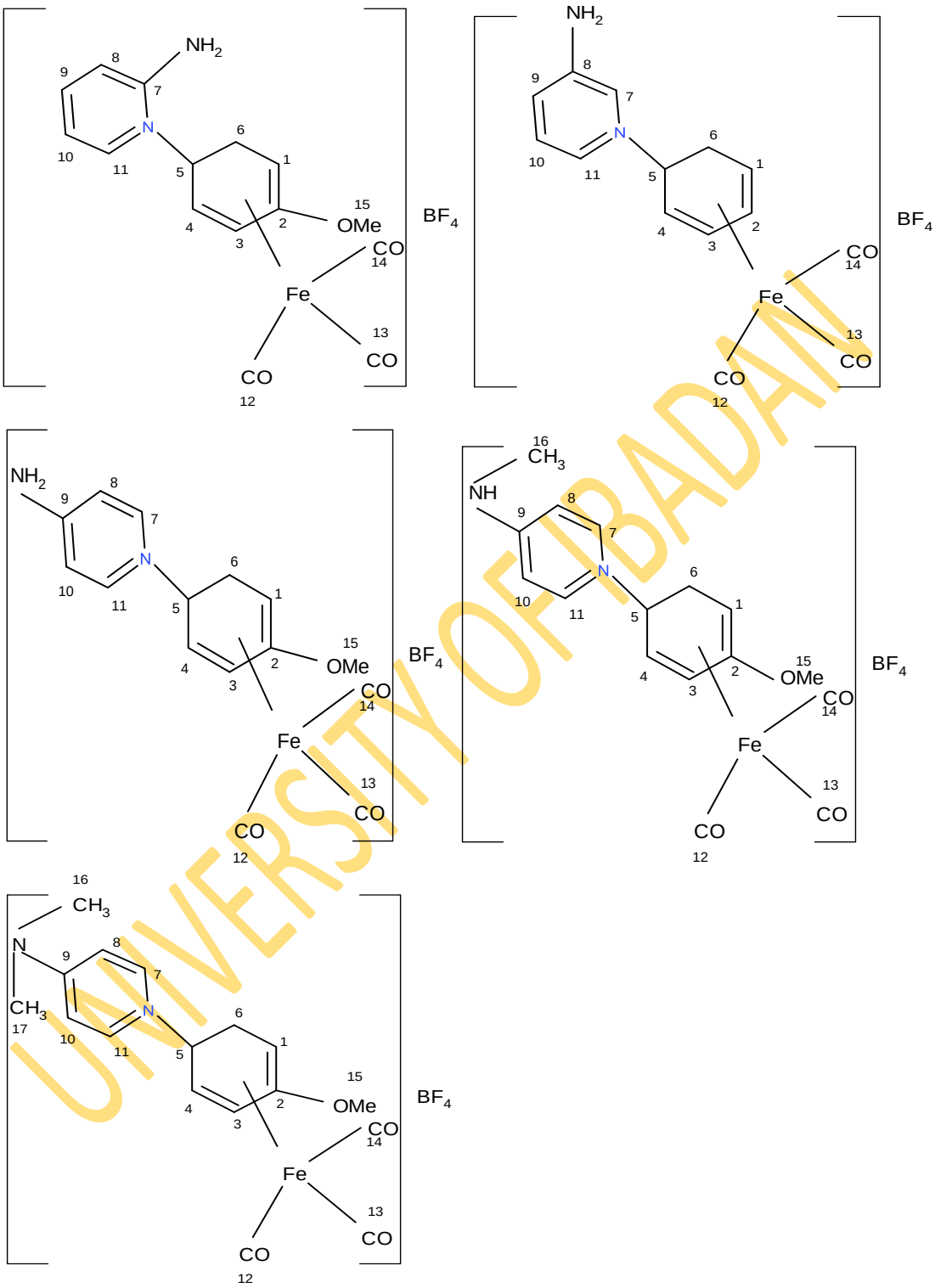

Figure 3.6: Structures of Tricarbonyl (1-4-η-5-exo-N-X-aminopyridino-2-methoxycyclohexa-1,3-diene) iron tetrafluoroborate complexes

3.12 Computation of Tricarbonyl (1-4-η-5-exo-N-X-aminopyridino-2-methoxy-cyclohexa-1,3-diene) irontetrafluoroboratecomplexes

All the complexes were modeled using Spartan ’10. Semi-empiricalmolecular orbital calculations were carried out on all the species involved. The PM3was employed throughout the study and all structures were fully optimized. The theoretical ground state geometries, electronic structure, thermodynamic parameters and vibrational frequencies of these modeled compounds were all investigated using the Semi-empirical PM3 and the results are discussed. The structures of these complexes are shown in Figure 3.6 while the optimized geometries of these amino pyridino-1-4-η-2-methoxycyclohexa-1,3-diene irontricarbonyl complexes are shown in Plate 3.6.

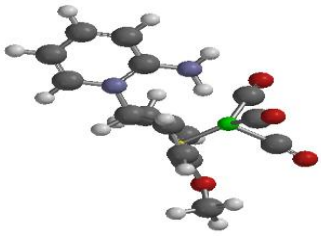

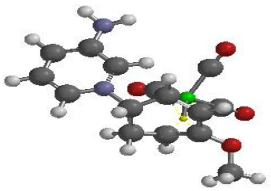

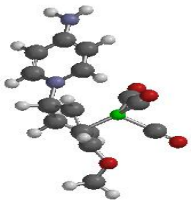

Plate 3.6: Optimized Structures of Tricarbonyl (1-4-η-5-exo-N-X-aminopyridino-2-methoxycyclohexa-1,3-diene) iron tetrafluoroborate complexes (the BF_4 is excluded for clarity)

3.13 Computation of complexes using Density Functional Theory (DFT)

All the structures shown in Plate 3.1 to 3.6 were re-optimized. All the calculations were performed using Spartan 10 program package using B3LYP methods which uses the exchange functional proposed by Becke and the correlation functional given by Lee, Yang and Parr. The 6-31(D) basis set(Hehre *et al.,* 1986) has been used in conjunction with DFT method. This basis set has the advantage of being flexible enough to guarantee reliable theoretical results and being small enough for rapid calculations. It represents an excellent compromise between completeness and economy. The molecular geometry was fully optimized without any constraint using analytical gradient procedure implemented within the programme. A restricted HF-DFT self consistent field calculations was carried out using Pulay DIIS and Geometry direct minimization implemented within the programme.

3.14 Computation of Electronic Properties using Hartree-Fock

The Spartan ’10 package was used as the calculation tool; Full optimization was initially achieved by using molecular mechanics and then semi empirical PM3 method. The results from the PM3 method were selected as input and the structures were further optimized by employing spin-restricted Hartree-Fock (RHF) approach at the level of the 6-31G (D) basis set.

3.15 Computation of Excited state Properties using TDDFT

In order to obtain the Ultraviolet visible absorption for our complexes, we employed the excited state computation with Time-dependent density functional theory with B3LYP and basis set of 6-31(D). The basis set 6-31(D) has been used in conjunction with TDDFT method because of its advantage of being flexible enough to guarantee reliable theoretical results and being small enough for rapid calculations. It represents an excellent compromise between completeness and economy. We computed the properties of five excited states with keyword “INCLUDE TRIPLETS”. The molecular geometry was fully optimized without any constraint using analytical gradient procedure implemented within the Spartan ’10 software programme.

CHAPTER FOUR

RESULTS AND DISCUSSION

4.1 Addition of pyridines to Tricarbonyl (1-5-η-cyclohexadienyl) irontetrafluoroborate $[Fe(CO)_3(1\text{-}5\text{-}\eta\text{-}C_6H_7)]BF_4$

The products (I-VI) isolated from the reactions of the organometallic compound $[Fe(CO)_3(1\text{-}5\text{-}\eta\text{-}C_6H_7)]BF_4$ with pyridine, 2-methylpyridine, 3-methylpyridine, 4-methylpyridine, 4-aminopyridine and 4-N-dimethylaminopyridine showed intense sharp ν_{CO} bands (KBr disc) at 2055 cm^{-1} and 1980 cm^{-1} as well as a broad band due to tetrafluoroborate anion at ca 1060 cm^{-1} in their infrared spectra. Product I was isolated as pale yellow crystalline, air stable solid characterized by infra-red, elemental analysisand ^1H N.M.R spectroscopy (Table 4.1 and Table 4.2). Products II-IV were isolated as brown air stable oils and were characterized by infra-red and elemental analysis. Products V and VI were isolated as brown solids and characterized by infra-red and elemental analysis. The spectra for the pyridine derivatives were carried out in KBr disc in the range 2500 cm^{-1} and 800 cm^{-1} and that for product I, shown in Figure 4.19 is typical for all the products (I-VI) with ν_{CO} bands at ca. 2055 cm^{-1} and 1980 cm^{-1} as well as the BF^-_4anion located at ca. 1050 cm^{-1}. These bands are characteristic features for a wide variety of 1,3-diene pyridine derivatives involving exo-addition at the dienyl ring of $[Fe(CO)_3(1\text{-}5\text{-}\eta\text{-}C_6H_7)]BF_4$.

Table 4.1: Nature of compound, infra-red spectra and micro analytical data for Tricarbonyl (1-4-η-5-exo-N-pyridino-cyclohexa-1,3-diene) iron complexes

No	Structure X	Nature of compound	IR ν_{CO} (ν_{BF_4})	Microanalysis Found (Calculated)%	
				C	H
I	H	yellow solid	1980, 2055 (1060)	54.1 (54.9)	4.2 (4.3)
II	2-Me	Brown Oil	1980, 2055 (1060)	55.8 (56.14)	4.4 (4.7)
III	3-Me	Brown Oil	1980, 2055 (1060)	54.9 (56.14)	4.3 (4.7)
IV	4-Me	Brown Oil	1980, 2055 (1060)	55.14 (56.14)	4.5 (4.7)
V	4-NH_2	Brown Solid	1980, 2055 (1060)	51.95 (52.23)	4.8 (4.65)
VI	4-$N(CH_3)_2$	Brown Solid	1980, 2055 (1060)	55.1 (54.84)	5.51 (5.38)

Table 4.2: Experimental ^{1}H NMR Spectra data for Tricarbonyl (1-4-η-5-exo-N- pyridino-cyclohexa-1,3-diene) iron tetrafluoroborate complexes

Complex X	proton	Chemical Shift/ppm	Relative Intensity	Multiplicity
H	$H^{1,4}$	3.10	2	m
	H^{2}	4.80	1	m
	H^{3}	4.40	1	m
	H^{5}	4.10	1	m
	exoH^{6}	2.10	1	m
	endoH^{6}	1.60	1	m
	Aromatic	7.70	2	t
	protons	7.10	1	t
		6.70	2	t
2-Me	$H^{1,4}$	3.05	2	m
	H^{2}	4.90	1	m
	H^{3}	4.50	1	m
	H^{5}	4.05	1	m
	exoH^{6}	2.00	1	m
	endoH^{6}	1.70	1	m
	CH_3	2.50	3	s
	Aromatic	7.30	2	t
	protons	6.90	1	t
		6.50	1	t
3-Me	$H^{1,4}$	3.05	2	m
	H^{2}	4.70	1	m
	H^{3}	4.50	1	m
	H^{5}	4.05	1	m
	exoH^{6}	2.00	1	m
	endoH^{6}	1.70	1	m
	CH_3	2.50	3	s
	Aromatic	7.60	2	d
	protons	6.45	2	d
	$H^{1,4}$	3.15	2	m

	H^2	4.90	1	m
	H^3	5.70	1	m
	H^5	5.10	1	m
4-Me	exoH^6	2.60	1	m
	endoH^6	1.70	1	m
	CH_3	2.55	3	s
	Aromatic	8.50	2	d
	protons	7.70	2	d
	$H^{1,4}$	3.20	2	m
	H^2	5.10	1	m
	H^3	4.60	1	m
	H^5	4.90	1	m
4-NH_2	exoH^6	2.40	1	m
	endoH^6	1.50	1	m
	Aromatic	8.40	2	d
	protons			
	$H^{1,4}$	3.10	2	m
	H^2	4.95	1	m
	H^3	4.50	1	m
	H^5	4.90	1	m
4-$N(CH_3)_2$	exoH^6	2.30	1	m
	endoH^6	1.40	1	m
	OCH_3	3.20	3	s
	CH_3	2.60	3	s
	Aromatic	8.40	2	d
	protons			
		7.50	2	d

4.2 Addition of pyridines to Tricarbonyl (1-5-η-2-methoxycyclohexadienyl) irontetrafluoroborate[$Fe(CO)_3$(1-5-η-2-$MeOC_6H_7$)]BF_4

The products (VII-XII) isolated from the reactions of the organometallic compound [$Fe(CO)_3$(1-5-η-2-$MeOC_6H_6$)]BF_4 with pyridine, 2-methylpyridine, 3-methylpyridine, 4-methylpyridine, 4-aminopyridine and 4-N-dimethylaminopyridine showed intense sharp ν_{CO} bands (KBr disc) at 2055 cm^{-1} and 1980 cm^{-1} as well as a broad band due to the tetrafluoroborate anion at ca 1060 cm^{-1} in their infrared spectra (Odiaka, T. I, 1980). Product VII was isolated as a pale yellow crystalline, air stable solid characterized by infra-red, elemental analysisand^{1}H N.M.R spectroscopy (Table 4.3 and Table 4.4). Products (VII-XII) were isolated as brown air stable oils and were characterized by infra-red and elemental analysis. Their^{1}H N.M.R spectra(Figure 4.25, page 249) clearly demonstrates that products (VII-XII) are complexes of Tricarbonyl (1-4-η-5-exo-N-pyridino-2-methoxycyclohexa-1,3-diene) tetrafluoroborate derivatives. The features shown in these spectra together with ν_{CO} infra-red bands at 2055 cm^{-1} and 1980 cm^{-1} have been reported as characteristic features for a wide variety of 1,3-diene pyridino derivatives involving exo-addition at the dienyl ring of novel organometallics(Odiaka, 1980; Odiaka and Okogun, 1985; Odiaka, 1988a, 1988b; Odiaka *et al*., 2007). For instance, the ^{1}HN.M.R spectrum of Product VII in d_6-acetone showed well-separated overlapping multiplets characteristics of the outer (H^1 and H^4) and inner (H^2 and H^3) diene protons at 3.10 ppm and 4.40 ppm respectively. The endo ($H^{6'}$) and exo (H^6) methylene protons appeared at 2.10 ppm and 1.60 ppm while the $H^{5'}$ proton adjacent to the N-pyridino-substituent is shifted downfield to 4.10 ppm. The aromatic protons of the pyridine substituent appear as triplets at 7.10 ppm and 7.00 ppm and a doublet at 7.70 ppm. The methoxy protons appeared at 2.43 ppm as a singlet as expected. An in "situ" ^{1}H N.M.R spectrum of product (X) from the reaction of 4-methylpyridine with the 2-methoxycomplex was carried out. (Table 4.3) showed characteristics features of the expected 1,3-diene derivative. Product (X) and the other pyridino derivatives isolated in this work are air sensitive yellow oils, decomposing readily to unknown species on exposure to air. Majority of these products were characterized by infra-red spectroscopy. The υ_{BF4} band found for all the products at ca. 1060 cm^{-1} clearly revealed the ionic nature of products (VII-XII). The instability of

products (VIII-XII) may be due to their oily nature and thus require preparation and storage under a dinitrogen atmosphere.

Table 4.3: Nature of compound, infra-red spectra and micro analytical data for Tricarbonyl (1-4-η-5-exo-N-pyridino-2-methoxycyclohexa-1,3-diene) iron complexes

No	Structure X	Nature of compound	IR ν_{CO} (ν_{BF_4})	Microanalysis Found (Calculated)%	
				C	H
VII	H	Pale yellow solid	1980, 2055 (1060)	43.46 (43.6)	3.15 (3.20)
VIII	2-Me	Brown Oil	1980, 2055 (1060)	44.83 (45.1)	3.62 (3.55)
IX	3-Me	Brown Oil	1980, 2055 (1060)	44.96 (45.1)	3.52 (3.55)
X	4-Me	Brown Oil	1980, 2055 (1060)	44.96 (45.1)	3.53 (3.55)
XI	4-NH_2	Brown Solid	1980, 2055 (1060)	42.7 (42)	3.32 (3.27)
XII	4-$N(CH_3)_2$	Brown Solid	1980, 2055 (1060)	44.49 (44.9)	3.95 (4.00)

Table 4.4: Experimental ^{1}H NMR Spectra data for Tricarbonyl (1-4-η-5-exo-N-pyridino-2-methoxycyclohexa-1,3-diene) iron tetrafluoroborate complexes

Complex X	proton	Chemical Shift/ppm	Relative Intensity	Multiplicity
	$H^{1,4}$	3.10	2	m
	H^{3}	4.40	1	m
	H^{5}	4.10	1	m
	$exoH^{6}$	2.10	1	m
	$endoH^{6}$	1.60	1	m
H	CH_3	2.43	3	s
	Aromatic	7.70	2	t
	protons	7.10	1	t
		6.70	2	t
	$H^{1,4}$	3.05	2	m
	H^{3}	4.50	1	m
	H^{5}	4.05	1	m
	$exoH^{6}$	2.00	1	m
	$endoH^{6}$	1.70	1	m
2-Me	OCH_3	3.30	3	s
	CH_3	2.50	3	s
	Aromatic	7.30	2	t
	protons	6.90	1	t
		6.50	1	t
	$H^{1,4}$	3.05	2	m
	H^{3}	4.50	1	m
	H^{5}	4.05	1	m
	$exoH^{6}$	2.00	1	m
3-Me	$endoH^{6}$	1.70	1	m
	OCH_3	3.30	3	s
	CH_3	2.50	3	s

	Aromatic	7.60	2	d
	protons	6.45	2	d
	$H^{1,4}$	3.15	2	m
	H^{3}	5.70	1	m
	H^{5}	5.10	1	m
	$exoH^{6}$	2.60	1	m
4-Me	$endoH^{6}$	1.70	1	m
	OCH_3	3.80	3	s
	CH_3	2.55	3	s
	Aromatic	8.50	2	d
	protons	7.70	2	d
	$H^{1,4}$	3.20	2	m
	H^{3}	4.60	1	m
	H^{5}	4.90	1	m
	$exoH^{6}$	2.40	1	m
$4\text{-}NH_2$	$endoH^{6}$	1.50	1	m
	OCH_3	3.40	3	s
	CH_3	2.50	3	s
	Aromatic	8.40	2	d
	protons			
	$H^{1,4}$	3.10	2	m
	H^{3}	4.50	1	m
	H^{5}	4.90	1	m
	$exoH^{6}$	2.30	1	m
$4\text{-}N(CH_3)_2$	$endoH^{6}$	1.40	1	m
	OCH_3	3.20	3	s
	CH_3	2.60	3	s
	Aromatic	8.40	2	d
	protons			
		7.50	2	d

4.3 Geometric parameters

4.3.1 Tricarbonyl (1-4-η-5-exo-N-pyridino-cyclohexa-1,3-diene) iron complexes

Geometrical parameters were obtained for all the organometallics after total optimization of the equilibrium geometries by Semi-empirical PM3. In order to investigate the effect of the substituent on the pyridine ring, geometries, electronic and thermodynamics properties were compared with the parent Tricarbonyl (1-4-η-5-exo-N-pyridino-cyclohexa-1,3-diene)iron complex. For the unsubstituted 1-4-η-5-exo-pyridino-cyclohexa-1,3-diene complex at PM3 level, calculations predict the bond length, bond angles and dihedral angles with remarkable changes. The effect of grafting on the position 2,3 and 4 of the pyridine ring was clearly observed. The increase in the bond length adjacentto the methyl group was clearly visible and was attributed to the strong electron-donating effect of the substituent. There were no significant changes in bond length (Table 4.5).

Table 4.5: Geometric parameters ofTricarbonyl (1-4-η-5-exo-N-pyridino-cyclohexa-1,3-diene) iron complexes

(a) Selected bond length

Bond length/Å	H	2-Me	3-Me	4-Me
C_1-C_2	1.479	1.479	1.479	1.479
C_2-C_3	1.404	1.404	1.404	1.404
C_3-C_4	1.488	1.488	1.488	1.488
C_4-C_5	1.490	1.490	1.490	1.490
C_5-C_6	1.544	1.544	1.544	1.544
C_6-C_1	1.492	1.492	1.492	1.492
N-C_5	1.529	1.530	1.528	1.528
N-C_{11}	1.374	1.384	1.374	1.375
C_7-C_8	1.392	1.389	1.394	1.389
C_8-C_9	1.393	1.394	1.390	1.400
C_9-C_{1O}	1.395	1.391	1.402	1.402
C_{10}-C_{11}	1.392	1.401	1.397	1.388
O_1-C_{12}	1.157	1.147	1.147	1.147
O_2-C_{13}	1.147	1.157	1.157	1.157

O_3-C_{14}	1.147	1.147	1.147	1.147
C_{12}-Fe	1.735	-	-	-
C_{13}-Fe	1.795	1.784	1.734	1.734
C_{14}-Fe	1.797	1.795	1.795	1.795
Fe-Lig	1.679	1.679	1.679	1.679
C_{15}-Fe	-	1.797	1.796	1.796
C_{10}-C_{12}	-	-	1.482	-
C_{11}-C_{12}	-	1.491	-	-

(b) Selected bond angles

Bond angles/°				
Lig-Fe-C_{13}	128.77	128.76	128.74	128.68
Lig-Fe-C_{14}	117.39	117.33	117.38	117.40
Lig-Fe-C_{15}	118.38	118.35	118.35	115.38
Fe-lig-C_2	105.11	105.08	105.09	105.10
Fe-C_{15}-O	174.15	174.69	174.75	174.77
C_5-N-C_7	119.95	118.69	120.14	119.99

(c) Selected dihedral angles

Dihedral angle/°				
C_{13}-Fe-lig-C_2	128.50	128.23	128.51	128.51
C_{15}-Fe-lig-C_3	-8.86	-8.95	-8.88	-8.81
C_5-N-C_2-H_{10}	0.94	0.97	0.97	1.02
C_5-N-C_{11}-H_{14}	-0.30	-	-0.47	-0.39
C_4-C_3-C_2-C_1	0.64	0.59	0.58	0.60

4.3.2 Tricarbonyl (1-4-η-5-exo-N-X,X-dimethylpyridino-cyclohexa-1,3-diene)iron complexes

The ground state geometric parameters were obtained using Semi-empirical PM3. In order to investigate the effect of substituent on the pyridine ring, the geometries, electronic and thermodynamic properties were calculated (Bouzakaraoui *et al.*, 2005; Hehnre, 2003). The Tricarbonyl (1-4-η-5-exo-N-X,X-dimethylpyridino-cyclohexa-1,3-diene) iron complexesstudy at PM 3 level, predict the bond length, bond angles and dihedral angles as shown in Table 4.6. For each model, Nine bond angles and dihedral angles which greatly contribute to the internal energy were measured. All the bond distances of C-H predicted are within the range of 1.088Å and 1.126Å. The bond distance from Iron to ligand in the 2,3-dimethylpyridino organometallic complex is 2.020Å, Fe-C_{13}, Fe-C_{14}, Fe-C_{15} measuring 2.162Å, 2.188 Å, and 2.163 Å respectively. These are the largest values recorded for these series, of complexes and is attributed to the strong electron-donating effect of the two adjacent methyl substituent on the pyridine ring which push electron towards the cyclohexa-1,3-diene ring, with the methyl group getting separated and the bond length becoming reduced. These are shown in Table 4.6.

Table 4.6: Geometric parameters of Tricarbonyl (1-4-η-5-exo-N-X,X-dimethylyridino-cyclohexa-1,3-diene ironcomplexes showing (a) selected bond length in Å, (b) bond angles(c) dihedral angles

(a) Selected bond length

Structure Bond length/Å	2,3-diMe	2,4-diMe	2,5-diMe	2,6-diMe	3,4-diMe
C_1-C_2	1.482	1.481	1.481	1.481	1.479
C_2-C_3	1.407	1.406	1.406	1.405	1.404
C_3-C_4	1.485	1.485	1.485	1.486	1.487
C_4-C_5	1.493	1.493	1.493	1.493	1.491
C_5-C_6	1.512	1.540	1.541	1.541	1.544
C_6-C_1	1.541	1.494	1.494	1.493	1.493
N-C_5	1.513	1.534	1.535	1.534	1.525
N-C_7	1.376	1.382	1.378	1.386	1.370
N-C_{11}	1.361	1.385	1.385	1.396	1.373
C_7-C_8	1.422	1.404	1.409	1.402	1.390
C_8-C_9	1.395	1.392	1.381	1.386	1.398
C_9-C_{10}	1.379	1.403	1.404	1.392	1.410
C_{10}-C_{11}	1.382	1.382	1.390	1.396	1.396

Fe-lig	2.020	1.678	1.678	1.679	1.679
Fe-C_{13}	2.162	1.734	1.734	1.733	1.734
Fe-C_{14}	2.188	1.795	1.795	1.795	1.795
Fe-C_{15}	2.163	1.796	1.796	1.796	1.796
O_1-C_{13}	1.149	1.157	1.157	1.158	1.157
O_2-C_{14}	1.149	1.147	1.147	1.147	1.147
O_3-C_{15}	1.149	1.147	1.147	1.147	1.147

(b) Selected bond angles in degree

Bond angle/°	2,3-diMe	2,4-diMe	2,5-diMe	2,6-diMe	3,4-diMe
C_{15}-Fe-C_{14}	93.46	93.40	93.45	93.52	95.36
C_{15}-Fe-lig	118.17	118.17	118.19	118.13	118.40
C_{14}-Fe-lig	117.11	117.14	117.16	116.99	117.42
C_{13}-Fe-lig	129.54	129.42	129.43	129.71	125.25
C_5-N-C_7	125.14	125.17	125.02	122.76	119.87
C_5-N-C_{11}	115.50	116.11	115.91	118.26	120.14

O_1-C_{13}-Fe	174.63	174.63	174.69	174.73	174.90
O_2-C_{14}-Fe	171.86	171.86	171.88	171.91	171.34
O_3-C_{15}-Fe	174.59	174.59	174.70	174.66	174.83

(c) Dihedral angles in degree

Dihedral angles/°	2,3-diMe	2,4-diMe	2,5-diMe	2,6-diMe	3,4-diMe
Lig-Fe-C_{13}-O_1	0.00	0.53	0.50	-0.69	3.63
O_3-C_{15}-Fe-lig	-5.74	-6.91	-6.26	-8.13	0.18
Fe-C_{14}-lig-C_2	-174.95	-174.84	-174,81	-175.11	-174.35
O_2-C_{14}-Fe-lig	-15.61	-14.64	-14.28	-14.72	-10.09
C_1-lig-Fe- C_{14}	-31.17	-31.17	-31.16	-31.30	-31.50

4.3.3 Tricarbonyl (1-4-η-5-exo-N-pyridino-2-methoxycyclohexa-1,3-dieneiron) complexes

The geometrical parameters were obtained after total optimization of the equilibrium geometries by Semi-empirical PM3. In order to investigate the effect of the substituent on the pyridine ring, the geometries were compared with the parent Tricabonyl (1-4-η-5-exo-N-pyridino-cyclohexa-1,3-diene) iron complex. For the unsubstituted Tricabonyl (1-4-η-5-exo-N-pyridino-cyclohexa-1,3-diene) iron complex at PM3 level, calculations predict the bond length, bond angles and dihedral angles with remarkable changes. The effect of the methyl group grafted on the position 2,3 and 4 of the pyridine ring was clearly observed with the increase in bond length adjacent to the methyl group resulting from the strong electron-donating effect of the substituent. The ground state geometrical parameters were compared with those of the unsubstituted tricarbonyl (1-4-η -cyclohexa-1,3-diene) ironcomplex. The replacement of hydrogen with the methoxy group resulted in the increase in bond length within the cyclohexa-1,3-diene ring. For instance, the bond length of C_2-C_3 generally increased when compared to the unsubstituted diene derivatives. For each compound, there were remarkable changes in bond length with the bond distances of C- H occurring within the range of 1.088-1.126Å. While the C-C and C = C bonds are within the range of 1.373- 1.545Å and 1.373-1.488Å respectively. The metal- carbon bond distances ranged from 1.736Å to 1.806Å, while the metal-ligand bond appears to be unchanged at 1.663Å. However, the bond angles and dihedral angles exhibit changes which depend on the position of the methyl group (Table 4.7).

Table 4.7: Geometrical parameters of Tricarbonyl (1-4-η-5-exo-N-pyridino-2-methoxycyclohexa-1,3-diene ironcomplexes showing (a) selected bond length (b) bond angles and (c) dihedral angles

(a) Selected bond length

Bond length/Å	H	2-Me	3-Me	4-Me
C_1-C_2	1.417	1.417	1.417	1.417
C_2-C_3	1.486	1.487	1.486	1.486
C_3-C_4	1.488	1.487	1.488	1.488
C_4-C_5	1.545	1.535	1.545	1.545
C_5-C_6	1.489	1.490	1.489	1.489
C_6-C_1	1.491	1.492	1.491	1.491
C_2-O_1	1.375	1.376	1.375	1.375
O_1-C_{12}	1.414	1.414	1.414	1.414
C_5-N	1.529	1.535	1.528	1.528
C_7-N	1.371	1.382	1.370	1.373
C_{11}-N	1.374	1.383	1.372	1.375
C_7-C_8	1.393	1.406	1.398	1.373
C_8-C_9	1.393	1.386	1.400	1.400
C_9-C_{10}	1.395	1.396	1.392	1.402
C_{10}-C_{11}	1.391	1.385	1.393	1.388

Fe-Lig	1.662	1.663	1.662	1.662
Fe-C_{13}	1.737	1.796	1.796	1.796
Fe-C_{14}	1.804	1.804	1.736	1.736
Fe-C_{15}	1.797	1.796	1.806	1.806
C_{13}-O_2	1.157	1.157	1.157	1.147
C_{14}-O_3	1.145	1.147	1.147	1.147
C_{15}-O_4	1.147	1.145	1.145	1.145

(b) Bond Angles in degrees

Angles/°				
C_{13}-Fe-C_{14}	94.63	96.52	96.63	96.63
C_{14}-Fe-C_{15}	92.49	96.04	94.62	94.67
C_{13}-Fe-C_{15}	96.63	96.52	92.55	92.53
Lig-Fe-C_{15}	118.38	118.34	118.59	118.59
C_2-O_1-C_{12}	114.96	114.67	114.94	115.00
Fe-lig-C_2	103.69	103.30	103.65	103.66
Fe-lig-C_1	80.55	80.63	80.56	80.56

Fe-C_{15}-O_4	174.77	177.13	177.18	177.14
C_5-N-C_7	120.12	124.74	119.91	120.09
C_5-N-C_{11}	119.84	116.14	119.85	120.01

(c) Dihedral angles in degrees

C_{15}-Fe-lig-C_3	101.09	101.11	101.67	101.69
C_{12}-O_1-C_2-C_1	-67.14	-68.39	-67.45	-66.83
C_4-C_5-N-C_7	-41.78	-51.62	-43.51	-43.70
C_{10}-C_{11}-N-C_5	179.61	179.47	179.69	179.70
C_{11}-N-C_7-C_8	-0.32	-1.13	-0.26	-0.28
C_2-C_3-lig-Fe	-104.85	-104.44	-104.81	-104.83

4.4.4 Tricarbonyl (1-4-η-5-exo-N-X,X-dimethylyridino-2-methoxycyclohexa-1,3-diene) iron complexes

Geometric parameters (bond length/Å, bond angles and dihedral angles in degrees) of the studied Tricarbonyl (1-4-η-5-exo-N-X,X-dimethylpyridino-2-methoxycyclohexa-1,3-dieneiron complexes in their global minimum obtained by Semi-empirical PM3 are shown Table 4.8. The ground state geometrical parameters were compared with the unsubstituted 1-4-η-cyclohexa-1,3-diene iron complex. The replacement of hydrogen by the methoxy group led to the increase in bond length within the cyclohexa-1,3-diene ring. For instance, the bond length of C_2-C_3 generally increased whencompared to the unsubstituted derivatives. For each compound, there were remarkable changes in bond length and all the bond distances of C- H predicted are within the range of 1.088Å-1.126Å.The C-C and C = C bonds are between 1.383 - 1.544Å and 1.343 - 1.488Å. The metal - carbon bond distances range from 1.735 - 2.198Å while the metal-ligand bond distance range between 1.662Å and 2.020Å However, the bond angles and dihedral angles changed as the position of the methyl group also changed. The results are collected in Table 4.8.

Table 4.8: Geometric parameters of Tricarbonyl (1-4-η-5-exo-N-X,X-dimethyl pyridino-2-methoxycyclohexa-1,3-diene iron complexes showingbond length, bond angles and dihedral angles

(a) Bond length in Angstrom units

Bond/Å	2,3-diMe	2,4-diMe	2,5-diMe	2,6-diMe	3,4-diMe	3,5-diMe
C_1-C_2	1.487	1.343	1.488	1.487	1.486	1.486
C_2-C_3	1.417	1.417	1.443	1.418	1.417	1.417
C_3-C_4	1.486	1.339	1.486	1.486	1.488	1.488
C_4-C_5	1.499	1.508	1.493	1.493	1.490	1.490
C_5-C_6	1.543	1.544	1.541	1.542	1.545	1.545
C_6-C_1	1.492	1512	1.493	1.493	1.491	1.491
C_2-O_1	1.376	1.365	1.376	1.376	1.375	1.375
O_1-C_{12}	1.414	1.423	1.414	1.414	1.413	1.413
Fe-lig	1.663	2.020	1.662	1.663	1.662	1.662
Fe-C_{13}	1.796	2.169	1.796	1.796	1.796	1.796
Fe-C_{14}	1.736	2.169	1.736	1.735	1.736	1.736

Fe-C_{15}	1.804	2.198	1.805	1.805	1.803	1.803
C_5-N	1.534	1.510	1.535	1.534	1.527	1.527
C_7-N	1.383	1.371	1.378	1.386	1.370	1.368
C_7-C_8	1.402	1.410	1.408	1.402	1.390	1.400
C_8-C_9	1.393	1.391	1.382	1.386	1.398	1.396
C_9-C_{10}	1.403	1.385	1.404	1.392	1.410	1.399
C_{10}-C_{11}	1.383	1.388	1.390	1.396	1.395	1.397
C_{11}-N	1.384	1.362	1.384	1.395	1.374	1.372
C_{13}-O_2	1.157	1.157	1.157	1.157	1.157	1.147
C_{14}-O_3	1.145	1.147	1.147	1.147	1.147	1.147
C_{15}-O_4	1.147	1.145	1.145	1.145	1.145	1.145

(b) Bond Angles in degrees

Bond Angle / °	2,3-diMe	2,4-diMe	2,5-diMe	2,6-diMe	3,4-diMe	3,5-diMe
O_3-C_{14}-Fe	171.35	171.16	171.26	171.24	171.41	171.19
C_{15}-Fe-C_{14}	94.02	94.14	94.12	93.95	94.13	94.20
C_{13}-Fe-C_{15}	92.65	92.68	92.66	92.64	92.49	92.56
C_{14}-Fe-lig	129.13	129.00	129.02	129.29	128.96	129.06
Fe-lig-C_2	103.11	103.26	103.10	103.18	103.67	103.67
Fe-lig-C_1	80.68	80.64	80.66	80.68	80.56	80.56
C_2-O_1-C_{12}	114.75	114.63	114.55	114.67	114.97	115.00
C_5-N-C_7	125.06	124.82	124.95	122.71	120.22	120.08
C_5-N-C_{11}	115.55	116.21	115.97	118.29	119.79	119.51
C_{16}-C_7-N	122.18	122.50	122.54	122.61	-	-

(c) Dihedral Angles in degrees

Bond/°	2,3-diMe	2,4-diMe	2,5-diMe	2,6-diMe	3,4-diMe	3,5-diMe
C_{14}-Fe-lig-C_2	127.74	127.83	127.92	127.42	128.51	128.50
C_{15}-Fe-lig-C_1	-62.68	-62.55	-62.59	-62.87	-62.06	-62.14
Fe-lig-C_2-O_1	60.28	60.34	59.99	60.12	60.54	60.71
C_{12}-O_1-C_2-C_1	-68.61	-69.31	-70.59	-69.34	-67.05	-66.32
C_3-C_4-C_5-C_6	-28.81	-28.96	-29.30	-27,40	-35.32	-35.12
C_5-N-C_7-C_{16}	0.65	-0.17	041	-4.65	-	-
C_5-N-C_{11}-C_{10}	-179.70	-179.36	-179.69	-175.28	-179.57	179.72

4.3.5 Tricarbonyl (1-4-η-5-exo–N-aminopyridino-cyclohexa-1,3-diene)iron

The geometrical parameters were obtained after total optimization of the equilibrium geometries by Semi-empirical PM3. Bond length, bond angles and dihedral angles which contribute to the internal energies were measured and recorded in Table 4.9. The effects of substituent amino group on the pyridine are clearly noticeable around the adjacent carbon atoms. For instance, the bond length of N-C_7 in 2-aminopyridino complex is 1.398Å because the amino substituent is attached to C_7, C_7-C_8 bond length is also1.432Å, these values are more than the values obtained for other pyridino substituents and this can be attributed to the electron donor capacity of the amino group.C_7-N_2 is also 1.366Å which is low in comparison with other C-N amino substituents, C_8-N_2 (1.399Å), C9-N_2 (1.377Å), and C_9-N_2 1.470Å and 1.380Å for N-methyl and N-diethyl substituents respectively. With the amino substituent on C_8, the bond length C_7-C_8 reduces to 1.412Å while C_8-C_9 increases to 1.413Å and the adjacent C_9-C_{10} reduces to 1.383Å. This is a clear manifestation of the substituent effect on the attached pyridine ring. The entire C-C single and double bonds are within the range of 1.432-1.529Å and 1.368-1.489Å respectively. The metal-carbon bonds are in the range 1.730-1.817Å, while the entire metal-ligand bond is within 1.697-1.701Å with little or no significant changes. All the C-H bonds fall within 1.090Å and 1.122Å. However, the bond and dihedral angles are shown in Table 4.9.

Table 4.9: Geometric parameters of Tricarbonyl (1-4-η- 5-exo-N-X-amino pyridino-cyclohexa-1,3-diene) iron complexes

(a) Selected bond length

Bond length / Å	2-NH_2	3-NH_2	4-NH_2	4-$NH(CH_3)$	4-$N(CH_3)_2$
$C_1 – C_2$	1.465	1.477	1.473	1.473	1.473
$C_2 – C_3$	1.405	1.396	1.398	1.398	1.398
$C_3 – C_4$	1.489	1.485	1.489	1.487	1.487
$C_4 – C_5$	1.509	1.496	1.498	1.499	1.499
$C_5 – C_6$	1.539	1.539	1.540	1.540	1.540
$C_6 – C_1$	1.498	1.494	1.495	1.495	1.495
$C_5 – N_1$	1.510	1.519	1.519	1.515	1.514
$N_1 – C_7$	1.398	1.366	1.378	1.378	1.379
$C_7 – C_8$	1.432	1.412	1.379	1.378	1.377
$C_8 – C_9$	1.368	1.413	1.418	1.419	1.424
$C_9 – C_{10}$	1.416	1.383	1.420	1.424	1.426
$C_{10} – C_{11}$	1.369	1.398	1.377	1.375	1.375
$C_{11} – N_1$	1.399	1.369	1.383	1.384	1.383
lig – Fe	1.701	1.700	1.697	1.697	1.697

$Fe - C_{12}$	1.765	1.734	1.730	1.730	1.730
$Fe - C_{13}$	1.815	1.799	1.798	1.797	1.797
$Fe - C_{14}$	1.817	1.809	1.804	1.803	1.802
$C_{12} - O_1$	1.154	1.159	1.160	1.160	1.160
$C_{13} - O_2$	1.145	1.148	1.148	1.148	1.148
$C_{14} - O_3$	1.144	1.145	1.146	1.146	1.146
$N_2 - H$	0.990	0.993	0.991	-	-
$C_7 - N_2$	1.367	-	-	-	-
$C_8 - N_2$	-	1.399	-	-	-
$C_9 - N_2$	-	-	1.377	1.470	1.380
$N_2 - C$	-	-	-	1.480	1.480
C – H	1.090-.122	1.091-1.123	1.090-1.124	1.090-1.124	1.090-1.124

(b) Bond angles in degrees

Bond angle/°	2-NH_2	3-NH_2	4-NH_2	4-$NH(CH_3)$	4-$N(CH_3)_2$
C_{12}-Fe-lig	133.62	133.04	132.22	132.17	132.13
C_{13}-Fe-lig	120.41	119.15	119.61	119.65	119.62
C_{14}-Fe-lig	109.29	111.27	111.91	111.95	112.02

Fe-C_{12}-O_1	169.89	170.41	171.52	171.65	171.61
Fe-C_{13}-O_2	174.23	174.86	174.92	174.97	174.82
Fe-C_{14}-O_3	170.13	170.75	170.98	170.94	171.07
C_5-N_1-C_{11}	118.51	117.46	119.09	119.25	119.42
C_5-N_1.C_7	122.18	122.05	121.03	120.97	121.12
N_1-C_7-N_2	119.19	-	-	-	-
C_7-N_1-C_{11}	119.19	120.47	119.89	119.78	119.89
C_7-C_8-N_2		119.73	-	-	-
C_8-C_9-N_2	-	-	120.97	122.67	121.70
C_9-N_2-C_{15}	-	-	-	122.83	118.26

(c) Dihedral angles in degrees

Dihedral angles /°	2-NH_2	3-NH_2	4-NH_2	4-$NH(CH_3)$	4-$N(CH_3)_2$
C_4-lig-Fe-C_{13}	51.20	55.48	52.85	52.57	52.51
C_3-lig-Fe-C_{14}	83.80	91.81	90.61	90.47	90.57
C_2-lig-Fe-C_{12}	92.23	105.30	105.93	106.02	106.14
N_2-C_7- N_1-C_5	0.86	-	-	-	-
C_5-N_1-C_7- N_2	0.25	3.16	0.38	0.20	0.23
N_2-C_8-C7-N1	-	-175.60	-	-	-
N_2-C_9-C_8-C_7	-	-	-176.03	-179.77	-179.80

4.3.6 Tricarbonyl (1-4-η-5-exo-N-aminopyridino-2-methoxycyclohexa-1,3-diene) iron complexes

The geometrical parameters were obtained after total optimization of the equilibrium geometries by Semi-empirical PM3. Bond length, bond angles and dihedral angles which contribute to the internal energies were measured and recorded (See Table 4.10). The effects of the substituent amino group on the pyridine are clearly noticeable around the adjacent carbon atoms; for instance, the bond length of N-C_7 in the 2-aminopyridino complex is 1.398Å because the amino substituent is attached to C_7. C_7-C_8 bond length is also 1.432Å. These values are more than the values obtained for other pyridino substituents and this can be attributed to the electron donor property of the amino group. C_7-N_2 is also 1.366Å.The C_7- C_8 bond length is 1.412Å while the bond length of C_8 – C_9 is 1.413Å. In all the complexes C_8 – C_9 and C_9 – C_{10} which are low in both 2- and 3-aminosubstituents increased significantly in the 4-amino-, 4-N-methylamino and 4-N-dimethylamino substituents respectively. This is comparable with 1.377Å (4-NH_2), 1.381Å {4-NH (CH_3) and 4-N $(CH_3)_2$ for the C_9-N_2 bond length (Table 4.10). With the amino substituent on C_8, the bond lengths C_7-C_8 and C_8-C_9 occur at 1.412Å and 1.413Å respectively while the adjacent C9-C_{10} bond length reduces to 1.383Å. This is a clear manifestation of the substituent effect on the attached pyridine ring. All the C-C single and double bonds are within the range of 1.432-1.529Å and 1.368-1.489Å respectively. The metal-carbon bond falls within the range 1.731-1.820Å while the entire metal-ligand bond is 1.681Å in all the complexes except for the 2-aminnopyridino complex whose metal-ligand bond is 1.692Å. All the C-H bonds fall within 1.090Å and 1.122Å. The bond distances, bond angles and dihedral angles for all the complexes are collected in Table 4.10.

Table 4.10: Geometric parameters of Tricarbonyl (1-4-η-5-exo-N-X-amino-pyridino-2-methoxycyclohexa-1,3-diene) iron complexes

(a) Selected bond length

Bond length / Å	2-NH_2	3-NH_2	4-NH_2	4-$NH(CH_3)$	4-$N(CH_3)_2$
$C_1 – C_2$	1.474	1.483	1.483	1.483	1.483
$C_2 – C_3$	1.419	1.409	1.408	1.408	1.408
$C_3 – C_4$	1.492	1.484	1.483	1.483	1.483
$C_4 – C_5$	1.509	1.495	1.495	1.495	1.495
$C_5 – C_6$	1.540	1.540	1.539	1.539	1.539
$C_6 – C_1$	1.496	1.493	1.494	1.493	1.494
$C_5 – N_1$	1.510	1.519	1.520	1.519	1.518
$N_1 – C_7$	1.398	1.366	1.377	1.377	1.378
$C_7 – C_8$	1.432	1.412	1.381	1.381	1.379
$C_8 – C_9$	1.367	1.413	1.416	1.417	1.422
$C_9 – C_{10}$	1.416	1.383	1.420	1.424	1.426
$C_{10} – C_{11}$	1.368	1.398	1.376	1.374	1.374
$C_{11} – N_1$	1.399	1.369	1.385	1.386	1.385
lig – Fe	1.692	1.681	1.681	1.681	1.681
Fe – C_{12}	1.820	1.736	1.732	1.732	1.731
Fe – C_{13}	1.770	1.797	1.801	1.801	1.800
Fe – C_{14}	1.814	1.821	1.820	1.820	1.818

$C_{12} – O_1$	1.153	1.159	1.161	1.161	1.616
$C_{13} – O_2$	1.142	1.148	1.148	1.148	1.148
$C_{14} – O_3$	1.144	1.143	1.143	1.143	1.144
$C_2 – O_4$	1.355	1.376	1.377	1.377	1.377
$O_4 – C_{15}$	1.414	1.414	1.415	1.415	1.414
$C_7 – N_2$	1.366	-	-	-	-
$C_8 – N_2$	-	1.399	-	-	-
$C_9 – N_2$	-	-	1.377	1.377	1.381
$N_2 – C$	-	-	-	1.476	1.480
C – H	1.089-1.121	1.091-1.121	1.090-1.121	1.090-1.122	1.091-1.122
N_2- H	0.989	0.993	0.991	0.995	-

(b) Bond Angles in degrees

Bond angle /°	2-NH_2	3-NH_2	4-NH_2	4-$NH(CH_3)$	4-$N(CH_3)_2$
C_{12}-Fe-lig	132.91	132.25	132.64	132.78	132.49
C_{13}-Fe-lig	120.58	118.88	118.55	118.44	118.49
C_{14}-Fe-lig	110.78	113.60	113.52	113.48	113.64
C_{12}-Fe-C_{14}	88.58	88.57	88.43	88.35	88.63
C_{13}-Fe-C_{14}	89.14	90.11	90.00	89.97	90.18

C_{12}-Fe-C_{13}	102.51	101.83	101.94	101.98	101.81
C_2-O_4-C_{15}	117.60	114.55	114.48	114.33	114.53
C_5-N_1-C_7	122.05	121.89	122.56	122.75	122.75
N_1-C_7-N_2	119.07	-	-	-	-
N_1-C_7-C_8	119.18	120.31	120.88	120.00	121.04
C_7-C_8-N_2	-	119.71			
H-N-H	120.20	114.49	116.78	-	-
N_2-C_7-C_8	121.74	-	-	-	-
C_9-N_2-C_{16}	-	-	-	122.74	120.81

(c) Dihedral Angles in degrees

Dihedral angles /°	2-NH_2	3-NH_2	4-NH_2	4-$NH(CH_3)$	4-$N(CH_3)_2$
C_3-C_2-O_4-C_{15}	128.48	128.50	127.90	126.24	128.64
C_{13}-Fe-C_{14}-O_3	68.67	68.79	69.12	69.16	68.30
C_{14}-Fe-lig-C_3	91.56	91.62	91.68	91.74	91.79
C_4-lig-Fe-C_{13}	54.95	55.07	55.42	55.57	55.20
C_4-C_5-N_1-C_7	11.54	11.34	10.38	9.21	10.66
C_8-C_7-N_2-H	11.73	11.78	-	-	-
H-C_7-C_8-N_2	-	3.61	-	-	-
C_{10}-C_9-N-C_{16}	-	-	-	171.98	171.98

4.4 Electronic properties

4.4.1 Tricarbonyl (1-4-η-5-exo-N-X-pyridino-cyclohexa-1,3-diene)iron complexes

It is expedient to visualize the HOMO and the LUMO for these new organometallics (Riggs and Sun, 2000; Bouzzine *et al*., 2004; Manna *et al*., 2003; Bingham *et al*., 1975; Dewar and Thiel, 1977; Dewar *et al*., 1985, 1977a, 1977b; Mclver *et al*., 1977)compounds because the relative ordering of occupied and virtual orbital provide a reasonable qualitative indication of both ground and excited state properties. The HOMO of these complexes possesses a π-bonding character within the subunit and π–antibonding character exited state properties between the consecutive subunits. On the other hand, the LUMO possesses a π -antibonding character within the subunit and a π-bonding character between the subunits. In practice, the HOMO and LUMO energies are obtained from an empirical formula based on the onset of oxidation-reduction of peaks measured by cyclic voltametry. Theoretically, the HOMO and LUMO energies are calculated using Semi-empirical PM3 (Stewart, 1989).These calculations however, do not have solid-state packing effect and aqueous state is not taken into consideration. Even if these energy levels are not accurate, it is still possible to use them to obtain information by comparing them with other compounds. Table 4.11 lists the theoretical electronic parameters of these new organometallics. The calculated electronic properties (energy band gap LUMO-HOMO) of the Tricarbonyl (1-4-η-5-exo-N-X-substituted pyridino-cyclohexa-1,3-dieneironcomplexes are 7.32eV,7.40eV, 7.40eV and 3.70eV respectively for X = H, 2-Me, 3-Me and 4-Me. There is no significant change in the electronic properties of the first three complexes; thereduction of band-gap observed in 4-methylpyridino complex may be attributed to thesymmetrical occupation of the methyl substituent on the pyridine ring. The LUMO-HOMO diagrams are presented in Plate 4.1.

Table 4.11: Electronic parameters for Tricarbonyl (1-4-η-5-exo-N-X-pyridino-cyclohexa-1,3-diene) iron complexes

Substituent	Dipole moment//Debye	HOMO energy /eV	LUMO energy /eV	Band gap/ eV
H	4.88	-5.09	-12.41	7.32
2-Me	4.12	-4.99	-12.39	7.40
3-Me	3.44	-4.97	-12.37	7.40
4-Me	3.31	-4.99	-8.79	3.70

4.4.2 Tricarbonyl (1-4-η-5-exo-N-X,X-dimethylpyridino-cyclohexa-1,3-diene) iron complexes

The HOMO of these complexes possesses a π-bonding character within the subunit and π-antibonding character excited state properties between the consecutive subunits. On the other hand, the LUMO possesses a π -antibonding character within the subunit and a π-bonding character between the subunits. In practice, the HOMO and LUMO energies are obtained from an empirical formula based on the onset of oxidation-reduction of peaks measured by cyclic voltametry.Theoretically the HOMO and LUMO energies are calculated using Semi-empirical PM3.These calculations however, do not have solid-state packing effect and aqueous state is not taken into consideration. Even if these energy levels are not accurate, it is still possible to use them to obtain information by comparing them with other compounds. Table 4.12 lists the theoretical electronic parameters of these new organometallics. The calculated electronic properties (LUMO-HOMO band gap) of compounds Tricarbonyl (1-4-η-5-exo-N-X,X-dimethylpyridino-cyclohexa-1,3-diene)ironcomplexes are 7,42eV, 7.40eV, 7.42eV, 7.40eV and 7.43eV respectively. There is no significant change in the electronic properties of these complexes. The calculated, HOMO and LUMO energies and the band gap are displayed in Table 4.12 while the LUMO-HOMO diagrams are presented in appendix 1, (Plate 4.2).

Table 4.12: Electronic parameters of Tricarbonyl (1-4-η-5-exo-N- X,X-dimethyl pyridino-cyclohexa-1,3-diene) iron complexes

Dimethyl	Dipole moment/Debye	E_{HOMO}/eV	E_{LUMO}/Ev	Band gap E/eV
2,3-	3.21	-12.31	-4.89	7.42
2,4-	2.94	-12.39	-4.90	7.40
2,5-	3.04	-12.31	-4.89	7.42
2,6-	3.58	-12.31	-4.92	7.40
3,4-	2.29	-12.31	-4.88	7.43

4.4.3 Tricarbonyl (1-4-η-5-exo-N-X-pyridino-2-methoxycyclohexa-1,3-diene) iron complexes

In order to explain the electronic properties of these compounds, the HOMO and the LUMO for these new organometallic compounds were visualized since the relative ordering of occupied and virtual orbitals provide a reasonable qualitative indication of both ground and excited state properties. Both the HOMO and the LUMO of these complexes possesses a combination of π-bonding character within subunit and π-antibonding character exited state properties between the consecutive subunits. On the other hand, the LUMO possesses a π-antibonding character within the subunit and a π -bonding character between the subunits. Experimentally, the HOMO and LUMO energies are obtained from an empirical formula based on the onset of oxidation-reduction of peaks measured by cyclic voltametry (Follett *et al*., 2007; Pratt and Vander Donk, 2005; Birke *et al*., 2006; Jensen and Ryde, 2003; Morschel *et al*., 2008; Huang *et al*., 2007; Hu and Boyd, 2000; Praetorius *et al*., 2008).Theoretically the HOMO and LUMO energies are calculated using theoretical models. These calculations however, do not have solid-state packing effect and aqueous state is not taken into consideration. Table 4.13 lists the theoretical electronic parameters for these new organometallics. The calculated electronic properties (energy band gap LUMO-HOMO) of the Tricarbonyl (1-4-η-5-exo-N-X-substituted pyridino-2-methoxycyclohexa-1,3-diene) iron complexes are 7.21, 7.20, 7.18 and 7.24eV respectively for X = H, 2-Me, 3-Me and 4-Me.There is no significant change in the electronic properties of these complexes. The LUMO-HOMO diagrams are presented in appendix 1 (Plate 4.3).

Table4.13: Electronic parameters for Tricarbonyl (1-4-η-5-exo-N-X-pyridino-2-methoxycyclohexa-1,3-diene) iron complexes

Substituent	Dipole moment/Debye	HOMO energy /eV	LUMO energy /eV	Band gap/ eV
H	6.69	-5.08	-12.29	7.21
2-Me	6.62	-5.00	-12.30	7.20
3-Me	5.58	-4.97	-12.25	7.18
4-Me	5.24	-4.99	-12.23	7.24

4.4.4 Tricarbonyl (1-4-η-5-exo-N-X,X-dimethylpyridino-2-methoxycyclohexa-1,3-diene) iron complexes

Spectroscopic data for a number of π-systems are usually determined either in solution or in the solid state (crystals or thin film). Our calculations are for isolated molecules in the gas phase. Experimentally, the HOMO and the LUMO energies can be obtained from an empirical data based on the onset of the oxidation and reduction of peaks measured by cyclic voltametry, in gas-phase chemistry, the HOMO and the LUMO energies are calculated using Semi-empirical PM3. However, solid state packing effects are not included in our calculations as this tends to affect the HOMO and the LUMO energy levels in a thin film compared to an isolated molecule. The calculated electronic parameters (energy band gaps, i.e. HOMO- LUMO) of the X, X-substituted pyridino-organometallic complexes are 7.27, 7.25, 7.30, 7.25, 7.32 and 7.35eV respectively for X = 2,3-Me_2, 2,4-Me_2, 2,5-Me_2, 2,6-Me_2, 3,4-Me_2 and 3,5-Me_2.Even with no change in band gap, they exhibit destabilization of both the HOMO and the LUMO levels in comparison with the new Tricarbonyl (1-4-η-pyridino-cyclohexa-1,3-diene ironcomplexes. This is due to the presence of the electron-donating methoxy group on the cyclohexa-1,3-diene ring and methyl substituent on the pyridine ring. There are no significant changes in band gap even though the position of the substituent changes. The HOMO and LUMO energies and energy band gaps are shown in Table 4.14, while the HOMO and LUMO diagrams are presented in appendix 1, (Plate 4.4).

Table 4.14: Electronic parameters for Tricarbonyl (1-4-η-5-exo-N-X,X dimethyl pyridino-2-methoxycyclohexa-1,3-diene) iron complexes

Dimethylgroup	Dipole moment/Debye	E_{HOMO}/eV	E_{LUMO}/eV	Bandgap Eg/Ev
2,3-	5.22	-12.16	-4.89	7.27
2,4-	4.97	-12.15	-4.90	7.25
2,5-	4.96	-12.17	-4.89	7.30
2,6-	5.43	-12.17	-4.92	7.25
3,4-	4.02	-12.19	-4.87	7.32
3,5-	4.23	-12.21	-4.86	7.35

4.4.5 Tricarbonyl (1-4-η-5-exo-N-X-aminopyridino-cyclohexa-1,3-diene) iron complexes

The HOMO of these complexes possesses a π-bonding character within sub-units and π-antibonding character excited state properties between the consecutive subunits. On the other hand, the LUMO possesses a π-antibonding character within the subunits and a π-bonding character between the subunits. Experimentally, the HOMO and the LUMO energies were obtained from an empirical formula based on the onset of oxidation-reduction of peaks measured by cyclic voltametry. Theoretically, the HOMO and LUMO energies are calculated using Semi-empirical PM3. These calculations however, do not have solid- state packing effect and aqueous state is not taken into consideration. The HOMO-LUMO energy gap is the difference in energy between the LUMO and HOMO;this is an important stability index. The calculated electronic properties (energy band gap, LUMO-HOMO) of these complexes were found to be within 7.30 – 7.80eV, the calculated values are shown in Table 4.15, while the LUMO-HOMO structures are shown in appendix 1 Plate 4.5. There is a significant change in the values recorded for dipole moments.

Table 4.15: Electronic parameters for Tricarbonyl (1-4-η-5-exo-N-X-amino-pyridino-cyclohexa-1,3-diene) iron complexes

X-aminopyridino	Dipole moments / Debye	HOMO energy / eV	LUMO energy / eV	Band gaps / eV
2-NH_2	2.19	-12.14	-4.34	7.80
3-NH_2	4,39	-12.13	-4.83	7.30
4-NH_2	6.06	-12.02	-4.67	7.35
4-$NHCH_3$	4.55	-11.97	-4.55	7.42
4–$N(CH_3)_2$	3.23	-11.92	-4.43	7.49

4.4.6 Tricarbonyl (1-4-η-5-exo-N-X-aminopyridino-2-methoxycyclohexa-1,3-diene) ironcomplexes

The HOMO-LUMO energy of these complexes was obtained in order to explain the electronic properties of these new organometallics. The HOMO of these complexes comprises of π-bonding combination and π-antibonding character excited state properties between the consecutive subunits. The LUMO possesses combination of π-antibonding characterand a π-bonding character between the sub-units. Experimentally, the HOMO and the LUMO energies were obtained from an empirical formula based on the onset of oxidation-reduction of peaks measured by cyclic voltametry. Theoretically, the HOMO and LUMO energies are calculated using Semi-empirical PM3. These calculations however, do not have solid-state packing effect and aqueous state is not taken into consideration. Although these energy levels may not be accurate, it is possible to use them to obtain information by comparing them with other compounds. The calculated electronic properties (energy band gap,LUMO-HOMO) of these complexes were found to be within 7.20–7.76eV, the highest been the Tricarbonyl (1-4-η-5-exo-N-2-aminopyridino-2-methoxycyclohexa-1,3-diene) iron complex, the calculated values are shown in Table 4.16 while the LUMO-HOMO structures are shown in appendix 1 Plate 4.6. However, there is a significant change in the values recorded for dipole moments.

Table 4.16: Electronic parameters for Tricarbonyl (1-4-η-5-exo-N-X-amino-pyridino-2-methoxycyclohexa-1,3-diene) iron complexes

X-aminopyridino	Dipole moments / Debye	HOMO energy / eV	LUMO energy / eV	Band gaps / eV
2-NH_2	3.52	-12.04	-4.28	7.76
3-NH_2	6.51	-12.01	-4.81	7.20
4-NH_2	8.27	-11.85	-4.65	7.20
4-$NH(CH_3)$	6.76	-11.80	-4.53	7.27
4-$N(CH_3)_2$	5.44	-11.76	-4.41	7.35

4.5 Thermodynamic parameters and Stability

4.5.1 Tricarbonyl (1-4-η-5-exo-N-X-pyridino-cyclohexa-1,3-diene) iron complexes

The formations of these complexes are highly exothermic. Thermodynamic stabilities is expected when a negative ΔH,ΔG and positive ΔS.The more negative the values of ΔG and ΔH, positive ΔS, the more stable the pyridino complexes.A closer look at the Table 4.13 confirms that the formation of Tricarbonyl (1-4-η-5-exo-N-4-methylpyridino-cyclohexa-1,3-diene iron complex is more exothermic than that of 2-methylpyridino and 3-methylpyridino organometallic complexes, hence the order stability is H>4-Me> 3-Me >2-Me. All the calculated free energies are negative, the calculated enthalpies are negative, all entropies are positive, and this implies that the formation of these complexes is spontaneous. There are no experimental or theoretical data for comparison; however, present calculations reveal that all the complexes are thermodynamically stable as shown in Table 4.17.

Table 4.17: Thermodynamic parameters forTricarbonyl (1-4-η-5-exo-N-X-pyridino-cyclohexa-1,3-diene) iron complexes. (T= 298.15K)

X-pyridino	Heat of formation H_f $kJmol^{-1}$	Free Energy G $kJmol^{-1}$	Entropy S $Jmol^{-1}K^{-1}$	Enthalpy H $kJmol^{-1}$
H	-799.78	-317.334	558.78	-150.74
2-Me	-840.68	-285.43	579.20	-112.75
3-Me	-845.34	-295.64	594.22	-118.48
4-Me	-847.73	-298.03	593.70	-121.02

4.5.2 Tricarbonyl (1-4-η-5-exo-N-X, X-dimethylpyridino-cyclohexa-1,3-diene) iron complexes

The formation of these 1,3-diene compounds are spontaneous. Thermodynamic stabilities results from negative Δ H, ΔG values and positive ΔS. The more negative the values of ΔG and ΔH and positive ΔS, the more stable will be the complexes. This is clearly confirmed in Table 4.18 with the Tricarbonyl (1-4-η-5-exo-N-2,6-dimethylpyridino-cyclohexa-1,3-diene iron complex being the most stable. All the calculated free energies are negative, the enthalpies are negative and entropies are all positive, suggesting that, the formation of these complexes is spontaneous. From the thermodynamic data, all the complexes are thermodynamically stable. The thermodynamic properties are shown in Table 4.18.

Table 4.18: Thermodynamic parameters for the Tricarbonyl (1-4-η-5-exo-N-X,X-dimethylpyridino-cyclohexa-1,3-diene) iron complexes (T = 298.15 K)

X,X-dimethyl	Heat of formation./ $kJmol^{-1}$	Free energy /$kJmol^{-1}$	Entropy /$Jmol^{-1}K^{-1}$	Enthalpy/ $kJmol^{-1}$
2,3-	-863.99	-235.57	598.17	-51.27
2,4-	-873..36	-248.70	607.31	-67.63
2,5-	-870.82	-246.55	609.26	-64.90
2,6-	-858.95	-228.71	595.21	-51.25
3,4-	-889.62	-269.37	620.04	-84.50

4.5.3 Tricarbonyl (1-4-η-5-exo-N-X-pyridino-2-methoxycyclohexa-1,3-diene) iron complexes

The quantities calculated include the standard enthalpy of formation, absolute enthalpy, entropy and free energy change; these are presented in Table 4.19. The heat of formation, absolute enthalpy and free energy are all negative while the entropy is positive. Thermodynamic stabilities are expected when ΔH and ΔG are negative. The more negative these values are and the more positive ΔS, the more stable would be the pyridino complexes. A closer look at Table 4.19 confirms that the formation of Tricarbonyl (1-4-η-5-exo-N-4-methylpyridino-2-methoxycyclohexa-1,3-dieneiron complex is more rapid than that of 2-methylpyridino and 3-methyl-pyridino organometallic complexes, hence the order of stability is H > 4-Me > 3-Me > 2-Me. All the calculated free energy values are negative and the calculated enthalpies are negative while all entropies are positive thus confirming that the formation of these complexes is spontaneous. There are no experimental or theoretical data for comparison. However, the present calculations reveal that all the complexes are thermodynamically stable as shown in Table 4.19.

Table 4.19: Thermodynamic parameters for Tricarbonyl (1-4-η-5-exo-N-X-pyridino-2-methoxycyclohexa-1,3-diene) iron complexes (T=298.15K)

X-pyridino	Heat of formation ΔH_f/kJmol^{-1}	Free Energy ΔG/ kJmol^{-1}	Entropy ΔS /Jmol^{-1}K^{-1}	Enthalpy ΔH /kJmol^{-1}
H	-976.54	-420.10	616.03	-237.33
2-Me	-1001.90	-371.57	630.71	-183.52
3-Me	-1021.94	-398.59	649.75	-204.87
4-Me	-1024.46	-401.13	649.26	-207.56

4.5.4 Tricarbonyl (1-4-η-5-exo-N-X,X-dimethylpyridino-2-methoxycyclohexa-1,3-diene) iron complexes

The calculated thermodynamic parameters include the standard heat of formation, absolute enthalpy, free energy and absolute entropyfor these complexes. Thermodynamic stabilities are expected when ΔH and ΔG values are negative thus indicating the spontaneity of the formation of these group of complexes. The more negative these values areand the more positive ΔS, the more stable would be the pyridino complexes. A closer look at Table 4.20 confirms that the formation of Tricarbonyl (1,4-η-5-exo-N-3,5-dimethylpyridino-2-methoxycyclohexa-1,3-diene iron complex is the most rapid followed by 3,4-dimethylpyridino-organometallic cationic complex while Tricarbonyl (1-4-η-5-exo-N-2,6-dimethylpyridino-2-methoxycyclohexa-1,3-diene) iron is the least. All the calculated free energy values are negative and the calculated enthalpies are negative while all entropies are positive, implying that the formation of these complexes is spontaneous. There are no experimental or theoretical data for comparison. However, the present calculations reveal that all the complexes are thermodynamically stable as shown in Table 4.20.

Table4.20: Thermodynamic parameters for Tricarbonyl (1-4-η-5-exo-N-X,X-dimethylpyridino-2-methoxycyclohexa-1,3-diene)iron complexes (T= 298.15K)

Structure, dimethyl	Heat of formation ΔH_f /kJmol^{-1}	Free Energy ΔG /kJmol^{-1}	Entropy ΔS /Jmol^{-1}K^{-1}	Enthalpy ΔH /kJmol^{-1}
2,3-	-1040.72	-339.09	654.70	-143.90
2,4-	-1049.45	-352.04	666.18	-153.41
2,5-	-1047.60	-350.04	665.54	-151.61
2,6-	-1035.90	-332.15	651.39	-137.93
3,4-	-1066.34	-372.80	667.23	-170.89
3,5-	-1067.05	-375.85	683.73	-172.00

4.5.5 Tricarbonyl (1-4-η-5-exo-N-X-aminopyridino-cyclohexa-1,3- diene) iron complexes

The formation of these amino pyridino-1-4-η-cyclohexa-1,3-diene irontricarbonylorganometallics are spontaneous. For complexes to be thermodynamically stable it isexpected that ΔG and ΔH are negative; the more stable would be the amino pyridino complexes. However all calculated free energy and enthalpy changes are negative while all calculated entropy values are positive, thus confirming that the formation of these complexes is spontaneous. Our calculations reveal that all the complexes are thermodynamically stable as shown in Table 4.21.

Table 4.21: Thermodynamic parameters for Tricarbonyl (1-4-η-5-exo-N-X-aminopyridino-cyclohexa-1,3-diene) iron complexes at 298.15K

X-aminopyridino	Heat of formation/ $kJmol^{-1}$	Free energy /$kJmol^{-1}$	Entropy / $Jmol^{-1}K^{-1}$	Enthalpy / $kJmol^{-1}$
2-NH_2	-823.56	-299.46	561.27	-132.11
3-NH_2	-824.92	-294.32	556.66	-125.37
4-NH_2	-827.87	-313.01	577.85	-140.72
4-$NH(CH_3)$	-843.48	-253.70	612.03	-71.22
4-$N(CH_3)_2$	-844.13	-188.50	648.50	4.86

4.5.6 Tricarbonyl (1-4-η-5-exo-N-X-aminopyridino-2-methoxycyclohexa-1,3-diene) ironcomplexes

A compound is essentially stable, if it has a negative heat of formation, negative free energy change and positive entropy. The formation of these amino pyridino-1-4-η-cyclohexa-1,3-diene irontricarbonylorganometallics are spontaneous as presented in Table 4.22. Among the five organometallics within the group, the Tricarbonyl (1-4-η-5-exo-N-4-aminopyridino-2-methoxycyclohexa-1,3-diene ironis the most stable, hence the order of stability is 4-NH_2> 2-NH_2> 3-NH_2> 4-$NHCH_3$> 4-$N(CH_3)_3$. Our calculations reveal that all the complexes are thermodynamically stable, 4-N-dimethylpyridino-1-4-η-2-methoxycyclo- hexa-1,3-diene irontricarbonyl with the highest value of free energy change being the least stable as shown in Table 4.22.

Table 4.22: Thermodynamic parameters for Tricarbonyl (1-4-η-5-exo-N-X-aminopyridino-2-methoxycyclohexa-1,3-diene) iron complexes at 298.15K

X-aminopyridino	Heat of formation/ $kJmol^{-1}$	Free energy /$kJmol^{-1}$	Entropy / $Jmol^{-1}K^{-1}$	Enthalpy / $kJmol^{-1}$
2-NH_2	-1002.52	-404.70	615.70	-221.12
3-NH_2	-1000.83	-397.57	625.70	-211.02
4-NH_2	-1015.10	-412.63	626.00	-225.97
4-$NH(CH_3)$	-1019.40	-353.14	660.08	-156.33
4-$N(CH_3)_2$	-1020.02	-288.13	697.32	-80.22

4.6 Vibrational Frequencies

4.6.1 Tricarbonyl (1-4-η-5-exo-N-pyridino-cyclohexa-1,3-diene) iron complexes

The calculated vibrational frequencies of the complexes are shown in figure appendix 3, Plate 4.7. According to group representation theory in Chemistry, we can deduce that, there are 87 and 96 vibrational modes for the pyridino-derivatives. Among these normal modes, the strongest infra-red absorption peaks and their intensities are displayed in Table 4.23. The simulated IR spectra of the derivatives are calculated by replacing one of its Hydrogen with methyl group. The total vibrations increase from 87 to 96.

Table 4.23: Vibrational frequencies and intensities forTricarbonyl (1-4-η-5-exo-N-X-pyridino-cyclohexa-1,3-diene) iron complexes

X-pyridino/assigned peaks.	Frequency/cm^{-1}	Intensity/$kMmol^{-1}$
H	1272	3676
	1736	6419
	2121	1654
	2170	1399
	2242	1226
2-Me	1272	3756
	1718	5264
	1755	4470
	2119	1603
	2170	1395
	2242	1216
3-Me	1284	3186

	1732	2134
	1748	3886
	2120	1661
	2170	1404
	2242	1244
4-Me	1290	3726
	1718	5732
	1749	1375
	2121	1663
	2170	1404
	2242	1256

4.6.2 Tricarbonyl (1-4-η-5-exo-N-X,X-dimethylpyridino-cyclohexa-1,3-diene) iron complexes

The calculated vibrational frequencies of the complexes are shown in Table 4.24. According to group representation theory in Chemistry, we can deduce that there are 105 vibrational modes for the pyridino- and methylpyridinoderivatives. Among these normal modes, the strongest infra-red absorption peaks and their intensities are displayed in Plate 4.7 in appendix 3.The simulated IR spectra of the derivatives are calculated by replacing one of its Hydrogen with methyl group. On replacing the hydrogen with methyl group, the total vibrations increase from 87 to 105.

Table 4.24: Vibrational frequencies and intensities forTricarbonyl (1-4-η-5-exo-N-X,X-dimethylpyridino-cyclohexa-1,3-diene) iron complexes

Bond.	Frequency/ cm^{-1}	Intensity/$kMmol^{-1}$
N-C_7	1272	3723
N=C_{11}	1727	6384
C≡ O	2123	1630
	2176	1301
	2244	1261
N-C_7	1270	2595
N=C_{11}	1713	6849
C2-O_1	1757	3938
C≡ O	2120	1572
	2175	1295
	2245	1266
N-C_7	1285	3906

$N=C_{11}$	1734	1307
C_9-C_{10}	1746	4193
C≡ O	2122	1640
	2175	1306
	2244	1286
N-C_7	1298	3667
$N=C_{11}$	1718	5700
C_7-C_8	1750	1374
C≡ O	2122	1638
	2174	1307
	2244	1285

4.6.3 Tricarbonyl (1-4-η-5-exo-N-X-pyridino-2-methoxycyclohexa-1,3-diene) iron complexes

According to group representation theory in Chemistry, we can deduce that, there are99 and 108 vibrational modes, for the pyridino- and methylpyridino-derivatives.Among these normal modes, the strongest infra-red absorption peaks and theirintensities are displayed in Table 4.25and in appendix 3, Plate 4.9. The simulated IR spectra of the derivatives are calculated by replacing one of its Hydrogen with methyl group. On replacing thehydrogen with methyl group, the total vibrations increase from 99 to 108.

Table 4.25: Vibrational frequencies and intensities forTricarbonyl (1-4-η-5-exo-N-X-pyridino-2-methoxycyclohexa-1,3-diene) iron complexes

X-pyridino/assigned peaks.	Bond	Frequency/ cm^{-1}	Intensity/$kMmol^{-1}$
H	N-C_7	1272	3723
	N=C_{11}	1727	6384
	C≡ O	2123	1630
		2176	1301
		2244	1261
2-Me	N-C_7	1270	2595
	N=C_{11}	1713	6849
	C2-O_1	1757	3938
	C≡ O	2120	1572
		2175	1295
		2245	1266

3-Me	N-C_7	1285	3906
	N=C_{11}	1734	1307
	C_9-C_{10}	1746	4193
	C≡ O	2122	1640
		2175	1306
		2244	1286
4-Me	N-C_7	1298	3667
	N=C_{11}	1718	5700
	C_7-C_8	1750	1374
	C≡ O	2122	1638
		2174	1307
		2244	1285

4.6.4 Tricarbonyl (1-4-η-5-exo-N-X,X-dimethylpyridino-2-methoxycyclohexa-1,3-diene) iron complexes

The calculated vibrational frequencies of X,X-dimethylpyridino-1-4-η-2-methoxycyclo-hexa-1,3-diene irontricarbonyl complexes are shown in appendix 3, Plate 4.10. There are 117 types of vibrational modes, according to group representation theory in chemistry, among these A modes of vibration, there are six strongest infra-red absorption peaks. The infra-red absorption bands and intensities are listed in Table 4.26. There are no experimental or other theoretical values for comparison.

Table 4.26: Vibrational frequencies and intensities for Tricarbonyl (1-4-η-5-exo-N-X, X-dimethylpyridino-2-methoxycyclohexa-1,3-diene) iron complexes

Structure, X, X-	Vibrating bond	Infra-red band/cm^{-1}	Intensity/$kMmol^{-1}$
2, 3-dimethyl-	$C_7 - C_8$	1250	2787
	$C_8 - C_{17}$	1291	1001
	$C_7 - C_{16}$	1578	1348
	$N - C_7$	1723	4291
	$N - C_{11}$	1750	5238
	$C \equiv O$	2120	1616
		2175	1283
		2244	1290
2, 4-dimethyl-	$C_9 - C_{10}$	1285	2913
	$N - C_7$	1709	7190
	$N - C_{11}$	1764	3243
	$C \equiv O$	2120	1582

		2175	1298
		2243	1293
2, 5-dimethyl-	$C_7 – C_8$	1290	3970
	$C_7 – C_{16}$	1608	1377
	$N – C_7$	1722	1890
	$N – C_{11}$	1763	5188
	$C \equiv O$	2119	1595
		2175	1311
		2243	1265
2, 6-dimethyl-	$C_7 – C_8$	1296	3472
	$N – C_7$	1724	12508
	$N – C_{11}$	1753	1301
	$C \equiv O$	2117	1507
		2175	1287

		2244	1250
3, 4-dimethyl-	$C_8 – C_9$	1302	2960
	$C_7 – C_{16}$	1538	1003
	$N – C_7$	1726	3854
	$N – C_{11}$	1745	1930
	$C \equiv O$	2121	1650
		2173	1306
		2244	1309
3, 5-dimethyl-	$C_7 – C_8$	1298	3662
	$N – C_{11}$	1760	4146
	$C \equiv O$	2122	1652
		2174	1302
		2244	1303

4.6.5 Tricarbonyl (1-4-η-5-exo-N-X-aminopyridino-cyclohexa-1,3-diene) iron complexes

There are 93 A type vibrational modes for these new aminopyridino organometallics. The vibrational modes change with the replacement of the hydrogen atom with methyl groups on the amino group, the vibrational modes increase to 102, with the hydrogen atoms completely replaced by methyl groups, the vibrational modes rose to 111. Among these normal modes, the strongest infra-red absorption peaks and their intensities are shown in Table 4.27 while the simulated infra-red spectra of these complexes are shown in appendix 3, Figure 4.7.

Table 4.27: Vibrational frequencies and intensities for Tricarbonyl (1-4-η-5-exo-N-X-aminopyridino-cyclohexa-1,3-diene) iron complexes

Structure	Vibrating bond	Infra-red band/ cm^{-1}	Intensity/$kMmol^{-1}$
2-NH_2	$C_5 – N_1$	1474	2721
	$C_7 – N_2$	1585	1721
	$C_8 – C_9$	1691	17658
	$C_{10} – C_{11}$	1784	1582
	$N_2 – H$, C≡ O	2129	2246
	C≡ O	2184	5951
	C≡ O	2192	3670
	$N_2 – H$	2307	1750
3-NH_2	$C_{11} – N_1$	1330	3015
	$C_8 – C_9$	1738	1978
	C≡ O	2106	1661
	C≡ O	2171	1217
	C≡ O	2241	1078
4-NH_2	$C_{11} – N_1$	1357	1616
	$C_{10} –C_{11}$	1561	2060

	$C_8 – C_9$	1682	10119
	$C_7 – C_8$	1735	1857
	C≡ O	2103	1728
	C≡ O	2169	1310
	C≡ O	2239	1204
	C_7 – H	2754	1219
4-NH(CH_3)	$C_{10} – C_{11}$	1568	2322
	$C_9 – N_2$	1626	1117
	$C_9 – C_{10}$	1676	11151
	$C_7 – C_8$	1734	1771
	C≡ O	2102	1739
	C≡ O	2168	1323
	C≡ O	2238	1208
	C_7 – H	2756	1310
4-N(CH_3)$_2$	$C_{11} – N_1$	1360	1567
	$C_{10} – C_{11}$	1571	1990
	$C_9 – C_8$	1663	12085

$C_7 – C_8$	1734	1835
C≡ O	2101	1742
C≡ O	2167	1329
C≡ O	2238	1210
$C_7 – H$	2763	1278

4.6.6Tricarbonyl (1-4-η-5-exo-N-X-aminopyridino-2-methoxycyclohexa-1,3-diene) iron complexes

By using group representation theory in Chemistry, there are 105 A types' vibrational modes for these new aminopyridino organometallics.The vibrational modes change with the replacement of the hydrogen atoms by methyl and methoxy groups on the pyridine moiety and cyclohexa-1,3-diene ring respectively, these vibrational modes increase to 114, when one of the hydrogen on the amino group is replaced by a methyl group. The vibrational modes further rose to 123 on replacing the two hydrogen atoms on the amino group with methyl groups. Among these normal modes, the strongest infra-red absorption peaks and their intensities are shown in Table 4.28, while the simulated infra-red spectra of these complexes are shown in appendix 3, Figure 4.8.

Table 4.28: Vibrational frequencies and intensities for simulated Tricarbonyl (1-4-η-5-exo-N-X-aminopyridino-2-methoxycyclohexa-1,3-diene) iron complexes

Structure X	Vibrating bond	Infra-red band/ cm^{-1}	Intensity/$kMmol^{-1}$
2-NH_2	$C_5 - N$	1474	2583
	$C_7 - N$	1585	1914
	$C_9 - C_{10}$	1690	17707
	$C_8 - C_9$	1785	1355
	N_2-H& C≡O	2111	5676
	N_2-H& C≡O	2159	5890
	C≡O	2190	1844
3-NH_2	N_1-C_7&$C_8 - C_9$	1333	2842
	$C_9 - C_{10}$	1738	1883
	C≡O	2106	1656
	C≡O	2177	1085
	C≡O	2247	1094
4-NH_2	N_1– C_7& C_8 – C_9	1351	2167
	$C_7 - C_8$	1557	2264
	$C_{10} - C_{11}$	1735	1884
	C≡O	2099	1638

	C≡O	2178	1110
	C≡O	2246	1230
	C_7 – H	2803	1048
4-NH(CH_3)	C_{10} –C_{11}	1563	2629
	C_9 – N_2	1626	1129
	C_9 – C_{10}	1677	12093
	C_7 – C_8	1734	1786
	C≡O	2098	1630
	C≡O	2178	1109
	C≡O	2245	1241
	C_7 – H	2816	1100
4-N(CH_3)$_2$	N_1 – C_7	1355	1623
	C_7 – C_8	1568	2200
	C_8 –C_9	1663	12893
	C_{10} – C_{11}	1734	1861
	C≡O	2098	1665
	C≡O	2176	1121
	C≡O	2244	1245
	C_7 – H	2813	1115

4.7 Infra-red Spectroscopic Studies using DFT: Vibrational analysis

4.7.1 Vibrational analysis of Tricarbonyl (1-4-η-5-exo-N-X-methylpyridino-cyclohexa-1,3-diene) iron complexes

There is no obvious deviation in optimized geometries for the Tricarbonyl (1-4-η-5-exo-N-Substituted pyridino-2-cyclohexa-1,3-diene) iron complexes.We present the calculated vibrational frequencies from gas phase infra-red spectra of the complexes without any scale factor. The absence of any imaginary frequency indicates that all the optimized structures correspond to the minimum point on the intermolecular potential energy surface. Analysis of the calculated vibrational frequencies of all the complexes shows no large deviation. We observed that the complexes have very sharp peaks between 2111 cm^{-1} – 2171 cm^{-1} corresponding to the stretching vibrations of the C≡O bond. It is clearly seen that these groups have corresponding IR signatures which are expected to provide useful information for further studies. Our theoretical vibrational frequencies agree with the experimental values(Odiaka, 1980; Odiaka and Okogun, 1985; Odiaka, 1988a, 1988b; Odiaka *et al*., 2007, 2011).

4.7.2 Vibrational analysis of Tricarbonyl (1-4-η-5-exo-N-X,X-dimethylpyridino-cyclohexa-1,3-diene) iron complexes

Analysis of the calculated vibrational frequencies of the six complexes shows no large deviation. We observed that the complexes have very sharp peak between 2103cm^{-1}–2170cm^{-1} corresponding to the stretching vibration of the C≡O bond. It is clearly seen that these groups have corresponding IR signatures which are expected to provide useful information for further studies.

4.7.3 Vibrational analysis of Tricarbonyl (1-4-η-5-exo-N-X-pyridino-2-methoxy-cyclohexa-1,3-diene) iron complexes

There are 99 and 108 A normal modes of vibration for the pyridino- and the methylpyridino-1-4-η-2-methoxycyclohexa-1,3-diene irontricarbonyl complexes. There is no obvious deviation in optimized geometries for the methylpyridino-1-4-η-2-

methoxycyclohexa-1,3-diene irontricarbonyl complexes. We present the calculated vibrational frequencies from gas phase infra-red spectra of the complexes without any scale factor. The absence of any imaginary frequency indicates that all the optimized structures correspond to the minimum point on the intramolecular potential energy surface. Analysis of the calculated vibrational frequencies of the four complexes shows no large deviation. The complexes have very sharp strong peak between 2108 cm^{-1} – 2165 cm^{-1}corresponding to the stretching vibration of the C≡O bond. It is clearly seen that these groups have corresponding IR signatures which are expected to provide useful information for further studies. Our theoretical vibrational frequencies are in good agreement with the available experimental values.

4.7.4 Vibrational analysis of Tricarbonyl (1-4-η-5-exo-N-X,X-dimethylpyridino-2-methoxycyclohexa-1,3-diene) iron complexes

Analysis of the calculated vibrational frequencies of the six complexes shows no large deviation, the complexes have very sharp peaks between 2102$cm^{-1}$and 2163cm^{-1} corresponding to the stretching vibration of the C≡O bond. The spectra of these complexes are presented in appendix 4, Figures 4.9 to 4.14.

4.8 Electronic States of the complexes using DFT

4.8.1 Tricarbonyl (1-4-η-5-exo-N-pyridino-cyclohexa-1,3-diene) iron complexes

The HOMO and LUMO densities are all over the cyclohexa-1,3-diene and pyridine and the methylpyridino moiety respectively. This gives an insight into the reactivity of the molecules. The HOMO and LUMO energies are given in Table 4.29a.

Reactivity parameters

All the calculated reactivity parameters are based on the values of the chemical potential, μ, and the global chemical hardness, η. they were calculated using finite difference and the frozen orbital approximations, which yield them in terms of the highest occupied molecular orbital energy, E_H, and the lowest unoccupied molecular orbital energy, E_L.

The validity of the Koopman's theorem within the DFT approximation is still controversial. However, it has been shown that, the Kohn Sham orbitals may differ in shape and energy from the Hartree-Fock orbitals and the combination of the two produces conceptual DFT reactivity descriptors that correlate quite well with the reactivity descriptors obtained through Hartree-Fock calculations. Thus, it is worth calculating the electronegativity, global hardness and global electrophilicity index for these complexes using both approximations in order to verify the quality of the procedures, Since the Self Consistent Field (SCF) model used in our calculations is restricted Hybrid HF-DFT SCF calculation were performed using Pulay Direct Inversion Iteration Substrate (DIIS) + Geometric Direct Minimization. The combination of the two theories produces a result which is expected to further validate Koopman's theorem. The results for the vertical ionization energies and electron affinities of these complexes were obtained through energy difference between the ionized and neutral state; calculated from the geometry of the molecule are listed and reported in Table 4.29b while the calculated values of the electronegativity, global hardness and global electrophilicity using I and A are also listed in Table 4.29b.

Using the HOMO and LUMO energies within the Koopman's theorem, the corresponding reactivity global indexes are also listed in Table 4.29b.

Although, the Hartree –Fock model could not successfully complete the calculations, but a mixture of Hartree-Fork and Density Functional Theory (HF-DFT) self consistent force field (SCF) procedure produces excellent result for these group of complexes. We may therefore conclude that, for these complexes we have been able to predict with qualitative accuracy, the DFT reactivity indices calculated through HOMO and LUMO energies as well as from the I and A obtained through energy differences. The orbital energy diagram showing HOMO and LUMO values shown in appendix 2, Figure (4.1).

From the present calculation, the total energy, the total dipole moment and the isotropic polarizability of the ground state with the DFT B3LYP basis set listed in Table 4.29a. The results for the dipole moment and polarizability may be an indication of solubility and

chemical reactivities for its synthesis and potential application in the synthesis of new derivatives.

Table 4.29: Electronic and reactivity parameters for Tricarbonyl (1-4-η-5-exo-N-X-pyridino-cyclohexa-1,3-diene) iron complexes

Table 4.29a: Electronic properties ofTricarbonyl (1-4-η-5-exo-N-X-pyridino-cyclohexa-1,3-diene) iron complexes

X	Total energy (a.u)	Dipole moment (debye)	E_{HOMO} (eV)	E_{LUMO} (eV)	Band Gap (eV)	Polarizability (eV)
H	-2084.56	12.21	-9.60	-6.14	3.46	62.12
2-Me	-2123.90	11.38	-9.56	-5.92	3.64	63.49
3-Me	-2123.90	11.74	-9.52	-5.96	3.56	63.58
4-Me	-2123.90	12.03	-9.49	-5.87	3.62	63.57

Table 4.29b: Reactivity global indexes of the structure of substituted Tricarbonyl (1-4-η-5-exo-N-X-pyridino-cyclohexa-1,3-diene) iron complexes**.**{I = ionization potential, A = electron affinity, μ = chemical potential, η = global chemical hardness, χ = electronegativity and ω = electrophilicity index}

X	I/eV	A/eV	μ/eV	η/eV	ω/eV
H	9.60	6.14	-7.87	1.73	17.90
2-Me	9.56	5.92	-7.74	1.82	16.37
3-Me	9.52	5.96	-7.74	1.78	16.83

4-Me	9.49	5.87	-7.69	1.81	16.34

4.8.2 Tricarbonyl (1-4-η-5-exo-N-X,X-dimthylpyridino-cyclohexa-1,3-diene) iron complexes

Theoretically the HOMO and LUMO energies are calculated using DFT B3LYP (6-31G(D)). These calculations however, do not have solid-state packing effect and aqueous state is not taken into consideration. The HOMO and LUMO densities are all over the cyclohexa-1,3-diene and dimethylpyridino moiety respectively, thus giving an insight into the reactivity of the complexes. The HOMO and LUMO energies together with calculated energy band gap are shown in Table 4.30a. The orbital energy diagrams are displayed in Figure4.2 (appendix 2).

Reactivity parameters

All the calculated reactivity parameters are based on the values of the chemical potential, μ, and the global chemical hardness, η. they were calculated using finite difference and the frozen orbital approximations, which yield them in terms of the highest occupied molecular orbital energy E_H, and the lowest unoccupied molecular orbital energy E_L. The validity of the Koopman's theorem within the DFT approximation is still controversial. However, it has been shown that, the Kohn Sham orbitals may differ in shape and energy from the Hartree-Fock orbitals; the combination of the two produces conceptual DFT reactivity descriptors that correlate quite well with the reactivity descriptors obtained from the combination of these two theories i.e Hartree-Fock and Density Functional theory. Thus, it is expedient to calculate the electronegativity, global hardness and global electrophilicity index for these complexes using both approximations in order to verify the quality of the procedures. Since the SCF model used in our calculations is a restricted hybrid HF-DFT self consistent field (SCF), calculations were performed using Pulay DIIS + Geometric Direct Minimization the combination of the two theories produces a result which further revalidates Koopman's theorem. The results for the vertical ionization energies and electron affinities of these complexes obtained through energy difference between the ionized and neutral state, calculated from the optimized geometry of the

molecule are listed and collected in Table 4.30b while the values of the electronegativity, global hardness and global electrophilicity are calculated using I and A are also listed in Table 4.30b.

Table 4.30: Electronic and reactivity parameters for Tricarbonyl (1-4-η-5-exo-N-X,X-dimethylpyridino-cyclohexa-1,3-diene) iron complexes

Table 4.30a: Total energy, Dipole moment, Polarizability and Energy band gaps for Tricarbonyl (1-4-η-5-exo-N-X,X-dimethylpyridino-cyclohexa-1,3-diene) iron complexes

X,X-diMethyl	Total Energy/ a.u	Dipole moment/D	E_{HOMO}/ eV	E_{LUMO}/ eV	Energy band gap/eV	Polarizability
2,3-	-2163.21	10.83	-9.51	-5.72	3.89	64.89
2,4-	-2163.20	11.21	-9.47	-5.65	3.82	64.93
2,5-	-2163.21	10.96	-9.49	-5.79	3.70	64.96
2,6-	-2163.20	10.61	-9.50	-5.78	3.72	64.83
3,4-	-2163.21	11.54	-9.44	-5.69	3.75	64.99
3,5-	-2163.21	11.26	-9.64	-5.82	3.82	65.04

Table 4.30b: Reactivity global indexes of Tricarbonyl (1-4-η-5-exo-N-X,X-dimethyl pyridino-cyclohexa-1,3-diene) iron complexes

$X,X(Me)_2$	I/eV	A/eV	μ/eV	η/eV	ω/eV
2,3-	9.51	5.72	-7.62	1.95	14.89
2,4-	9.47	5.65	-7.56	1.91	14.96
2,5-	9.49	5.79	-7.64	1.85	15.80
2,6-	9.50	5.78	-7.64	1.86	15.69
3,4-	9.44	5.69	-7.57	1.88	15.28
3,5-	9.64	5.82	-7.73	1.91	15.64

4.8.3 Tricarbonyl (1-4-η-5-exo-N-X-pyridino-2-methoxycyclohexa-1,3-diene) iron complexes

It is expedient to visualize the HOMO and LUMO of these new organometallic compounds because the relative ordering of occupied and virtual orbital provide a reasonable qualitative indication of both ground and excited state properties.The HOMO of these complexes possesses a π-bonding character within the subunit and π-antibonding character excited state properties between the consecutive subunits. On the other hand, the LUMO possesses a π -antibonding character within thesubunit and a π-bonding character between the subunits.In practice, the HOMO and LUMO energies are obtained from an empirical formula based on the onset of oxidation-reduction of peaks measured by cyclic voltametry.Theoretically, the HOMO and LUMO energies are calculated using DFT B3LYP (6-31G(D)). These calculations however, do not have solid-state packing effect and aqueous state is not taken into consideration. The HOMO and LUMO densities are all over the cyclohexa-1,3-diene and methylpyridino moiety respectively, thus giving an insight into the reactivity of these complexes. The HOMO and LUMO energies together with calculated energy band gap are collected in Table 4.31a. The HOMO and LUMO energy diagrams and the orbital energy diagram are shown in Plate4.3, appendix 1 and Figure 4.3 in appendix 2respectively.

Reactivity parameters

All the calculated reactivity parameters are based on the values of the chemical potential, μ, and the global chemical hardness, η. they were calculated using finite difference and the frozen orbital approximations, which yield them in terms of the highest occupied molecular orbital energy, E_H, and the lowest unoccupied molecular orbital energy, E_L. The validity of the Koopman's theorem within the DFT approximation is still controversial. However, it has been shown that, the Kohn Sham orbitals may differ in shape and energy from the Hartree-Fock orbitals. The combination of the two produces conceptual DFT reactivity descriptors that correlate quite well with the reactivity descriptors obtained

through Hartree-Fock calculations. Thus, it is expedient to calculate the electronegativity, global hardness and global electrophilicity index for these complexes using both approximations in order to verify the quality of the procedures, Since the SCF model used in our calculations is a restricted hybrid HF-DFT-SCF calculations were performed using Pulay DIIS + Geometric Direct Minimization. The combination of the two theories produces a result which further revalidates Koopman's theorem. The results for the vertical ionization energies and electron affinities of these complexes obtained through energy difference between the ionized and neutral state, calculated from the optimized geometry of the molecule are listed and collected in Table 4.31b while the calculated values of the electronegativity, global hardness and global electrophilicity using I and A are also listed in Table 4.31b

Table 4.31: Electronic and Reactivity parameters for Tricarbonyl (1-4-η-5-exo-N-X-pyridino-2-methoxycyclohexa-1,3-diene) iron complexes

Table 4.31a: Electronic properties ofTricarbonyl (1-4-η-5-exo-N-X-pyridino-2-methoxy cyclohexa-1,3-diene) iron complexes

X	Total energy/ a.u	Dipole moment/D	E_{HOMO}/eV	E_{LUMO}/eV	Eg/eV	Polarizability
H	-2199.09	12.48	-9.33	-6.06	3.27	64.39
2-Me	-2138.41	11.73	-9.28	-5.83	3.45	65.75
3-Me	-2138.31	12.11	-9.24	-5.90	3.34	65.85
4-Me	-2138.41	12.37	-9.23	-5.79	3.44	65.82

Table 4.31b: Reactivity global indexes of Tricarbonyl (1-4-η-5-exo-N-X-pyridino-2-methoxycyclohexa-1,3-diene) iron complexes

Substituent	I/eV	A/eV	μ/eV	η/eV	ω/eV
H	9.33	6.06	-7.70	1.64	18.08
2-Me	9.28	5.83	-7.56	1.73	16.56
3-Me	9.24	5.90	-7.57	1.67	17.16
4-Me	9.23	5.79	-7.51	1.72	16.40

4.8.4 Electronic properties of Tricarbonyl (1-4-η-5-exo-N-X,X-dimethylpyridino-2-methoxycyclohexa-1,3-diene) iron complexes

The relative ordering of occupied and virtual orbital provide a reasonable qualitative indication of both ground and excited state properties.The HOMO of these complexes possesses a π-bonding character within the subunit and π-antibonding character excited state properties between the consecutive subunits. On the other hand, the LUMO possesses a π -antibonding character within the subunit and a π-bonding character between the subunits. In practice, the HOMO and LUMO energies are obtained from an empirical formula based on the onset of oxidation-reduction of peaks measured by cyclic voltametry. Theoretically, the HOMO and LUMO energies are calculated using DFT B3LYP (6-31G(D)). These calculations however, do not have solid-state packing effect and aqueous state is not taken into consideration. The HOMO and LUMO densities are all over the cyclohexa-1,3-diene and dimethylpyridino moiety respectively, thus giving an insight into the reactivity of these complexes. The HOMO and LUMO energies together with calculated energy band gaps are collected in Table 4.32a. The HOMO and LUMO energy diagrams and the energy band diagrams are displayed in Plate 4.4 (appendix 1) and Figure 4.4(appendix 2) respectively.

Reactivity parameters

All the calculated reactivity parameters are based on the values of the chemical potential, μ, and the global chemical hardness, η. They were calculated using finite difference and the frozen orbital approximations, which yields them in terms of the highest occupied molecular orbital energy, E_H, and the lowest unoccupied molecular orbital energy, E_L. The validity of the Koopman's theorem within the DFT approximation is still controversial. However, it has been shown that, the Kohn Sham orbitals may differ in shape and energy from the Hartree-Fock orbitals. The combination of the two produces conceptual DFT reactivity descriptors that correlate quite well with the reactivity descriptors obtained

through Hartree-Fock calculations, thus, it is expedient to calculate the electronegativity, global hardness and global electrophilicity index for these complexes using both approximations in order to verify the quality of the procedures. Since the SCF model used in our calculations is a restricted hybrid HF-DFT self consistent field (SCF), calculations were performed using Pulay DIIS + Geometric Direct Minimization. The combination of the two theories produces a result which further revalidates Koopman's theorem. The results for the vertical ionization energies and electron affinities of these complexes obtained through energy difference between the ionized and neutral state, calculated from the optimized geometry of the molecule are listed and collected in Table 4.32b while the values of the electronegativity, global hardness and global electrophilicity are calculated using I and A as shown in Table 4.32b.

Table 4.32: Electronic and Reactivity parameters for Tricarbonyl (1-4-η-5-exo-N-X,X-dimethylpyridino-2-methoxycyclohexa-1,3-diene) iron complexes

Table 4.32a: Total energy, Dipole moment, Polarizability and Energy band gaps for Tricarbonyl (1-4-η-5-exo-N-X,X-dimethylpyridino-2-methoxycyclohexa-1,3-diene) iron complexes

X,X-$(Me)_2$	Total Energy/ a.u	Dipole moment/D	EHOMO/ eV	ELUMO/ eV	Band gap/eV	Polarizability
2,3-	-2277.73	11.26	-9.21	-5.65	3.56	67.16
2,4-	-2277.73	11.62	-9.20	-5.58	3.58	67.19
2,5-	-2277.73	11.33	-9.22	-5.71	3.51	67.22
2,6-	-2277.73	11.02	-9.20	-5.72	3.48	67.10
3,4-	-2277.73	11.64	-9.20	-5.75	3.45	67.30
3,5-	-2277.73	11.64	-9.20	-5.75	3.45	67.30

Table 4.32b: Reactivity global indexes of Tricarbonyl (1-4-η-5-exo-N-X,X-dimethylpyridino-2-methoxycyclohexa-1,3-diene) iron complexes

X,X-$(Me)_2$	I/eV	A/eV	μ/eV	η/eV	ω/eV
2,3-	9.21	5.65	-7.43	1.78	15.51
2,4-	9.20	5.58	-7.39	1.79	15.26
2,5-	9.22	5.71	-7.47	1.76	15.90
2,6-	9.20	5.72	-7.46	1.74	15.99

3,4-	9.20	5.75	-7.48	1.73	16.22
3,5-	9.20	5.75	-7.48	1.73	16.22

4.8.5 Tricarbonyl (1-4-η-5-exo-N-X-aminopyridino-cyclohexa-1,3-diene) iron complexes

It is expedient to visualize the HOMO and LUMO of these new organometallic compounds because the relative ordering of occupied and virtual orbital provide a qualitative indication of both ground and exited state properties. The HOMO of these complexes possesses a π-bonding character within the subunit and π-antibonding character exited state properties between the consecutive subunits. On the other hand, the LUMO possesses a π-antibonding character within the subunit and π-bonding character between the subunits. In practice, the HOMO and LUMO energies are calculated using DFT B3LYP, 6-31(D). These calculations however, do not have solid-state packing effect and aqueous state is not taken into consideration. The HOMO and LUMO densities are all over the cyclohexa-1,3-diene irontricarbonyl and aminopyridino moiety respectively, thus giving an insight into the reactivity of these complexes. The HOMO and LUMO energies together with calculated energy band gap are collected and shown in Table 4.33awhile the reactivity indices are listed in Table 4.33b. The HOMO and LUMO energy diagrams and the energy band diagrams are displayed in Plate 4.5 and Figure 4.5 respectively.

Table 4.33: Electronic and Reactivity parameters for Tricarbonyl (1-4-η-5-exo-N-X-aminopyridino-cyclohexa-1,3-diene) iron complexes

Table 4.33a: Electronic properties of Tricarbonyl (1-4-η-5-exo-N-X-aminopyridino-cyclohexa-1,3-diene) iron complexes

X-pyridino-	Total energy/ a.u	Dipole moment/debye	E_{HOMO}/eV	E_{LUMO}/eV	Eg/eV	Polarizability
2-NH_2	-2139.92	8.76	-9.80	-5.43	4.37	62.60
3-NH_2	-2139.92	9.64	-9.61	-5.70	3.91	65.06
4-NH_2	-2139.94	12.50	-9.43	-5.11	4.32	62.70
4-$NH(CH_3)$	-2179.25	11.79	-9.37	-4.96	4.41	64.32
4-$N(CH_3)_2$	-2218.56	11.30	-9.32	-4.88	4.44	65.85

Table 4.33b: Reactivity global indexes of Tricarbonyl (1-4-η-5-exo-N-X-aminopyridino-cyclohexa-1,3-diene) iron complexes.{I = ionization energy, A = electron affinity, μ = chemical potential, η = global chemical hardness, and, ω = electrophilicity index}

X	I/eV	A/eV	μ/eV	η/eV	ω/eV
2-NH_2	9,80	5.43	-7.62	2.19	13.26
3-NH_2	9.61	5.70	-7.66	1.96	14.97

4-NH_2	9.43	5.11	-7.27	2.16	12.24
4-$NH(CH_3)$	9.37	4.96	-7.17	2.21	11.63
4-$N(CH_3)_2$	9.32	4.88	-7.10	2.22	11.35

4.8.6 Tricarbonyl (1-4-η-5-exo-N-X-aminopyridino-2-methoxycyclohexa-1,3-diene) iron complexes

It is expedient to visualize the HOMO and LUMO of these new organometallic compounds because the relative ordering of occupied and virtual orbital provide a reasonable qualitative indication of both ground and excited state properties. The HOMO of these complexes possesses a π-bonding character within the subunit and π-antibonding character excited state properties between the consecutive subunits. On the other hand, the LUMO possesses a π -antibonding character within thesubunit and a π-bonding character between the subunits. In practice, the HOMO and LUMO energies are obtained from an empirical formula based on the onset of oxidation-reduction of peaks measured by cyclic voltametry. Theoretically, the HOMO and LUMO energies are calculated using DFT B3LYP (6-31G(D)). These calculations however, do not have solid-state packing effect and aqueous state is not taken into consideration. The HOMO and LUMO densities are all over the 2-methoxycyclohexa-1,3-diene and aminopyridino moiety respectively, thus giving an insight into the reactivity of these complexes. The HOMO and LUMO energies together with calculated energy band gaps are collected in Table 4.34a while the reactivity indices are listed in Table 4.34b. The HOMO and LUMO energy diagrams and orbital energy diagrams are displayed in Plate 4.6 and Figure 4.6 respectively.

Table 4.34: Electronic and Reactivity parameters for Tricarbonyl (1-4-η-5-exo-N-X-aminopyridino-2-methoxycyclohexa-1,3-diene) iron complexes

Table 4.34a: Total energy, Dipole moment, Polarizability and Energy band gaps for Tricarbonyl (1-4-η-5-exo-N-X-aminopyridino-2-methoxycyclohexa-1,3-diene) iron complexes

X-pyridino	Total energy/ a.u	Dipole moment/ D	Polarizability	E_{HOMO}/eV	E_{LUMO}/eV	Eg/eV
2-NH_2	-2254.45	9.25	64.86	-9.56	-5.34	4.22
3-NH_2	-2254.45	10.20	65.06	-9.32	-5.62	3.70
4-NH_2	-2254.46	13.23	64.96	-9.16	-5.04	4.12
4-NH(CH_3)	-2293.77	12.55	66.58	-9.10	-4.89	4.21
4-N(CH_3)$_2$	-2333.08	11.82	68.10	-9.06	-4.81	4.25

Table 4.34b: Reactivity global indexes of Tricarbonyl (1-4-η-5-exo-N-X-aminopyridino-2-methoxycyclohexa-1,3-diene) iron complexes

X-pyridino	I/Ev	A/eV	μ/eV	χ/eV	η/eV	ω/eV
2-NH_2	9.56	5.34	-7.45	7.45	2.11	13.15
3-NH_2	9.32	5.62	-7.47	7.47	1.85	15.08

4-NH_2	9.16	5.04	-7.10	7.10	2.06	12.24
4-$NH(CH_3)$	9.10	4.89	-7.00	7.00	2.06	11.92
4-$N(CH_3)_2$	9.06	4.81	-6.94	6.94	2.08	11.61

4.9 Neutron magnetic resonance (N.m.r) spectroscopic studies of the complexes

4.9.1 Tricarbonyl (1-4-η-5-exo-N-X-pyridino-cyclohexa-1,3-diene) iron complexes

The ^{1}H, ^{13}C and ^{15}N NMR spectra of these complexes were analysed using Spartan '10 programme software. These complexes show well separated overlapping multiplets characteristics of the outer H^1 and H^4 and inner H^2 and H^3 -diene protons. The endo H^6 and exo H^6 protons appeared as shown in the Tables 4.35-4.45 and the spectra are displayed in Figures 4.15a. The H^5 proton adjacent to the N-methylpyridino substituent is shifted downfield. For instance, with the Tricarbonyl (1-4-η-5-exo-N-pyridino-cyclohexa-1,3-diene) iron complex, the Aromatic protons of the pyridine group appear as triplets and doublets while the methylene protons appeared as singlet between 2.18-2.90. These values are characteristic features of the 1,3-diene derivatives (Odiaka and Okogun, 1985; Odiaka, 1988a, 1988b; Odiaka *et al*., 2007). The ^{13}C chemical shifts calculated at the DFT B3LYP levels of theory with 6-31G(D) basis set are presented in Table 4.35 and 4.36 while the spectra are shown in Figure 4.15. The C_1, C_4 and C_6atoms appeared at 47.65,50.83 and 37.23ppm respectively, while the chemical shifts of C_2, C_3 and C_5 appeared at 85.91, 80.80 and79.08ppm correspondingly. All the Aromatic carbons of the pyridine $C_7 - C_{11}$ appeared at 120 – 157.20ppm while Carbonyl carbon due to the presence of oxygen and iron are deshielded and consequently have higher chemical shifts at 208-216ppm. However, the methylene carbon appeared in the range 19-23ppm. There are no experimental values for ^{13}C but ^{1}H NMR values agrees with available experimental values

(Odiaka and Okogun, 1985; Odiaka, 1988a, 1988b; Odiaka *et al*., 2007, 2011). The aromatic carbon to which the methylene carbon is attached is shifted downfield due to the electron releasing ability of the methyl substituent.

Table 4.35: ^{1}H N.m.r Chemical shifts (ppm) ofTricarbonyl (1-4-η-5-exo-N-X-pyridino-cyclohexa-1,3-diene) iron complexes

Proton	H	2-Me	3-Me	4-Me
H_1	2.71	2.59	2.57	2.68
H_2	5.80	5.78	5.79	5.76
H_3	5.57	5.70	5.65	5.55
H_4	2.35	2.20	2.28	2.32
H_5	4.80	5.16	4.85	4.70
H_{6exo}	2.97	2.70	2.75	2.95
$H_{6\ endo}$	1.74	1.32	1.51	1.70
H_7	8.13	-	7.80	7.90
H_8	7.81	7.62	-	7.51
H_9	8.39	8.20	8.21	-
H_{10}	7.93	7.75	7.82	7.63
H_{11}	8.61	8.68	8.41	8.30
CH_3	-	2.52-2.90	2.18-2.81	2.58-2.87

Table 4.36: **^{13}C N.m.r Chemical shifts (ppm) ofTricarbonyl (1-4-η-5-exo-N-X-pyridino-cyclohexa-1,3-diene) iron complexes**

Carbon	H	2-Me	3-Me	4-Me
C_1	47.65	45.85	46.22	47.80
C_2	85.91	85.63	85.71	85.55
C_3	80.80	81.97	81.57	80.73
C_4	50.83	47.72	48.24	50.48
C_5	79.08	71.05	78.22	77.30
C_6	37.23	32.92	36.08	37.07
C_7	136.21	148.95	135.80	132.42
C_8	122.38	124.70	137.39	122.79
C_9	139.76	138.71	140.40	157.19
C_{10}	123.07	120.34	122.23	123.72
C_{11}	133.89	134.01	130.40	132.46
C_{12}	214.69	215.38	215.14	214.85
C_{13}	208.61	208.67	208.74	208.71

C_{14}	208.16	208.42	208.39	208.45
C_{15}	-	20.25	19.01	22.33
^{15}N	-138.54	-143.89	-141.77	-147.24

4.9.2 Tricarbonyl (1-4-η-5-exo-N-X,X-dimethylpyridino-cyclohexa-1,3-diene) iron complexes

The complexes showed well separated overlapping multiplets characteristics of the outer H^1 and H^4 and inner H^3-diene protons. The endo H^6 and exo H^6all appeared as shown in Table 4.37 and displayed in Figure 4.16a. The H^5 proton adjacent to the N-methylpyridino substituent is shifted downfield. For instance, with the pyridino-1-4-η-cyclohexa-1,3-diene complex, the Aromatic protons of the pyridine group appear as triplets and doublets while the methylene protons appeared as singlet between 2.35-2.81ppm. These values are characteristic features of the 1,3-diene derivatives. The ^{13}C chemical shifts calculated at the DFT B3LYP levels of theory with 6-31G(D) basis set are presented in Table 4.38 while the spectra are shown in Figure 4.16b. The C_1, C_4 and C_6 atoms appeared 47.65,50.83 and 37.23ppm respectively while the chemical shifts of C_2, C_3 and C_5 atoms appeared respectively at 85.91, 80.80 and79.08ppm. All the Aromatic carbons of the pyridine $C_7 – C_{11}$ appeared between 120 and 157.20ppm while the carbonyl carbon due to the presence of oxygen and iron is deshielded and therefore has a higher chemical shifts at 208-216ppm. However, the methylene carbon appeared in the range 19-23ppm. The aromatic carbon to which the methylene carbon is attached is shifted downfield due to the electron releasing ability of the methyl substituent.

Table 4.37: **^{1}H N.m.r Chemical shifts (in ppm) of Tricarbonyl (1-4-η-5-exo-N-X,X-dimethylpyridino-cyclohexa-1,3-diene) iron complexes**

Proton	2,3-diMe	2,4-diMe	2,5-diMe	2,6-diMe	3,4-diMe	3,5-diMe
H_1	2.59	2.57	2.61	2.76	2.53	2.62
H_2	5.77	5.75	5.77	5.62	5.77	5.78
H_3	5.68	5.68	5.63	5.66	5.64	5.56
H_4	2.18	2.17	2.22	2.07	2.23	2.29
H_5	5.16	5.07	5.08	5.40	4.83	4.69
H_{6exo}	2.70	2.68	2.71	2.49	2.68	2.82
H_6 endo	1.33	1.28	1.43	1.71	1.45	1.62
H_7	8.04	7.32	7.49	7.46	7.66	7.61
H_8	7.60	7.48	8.00	8.00	7.58	8.00
H_9	8.54	8.46	8.29	7.43	8.27	8.07
H_{10}	2.75	2.35	2.53	2.59	2.49	2.74
H_{11}	2.24	2.80	2.50	2.65	2.50	2.71
H_{12}	2.61	2.70	2.79	2.98	2.24	2.10

H_{13}	2.40	2.48	2.74	2.65	2.58	2.75
H_{14}	2.65	2.45	2.77	3.17	2.57	2.79
H_{15}	2.61	2.81	2.17	2.49	2.48	2.19

Table 4.38: ^{13}C N.m.r. Chemical shifts (in ppm) of Tricarbonyl (1-4-η-5-exo-N-X,X-dimethylpyridino-cyclohexa-1,3-diene) iron complexes

Carbon	2,3-diMe	2,4-diMe	2,5-diMe	2,6-diMe	3,4-diMe	3,5-diMe
C_1	45.97	46.20	46.44	46.74	46.02	47.00
C_2	85.62	85.56	85.04	85.04	85.62	85.65
C_3	81.84	81.84	82.01	81.92	81.70	81.17
C_4	48.22	47.53	49.50	47.46	47.61	50.11
C_5	71.08	69.57	69.88	69.75	76.49	77.84
C_6	32.65	32.99	34.09	27.36	35.46	36.45
C_7	148.21	147.51	145.78	151.02	134.72	133.39
C_8	136.33	125.27	123.90	123.29	135.78	136.01
C_9	140.00	155.58	139.56	137.53	155.89	141.09
C_{10}	119.29	120.89	134.71	124.80	123.48	136.66
C_{11}	131.59	132.49	133.81	151.18	129.59	130.42
C_{12}	215.32	215.38	215.38	215.95	215.26	214.87

C_{13}	208.70	208.72	208.79	208.77	208.88	208.67
C_{14}	208.65	208.67	208.55	209.16	208.66	208.59
C_{15}	16.25	20.07	19.87	22.71	18.41	18.68
C_{16}	21.35	22.04	18.82	25.37	21.41	19.07

4.9.3 Tricarbonyl (1-4-η-5-exo-N-X-pyridino-2-methoxycyclohexa-1,3-diene) iron complexes

The calculated ^{1}H, ^{13}C and ^{15}N N.m.rchemical shift (in ppm) of substituted pyridino-1-4-η-2-methoxycyclohexa-1,3-diene irontricarbonyl complexes, are reported in Table 4.39. The spectra of the complexes show well separated overlapping multiplets characteristics of the outer H_1 and H_4 and inner H_3 -diene protons. The endo H_6 and exo H_6 protons all appeared as shown in the Table 4.39 and displayed in Figure 4.17a. The H_5 proton adjacent to the N-methylpyridino substituent is shifted downfield. For instance, the pyridino-1-4-η-cyclohexa-1,3-diene complex, the Aromatic protons of the pyridine group appear as triplets and doublets while the methylene protons appeared as singlet between 2.46-2.86 ppm. These values are characteristic features of the 1,3-diene derivatives. The ^{13}C chemical shifts calculated at the DFT B3LYP levels of theory with 6-31G(D) basis set are presented in Table 4.39while the spectra are shown in Figure 4.17b, The C_1 atom at appeared 139.23 ppm, and this is attributed to the presence of the methoxy group is attached to carbon 2 of the cyclohexa-1,3-diene ring, while the chemical shifts of C_2, C_3, C_4 and C_5 appeared at 63.83, 37.88, 42.64 and79.04 ppm. All the Aromatic carbons of the pyridine $C_7 – C_{11}$ appeared at 122.19 – 139.35 ppm while C≡O carbon due to the presence of oxygen and iron are deshielded and have higher chemical shifts at 209-215 ppm. However, the methylene carbon appeared in the range 19 – 23 ppm. There are no experimental values for ^{13}C but ^{1}H N.m.r values agrees with available experimental values. The aromatic carbon to which the methylene carbon is attached is downfield due to the electron releasing ability of the methyl substituent.

Table 4.39: **^{1}H and ^{13}C N.m.rChemical shifts (in ppm) of Tricarbonyl (1-4-η-5-exo-N-X-pyridino-2-methoxycyclohexa-1,3-diene) iron complexes**

Proton/Carbon	H	2-Me	3-Me	4-Me
$_{1}H$	2.84	2.76	2.83	2.81
$_{2}H$	-	-	-	-
$_{3}H$	5.16	5.34	5.17	5.15
$_{4}H$	2.08	1.92	2.05	2.04
$_{5}H$	4.56	4.88	4.49	4.47
$_{exo\ 6}H$	2.93	2.73	2.88	2.84
$_{endo\ 6'}H$	1.68	1.33	1.65	1.62
OCH_3	3.55-4.10	3.51-4.06	3.54-4.09	3.54-4.08
$_{7}H$	8.09	-	7.79	7.86
$_{8}H$	7.78	7.58	-	7.48
$_{9}H$	8.47	8.16	8.18	-
$_{10}H$	7.90	7.73	7.78	7.62
$_{11}H$	8.57	8.85	8.33	8.35

CH_3	-	2.46-2.84	2.13-2.79	2.57-2.86
C_1	139.23	139.51	139.21	139.13
C_2	63.87	64.44	64.19	64.06
C_3	37.88	36.94	38.00	37.82
C_4	42.64	39.31	42.48	42.23
C_5	79.04	71.33	78.40	77.54
C_6	38.59	34.21	38.16	37.98
C_7	136.19	148.85	135.79	135.15
C_8	122.19	124.43	137.03	122.57
C_9	139.35	138.48	140.01	156.80
C_{10}	123.03	120.18	122.13	123.64
C_{11}	133.99	134.52	131.11	132.59
OCH_3	54.08	54.07	53.99	54.00
C_{13}	214.46	214.93	214.80	214.52
C_{14}	206.90	206.99	207.11	206.99
C_{15}	209.60	209.80	209.81	209.81
C_{16}	-	20.26	18.91	22.30

4.9.4 Tricarbonyl (1-4-η-5-exo-N-X,X-dimethylpyridino-2-methoxycyclohexa-1,3-diene) iron complexes

The ^{1}H, ^{13}C and ^{15}N N.m.r spectra of these complexes show well separated overlapping multiplets characteristics of the outer H^1 and H^4 and inner H^3 -diene protons. The endo H^6 and exo H^6 all appeared as shown in Table 4.40 and displayed in Figure 4.18a. The H^5 proton adjacent to the N-methylpyridino substituent is shifted downfield to 4.44ppm and 5.15ppm for all the protons in the dimethylpyridino-1-4-η-cyclohexa-1,3-diene complexes, while the Aromatic protons of the pyridine group appeared as triplets and doublets located at 7.28 and 8.63ppm. The methylene protons appeared as a singlet between 2.07-2.93ppm. These values are characteristic features of the 1,3-diene derivatives. The ^{13}C chemical shifts calculated at the DFT B3LYP levels of theory with 6-31G(D) basis set are presented in Table 4.41 while the spectra are shown in Figure 4.28b. The C_1, C_4 and C_6 appeared at 36.87, 40.66 and 33.97ppm respectively while the chemical shifts of C_2 appeared at 139.27ppm due to its coordination to the methoxy C_{17}. $C_3$and C_5 atoms appeared at 64.79 and 70.85ppm respectively. All the Aromatic carbons of the pyridine $C_7 - C_{11}$ atoms appeared at 119.20 and 155.37ppm while carbonyl carbon due to the presence of oxygen and iron is deshielded and therefore has a higher chemical shift at 208-216ppm. However, the methylene carbon appeared in the range 16.34-25.70ppm. Our theoretical values agree with available experimental values for ^{1}H NMR spectra. The aromatic carbon to which the methylene carbon is attached is deshielded due to the electron releasing ability of the methyl group.

Table 4.40: ^{1}H N.m,r Chemical shifts (in ppm) of Tricarbonyl (1-4-η-5-exo-N-X,X-dimethylpyridino-2-methoxycyclohexa-1,3-diene) iron complexes

Proton	2,3-diMe	2,4-diMe	2,5-diMe	2,6-diMe	3,4-diMe	3,5-diMe
H^{1}	2.76	2.74	2.78	2.92	2.78	2.80
OCH_3	3.52-4.06	3.51-3.62	3.52-4.07	3.51-4.07	3.53-4.06	3.53-4.07
H^{3}	5.25	5.23	5.25	5.26	5.15	5.16
H^{4}	1.91	1.90	1.93	1.81	2.00	2.02
H^{5}	4.88	4.79	4.82	5.15	4.44	4.44
H^{6exo}	2.70	2.70	2.73	2.51	2.79	2.84
$H^{6\ endo}$	1.38	1.30	1.38	1.67	1.59	1.64
CH_3/H^{7}	2.20-2.69	2.39-2.76	2.43-2.76	2.55-2.93	7.65	8.05
CH_3/H^{8}	2.38-2.62	7.28	7.46	7.43	2.22-2.44	2.18-2.77
H^{9}/CH_3	8.00	2.27-2.80	7.98	7.96	2.46-2.57	7.98
H^{10}/CH_3	7.58	7.48	2.19-2.76	7.41	7.55	2.07-2.77
H^{11}/CH_3	8.63	8.58	8.41	2.29-2.62	8.23	7.58

Table 4.41: **^{13}C N.m.r Chemical shifts (in ppm) of Tricarbonyl (1-4-η-5-exo-N-X,X-dimethylpyridino-2-methoxycyclohexa-1,3-diene) iron complexes**

Carbon	2,3-diMe	2,4-diMe	2,5-diMe	2,6-diMe	3,4-diMe	3,5-diMe
C_1	36.87	36.89	37.33	37.12	37.65	38.02
C_2	139.27	139.48	139.26	136.73	139.12	139.29
C_3	64.79	64.76	64.79	69.05	64.34	64.16
C_4	40.66	39.70	40.69	39.04	42.04	42.39
C_5	70.85	69.69	69.98	70.38	76.98	77.85
C_6	33.97	34.35	35.17	28.81	37.63	37.39
C_7	148.21	147.60	145.67	151.07	134.76	133.37
C_8	135.97	125.07	123.71	123.17	135.35	135.67
C_9	139.74	155.23	139.28	137.34	155.37	140.74
C_{10}	119.20	120.83	134.58	124.73	123.49	136.53
C_{11}	132.23	132.95	134.08	151.26	130.42	130.69
C_{12}	16.34	20.12	19.18	22.81	18.35	18.68
C_{13}	21.21	21.93	18.80	25.70	27.42	19.04

C_{14}	215.16	214.99	215.07	215.45	214.82	214.60
C_{15}	207.08	207.09	207.11	207.02	207.22	207.16
C_{16}	209.83	209.95	209.92	210.39	209.92	209.81
C_{17}	54.06	53.98	54.04	54.02	53.94	53.95

4.9.5 Tricarbonyl (1-4-η-5-exo-N-X-aminopyridino-cyclohexa-1,3-diene) iron complexes

The ^{1}H and ^{13}C spectra of these complexes were analysed using Spartan 10 programme software. These complexes show well separated overlapping multiplets characteristic of the outer H1 and H2 and inner H2 and H3 –diene protons. The endo and the exo H6 protons appeared as shown in the Table 4.42 and displayed in Figure 4.19a. The H^{5} proton adjacent to the 4-aminopyridino substituent is shifted downfield. For instance, with the aminopyridino-1-4-η-cyclohexa-1,3-diene irontricarbonyl complex, the aromatic protons of the pyridine group appeared as triplets and doublets while the methylene protons appeared as singlet between 2.18-2.90 ppm. These values are characteristic features of the 1,3-diene derivatives. The ^{13}C chemical shifts calculated at the DFT b3LYP levels of theory with 6-31(D) basis set are presented in Table 4.43 while the spectra are shown in Figure 4.19b. The C1, C4, and C6 atoms appeared at ca: 47.65, 50.83 and 37.23ppm, while the chemical shifts of C2, C3, and C5 appeared at 85.91, 80.80 and 79.08ppm respectively. All the aromatic carbons of the pyridine ring C7 to C11 appeared at 120-157.20ppm while the carbonyl carbon due to the presence of oxygen and iron are deshielded and consequently have higher chemical shifts at 208-216ppm. However, the methylene carbon appeared in the range 19-23ppm. The aromatic carbon to which the amino substituent is attached is shifted downfield due to the electron releasing ability of the amino group. Our theoretical predictions agree with available experimental values.

Table 4.42: **^{1}H N.m.r Chemical shifts (in ppm) ofTricarbonyl (1-4-η-5-exo-N-X-aminopyridino-cyclohexa-1,3-diene) iron complexes**

Proton	2-NH_2	3-NH_2	4-NH_2	4-$NH(CH_3)$	4-$N(CH_3)_2$
H_1	3.32	3.00	2.93	2.91	2.93
H_2	5.49	5.47	5.44	5.45	5.34
H_3	5.68	5.61	5.56	5.56	5.55
H_4	2.25	2.24	2.08	2.11	2.15
H_5	3.98	4.20	4.02	4.07	3.96
H_6exo	2.35	1.86	1.81	1.75	1.80
H_6endo	2.46	2.63	2.55	2.55	2.53
H_8	-	7.94	7.39	8.27	8.32
H_9	6.54	-	6.37	6.58	6.59
H_{10}	7.80	7.14	-	-	-
H_{11}	6.81	7.42	6.54	6.28	6.42
H_{12}	7.25	7.20	8.34	7.28	7.33

N-H	4.92	3.89	4.48	4.48	-
N-H(CH_3)	7.21	3.98	4.51	-	3.06-3.25
$N(CH_3)_2$	-	-	-	2.99-3.17	3.06-3.30

Table 4.43: ^{13}C N.m.r Chemical shifts (in ppm) ofTricarbonyl (1-4-η-5-exo-N-X-aminopyridino-cyclohexa-1,3-diene) iron complexes

Carbon	2-NH_2	3-NH_2	4-NH_2	4-NH(CH_3)	4-$N(CH_3)_2$
C_1	58.72	55.16	54.59	54.12	54.74
C_2	88.15	86.15	86.03	85.72	85.87
C_3	78.54	78.98	78.98	79.29	78.92
C_4	50.39	48.52	48.09	48.01	49.12
C_5	70.77	70.16	66.96	65.91	65.98
C_6	38.84	42.98	41.47	41.18	42.14
C_7	143.55	118.31	133.97	133.59	131.90
C_8	108.55	138.66	104.61	101.20	104.31
C_9	138.20	120.72	146.14	146.91	146.64
C_{10}	109.84	122.31	104.33	105.92	103.70
C_{11}	135.30	124.11	135.96	134.18	134.14
C_{12}	214.23	218.70	217.50	217.18	217.68
C_{13}	209.99	209.33	209.45	209.75	209.91

C_{14}	208.07	208.24	208.63	208.77	208.75
C_{15}	-	-	-	29.46	40.69
C_{16}				-	40.73

4.9.6 Tricarbonyl (1-4-η-5-exo-N-X-aminopyridino-2-methoxycyclohexa-1,3-diene) iron complexes

The ^{1}H, ^{13}C and ^{15}N NMR spectra of theTricarbonyl (1-4-η-5-exo-N-substituted aminopyridino-cyclohexa-1,3-diene) iron complexesshow well separated overlapping multiplets characteristics of the outer H^1 and H^4 and inner H^2 and H^3 -diene protons. The endo H^6 and exo H^6 protons appeared as shown in the Table 4.44 and displayed in Figure 4.20a. The H^5 proton adjacent to the N-methylpyridino substituent is shifted downfield. For instance, with the pyridino-1-4-η-cyclohexa-1,3-diene complex, the Aromatic protons of the pyridine group appear as triplets and doublets while the methylene protons appeared as singlet between 2.18-2.90. These values are characteristic features of the 1,3-diene derivatives. The ^{13}C chemical shifts calculated at the DFT B3LYP levels of theory with 6-31G(D) basis set are presented in Table 4.45 while the spectra are shown in Figure 4.20b. The C_1, C_4 and C_6atoms appeared at 47.65,50.83 and 37.23ppm, while the chemical shifts of C_2, C_3 and C_5 appeared at 85.91, 80.80 and79.08ppm respectively. All the Aromatic carbons of the pyridine $C_7 – C_{11}$ appeared at 120 – 157.20ppm while carbonyl carbon due to the presence of oxygen and iron are deshielded and consequently have higher chemical shifts at 208-216ppm. However, the methylene carbon appeared in the range 19-23ppm. There are no experimental values for ^{13}C but ^{1}H NMR values agrees with available experimental values. The aromatic carbon to which the methylene carbon is attached isdeshielded due to the electron releasing ability of the methyl group.

Table 4.44: **^{1}H N.m.r Chemical shifts (in ppm)ofTricarbonyl (1-4-η-5-exo-N-X-aminopyridino-2-methoxycyclohexa-1,3-diene) iron complexes**

Proton	2-NH_2	3-NH_2	4-NH_2	4-$NH(CH_3)$	4-$N(CH_3)_2$
H_1	3.30	3.05	3.03	2.99	2.98
H_2	-	-	-	-	-
H_3	5.38	5.21	5.17	5.18	5.17
H_4	1.98	1.83	1.74	1.75	1.76
H_5	3.91	4.25	3.91	4.03	4.06
H_{6endo}	2.17	1.65	1.67	1.61	1.60
H_{6exo}	2.32	2.56	2.47	2.49	2.50
H_7	-	7.77	8.33	8.19	8.14
H_8	6.49	-	6.50	6.51	6.52
H_9	7.76	7.09	-	-	-
H_{10}	6.77	7.40	6.33	6.24	6.43

H_{11}	7.22	7.15	7.35	7.25	7.31
OCH_3	3.44-4.04	3.45-4.05	3.44-4.00	3.44-4.06	3.44-4.01
N-H	4.85	3.86	4.44	4.49	-
N-H	7.11	3.91	4.47	-	-
CH_3	-	-	-	2.97-3.15	3.04-3.29

Table 4.45: ^{13}C N.m.rChemical shifts (in ppm) ofTricarbonyl (1-4-η-5-exo-N-X-aminopyridino-2-methoxycyclohexa-1,3-diene) iron complexes

Carbon	2-NH_2	3-NH_2	4-NH_2	4-$NH(CH_3)$	4-$N(CH_3)_2$
C_1	47.15	44.22	44.50	43.61	43.69
C_2	140.92	139.29	139.04	139.11	139.19
C_3	63.98	62.69	62.94	62.97	62.96
C_4	42.93	39.63	40.84	39.84	40.26
C_5	71.52	69.94	67.45	66.11	65.71
C_6	38.32	41.77	41.52	40.45	40.28
C_7	143.37	118.39	134.19	133.85	131.96
C_8	108.46	138.21	104.61	100.91	103.47
C_9	137.89	120.13	146.08	146.91	146.41
C_{10}	109.60	122.39	104.12	105.87	104.10

C_{11}	135.23	123.74	135.99	134.16	133.84
C_{12}	54.74	54.38	54.27	54.21	54.21
C_{13}	214.20	217.46	217.23	216.76	216.74
C_{14}	210.66	210.66	210.84	210.97	211.11
C_{15}	206.16	206.61	206.72	207.11	207.02
C_{16}	-	-	-	29.40	40.55

4.10 Electronic states of the complexes using Hartree-Fock

According to Koopman in a closed-shell Hartree-Fock theory, the first ionization energy of a molecular system is equal to the negative of the orbital energy of the highest occupied molecular orbital (HOMO) while the negative of LUMO is the electron affinity. The HOMO and LUMO energies were calculated using Hartree-Fock with basis set 6-31G(D) for one complex within a group. The calculated values of Total energy, dipole moment, HOMO, LUMO energies, polarization and band gaps are reported in Table 4.46a. These values are calculated for the purpose of comparison with the calculated values using Density Functional Theory (DFT).

Reactivity parameters

By means of Koopman's theorem, the hardness is related to the HOMO-LUMO energy difference. A "hard" molecule has a large HOMO-LUMO gap, and is expected to be chemically unreactive; i.e hardness is related to chemical stability. A small HOMO-LUMO gap indicates a "soft" molecule and from second order perturbation theory, it follows that a small gap between occupied and unoccupied orbital will give a large contribution to the polarizability. i.e softness is a measure of how easily the electron density can be distorted by external fields.

The reactivity parameters were obtained using finite difference and frozen orbital approximation which yields them in terms of the highest occupied molecular orbital energy, E_H, and lowest unoccupied molecular orbital energy, E_L According to Koopman, the first ionization energy of a molecular system for a closed shell molecules is the negative of highest occupied molecular orbital and that of electron affinity is the negative of lowest unoccupied molecular orbital. The ionization energies and electron affinities for these complexes were obtained from Ab initio Hartree-Fock procedure with basis set 6-31G (D), and the values are presented in Table 4.46b.

Table 4.46: Electronic and Reactivity parameters of complexes using Hartree-Fock 6-31G(D)

Table 4.46a: Electronic properties of Tricarbonyl (1-4-η-5-exo-N-substituted pyridino-cyclohexa-1,3-diene) iron complexes

Substituent	Total energy/ a.u	Dipole moment/D	E_{HOMO} /eV	E_{LUMO} /eV	E_{GAP}/ eV	Polarisation
$[(MePyC_6H_7)Fe(CO)_3]^+$	-2117.17	5.41	-10.44	-1.26	9.18	62.93
$[(Me_2PyC_6H_7)Fe(CO)_3]^+$	-2156.19	4.69	-10.42	-1.27	9.15	64.21
$[(MePyC_6H_6OMe)Fe(CO)_3]^+$	-2231.00	8.88	-10.71	-1.66	9.05	64,49
$[(Me_2PyC_6H_6OMe)Fe(CO)_3]^+$	-2270.01	7.97	-10.71	-1.66	9.05	65.79
$[(MeHNPyC_6H_7)Fe(CO)_3]^+$	-2172.19	7.77	-10.37	-0.66	9.71	63.45
$[(Me_2NPyC_6H_6OMe)Fe(CO)_3]^+$	-2325.05	9.51	-10.64	-0.92	9.72	66.82

Table 4.46b: Reactivity global indexes of Tricarbonyl (1-4-η-5-exo-N-substituted pyridino-cyclohexa-1,3-diene) iron complexes

Substituent	I/eV	A/eV	μ/eV	η/eV	χ/eV	ω/eV
$[(MePyC_6H_7)Fe(CO)_3]^+$	10.44	1.26	-5.85	4.59	5.85	16.30
$[(Me_2PyC_6H_7)Fe(CO)_3]^+$	10.42	1.27	-5.85	4.58	5.85	15.69
$[(MePyC_6H_6OMe)Fe(CO)_3]^+$	10.71	1.66	-5.62	4.53	5.62	16.40
$[(Me_2PyC_6H_6OMe)Fe(CO)_3]^+$	10.71	1.66	-5.62	4.53	5.62	15.99
$[(MeHNPyC_6H_7)Fe(CO)_3]^+$	10.37	0.66	-5.52	4.86	5.52	11.63
$[(Me_2NPyC_6H_6OMe)Fe(CO)_3]^+$	10.64	0.92	-5.78	4.86	5.78	11.61

4.11 Time-dependent density functional theory(TDDFT) of the complexes

Time-dependent Density Functional Theory is presently enjoying enormous popularity in quantum Chemistry, as an important instrument for calculating and elucidating the electronic excited state energies. The theory applies ground state DFT philosophy to time dependent problems by replacing the complicated many-body time-dependent Schrodinger equation by a set of time-dependent single-particle equation whose orbitals yield the same time-dependent density. According to Runge and Gross, 1984, for a given initial wavefunction, particle statistics and interaction, a given time-dependent density can arise from at most one time-dependent external potential. This implies that the time dependent potential (all other properties inclusive) is a function of the time-dependent density. Considering the ground state Kohn-Sham theorem, the time-dependent Kohn-Sham (TDKS) (Bauernschmitt and Ahlrichs,1996,equations which describe the non-interacting electrons that evolves in a time-dependent Kohn-Sham potential, but yielded the same density as that of the interesting system of interest. The more difficult interacting time-dependent Schrodinger equation is replaced by a much simpler set of equations which easier to solve. The price of this simplification is that the exchange-correlation piece of the Kohn-Sham potential is to be approximated. The commonest time-dependent perturbation is a long wavelength electric field, oscillating with frequency. In this regard, the field is a weak perturbation of the molecule, and a linear response analysis can be performed, from which the optical absorption spectrum of the molecule due to the electronic excitations can be extracted. The linear response TDDFT predicts the transition frequencies to electronic excited states and many other properties (Stratmann *et al*., 1998; Casida *et al*., 1998;

Dominique and Shinichiro, 2000; Appel *et al.*, 2003; Brewer *et al*., 2005; Forslund *et al*., 2002; Ren *et al*., 2010; Bertsch *et al*., 2001; Liu, 2008; Morell *et al*., 2005; Shigeyoshi *et al*., 2010; Marques and Gross, 2004; Cave *et al*., 2002; Bernasconi *et al*., 2004; Roy and Hughbanks, 2006; Besley and Blundy, 2006; Hirose *et al*., 2004; Maitra *et al*., 2002; Petersilka *et al*., 1996; Della and Gorling, 2003; Grabo *et al*., 2000; Petersilka *et al*., 2000; Tao and Vignale, 2006).

4.11.1 TDDFT of Tricarbonyl (1-4-η-5-exo-N-pyridino-cyclohexa-1,3- diene) iron complexes

Electronic transitions were investigated to confirm the configuration for ground state geometry optimized with DFT B3LYP with basis set 6-31G(D). The transitions are from the ground state to excited states, and are all spin-allowed. Excitation energies and oscillation strengths for the transition from ground state (S_o) singlet, to first, S_1, second, S_2, third, S_3, fourth, S_4 and fifth, S_5 of each complex were calculated using TDDFT calculation in gas phase at the level B3LYP/6-31G(D) level. The calculated total time-dependent density functional theory (TDDFT) energy was -2084.46a.u. and the first excited state is a triplet with excitation energy of 2.7908eV i.e $S_o \rightarrow T_1$. However, it is found that the $S_o \rightarrow S_1$ transition corresponding to the excitation from the HOMO to the LUMO with absorption wavelength of 430.19nm is dominant. The calculated transition energies (eV), wavelengths (nm) and oscillator strengths showing its multiplicities are shown in Table 4.47 and UV-visible spectrum is shown figure 4.21, (appendix 6).

Table 4.47: Transition energies (eV), wavelengths (nm) and oscillator strengths for Tricarbonyl (1-4-η-5-exo-N-pyridino-cyclohexa-1,3-diene) iron complex

Excited states No.	Excitation Energy/eV	Multiplicity	Strength	Wavelength/nm
1	2.7908	Triplet	0.0000	444.25
2	2.8821	Singlet	0.0251	430.19
3	3.2187	Triplet	0.0000	385.20
4	3.2986	Triplet	0.0000	325.87
5	3.4262	Triplet	0.0000	361.87
6	3.4411	Triplet	0.0000	360.30
7	3.4965	Singlet	0.0004	354.60
8	3.5704	Singlet	0.0180	347.26
9	3.7591	Singlet	0.0113	330.61
10	3.7916	Singlet	0.0078	327.00

4.11.2 TDDFT ofTricarbonyl (1-4-η-5-exo-N-X,X-dimethylpyridino-cyclohexa-1,3-diene) iron complex

The electronic transitions of dimethylpyridino-1-4-η-cyclohexa-1,3-diene irontricarbonyl complexeswere investigated to confirm the configuration for ground state geometry optimized with DFT B3LYP with basis set 6-31G(D). The transitions are from the ground state to excited states, and are all spin-allowed. Excitation energies and oscillation strengths for the transition from ground state (S_o) singlet, to first, S_1, second, S_2, third, S_3, fourth, S_4, fifth, S_5 and sixth $S_6$of each complex were calculated using TDDFT calculation in gas phase at the level B3LYP/6-31G(D) level. The calculated total time-dependent density functional theory energy was -2163.0824a.u. and the first excited state is a triplet with excitation energy of 3.0019eV meaning first transition from ground state singlet to first excited state triplet. i.e $S_o \rightarrow T_1$. It is found that the $S_o \rightarrow S_1$ transition corresponding to the excitation from the HOMO to the LUMO with absorption wavelength of 396.25nm and $S_o \rightarrow T_4$ with the absorption wavelength of 358.38nm is dominant. However, a spin-forbidden transition exist because a singlet mixes to some extent with a triplet state due to a very similar molecular geometry of the excited state singlet and triplet states, and a strong spin-orbit coupling which allows the spin flip associated with a singlet-triplet transition to occur, although the degree of mixing is small, hence the oscillator strength associated with these transitions are very weak. These transitions are listed in Table 4.48 while the spectrum is shown Figure 4.22, (appendix6).

Table 4.48: Transition energies (eV), wavelengths (nm) and oscillator strengths for Tricarbonyl (1-4-η-5-exo-N-X,X-dimethylpyridino-cyclohexa-1,3-diene) iron complex

Excited states No.	Excitation Energy/eV	Multiplicity	Strength	Wavelength/nm
1	3.0019	Triplet	0.0000	413.02
2	3.1289	Singlet	0.0219	396.25
3	3.2534	Triplet	0.0000	381.09
4	3.2689	Triplet	0.0000	379.28
5	3.4596	Triplet	0.0219	358.38
6	3.4737	Triplet	0.0000	356.93
7	3.6847	Triplet	0.0000	336.49
8	3.7320	Singlet	0.0149	332.21
9	3.7748	Singlet	0.0009	328.45
10	3.7965	Singlet	0.0066	326.58

11	3.9749	Singlet	0.0014	311.84
12	4.0618	Singlet	0.0250	305.24

4.11.3 TDDFT of Tricarbonyl (1-4-η-5-exo-N-4-methylpyridino-cyclohexa-1,3-diene) iron complex

The electronic transitions of 4-methylpyridino-1-4-η-cyclohexa-1,3-diene irontricarbonyl were investigated to confirm the configuration for ground state geometry optimized with DFT B3LYP with basis set 6-31G(D). The transitions are from the ground state to excited states, Singlet states and are all spin-allowed. However spin-forbidden transitions occur due to some singlet state mixing to some extent with the triplet state as a result of spin-orbit coupling though with extremely weak bands. Excitation energies and oscillation strengths for the transition from ground state (S_o) singlet, to first, S_1, second, S_2, third, S_3, fourth, S_4, fifth, S_5 and sixth S_6 of each complex were calculated using TDDFT calculation in gas phase at the level B3LYP/6-31G(D) level. The calculated total time-dependent density functional theory energy was -2238.3086a.u. and the first excited state is a triplet with excitation energy of 3.2872eV meaning first transition from ground state singlet to first excited state triplet. i.e $S_o \rightarrow T_1$. It is found that the $S_o \rightarrow S_1$ transition corresponding to the excitation from the HOMO to the LUMO with absorption wavelength of 429.18nm and $S_o \rightarrow T_4$ with the absorption wavelength of 362.20nm is dominant. Although, intersystem crossing between singlet-triplet electronic states is forbidden in Born Oppenheimer approximation, for these molecules the probability of this happening is high. This is as a result of similar molecular geometry of the excited state singlet and triplet states, and a strong spin-orbit coupling which allows the spin flip

associated with a singlet-triplet transition to occur.These transitions are listed in Table 4.49 while the spectrum is shown figure 4.23, (appendix 6).

Table 4.49: Transition energies (eV), wavelengths (nm) and oscillator strengths for Tricarbonyl (1-4-η-5-exo-N-4-methylpyridino-cyclohexa-1,3-diene) iron complex

Excited states No.	Excitation Energy/eV	Multiplicity	Strength	Wavelength/nm
1	2.7844	Triplet	0.0000	445.28
2	2.8888	Singlet	0.0389	429.18
3	3.2872	Triplet	0.0000	377.18
4	3.3683	Triplet	0.0000	368.09
5	3.4231	Triplet	0.0389	362.20
6	3.5053	Triplet	0.0000	353.70
7	3.5301	Triplet	0.0000	351.22
8	3.5873	Singlet	0.0134	345.62
9	3.6879	Singlet	0.0001	336.19

10	3.7151	Singlet	0.0136	333.73
11	3.7905	Singlet	0.0057	327.09
12	3.8532	Singlet	0.0011	321.77

4.11.4 TDDFT of Tricarbonyl (1-4-η-5-exo-N-2,3-dimethylpyridino-cyclohexa-1,3-diene) iron complex

The electronic transitions of dimethylpyridino-1-4-η-cyclohexa-1,3-diene irontricarbonyl complexes were investigated to confirm the configuration for ground state geometry optimized with DFT B3LYP with basis set 6-31G(D). The transitions are from the ground state to excited states, and are all spin-allowed. Excitation energies and oscillation strengths for the transition from ground state (S_o) singlet, to first, S_1, second, S_2, third, S_3, fourth, S_4, fifth, S_5 and sixth S_6 of each complex were calculated using TDDFT calculation in gas phase at the level B3LYP/6-31G(D) level. The calculated total time-dependent density functional theory energy was -2163.0824a.u, and the first excited state is a triplet with excitation energy of 2.9952eV meaning first transition from ground state singlet to first excited state triplet. i.e $S_o \rightarrow T_1$. It is found that the $S_o \rightarrow S_1$ transition corresponding to the excitation from the HOMO to the LUMO with absorption wavelength of 413.94nm and $S_o \rightarrow T_4$ with the absorption wavelength of 364.44nm are dominant. Although, intersystem crossing between singlet-triplet electronic states is forbidden in Born Oppenheimer approximation, for many molecules the probability of this happening is high. The probability of intersystem crossing transitions is enhanced by two factors: a very similar molecular geometry in the excited state singlet and triplet states, and a strong spin-orbit coupling which allows the spin flip associated with a singlet-triplet transition to occur. In these complexes, intersystem crossing from excited state singlet to

triplet excited state occurs with same oscillator strength but at different energy bands.Although the degree of mixing may be small, but the bands associated with these transitions are very weak. These transitions are listed in Table 4.50 while the spectrum is shown Figure 4.24, (appendix 6).

Table 4.50: Transition energies (eV), wavelengths (nm) and oscillator strengths for Tricarbonyl (1-4-η-5-exo-N-2,3-dimethylpyridino-2-methoxycyclohexa-1,3-diene) iron complex

Excited states No.	Excitation Energy/eV	Multiplicity	Strength	Wavelength/nm
1	2.9273	Triplet	0.0000	423.54
2	2.9952	Singlet	0.0187	413.94
3	3.2864	Triplet	0.0000	377.26
4	3.3766	Triplet	0.0000	357.18
5	3.4021	Triplet	0.0187	364.44
6	3.5323	Triplet	0.0000	351.00
7	3.6125	Triplet	0.0000	342.95
8	3.7278	Singlet	0.0037	332.59

9	3.8320	Singlet	0.0020	323.54
10	3.8742	Singlet	0.0152	320.02
11	3.9053	Singlet	0.0043	317.47
12	3.9428	Singlet	0.0055	314.03

4.11.5 TDDFT of Tricarbonyl (1-4-η-5-exo-N-4-aminopyridino-cyclohexa-1,3-diene) iron complex

Electronic transitions were investigated to confirm the configuration for ground state geometry optimized with DFT B3LYP with basis set 6-31G(D). The transitions are from the ground state to excited states, and are all spin-allowed. Excitation energies and oscillation strengths for the transition from ground state (S_o) singlet, to first, S_1, second, S_2, third, S_3, fourth, S_4 and fifth, S_5 of each complex were calculated using TDDFT calculation in gas phase at the level B3LYP/6-31G(D) level. The calculated total time-dependent density functional theory energy was -2139.8138a.u and the first excited state is a triplet with excitation energy of 3.2855eV i.e $S_o \rightarrow T_1$. However, it is found that the$S_o \rightarrow S_1$ transition corresponding to the excitation from the HOMO to the LUMO with absorption wavelength of 285.91nm is dominant and this can be attributed to $n \rightarrow \pi^*$transition. The calculated transition energies (eV), wavelengths (nm) and oscillator strengths showing its multiplicities are shown in Table 4.51 and UV-visible spectrum is shown Figure 4.25, (appendix 6).

Table 4.51: Transition energies (eV), wavelengths (nm) and oscillator strengths for Tricarbonyl (1-4-η-5-exo-N-4-aminopyridino-cyclohexa-1,3-diene) iron complex

Excited states No.	Excitation Energy/eV	Multiplicity	Strength	Wavelength/nm
1	3.2855	Triplet	0.0000	377.37
2	3.3863	Triplet	0.0000	366.13
3	3.5424	Triplet	0.0000	350.00
4	3.6186	Triplet	0.0000	342.63
5	3.6864	Triplet	0.0000	336.32
6	3.7302	Singlet	0.0007	332.38
7	3.7464	Singlet	0.0000	330.94
8	3.8913	Singlet	0.0011	318.62
9	3.9715	Singlet	0.0003	312.18

10	4.1052	Singlet	0.0022	302.01
11	4.1547	Singlet	0.0036	298.42
12	4.3365	Singlet	0.0176	285.91

4.11.6 TDDFT of Tricarbonyl (1-4-η-5-exo-N-4-N-dimethylaminopyridino-cyclohexa-1,3-diene) iron complex

The electronic transitions of Tricarbonyl (1-4-η-5-exo-N-4-N-dimethylaminopyridino-cyclohexa-1,3-diene) iron complexeswere investigated to confirm the configuration for ground state geometry optimized with DFT B3LYP with basis set 6-31G(D). The transitions are from the ground state to excited states, and are all spin-allowed. Excitation energies and oscillation strengths for the transition from ground state (S_o) singlet, to first, S_1, second, S_2, third, S_3, fourth, S_4, fifth, S_5 and sixth S_6 of each complex were calculated using TDDFT calculation in gas phase at the level B3LYP/6-31G(D) level. The calculated total time-dependent density functional theory energy was -2218.4340a.u, and the first excited state is a triplet with excitation energy of 3.2847eV meaning first transition from ground state singlet to first excited state triplet. i.e $S_o \rightarrow T_1$.but with a very weak band. It is found that the $S_o \rightarrow S_1$ transition corresponding to the excitation from the HOMO to the LUMO with absorption wavelength of 285.57nm.is dominant and this is attributed to the transition from $n \rightarrow \pi^*$. However, a spin-forbidden transition exist because the singlets mix to some extent with the triplets state due to spin-orbit coupling, although the degree of mixing is small, hence the band associated with these transitions are very weak. The calculated transition energies (eV), wavelengths (nm) and oscillator strengths

showing its multiplicities are shown in Table 4.52and UV-visible spectrum is shown Figure 4.25 in appendix 6.

Table 4.52: Transition energies (eV), wavelengths (nm) and oscillator strengths for Tricarbonyl (1-4-η-5-exo-N-4-N-dimethylaminopyridino-cyclohexa-1,3-diene) iron complex

Excited states No.	Excitation Energy/eV	Multiplicity	Strength	Wavelength/nm
1	3.2841	Triplet	0.0000	377.46
2	3.3757	Triplet	0.0000	367.28
3	3.3839	Triplet	0.0000	366.40
4	3.5469	Triplet	0.0000	349.55
5	3.6102	Triplet	0.0000	343.42
6	3.7845	Triplet	0.0000	327.61
7	3.8452	Singlet	0.0015	322.44

8	3.8973	Singlet	0.0007	318.13
9	3.9704	Singlet	0.0002	312.27
10	4.1411	Singlet	0.0042	299.40
11	4.2785	Singlet	0.0001	289.78
12	4.3416	Singlet	0.0236	285.57

4.11.7 TDDFT of Tricarbonyl (1-4-η-5-exo-N-4-N-dimethylaminopyridino-2-methoxycyclohexa-1,3-diene) iron complex

The electronic transitions of Tricarbonyl (1-4-η-5-exo-N-4-N-dimethylaminopyridino-2-methoxycyclohexa-1,3-diene) iron complexeswere investigated to confirm the configuration for ground state geometry optimized with DFT B3LYP with basis set 6-31G(D). The transitions are from the ground state to excited states, and are all spin-allowed. Excitation energies and oscillation strengths for the transition from ground state (S_o) singlet, to first, S_1, second, S_2, third, S_3, fourth, S_4, fifth, S_5 and sixth S_6 of each complex were calculated using TDDFT calculation in gas phase at the level B3LYP/6-31G(D) level. The calculated total time-dependent density functional theory energy was -2332.9574a.u, and the first excited state is a triplet with excitation energy of 3.3092eV meaning first transition from ground state singlet to first excited state triplet. i.e $S_o \rightarrow T_1$.but with a very weak band. It is found that the $S_o \rightarrow S_1$ transition corresponding to the excitation from the HOMO to the LUMO with absorption wavelength of 288.62nm.is dominant and this is attributed to the transition from $n \rightarrow \pi^*$. However, a spin-forbidden transition exist because the singlets mix to some extent with the triplets state due to spin-orbit coupling, although the degree of mixing is small, hence the band associated with

these transitions are very weak. The calculated transition energies (eV), wavelengths (nm) and oscillator strengths showing its multiplicities are shown in Table 4.53 and UV-visible spectrum is shown Figure 4.26, (appendix 6).

Table 4.53: Transition energies (eV), wavelengths (nm) and oscillator strengths for Tricarbonyl (1-4-η-5-exo-N-4-N-dimethylaminopyridino-2-methoxy-cyclohexa-1,3-diene) iron complex

Excited states No.	Excitation Energy/eV	Multiplicity	Strength	Wavelength/nm
1	3.3092	Triplet	0.0000	374.66
2	3.3795	Triplet	0.0000	366.87
3	3.4358	Triplet	0.0000	360.86
4	3.4967	Triplet	0.0000	354.57
5	3.6030	Triplet	0.0000	344.11
6	3.6707	Singlet	0.0008	337.76
7	3.6738	Triplet	0.0000	337.48
8	3.9079	Singlet	0.0049	317.27

9	3.9801	Singlet	0.0014	311.51
10	4.0856	Singlet	0.0042	303.47
11	4.1435	Singlet	0.0044	299.23
12	4.2957	Singlet	0.0131	288.62

CHAPTER FIVE

SUMMARY AND CONCLUSION

5.1 Summary

The complexes 1-4-η-cyclohexa-1,3-diene derivatives of irontricarbonyl were synthesised and characterised using microanalytical method, infra-red, proton-nuetron magnetic resonance and ultra-violet light spectroscopy.

The geometry, thermodynamic and electronic properties were studied using Spartan ’10 molecular software package. The electronic excited state were investigated in order to determine the light emitting ability of the complexes.

The geometries of the complexes are functions of the various substituents on the rings while the formations were entirely spontaneous. The electronic parameters obtained are indicative of the reactivities as well as light emitting ability of the complexes.

5.2 Conclusion

The organometallic complex Tricarbonyl (1-4-η-5-exo-N-pyridino-cyclohexa-1,3-diene) iron and its derivatives were synthesized via addition of pyridines to the complexes $[Fe(CO)_3$ (1-5-η-dienyl)$]BF_4$ dienyl = C_6H_7 or 2-$OMeC_6H_6$ in acetonitrile.This synthesis has clearly demonstrated the application of organometallics to the synthesis of coordinated organics and the ease (room temperature and pressure) with which product I-XII (equation 4.1) could be prepared.

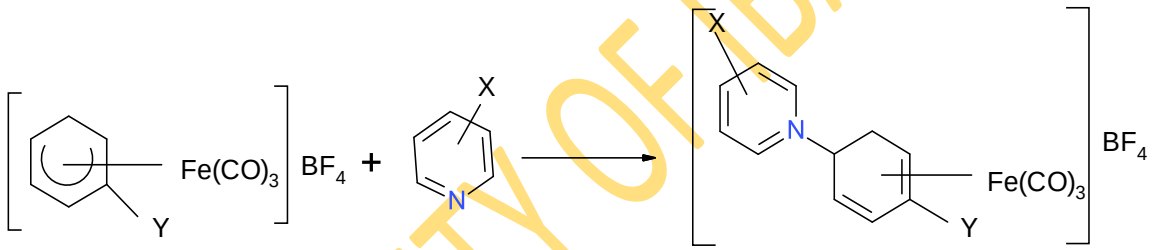

X = H, CH_3 , NH_2, $NH(CH_3)$, $N(CH_3)_2$

Y = H, OCH_3

..... 4.1

The C_1 symmetry ofTricarbonyl (1-4-η-5-exo-N-X-Substitutedpyridino-Y-substituted cyclohexa-1,3-diene) iron complexand its derivatives have been calculated using, quantum mechanical method which include Semi-empirical PM3, Hartree-Fock, Density functional theory and Time-dependent density functional theory. The properties investigated for the stable structures include, the optimized structures, electronic properties, dipole moments, thermodynamic properties and vibrational frequencies. Semi empirical PM3 model revealed that, all the complexes are stable. TheHOMO-LUMO energy band gaps of these complexes are calculated using all the three models, Band gaps calculated using Hartree-Fock model had the highest value followed by Semi empirical PM3 model while the least value of band gap was obtained from density functional theory.

Semi empirical studies revealed that all the complexes are thermodynamically stable as indicated by the values of free energy, enthalpy and entropy. However, the formation of these complexes is spontaneous from the calculated free energy values.

Infra-red vibrational analyses were carried out using both semi empirical and density functional theory for molecular characterization of these complexes. It was discovered that, these complexeshave very sharp peaks between 2103cm^{-1}– 2171cm^{-1} corresponding to the stretching vibrations of the C≡O bond. It is clearly seen that these groups have corresponding IR signatures which are expected to provide useful information for further studies.

^{1}H N.m.r spectroscopic studies on these groups of complexes show well separated overlapping multiplets characteristics of the outer H^{1}and H^{4} and inner H^{2} and H^{3} –diene protons (Odiaka and Okogun, 1985; Odiaka, 1988a, 1988b; Odiaka *et al*., 2007). The density functional theory and Time-dependent density functional theory were used to characterize the complexes while ultra-violet visible studies allowed the prediction ofthe electronic transition from ground state singlet to excited state mixtures of singlets (strong bands) and triplets (weak bands). The $S_o \rightarrow S_1$ transition corresponds to the excitation from the HOMO to the LUMO with the absorption wavelength ranging from of 430.19nm-368nm attributed to the transition from $\pi \rightarrow \pi^*$while the absorption wavelength of less than 300nm is attributed to the electronic transition from $n \rightarrow \pi^*$as observed for aminopyridino 1-4-η--cyclohexa-1,3-diene irontricarbonyl complexes.

The calculated IR Vco bands and ^{1}H NMR studies are in good agreement with the observed experimental values.

The HOMO and LUMO energies calculated using both Hartree-Fock and Density functional theory showed that the DFT significantly underestimated the LUMO energies in comparison to HF. Ionization energies obtained from HOMO are of the order 1.58eV greater in HFin comparison to DFT while the DFT underestimated the LUMO energies and hence predicted higher values of electron affinities.

The values of ionization energies and electron affinities obtained from HOMO and LUMO were used in calculating the chemical potential, global chemical hardness, electronegativity and electrophilicity index, all commonly referred to as reactivity parameters. The predicted value of reactivity parameters showed that under suitable conditions, these complexes will react with nucleophiles to give new products.

Finally, our results revealed that the excited state is a mixture of singlet and triplet. The relaxation from the excited state singlet ($S_1 \rightarrow S_0$) gives fluorescence while the relaxation from the excited state triplet to ground state singlet ($T_1 \rightarrow S_0$) results to phosphorescence. The aminopyridino complexes are purely fluorescent emitters while the methyl and dimethyl substituted pyridino complexes are phosphorescent emitters.

The electronic-excited state of synthesised methyl, dimethyl, and amino substituted Tricarbonyl (1-4-η-5-exo-N-4-N-dimethylaminopyridino-2-methoxycyclohexa-1,3-diene) iron complexesare capable of emitting light via phosphorescence and fluorescence, and may be useful in light emitting diodes.

APPENDICES

Appendix 1 HOMO-LUMO Energy diagrams

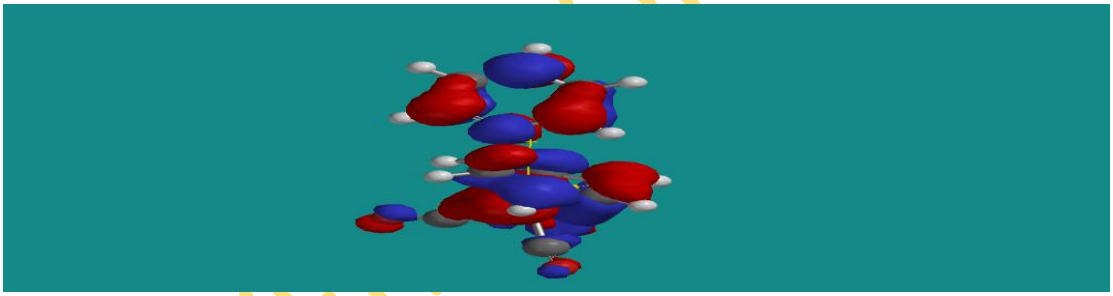

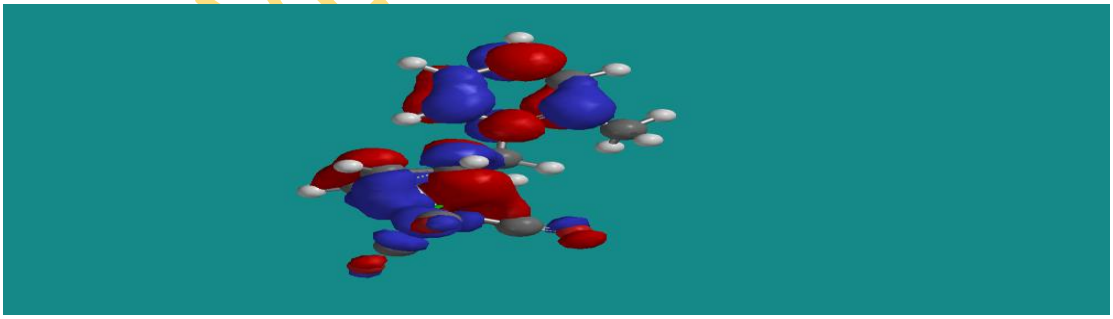

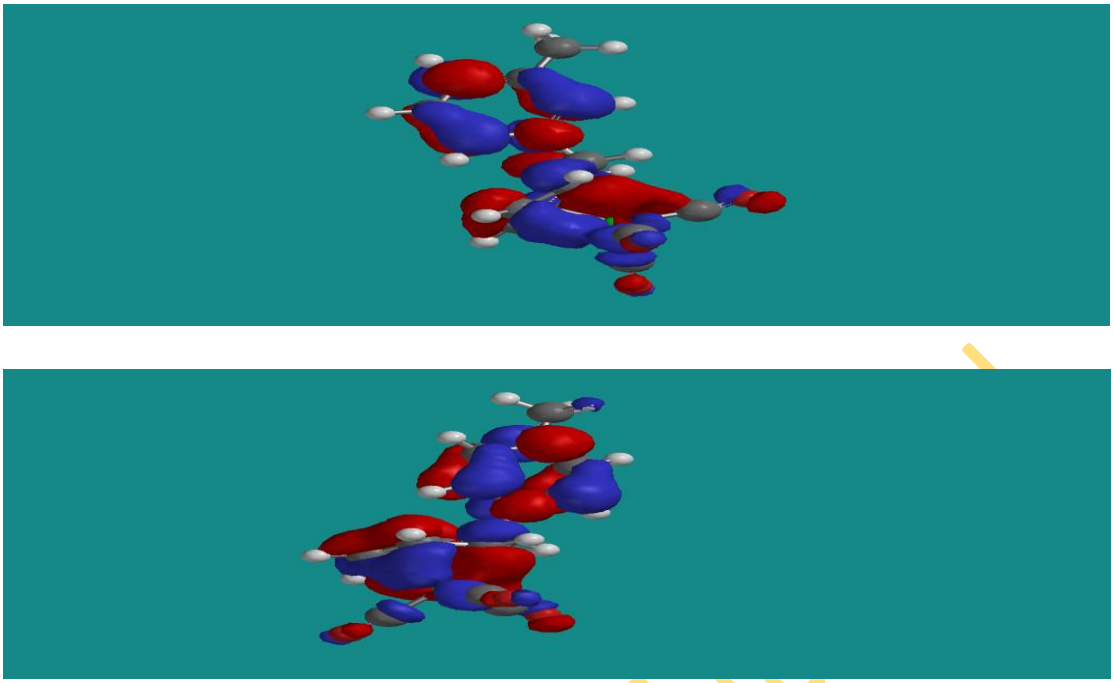

Plate 4.1: HOMO-LUMO Energy diagrams of Tricarbonyl (1-4-η-5-exo-N-X-pyridino-cyclohexa-1,3-diene) iron

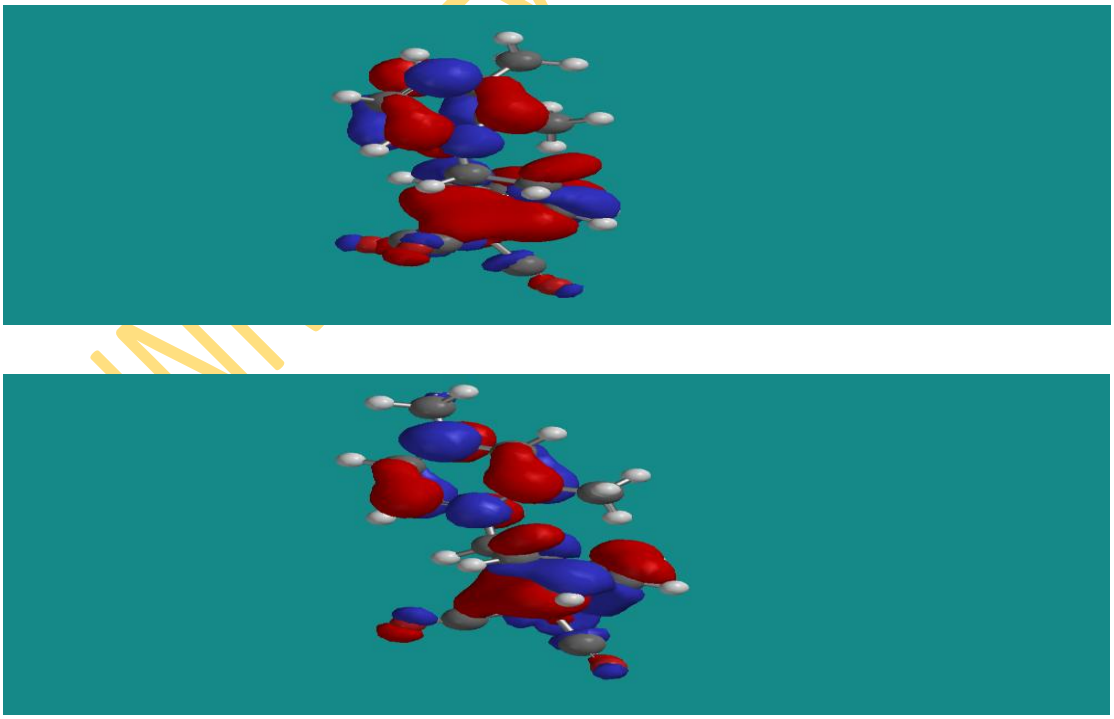

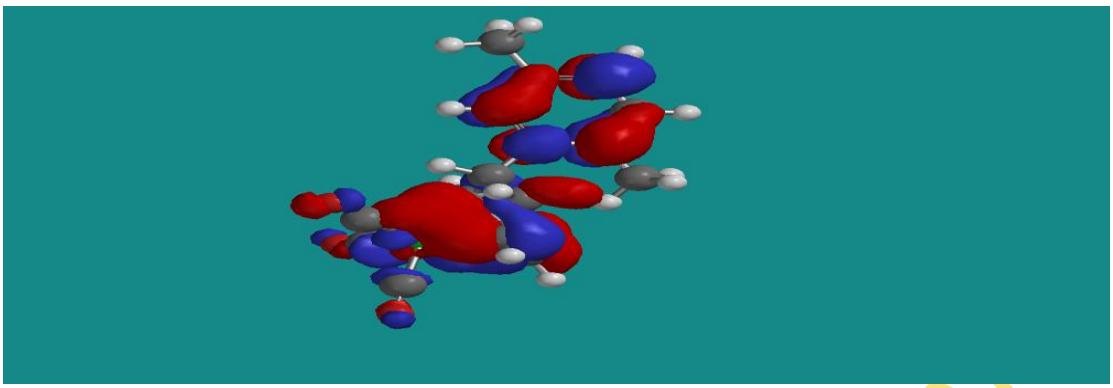

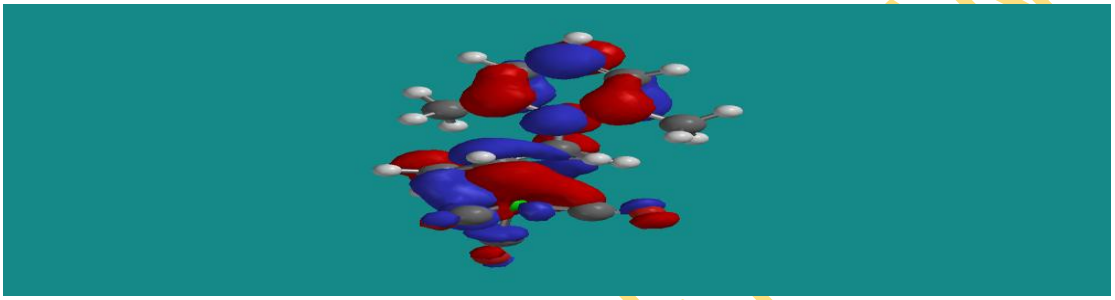

Plate 4.2: HOMO-LUMO diagrams ofTricarbonyl (1-4-η-5-exo-N-X,X-dimethyl-pyridino-cyclohexa-1,3-diene) iron

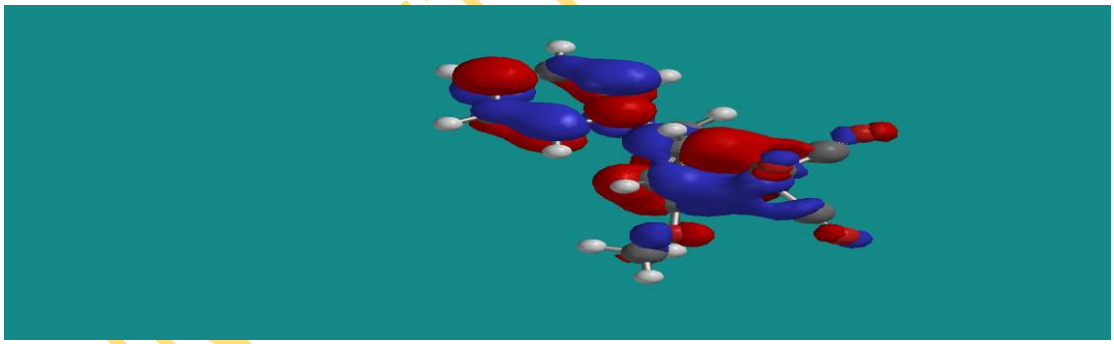

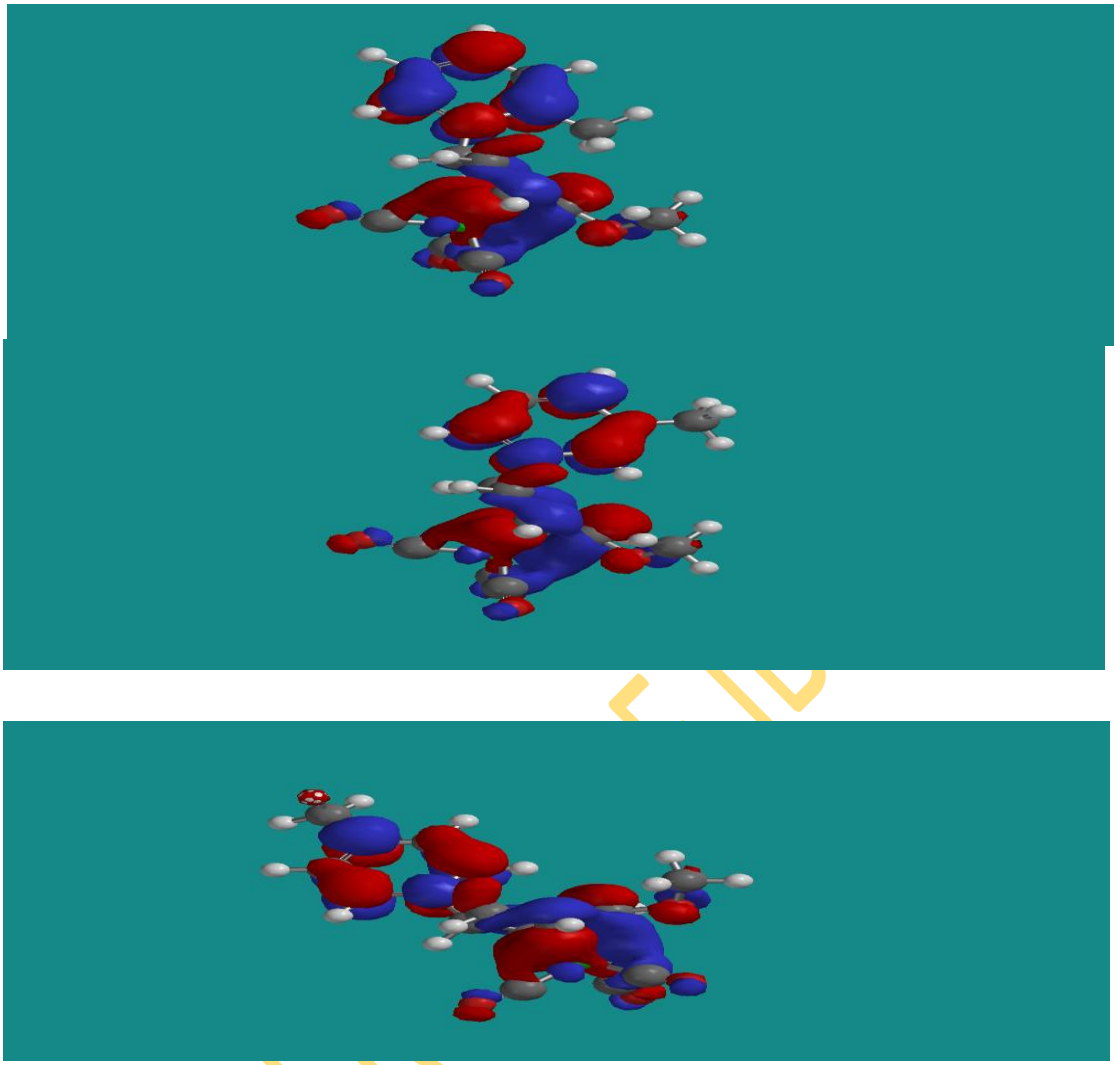

Plate 4.3: HOMO-LUMO Energy diagram of Tricarbonyl (1-4-η-5-exo-N-X-pyridino-2-methoxycyclohexa-1,3-diene) iron

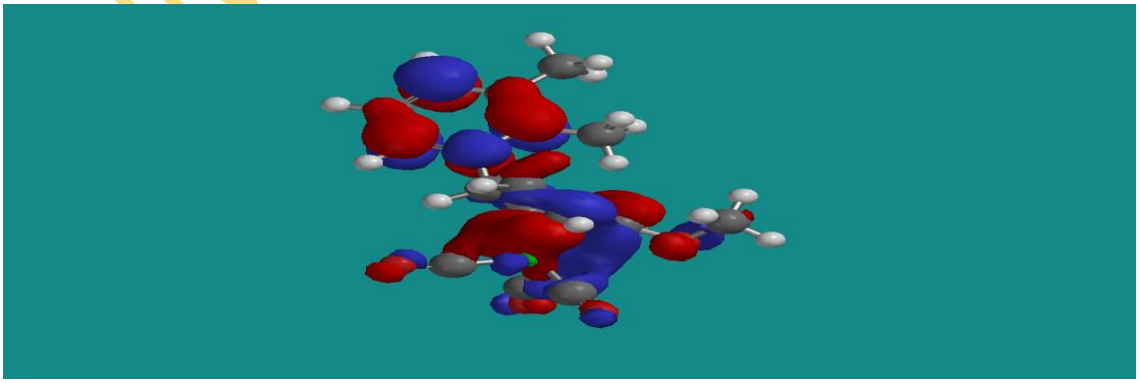

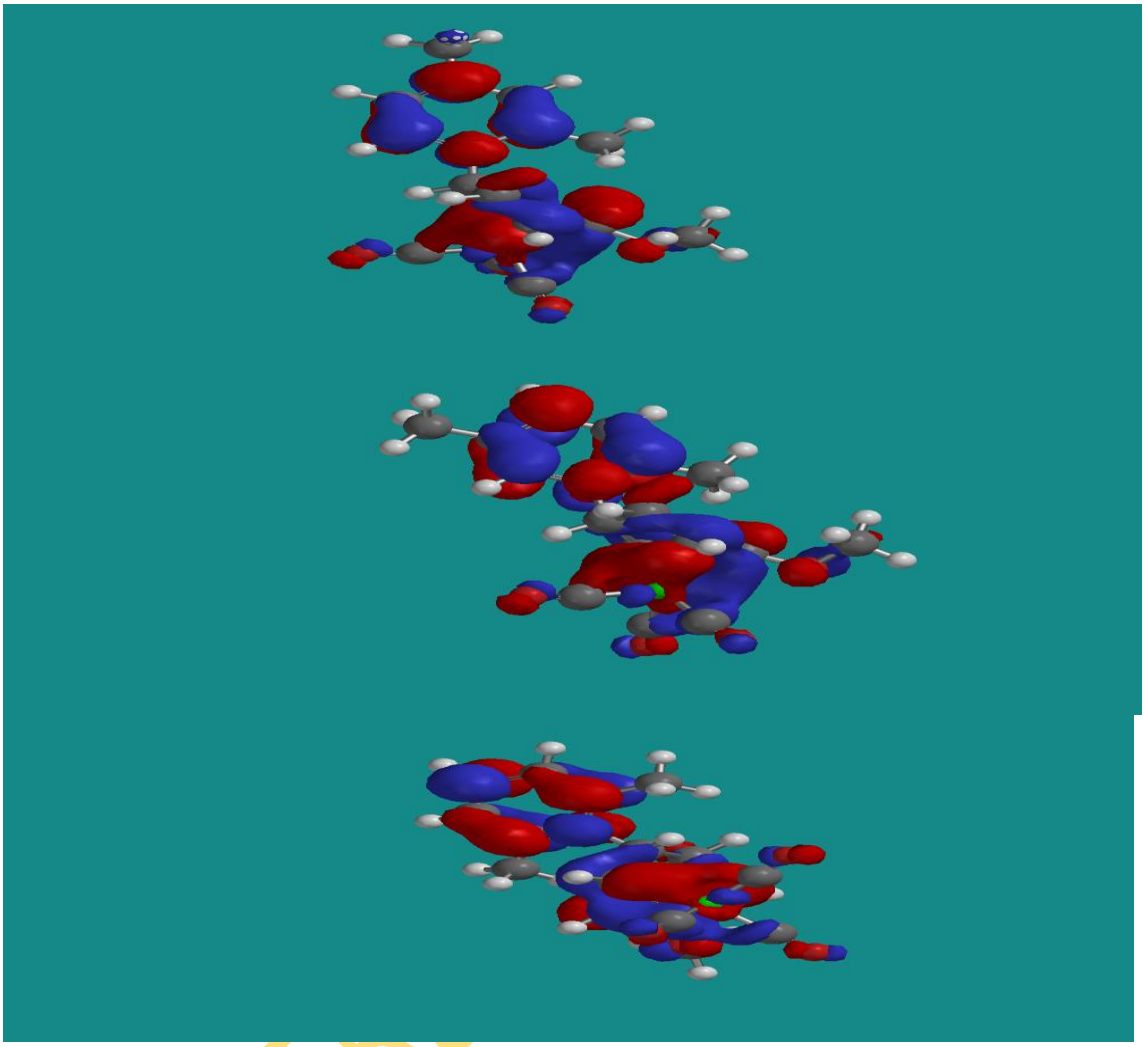

Plate 4.4: HOMO and LUMO energy diagrams of Tricarbonyl (1-4-η-5-exo- N-X, X-dimethylpyridino-2-methoxycyclohexa-1,3-diene) iron

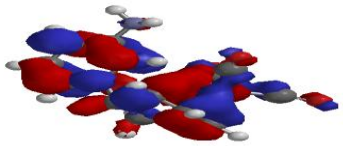

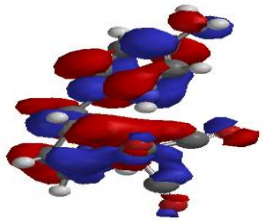

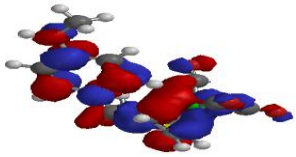

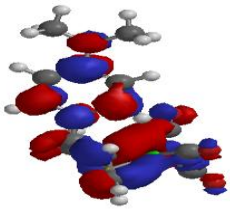

Plate 4.5: HOMO – LUMO Energy diagrams of Tricarbonyl (1-4-η-5-exo-N- X-aminopyridino-cyclohexa-1,3-diene) iron

Plate 4.6: HOMO – LUMO Energy diagrams of Tricarbonyl (1-4-η-5-exo-N-X-aminopyridino-2-methoxycyclohexa-1,3-diene) iron

Appendix 2: Orbital energy diagrams

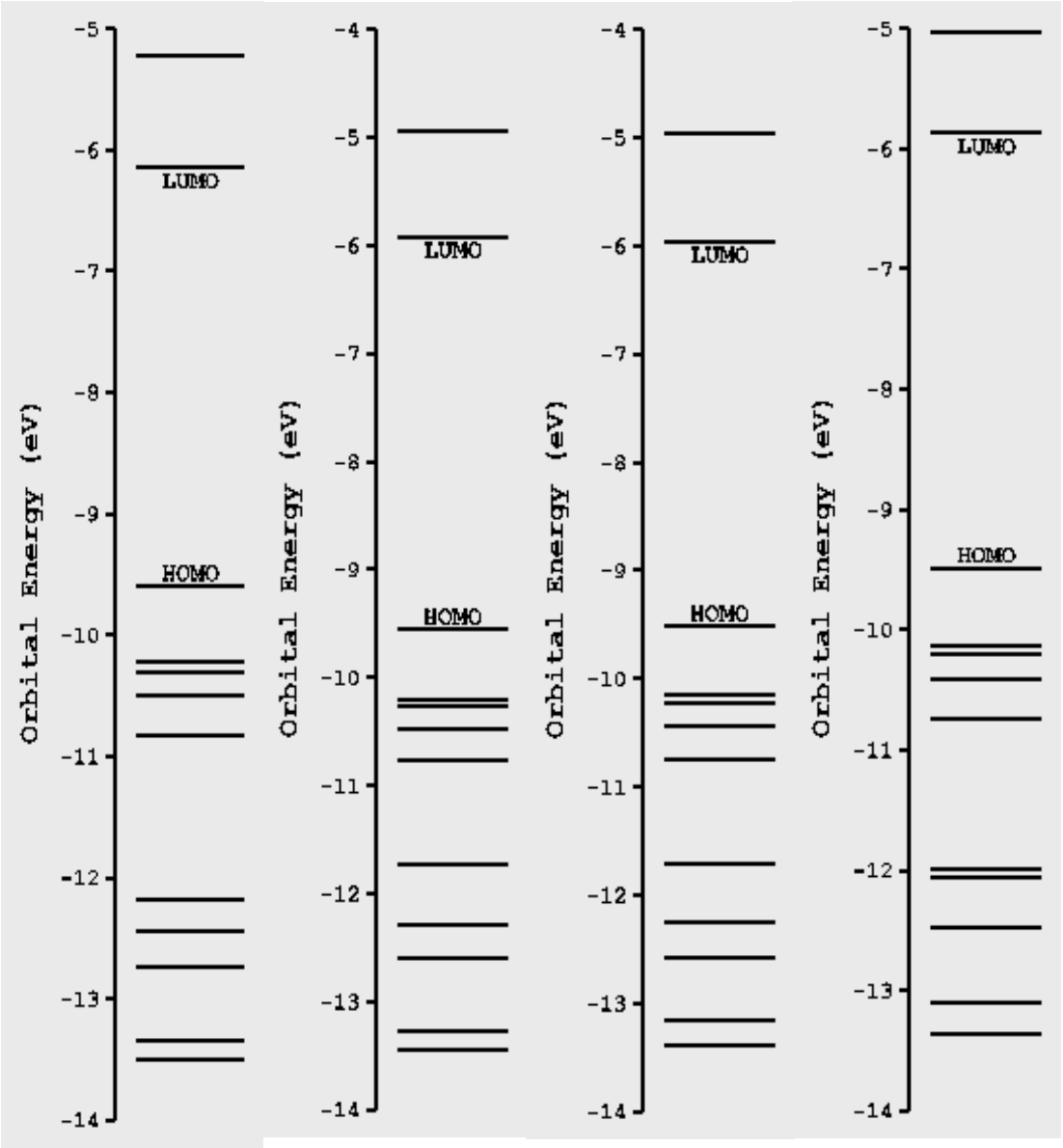

Figure 4.1: Orbital energy diagrams of Tricarbonyl (1-4-η-5-exo-N-X-pyridino-cyclohexa-1,3-diene) iron

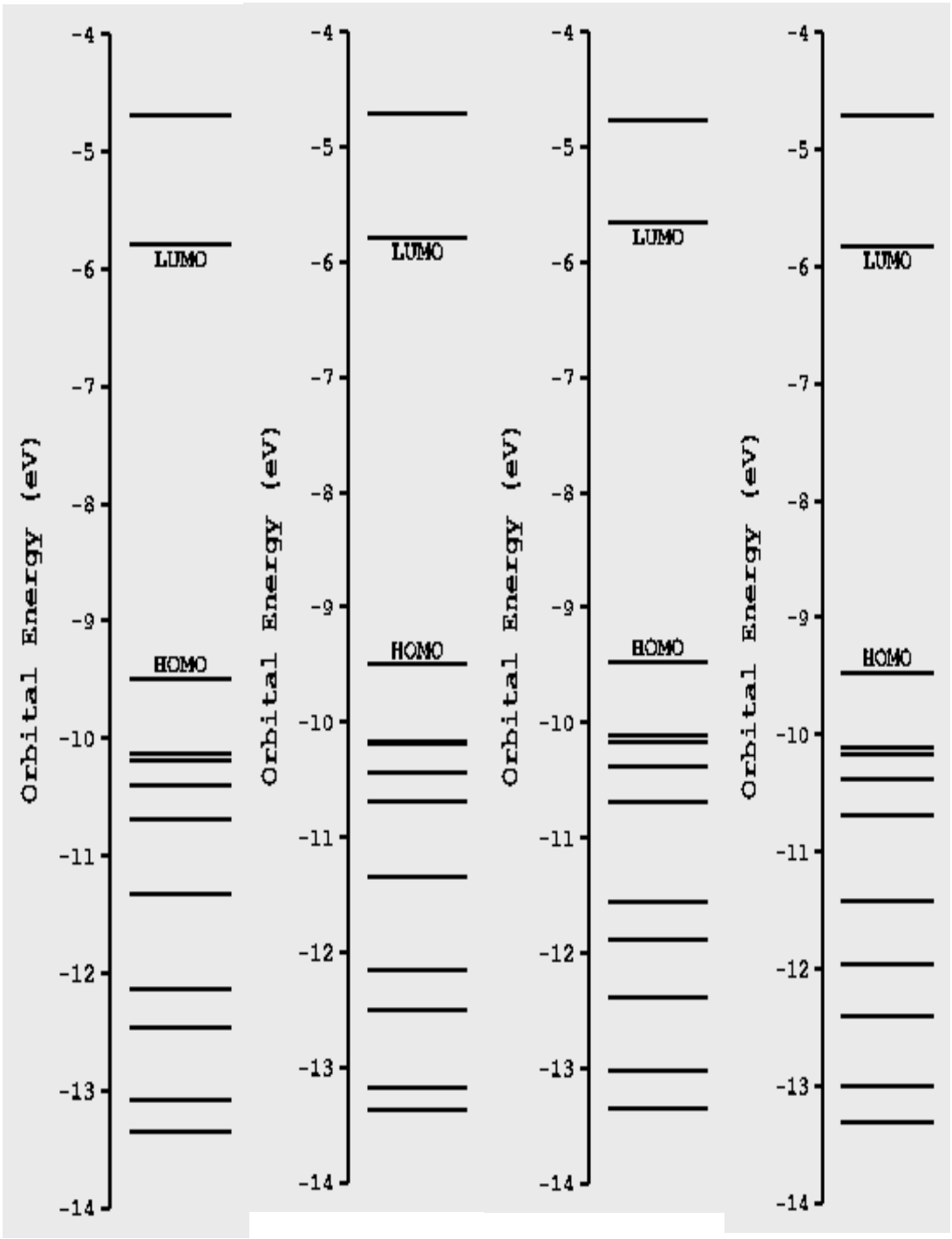

Figure 4.2: Orbital energy diagrams of Tricarbonyl (1-4-η-5-exo-N-X,X-dimethyl pyridino-cyclohexa-1,3-diene) iron

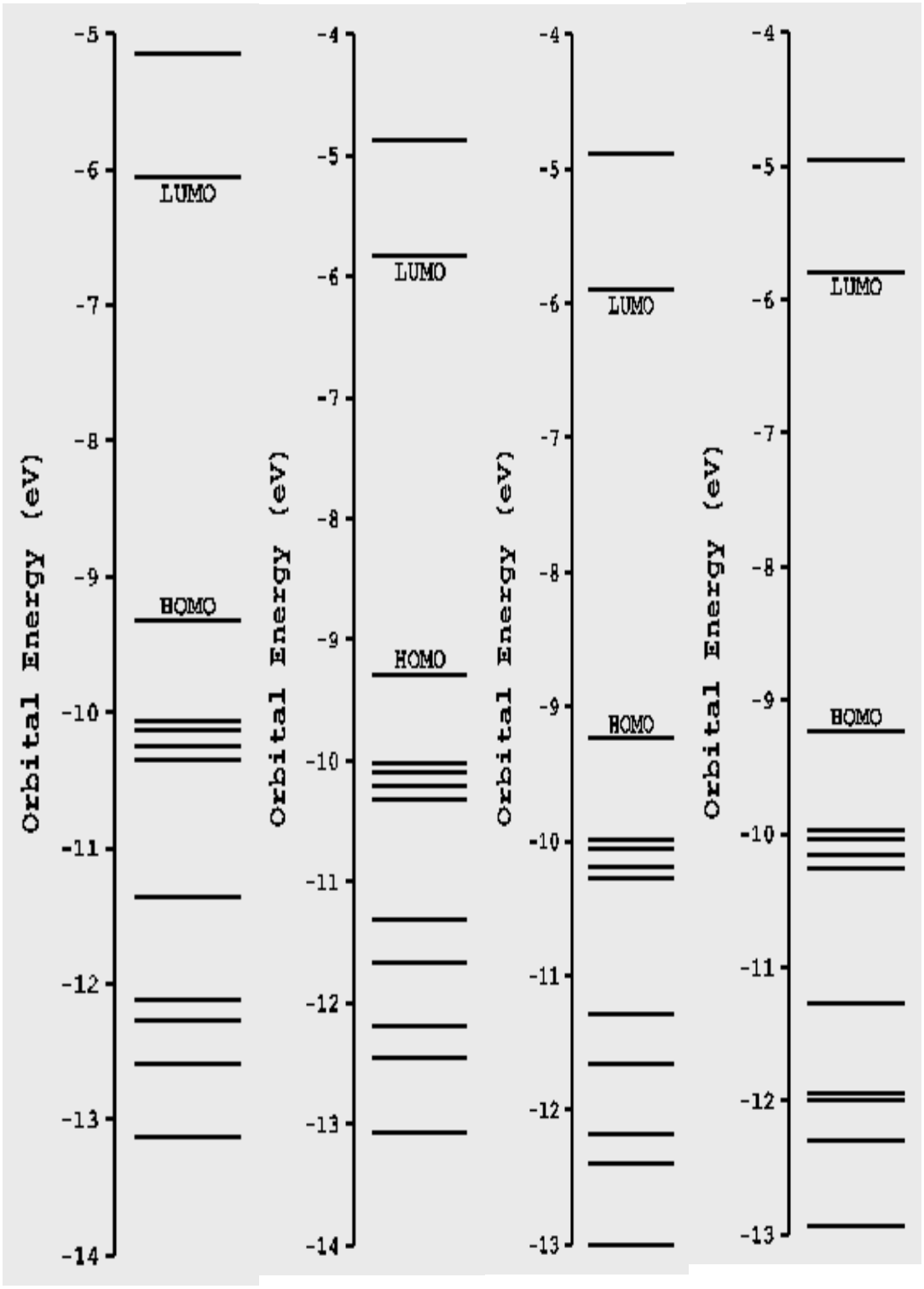

Figure 4.3: Orbital energy diagrams of Tricarbonyl (1-4-η-5-exo-N-X-pyridino-2-methoxycyclohexa-1,3-diene) iron

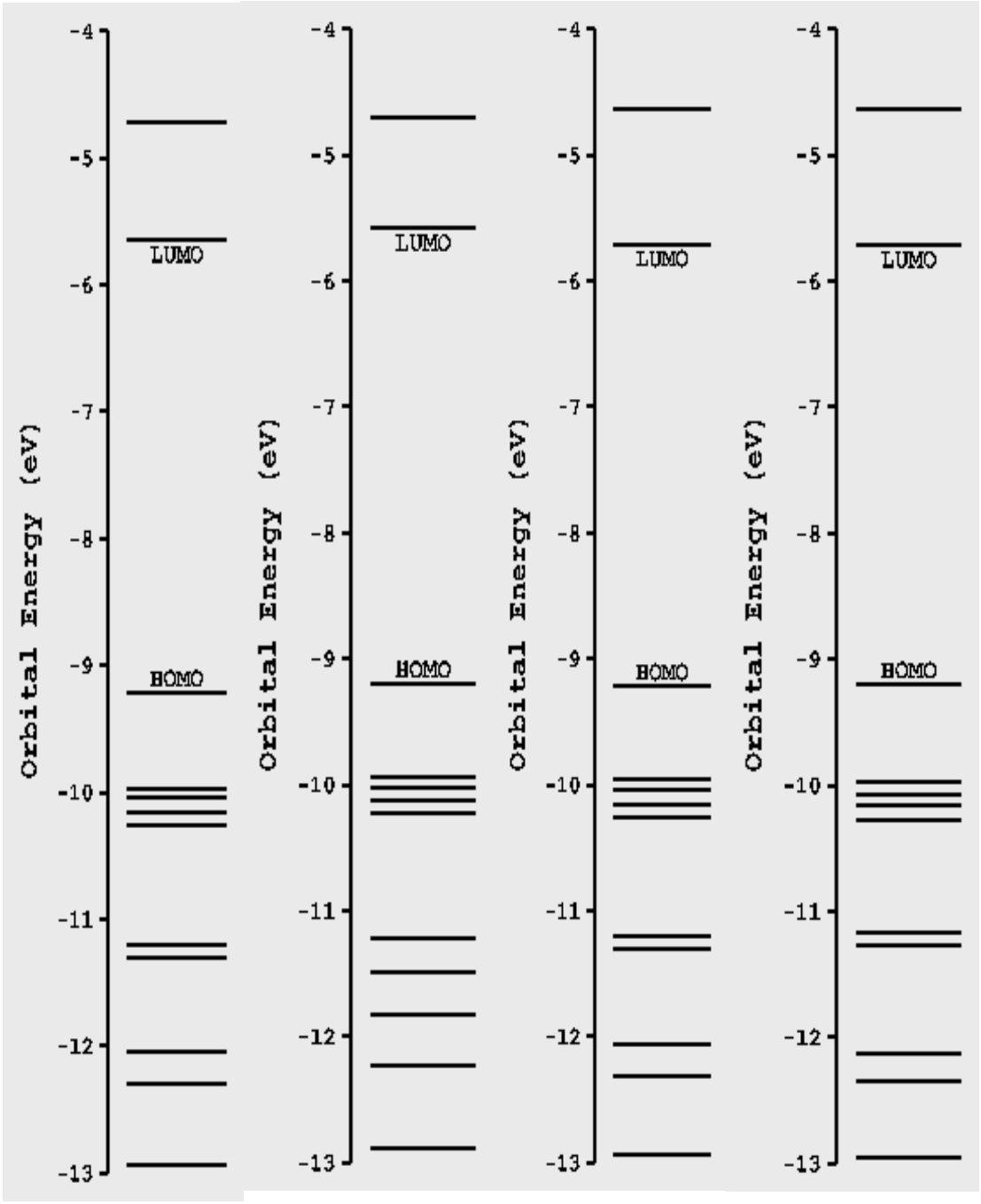

Figure 4.4: Orbital energy diagrams of Tricarbonyl (1-4-η-5-exo-N-X,X-dimethyl pyridino-2-methoxycyclohexa-1,3-diene) iron

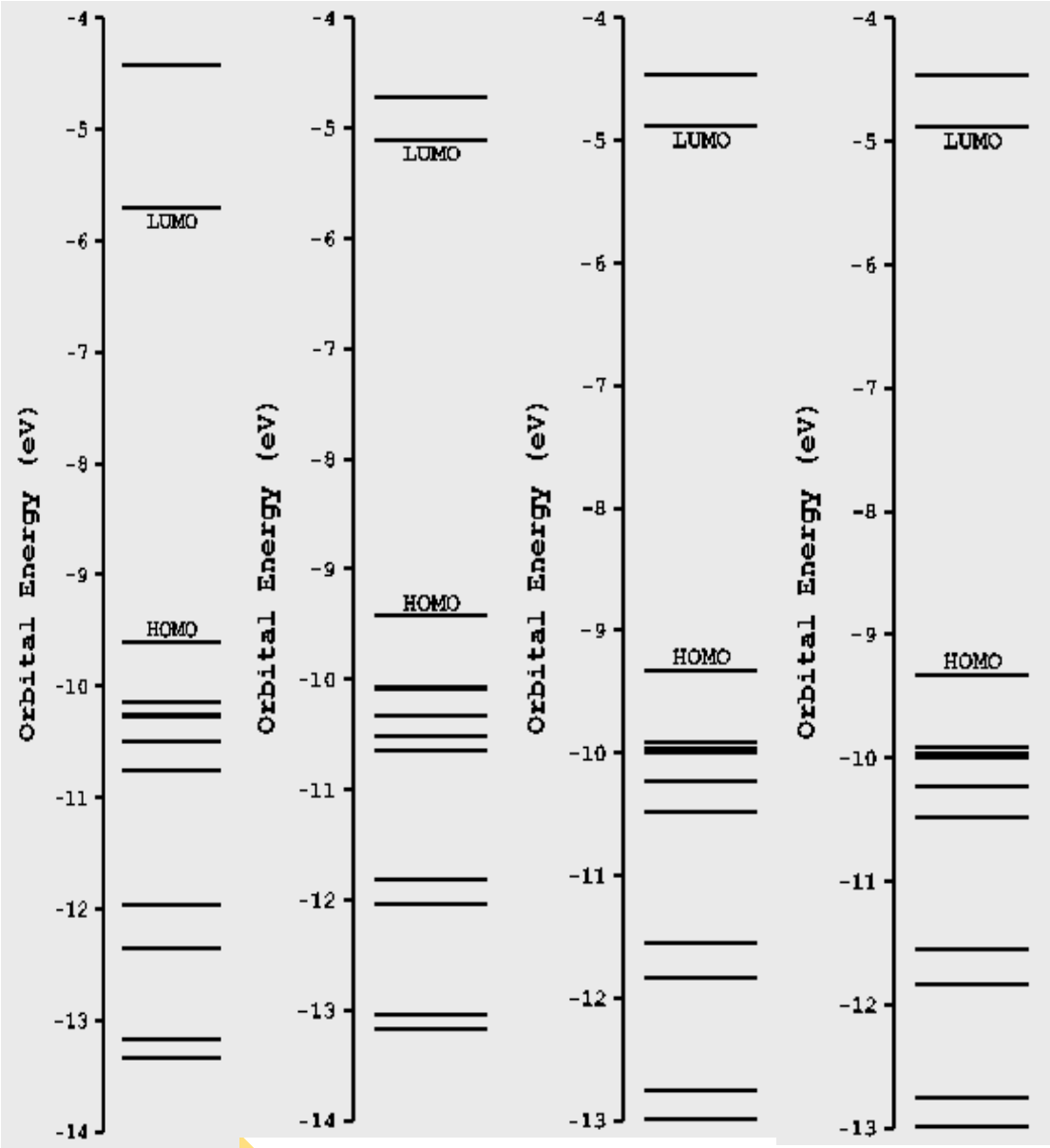

Figure 4.5: Orbital energy diagrams of Tricarbonyl (1-4-η-5-exo-N-X-aminopyridino-cyclohexa-1,3-diene) iron

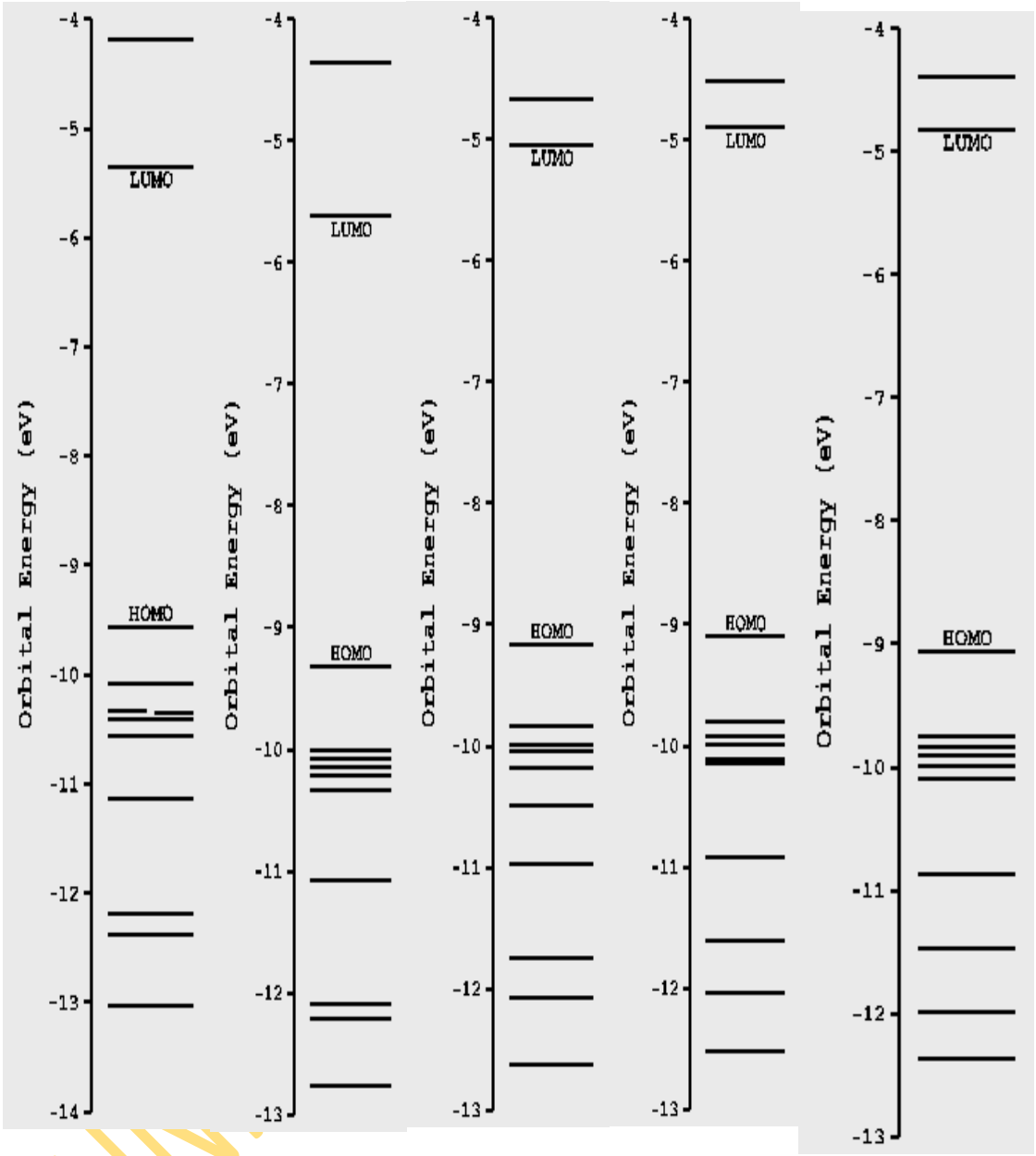

Figure 4.6: Orbital energy diagrams of Tricarbonyl (1-4-η-5-exo-N-X-aminopyridino-2-methoxycyclohexa-1,3-diene) iron

Appendix 3: Infra-red Spectra showing vibrational frequencies using PM3

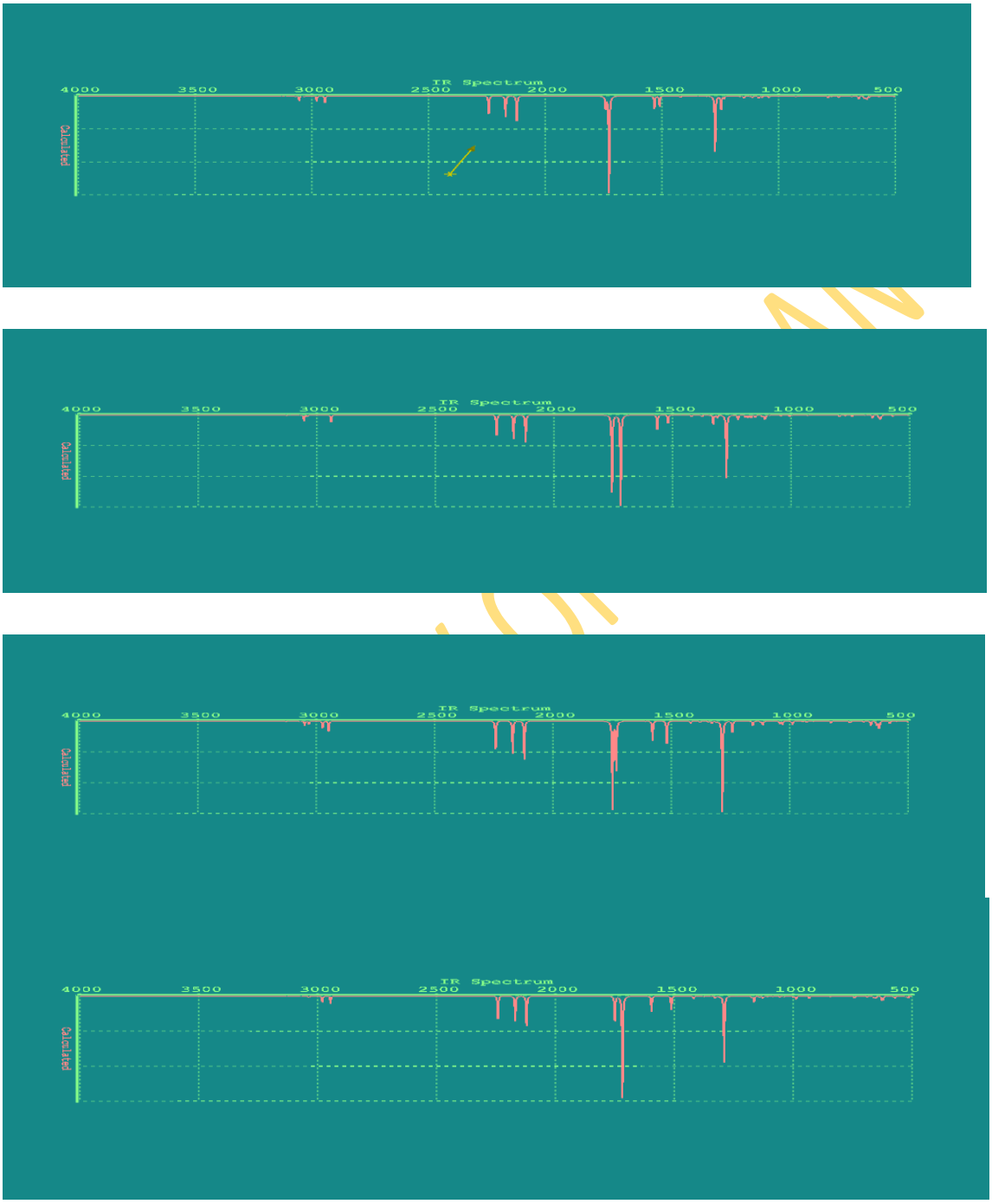

Plate 4.7: Infra-red spectraof Tricarbonyl (1-4-η-5-exo-N-X-pyridino-cyclohexa-1,3-diene) iron

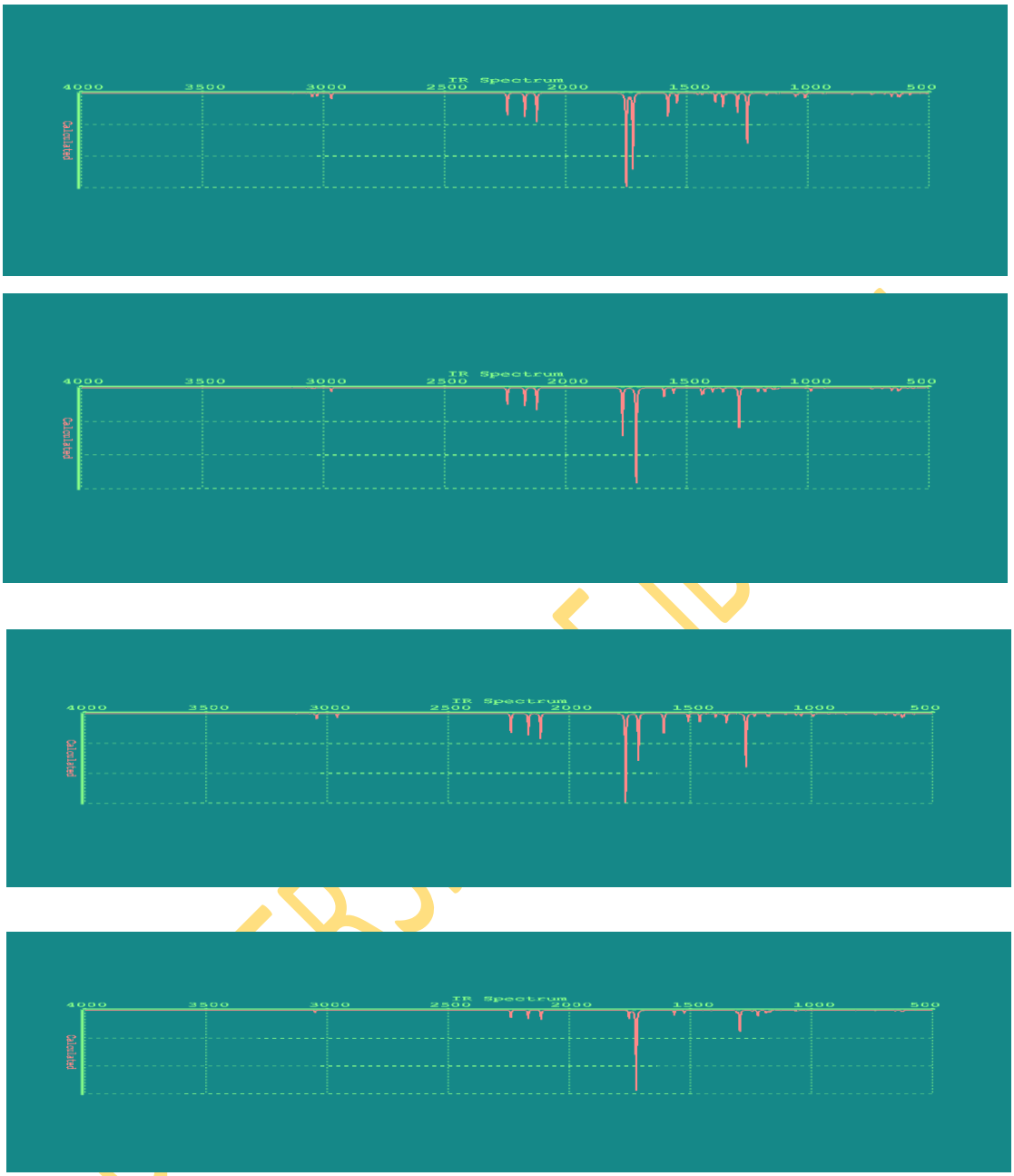

Plate4.8: Infra-red spectra of Tricarbonyl (1-4-η-5-exo-N-X,X-dimethylpyridino-cyclohexa-1,3-diene) iron

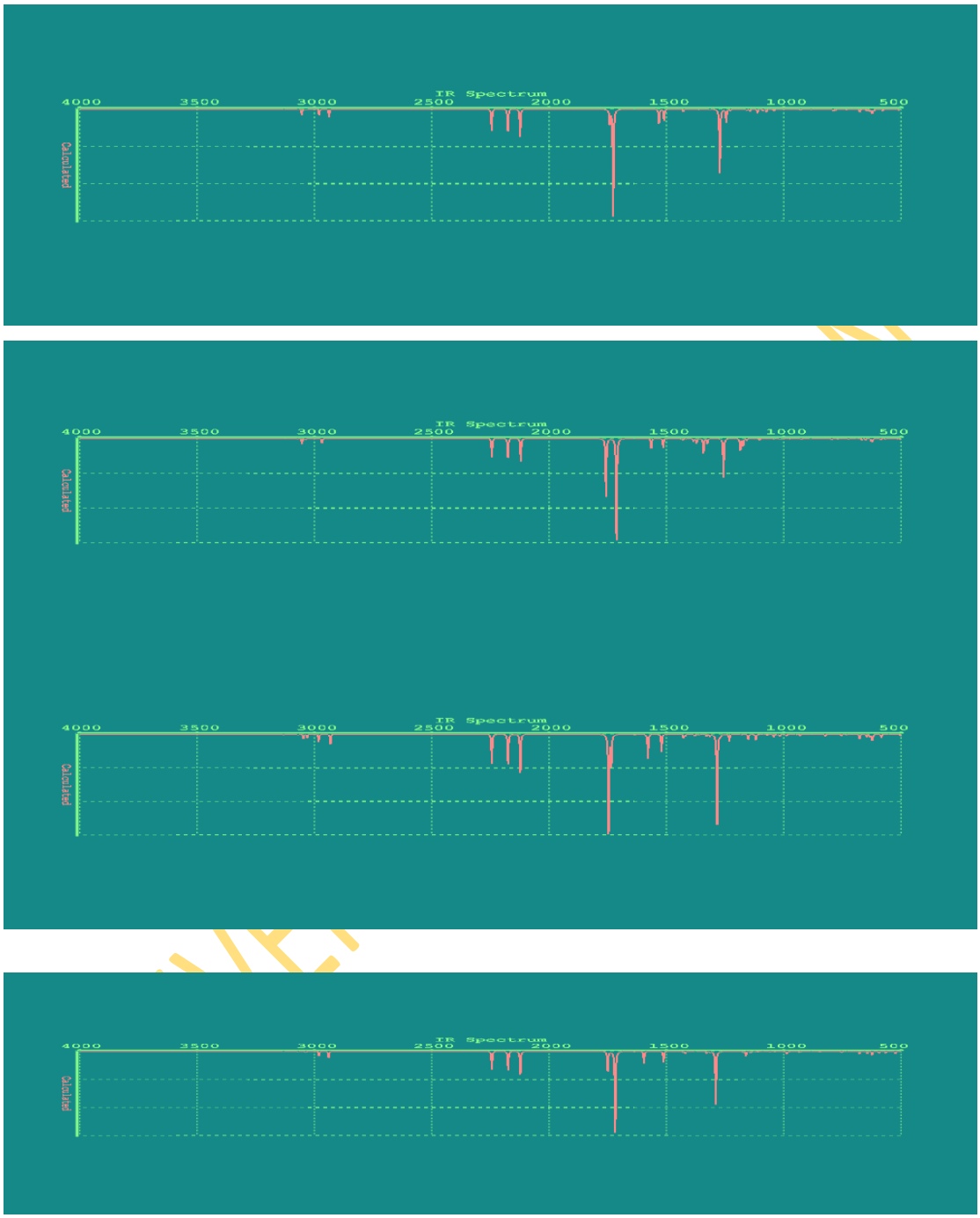

Plate 4.9: Infra-red spectra of Tricarbonyl (1-4-η-5-exo-N-X-pyridino-2-methoxy cyclohexa-1,3-diene) iron

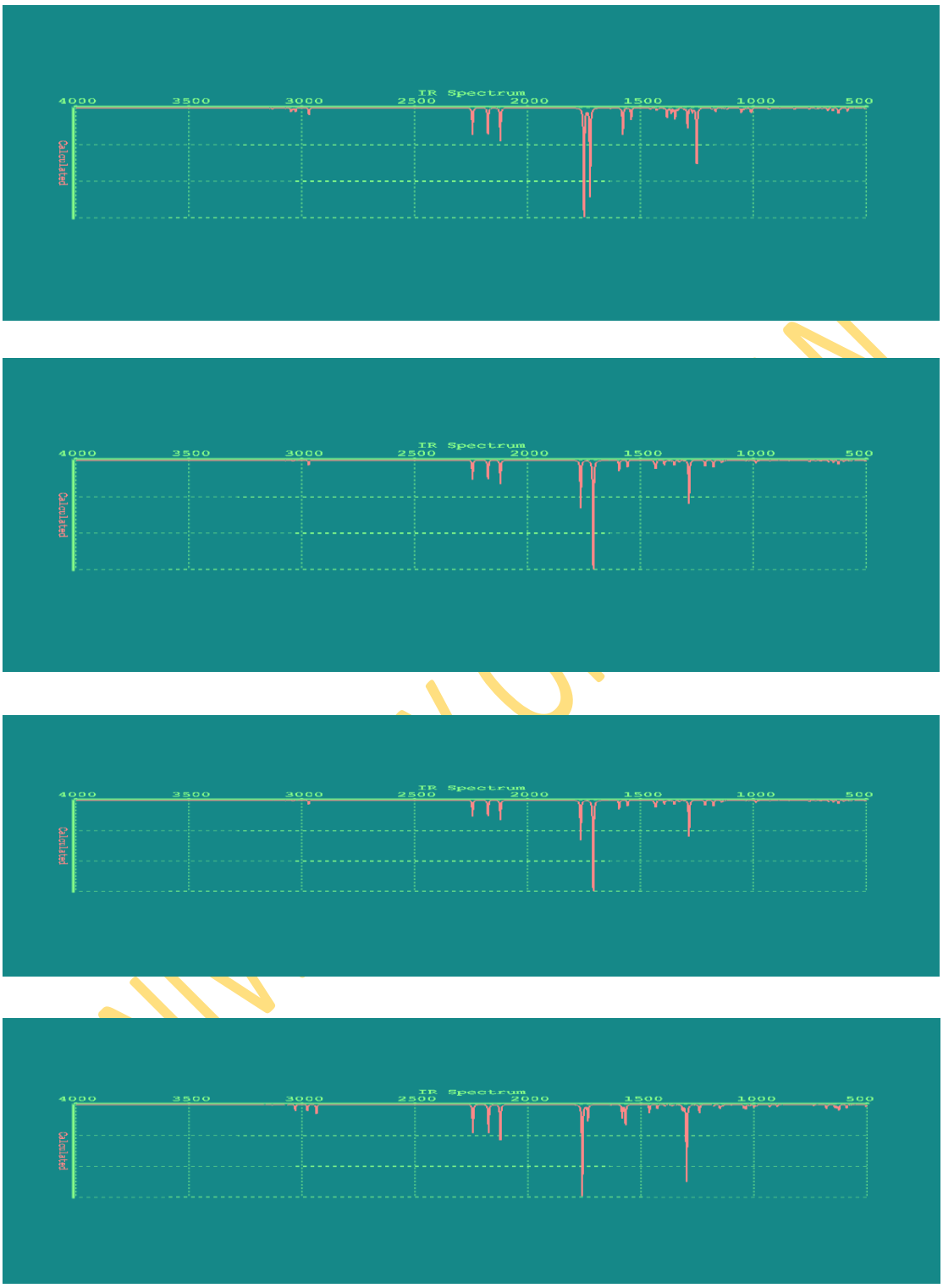

Plate 4.10: Infra-red spectra ofInfra-red spectrum of Tricarbonyl (1-4-η-5-exo-N-X,X-dimethylpyridino-2-methoxycyclohexa-1,3-diene) iron

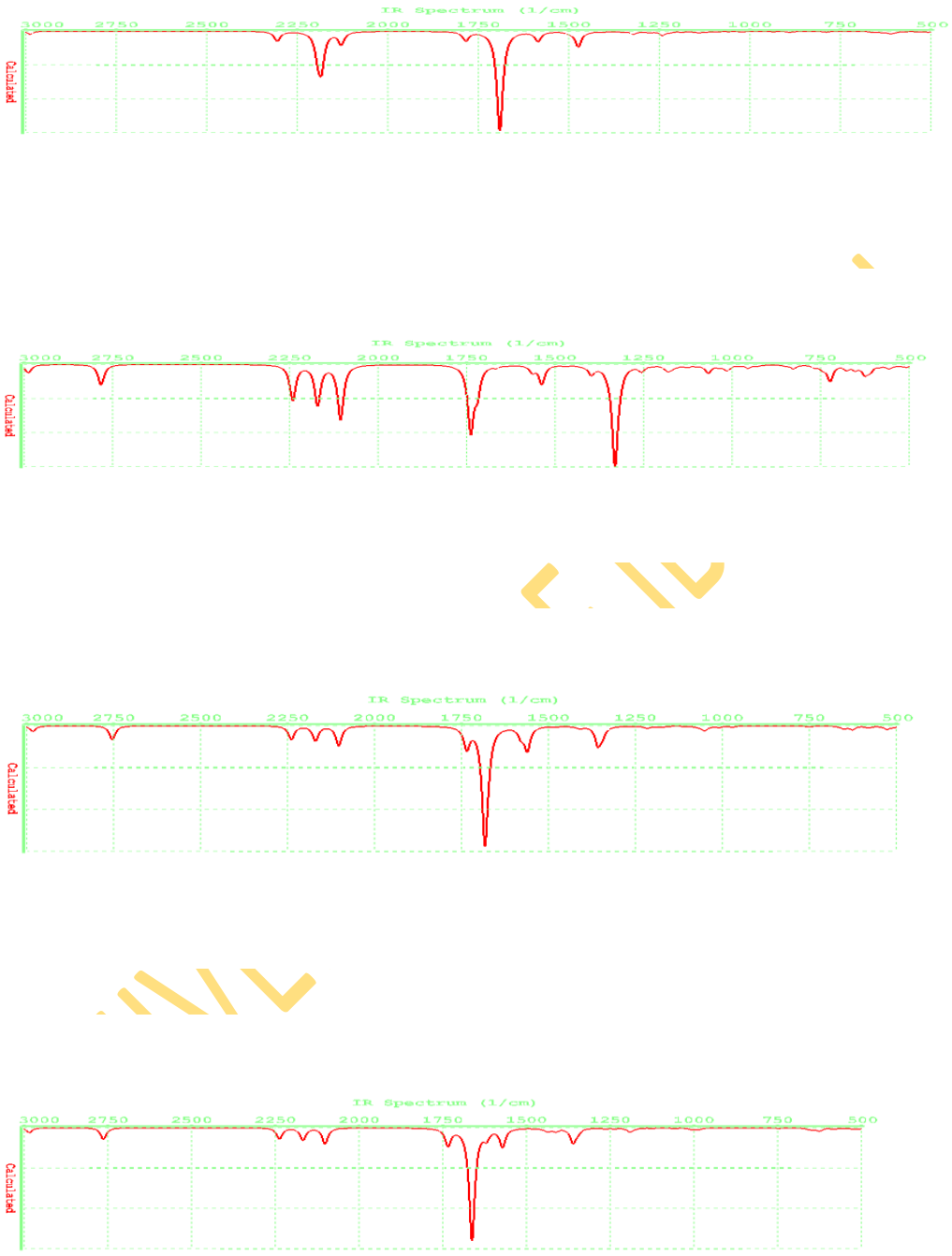

Figure 4.7: Infra-red spectra ofTricarbonyl (1-4-η-5-exo-N-4-N-Substitued amino pyridino-cyclohexa-1,3-diene) iron complexes

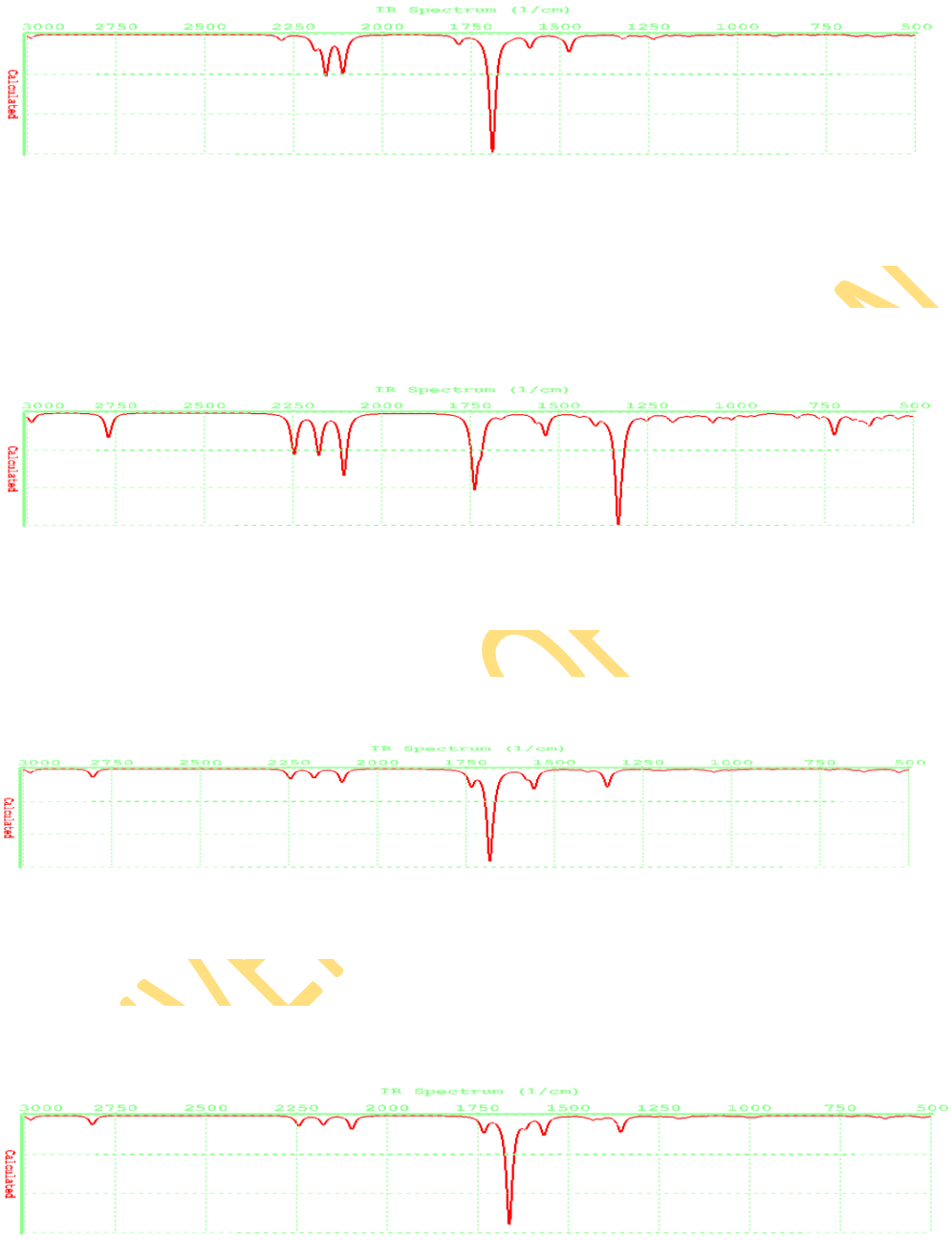

Figure 4.8: Infra-red spectra of Tricarbonyl (1-4-η-5-exo-N-4-N-substituted aminopyridino-2-methoxycyclohexa-1,3-diene) iron complexes

Appendix 4 Infra-red Spectra showing vibrational frequencies using DFT

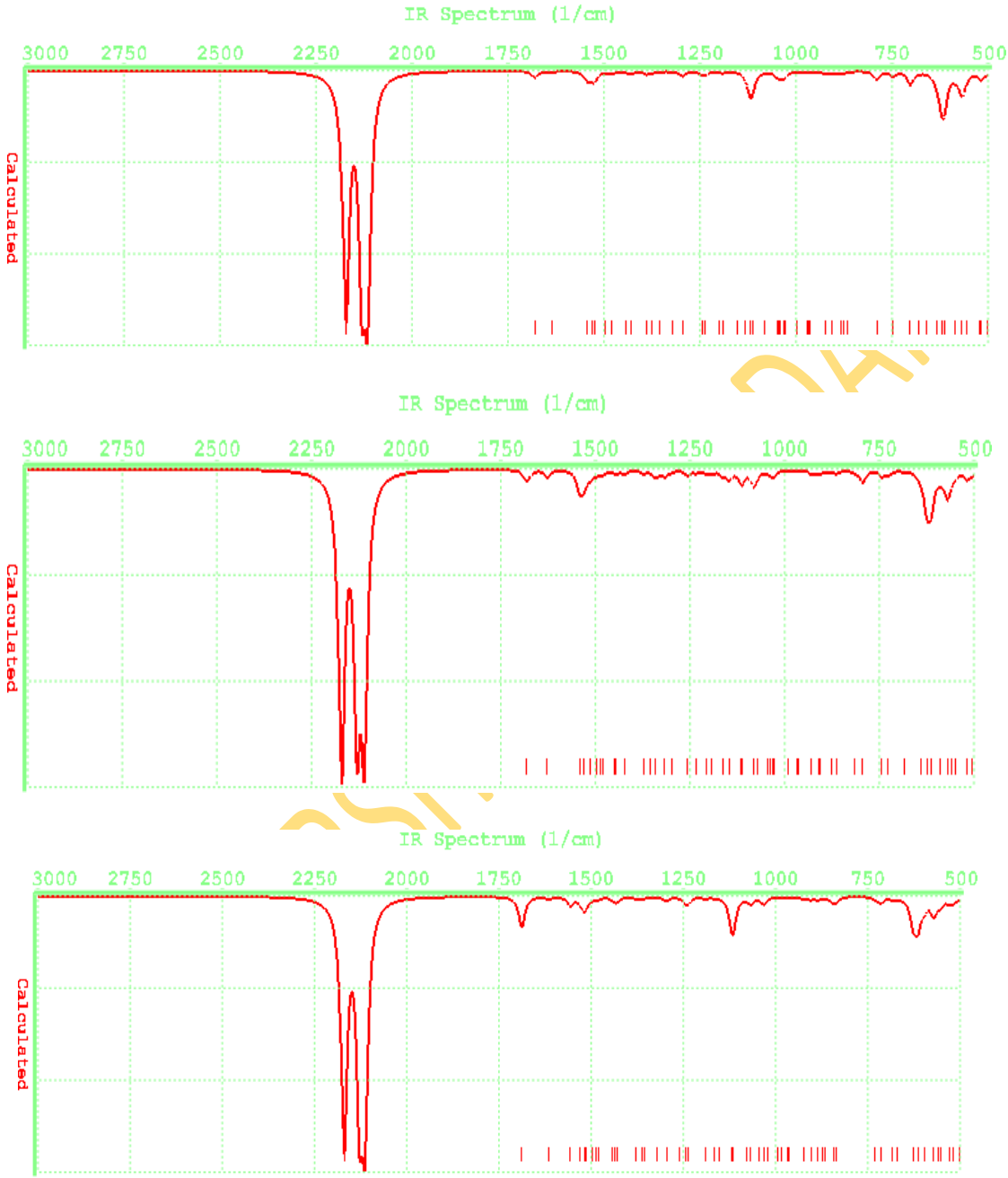

Figure 4.9: Infra-red spectra ofTricarbonyl (1-4-η-5-exo-N-X-pyridino-cyclohexa-1,3-diene) iron complexes

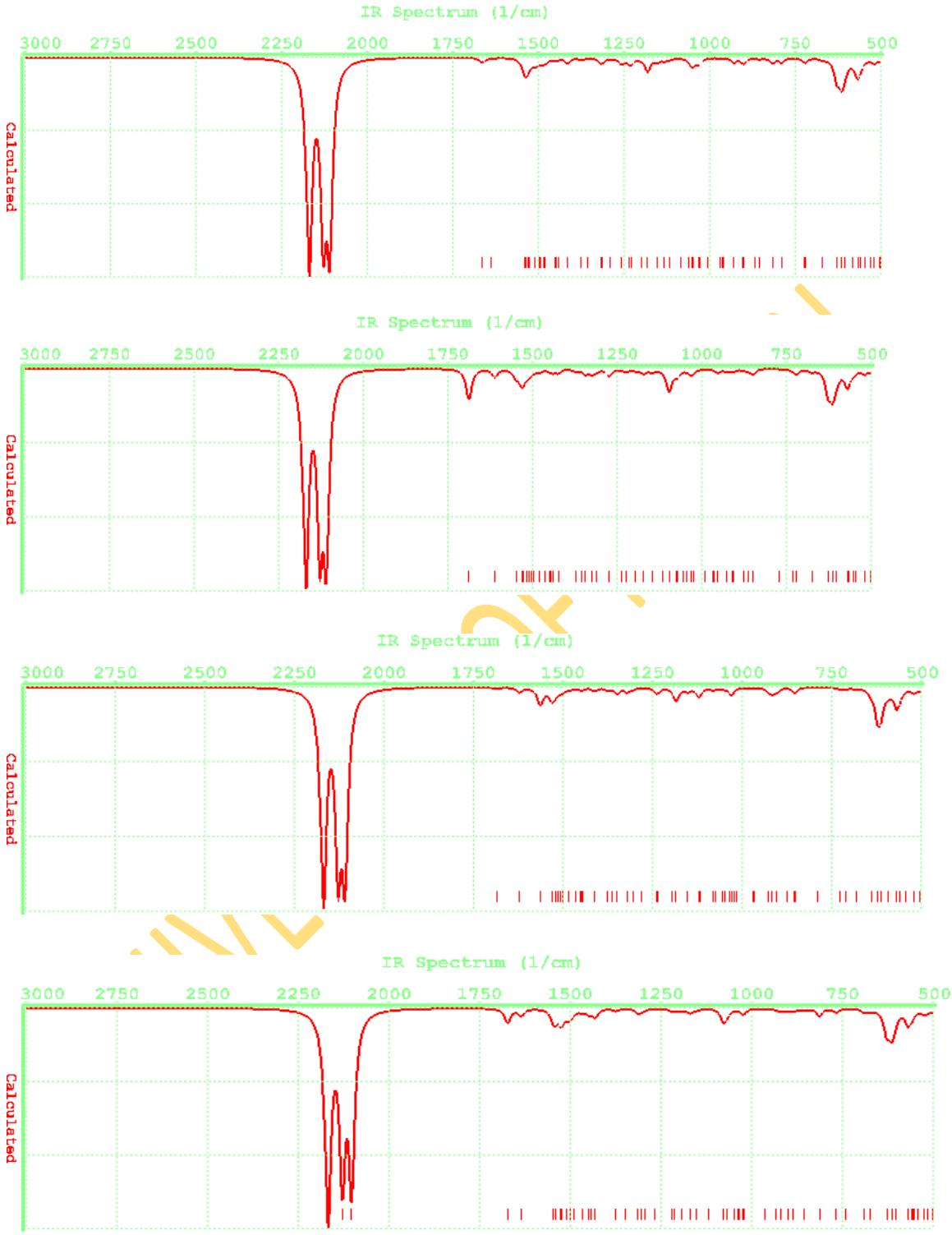

Figure 4.10: Infra-red spectra of Tricarbonyl (1-4-η-5-exo-N-X,X-dimethylpyridino-cyclohexa-1,3-diene) iron complexes

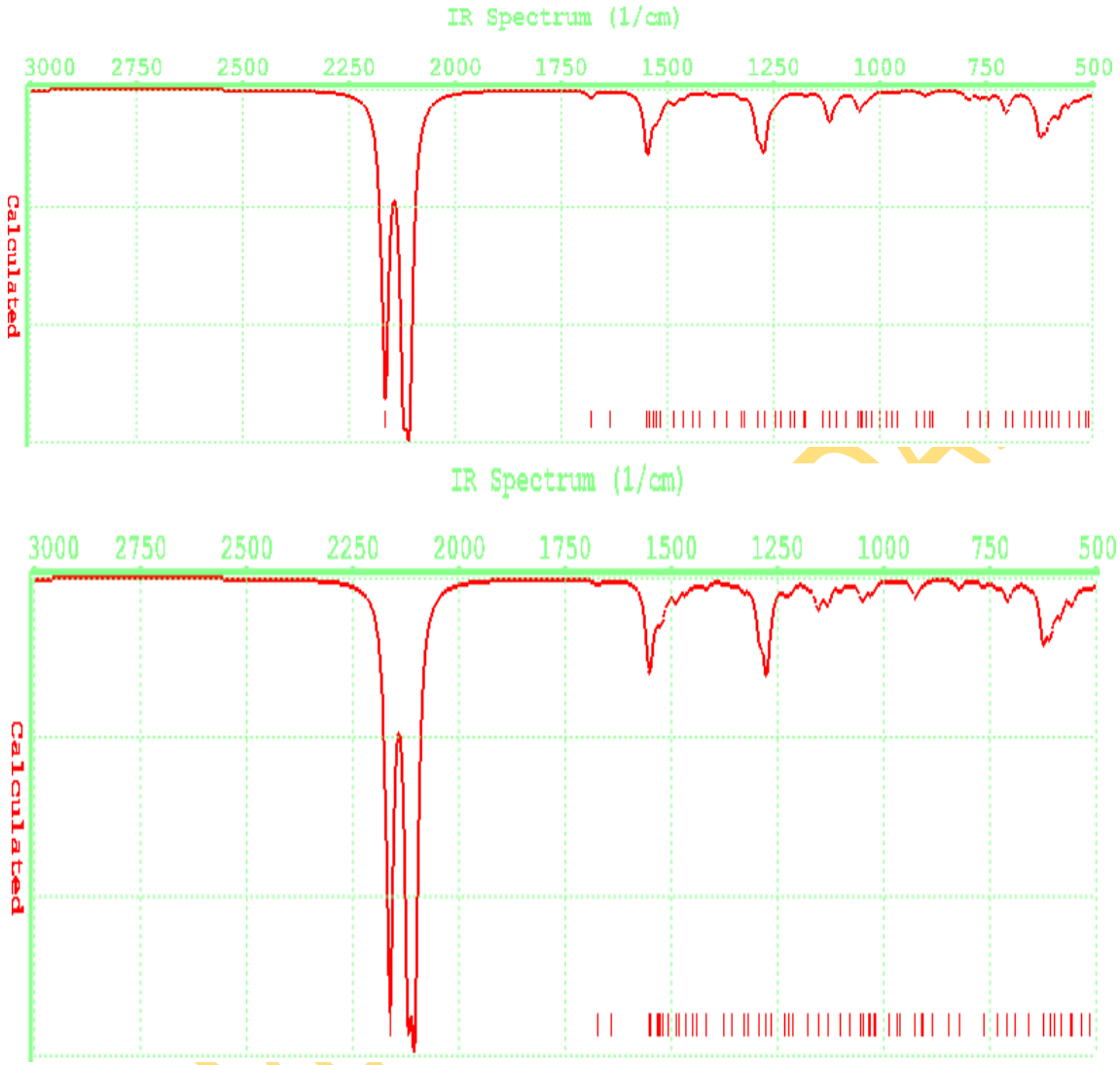

Figure 4.11: Infra-red spectra of Tricarbonyl (1-4-η-5-exo-N-Substituted pyridino-2-methoxy-cyclohexa-1,3-diene) iron complexes

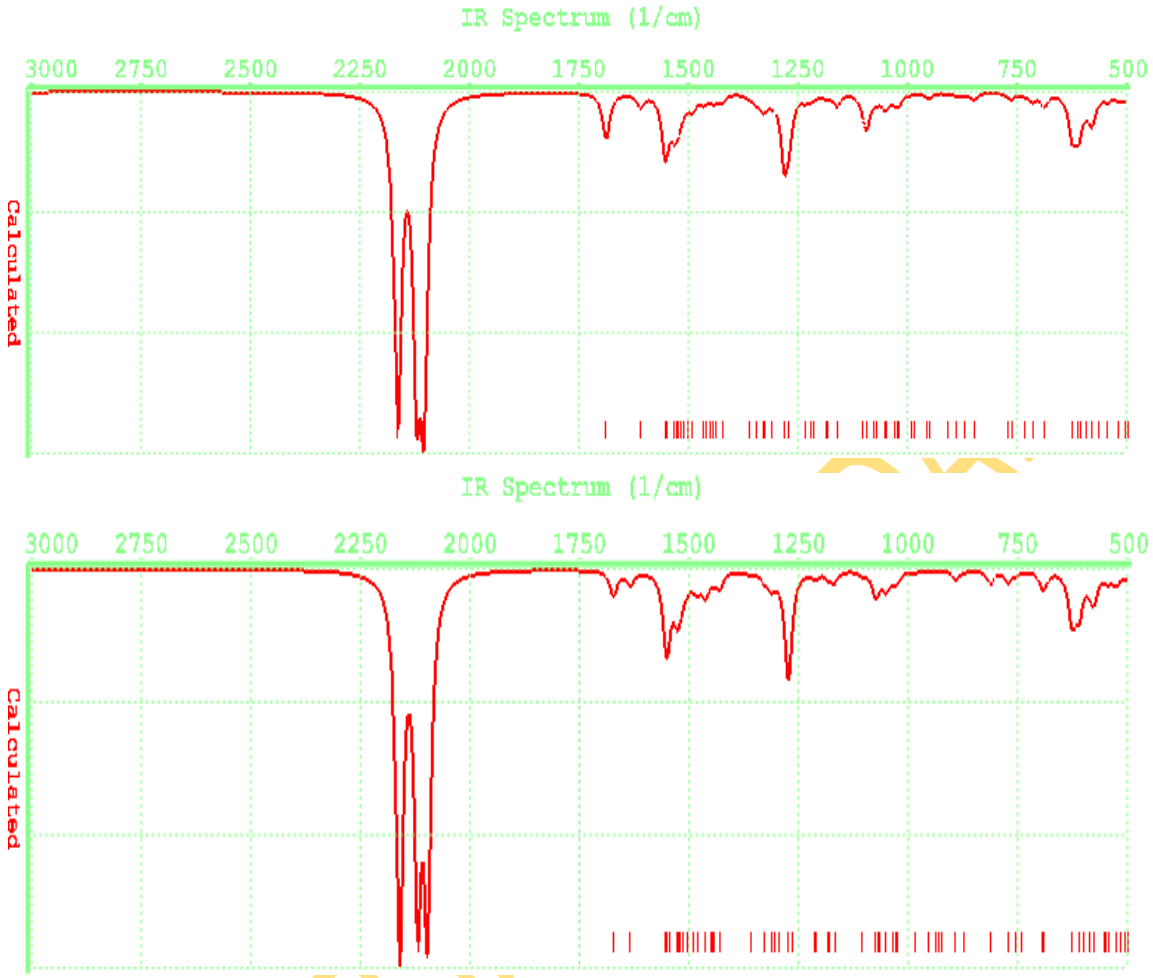

Figure 4.12: Infra-red spectra of Tricarbonyl (1-4-η-5-exo-N-X,X-dimethylpyridino-2-methoxycyclohexa-1,3-diene) iron complexes

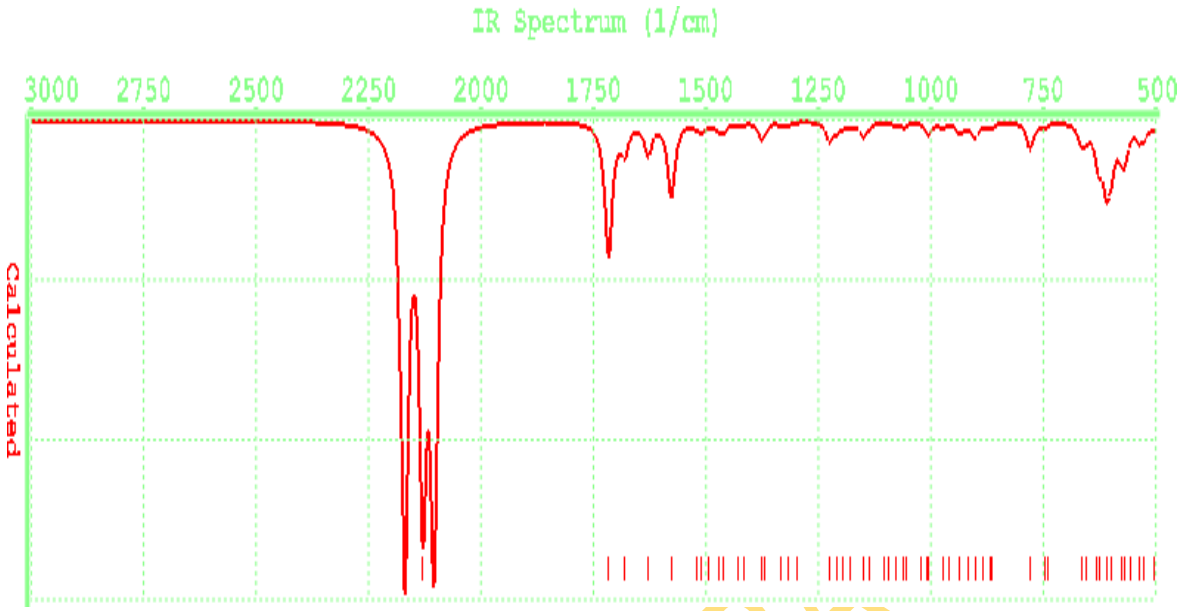
IR Spectrum (1/cm)
3000
2750
2500
2250
2000
1750
1500
1250
1000
750
500
Calculated

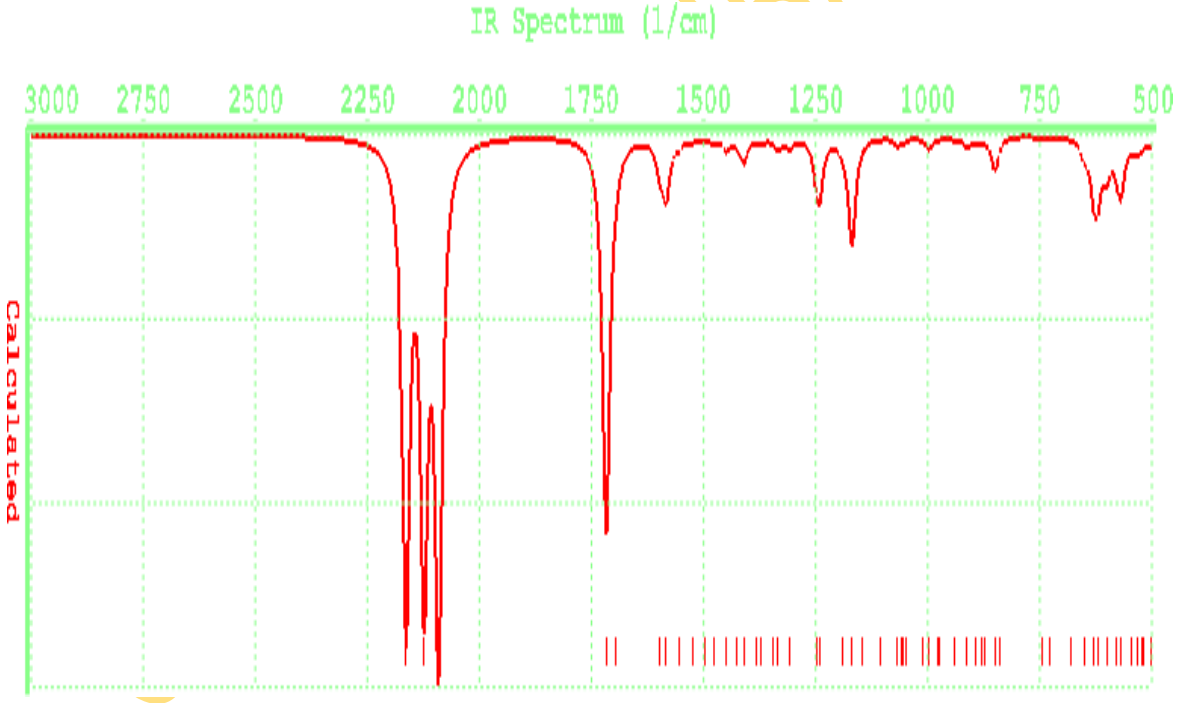
IR Spectrum (1/cm)
3000
2750
2500
2250
2000
1750
1500
1250
1000
750
500
Calculated

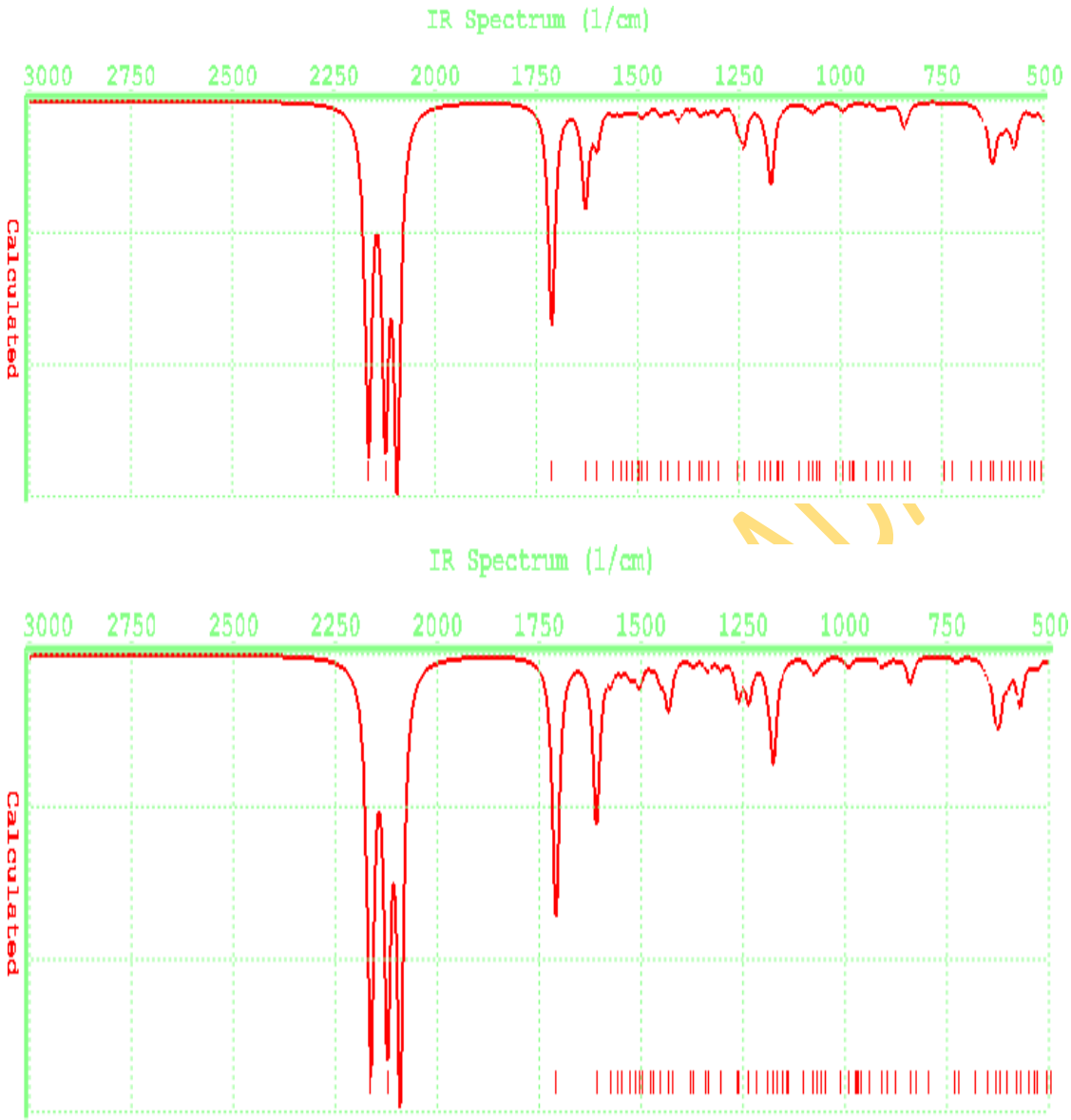

Figure 4.13: Infra-red Spectra of Tricarbonyl (1-4-η-5-exo-N-Substituted aminopyridino-cyclohexa-1,3-diene) iron complexes

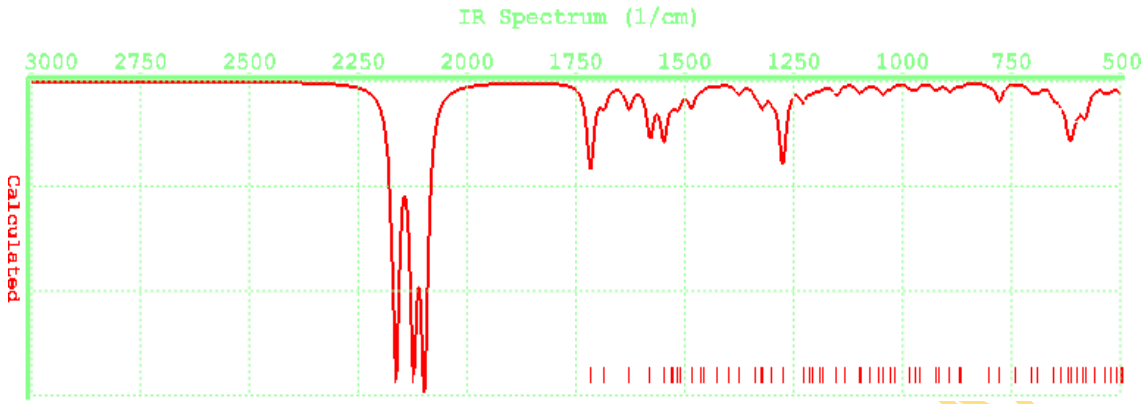
IR Spectrum (1/cm)
3000 2750 2500 2250 2000 1750 1500 1250 1000 750 500
Calculated

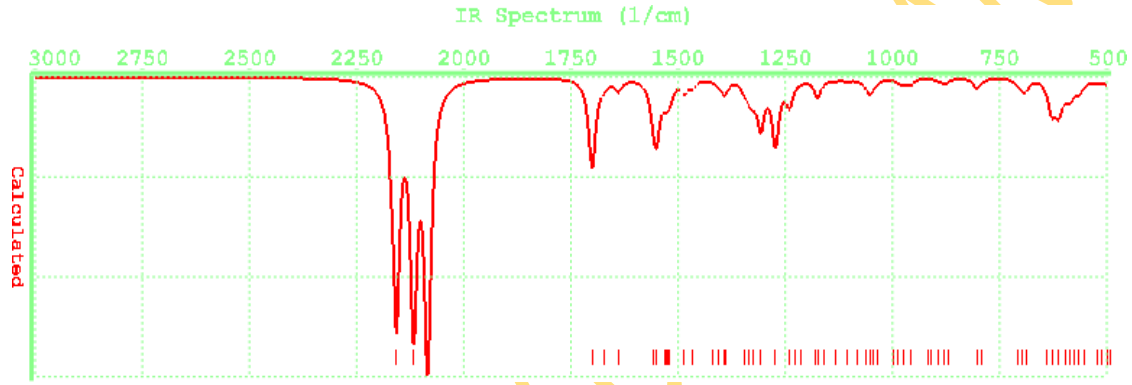
IR Spectrum (1/cm)
3000 2750 2500 2250 2000 1750 1500 1250 1000 750 500
Calculated

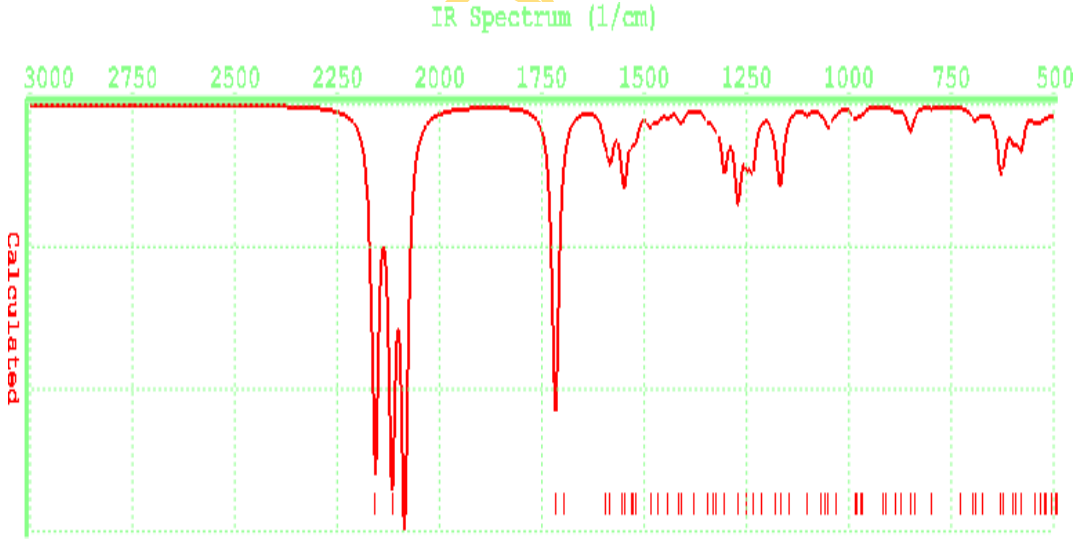
IR Spectrum (1/cm)
3000 2750 2500 2250 2000 1750 1500 1250 1000 750 500
Calculated

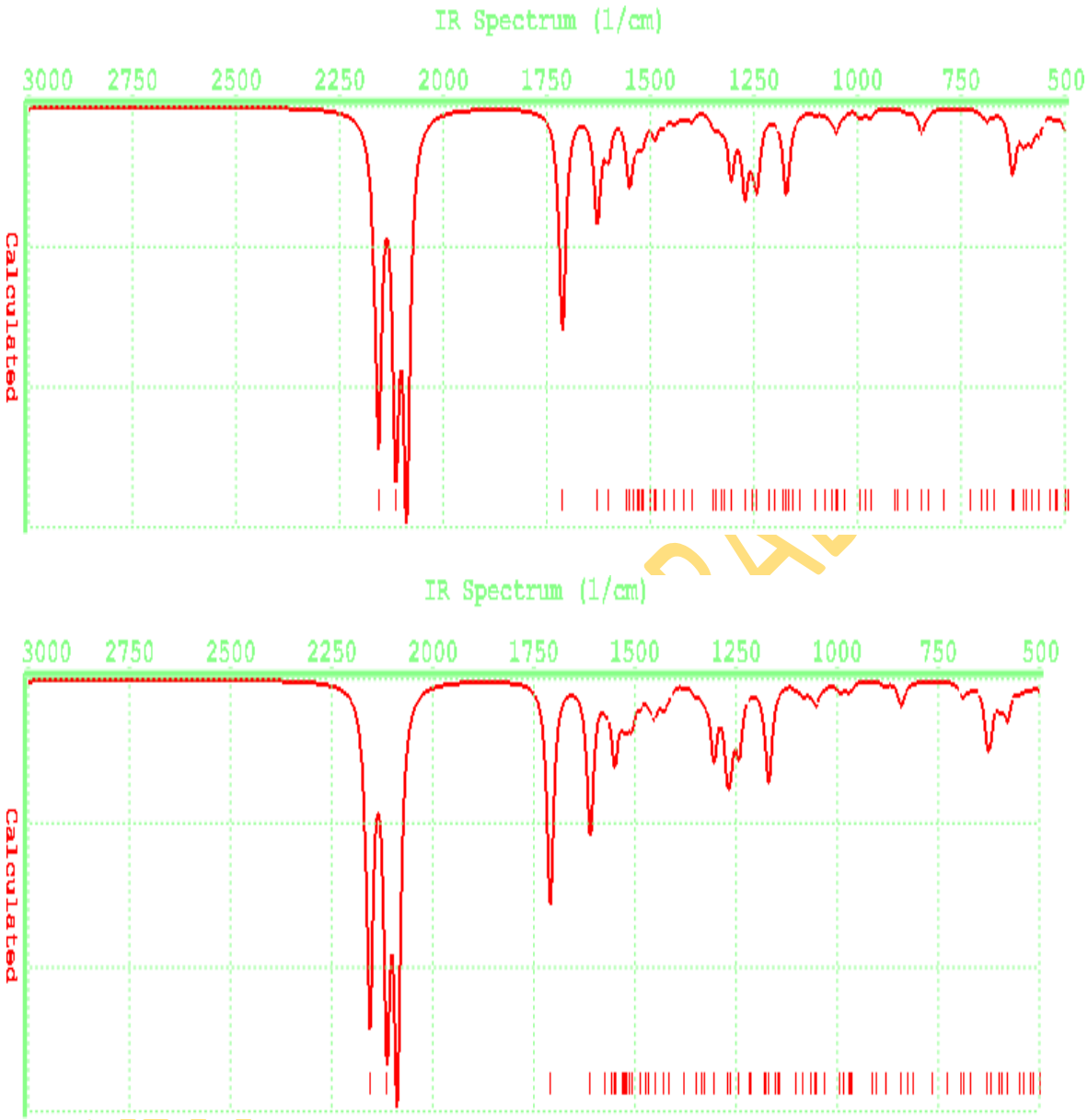

Figure 4.14: Infra-red spectra ofTricarbonyl (1-4-η-5-exo-N-Substituted amino-pyridino-2-methoxycyclohexa-1,3-diene) iron complexes

Appendix 5 Neutron Magnetic Resonance Spectra (NMR) of complexes

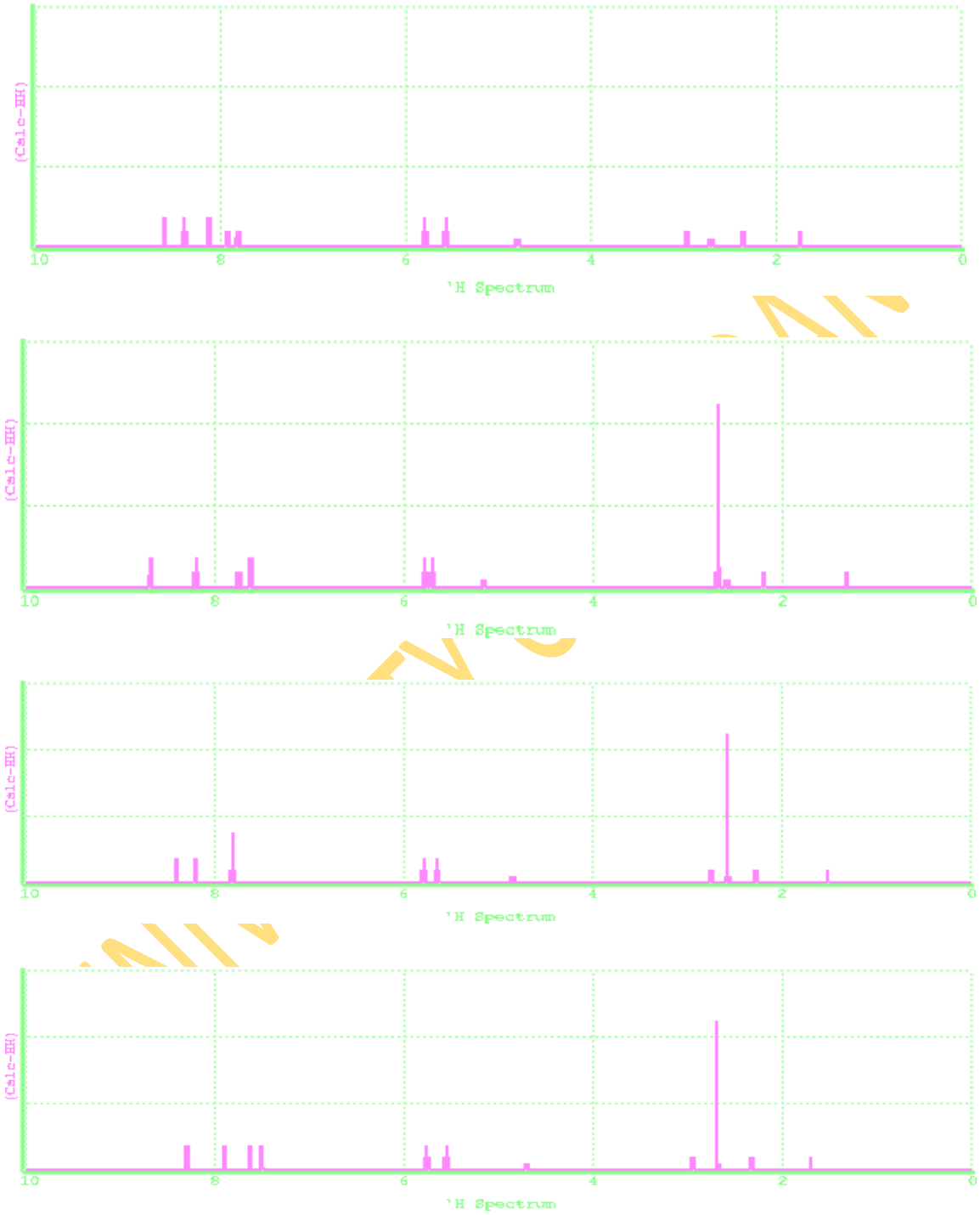

Figure 4.15a: ^{1}H n.m.r spectra of Tricarbonyl (1-4-η-5-exo-N-X-pyridino-cyclohexa-1,3-diene) iron complexes

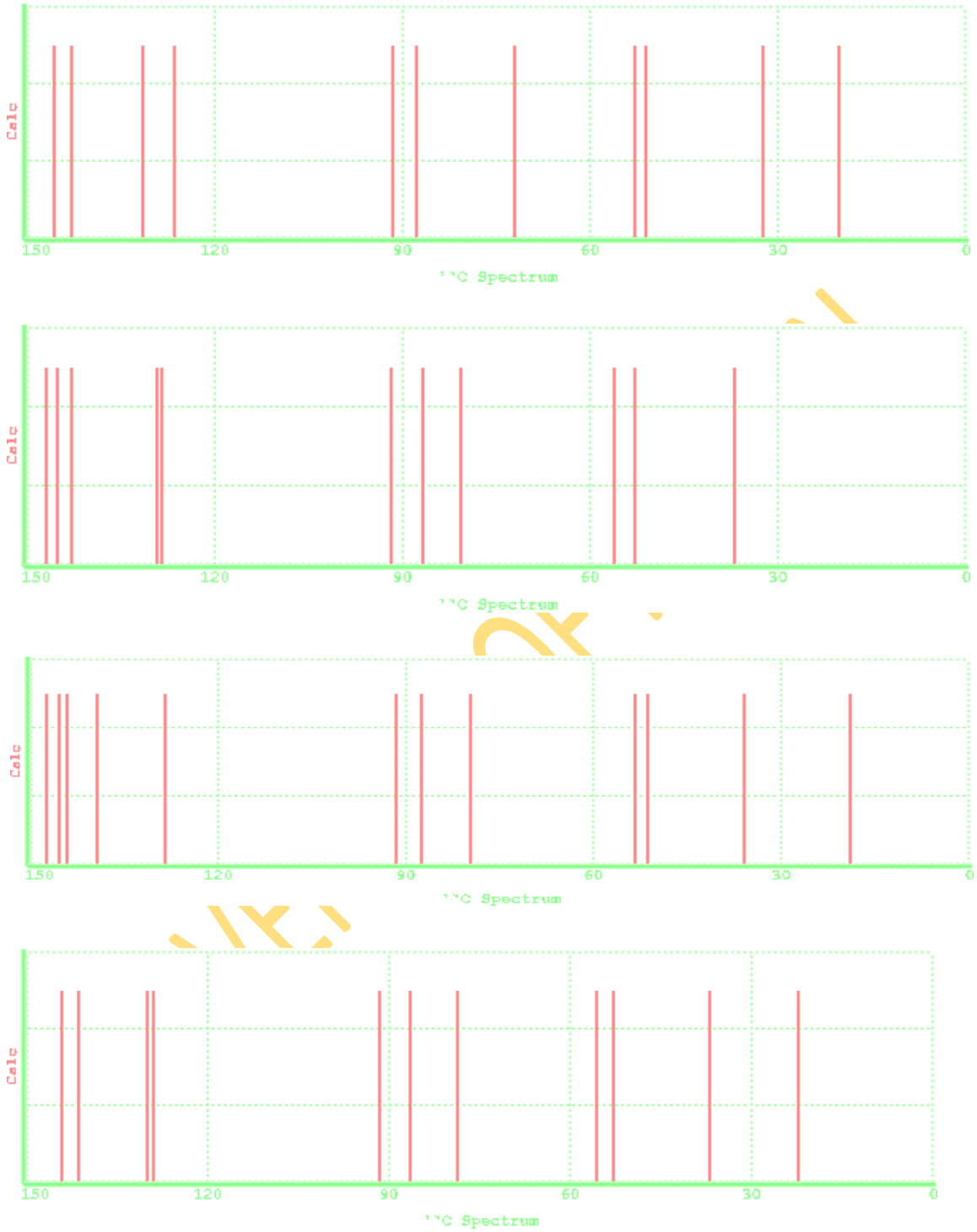

Figure 4.15b: ^{13}C N.m.r spectra of Tricarbonyl (1-4-η-5-exo-N-X-pyridino-cyclohexa-1,3-diene) iron complexes

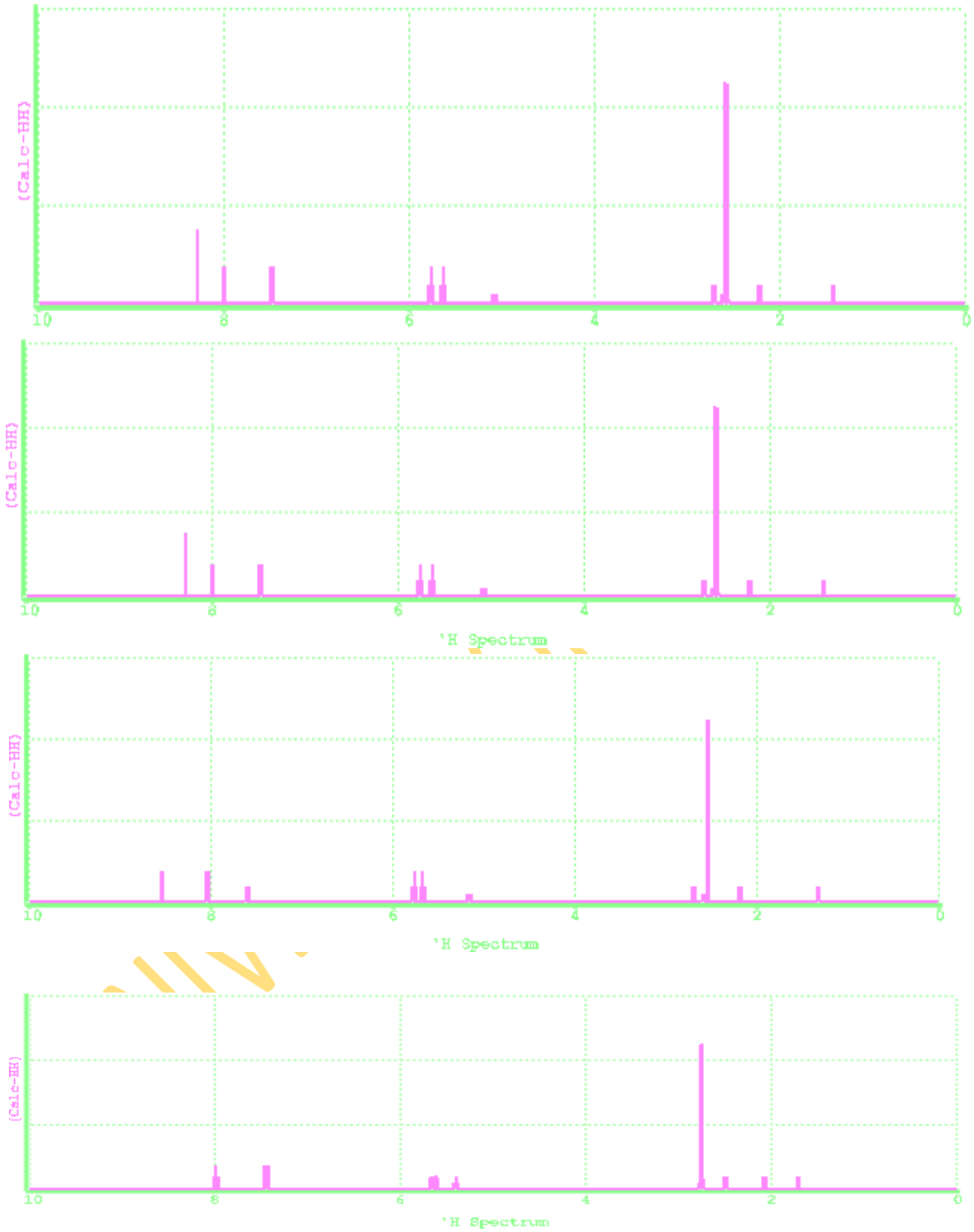

Figure 4.16a: ^{1}H n.m.r spectra of Tricarbonyl (1-4-η-5-exo-N-X,X-dimethylpyridino-cyclohexa-1,3-diene) iron complexes

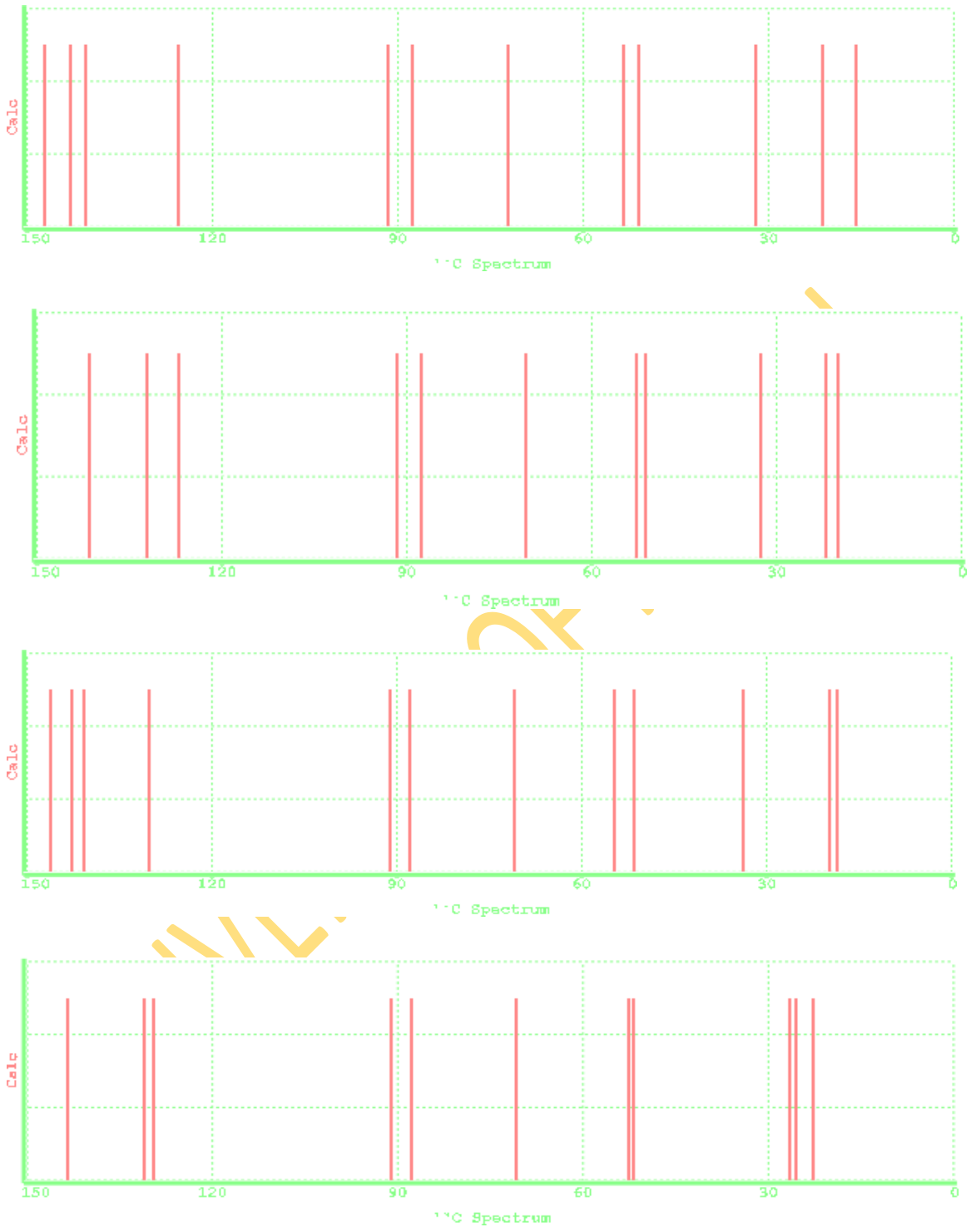

Figure 4.16b: ^{13}CN.m.r spectra of Tricarbonyl (1-4-η-5-exo-N-X,X-dimethylpyridino-cyclohexa-1,3-diene) iron complexes

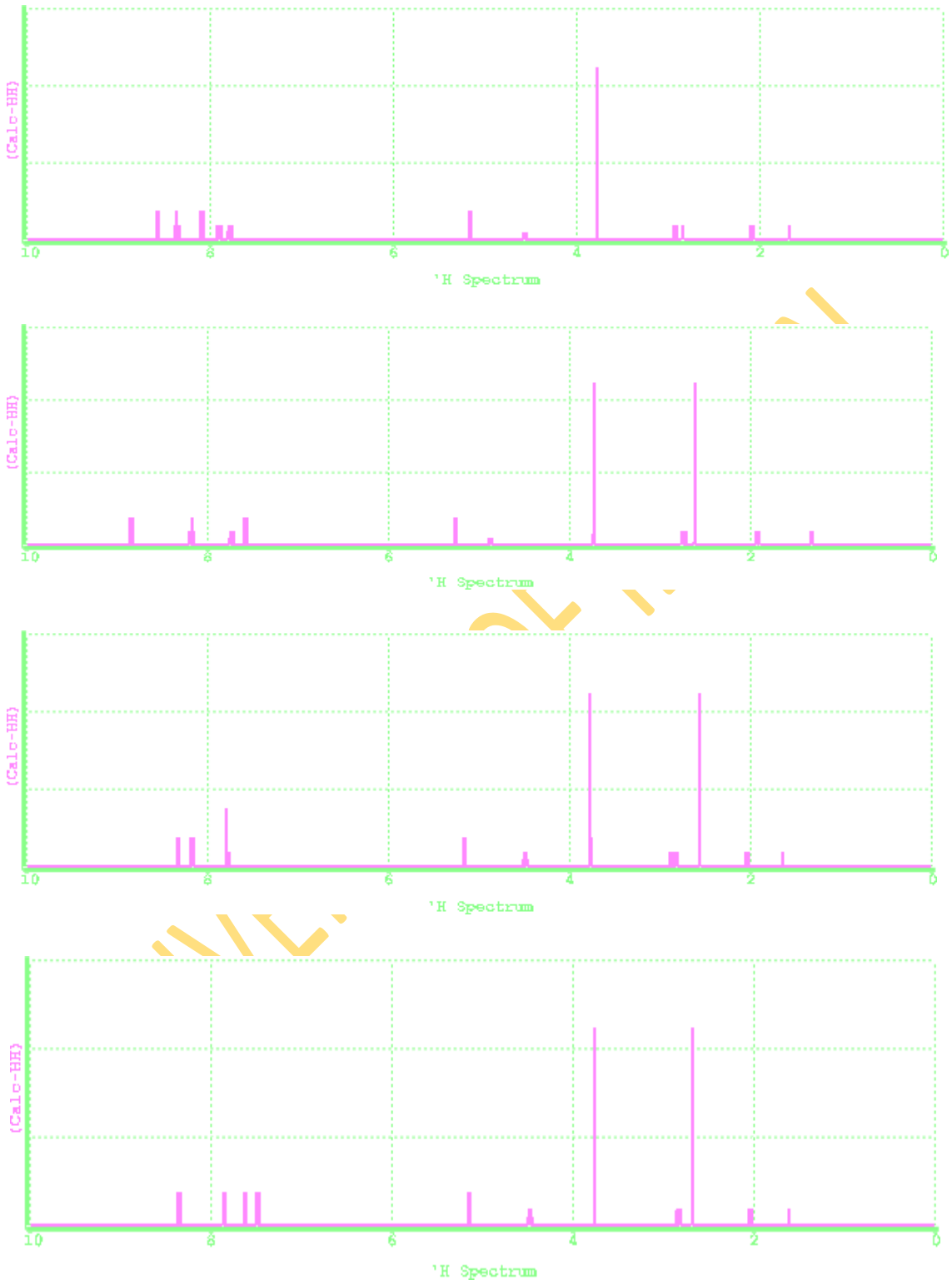

Figure 4.17a: ^{1}Hn.m.r. spectra of Tricarbonyl (1-4-η-5-exo-N-substiruted pyridino-2-methoxycyclohexa-1,3-diene) iron complexes

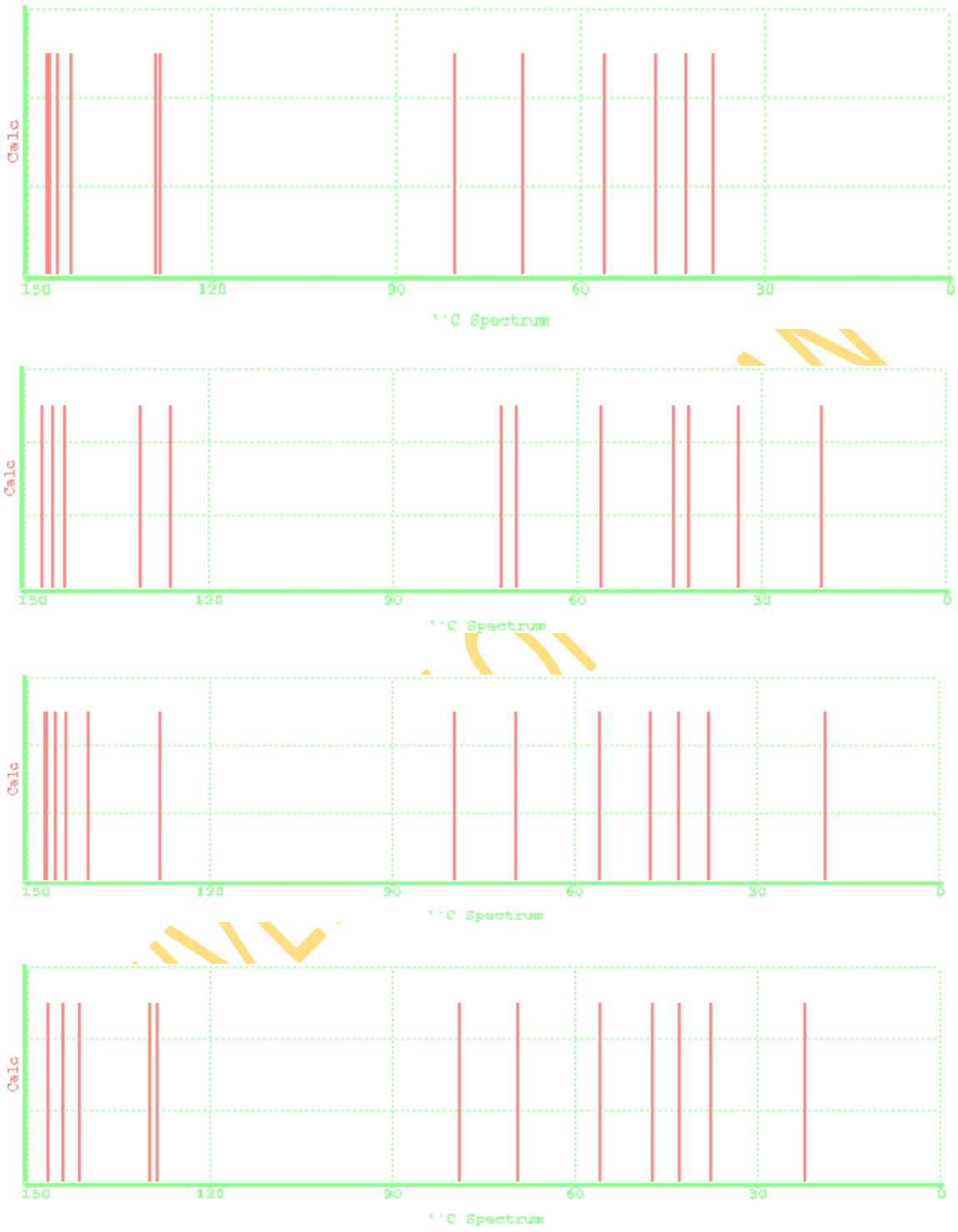

Figure 4.17b: ^{13}C N.m.r spectra of Tricarbonyl (1-4-η-5-exo-N- substituted pyridino-2-methoxycyclohexa-1,3-diene) iron complexes

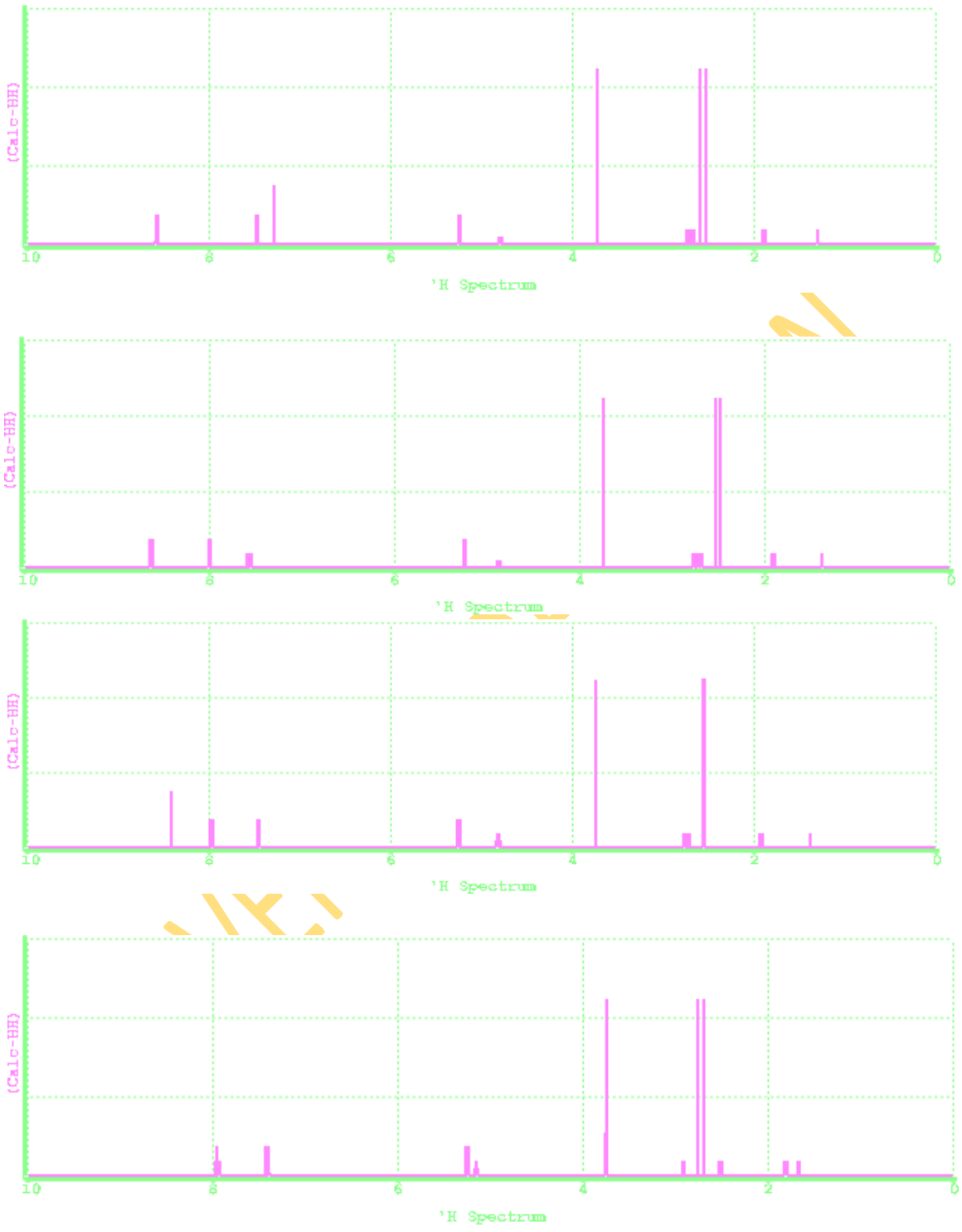

Figure 4.18a: [1]Hn.m.r spectra of Tricarbonyl (1-4-η-5-exo-N-X,X-dimethylpyridino-2-methoxycyclohexa-1,3-diene) iron complexes

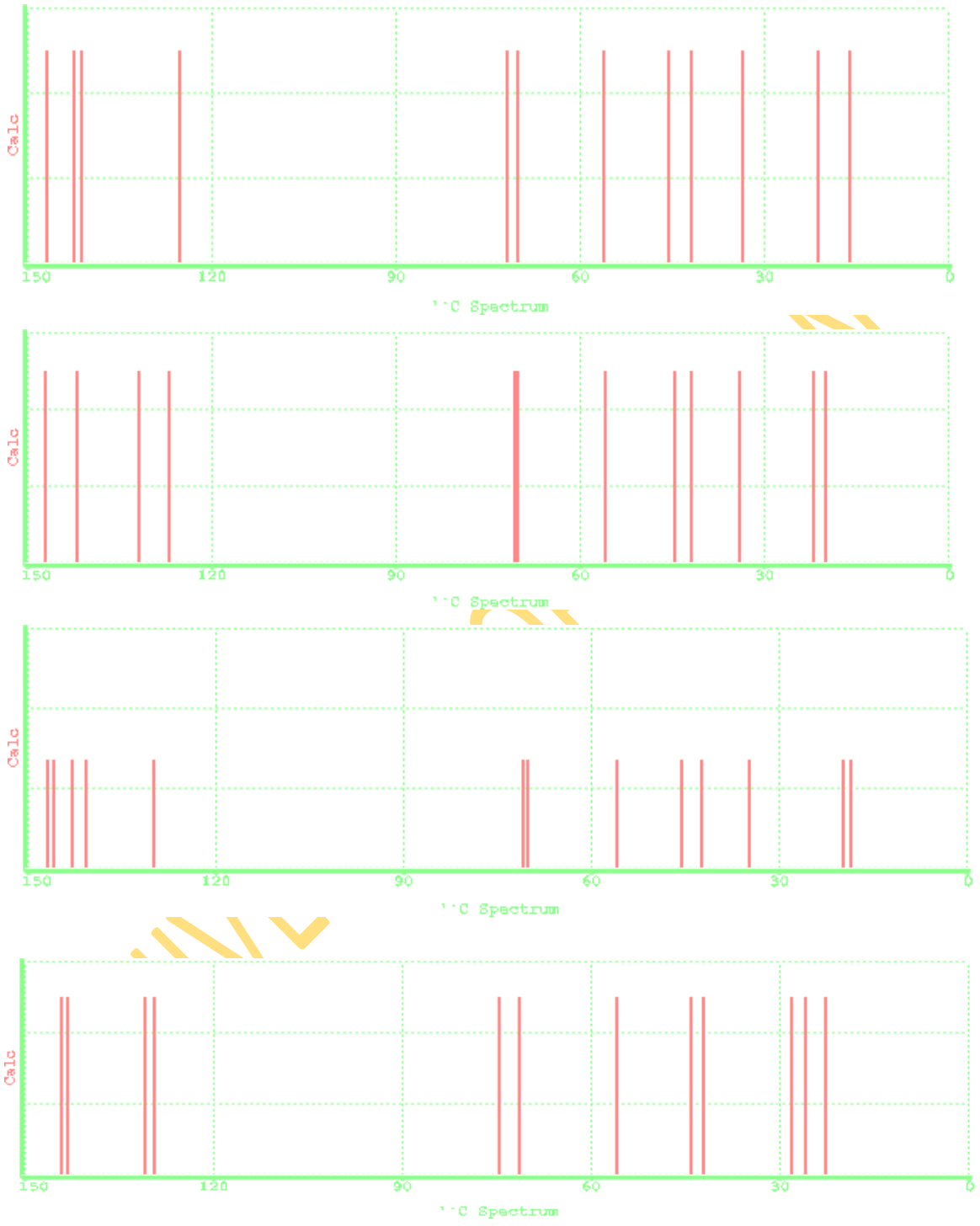

Figure 4.18b: ^{13}CN.m.rspectra of Tricarbonyl (1-4-η-5-exo-N- X,X-dimethyl-pyridino-2-methoxycyclohexa-1,3-diene) iron complexes

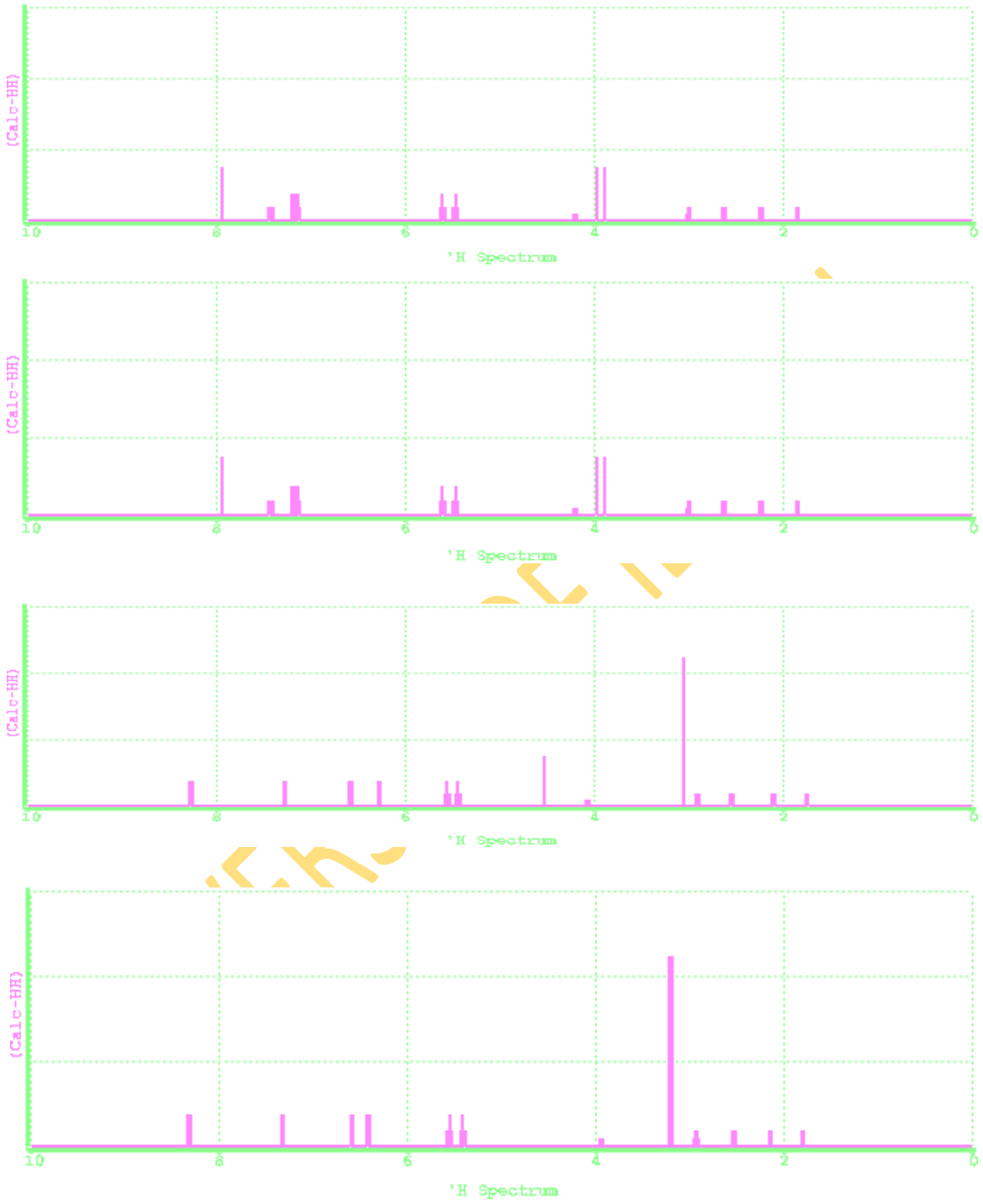

Figure 4.19a: ^{1}Hn.m.r spectra of Tricarbonyl (1-4-η-5-exo-N-Substituted methylamino-pyridino-cyclohexa-1,3-diene) iron complexes

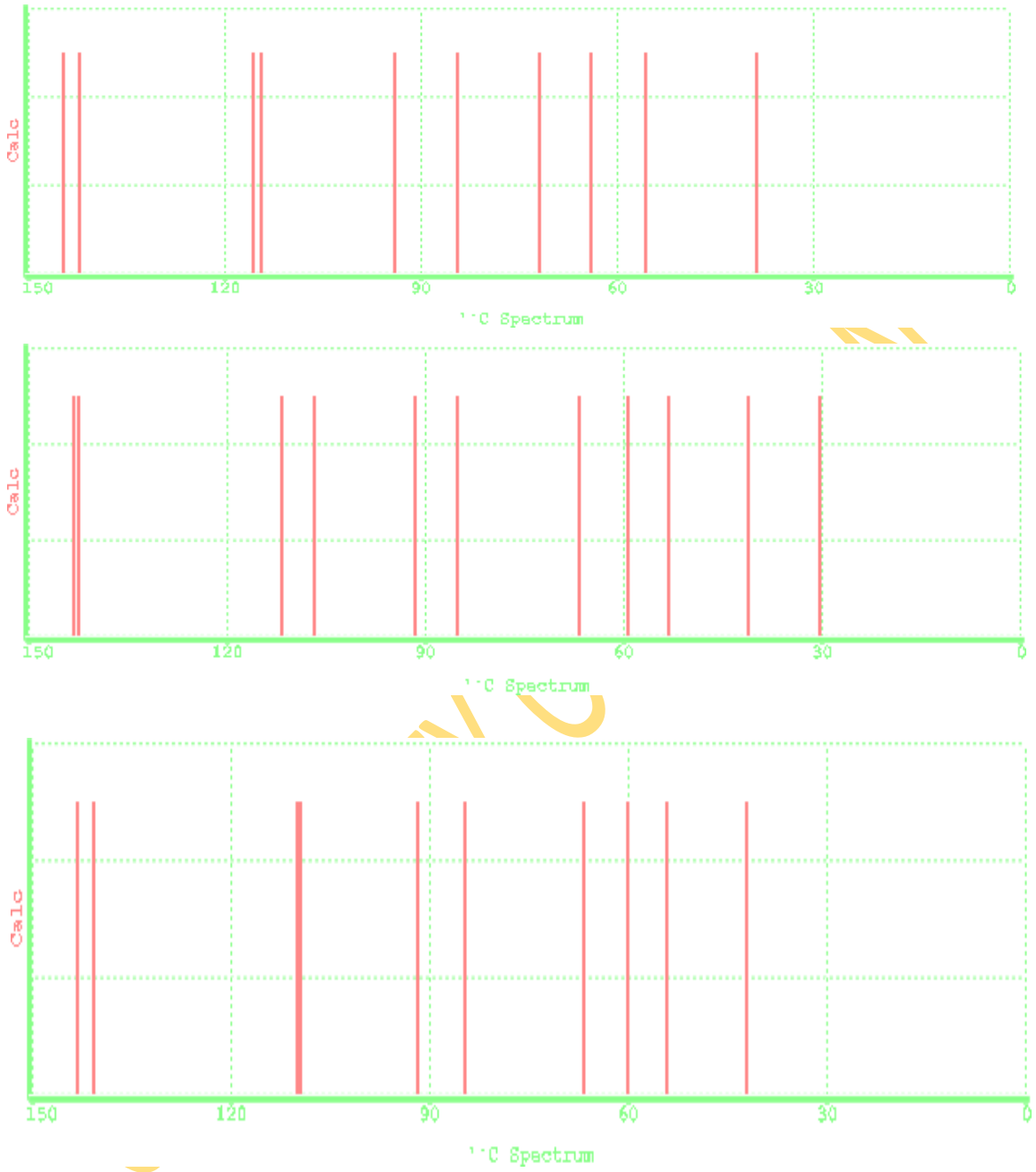

Figure 4.19b: ^{13}CN.m.r Spectra ofTricarbonyl (1-4-η-5-exo-N- substituted amino pyridino-cyclohexa-1,3-diene) iron complexes

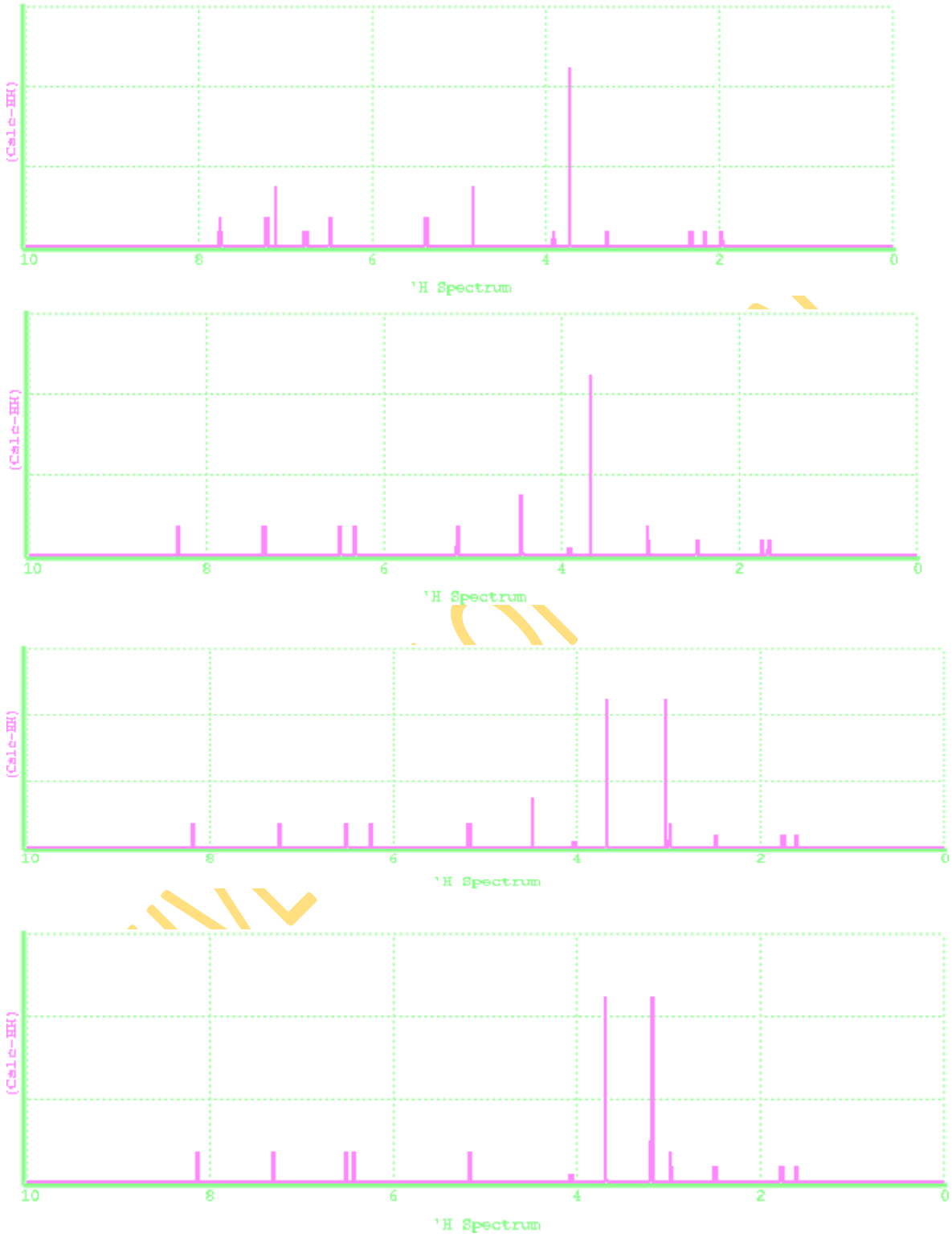

Figure 4.20a: [1]Hn.m.r spectra of Tricarbonyl (1-4-η-5-exo-N-substituted aminopyridino-2-methoxycyclohexa-1,3-diene) iron complexes

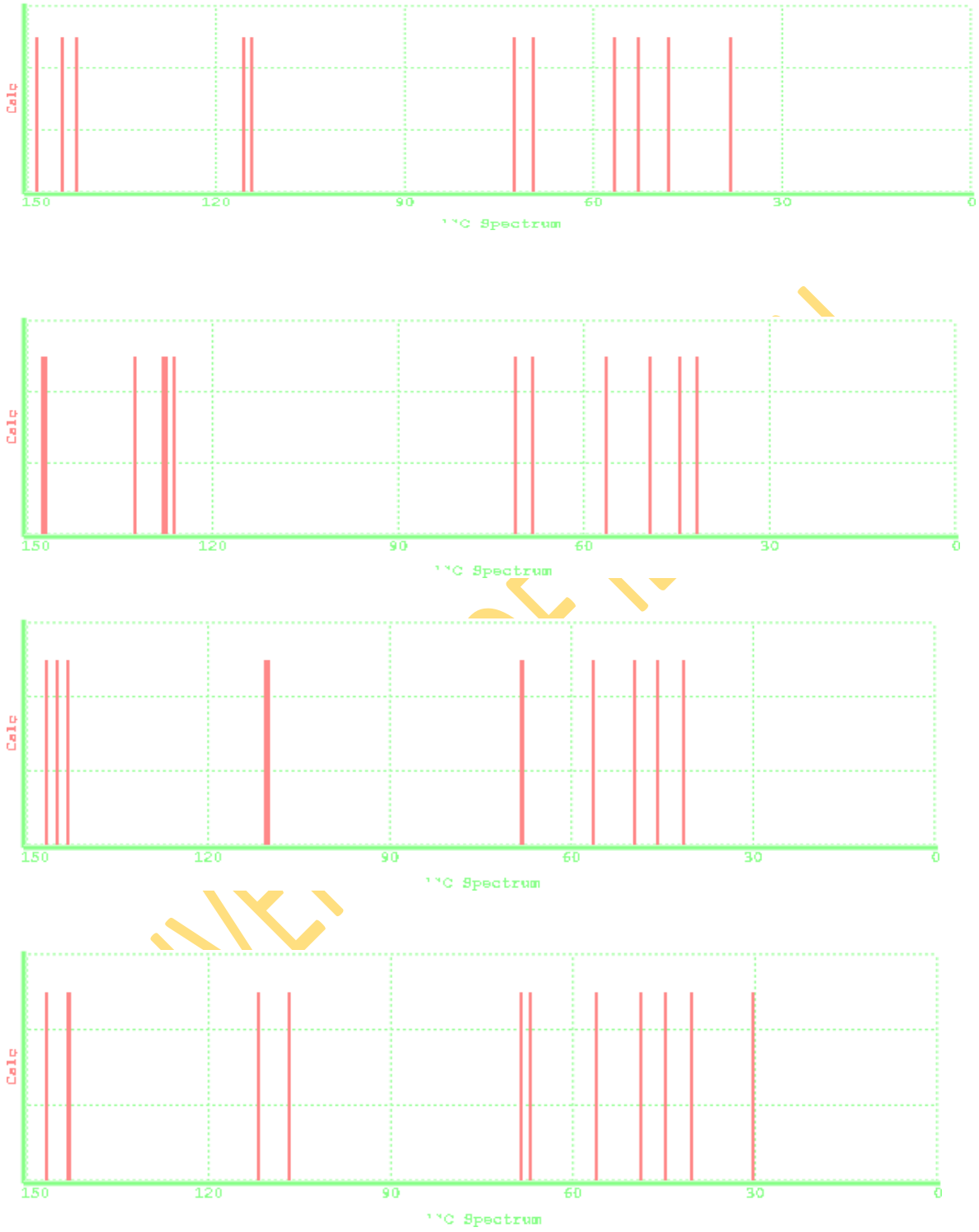

Figure 4.20b: ^{13}CN.m.rspectra of Tricarbonyl (1-4-η-5-exo-X-substituted aminopyridino-2-methoxycyclohexa-1,3-diene) iron complexes

Appendix 6 Uv-visible Spectra of complexes

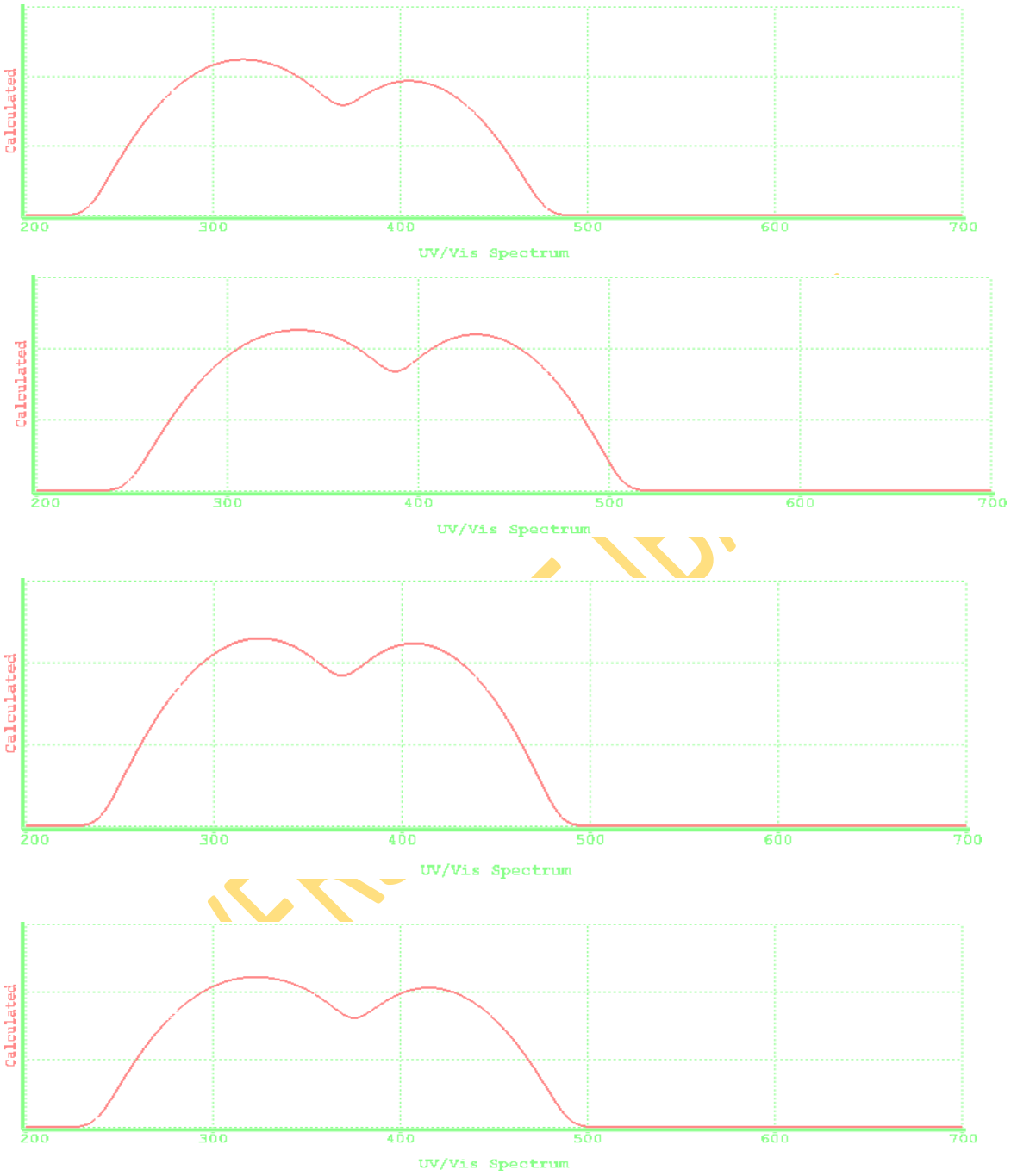

Figure 4.21: Uv-visible spectra of Tricarbonyl (1-4-η-5-exo-N-substituted pyridino-cyclohexa-1,3-diene) iron complexes

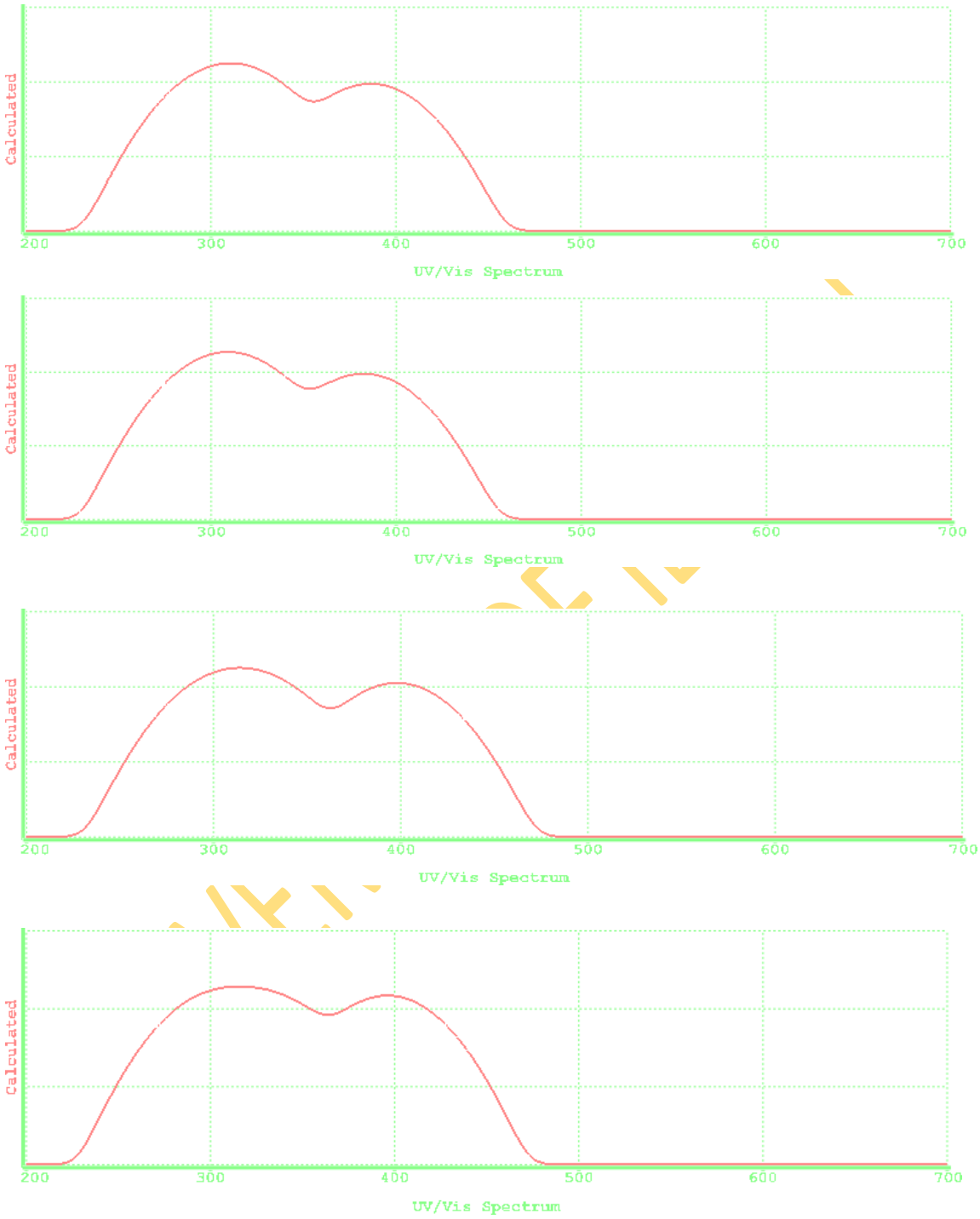

Figure 4.22: Uv-visible Spectra of Tricarbonyl (1-4-η-5-exo-N-X,X-dimethyl pyridino-cyclohexa-1,3-diene) iron complexes

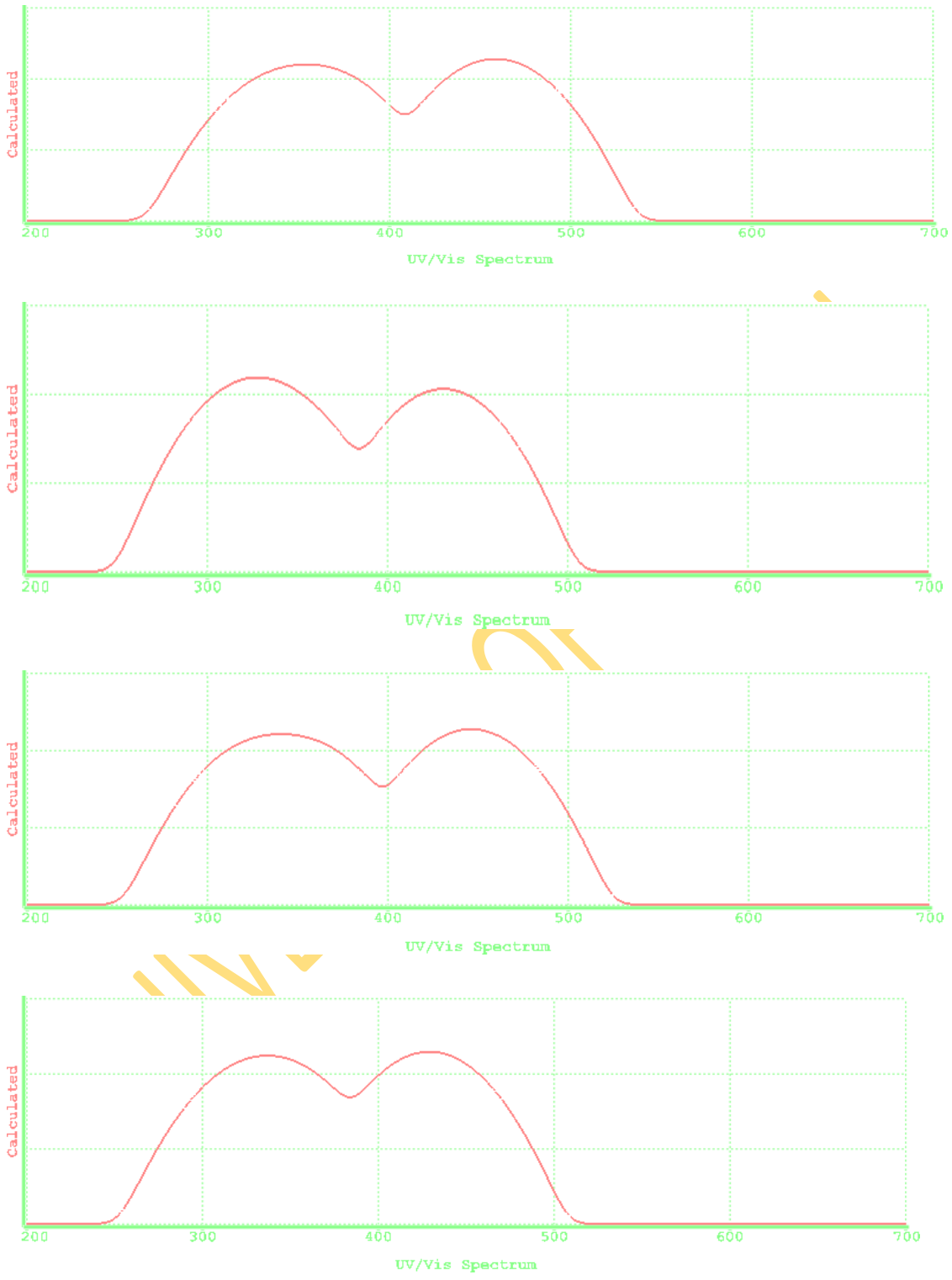

Figure 4.23: UV-visible spectra of Tricarbonyl (1-4-η-5-exo-N-Substituted pyridino-2-methoxycyclohexa-1,3-diene) iron complexes

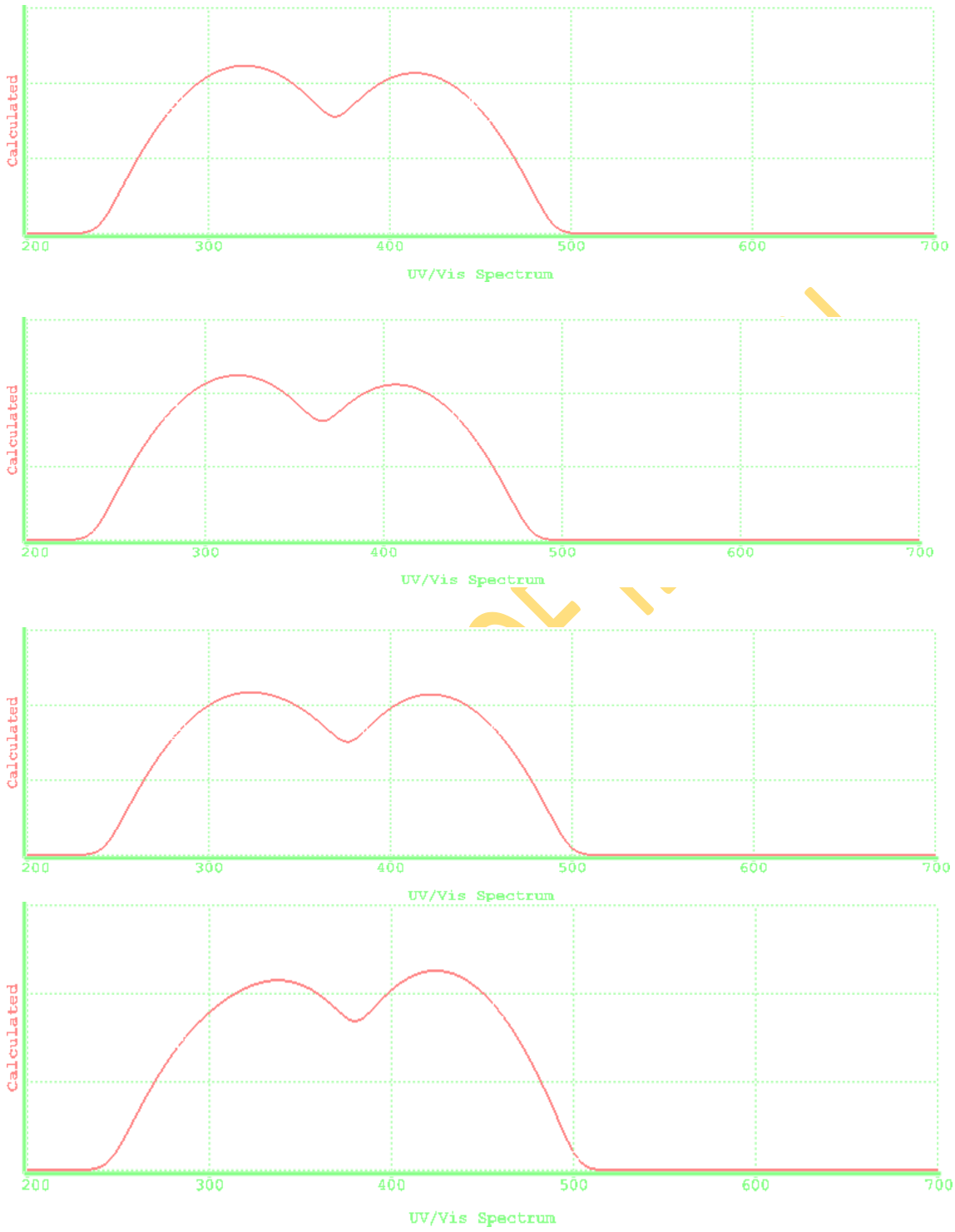

Figure 4.24: UV-visible spectra of UV-visible spectrum of Tricarbonyl(1-4-η-5-exo-N-X,X-dimethylpyridino-2-methoxycyclohexa-1,3-diene ironcomplexes

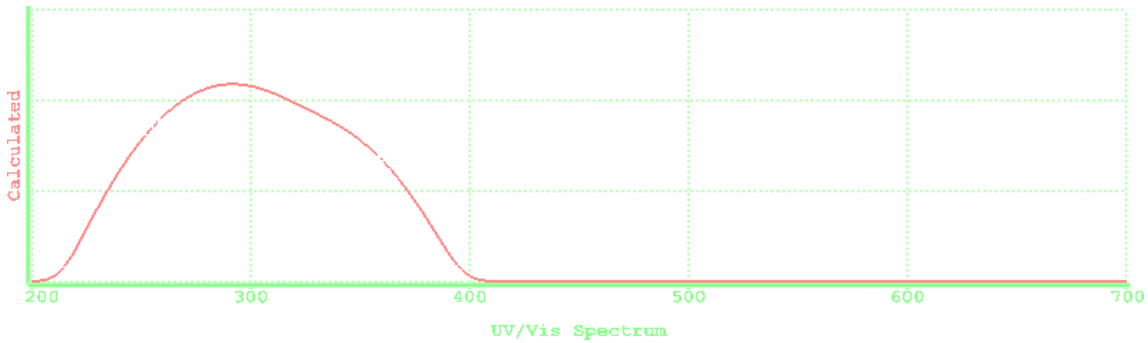
Calculated
200
300
400
500
600
700
UV/Vis Spectrum

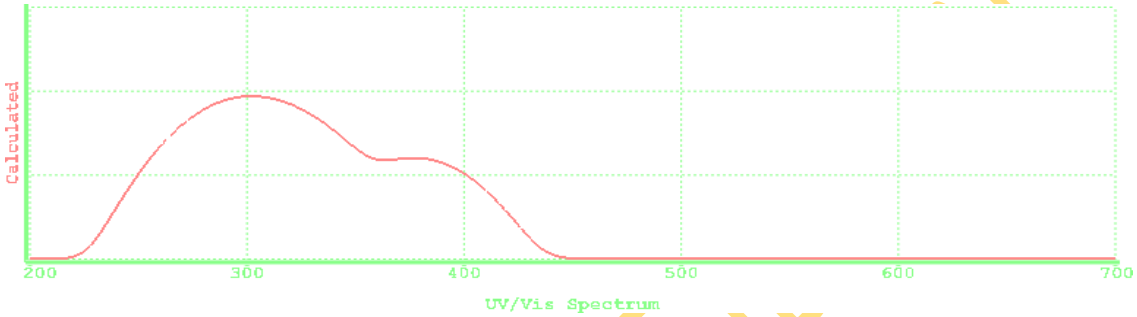
Calculated
200
300
400
500
600
700
UV/Vis Spectrum

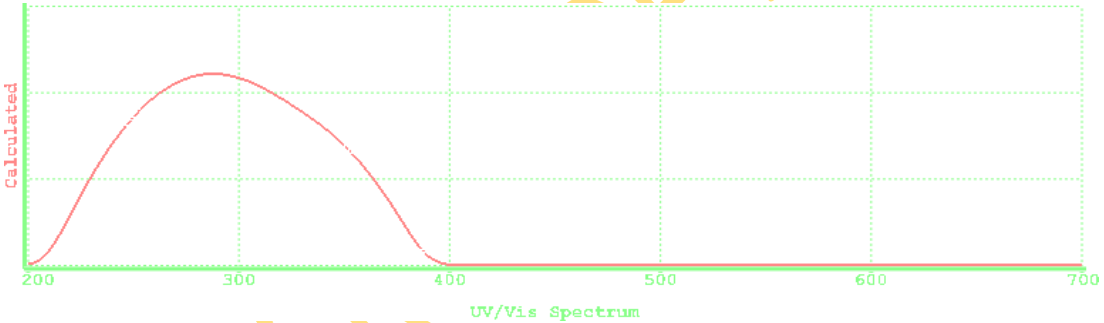
Calculated
200
300
400
500
600
700
UV/Vis Spectrum

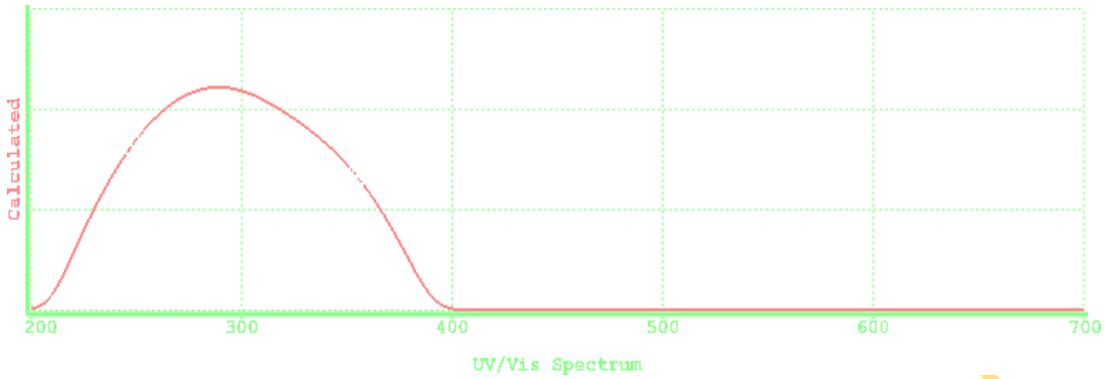

Figure 4.25: UV-visible spectra of Tricarbonyl (1-4-η-5-exo-N-substituted amino-pyridino-cyclohexa-1,3-diene) iron complexes

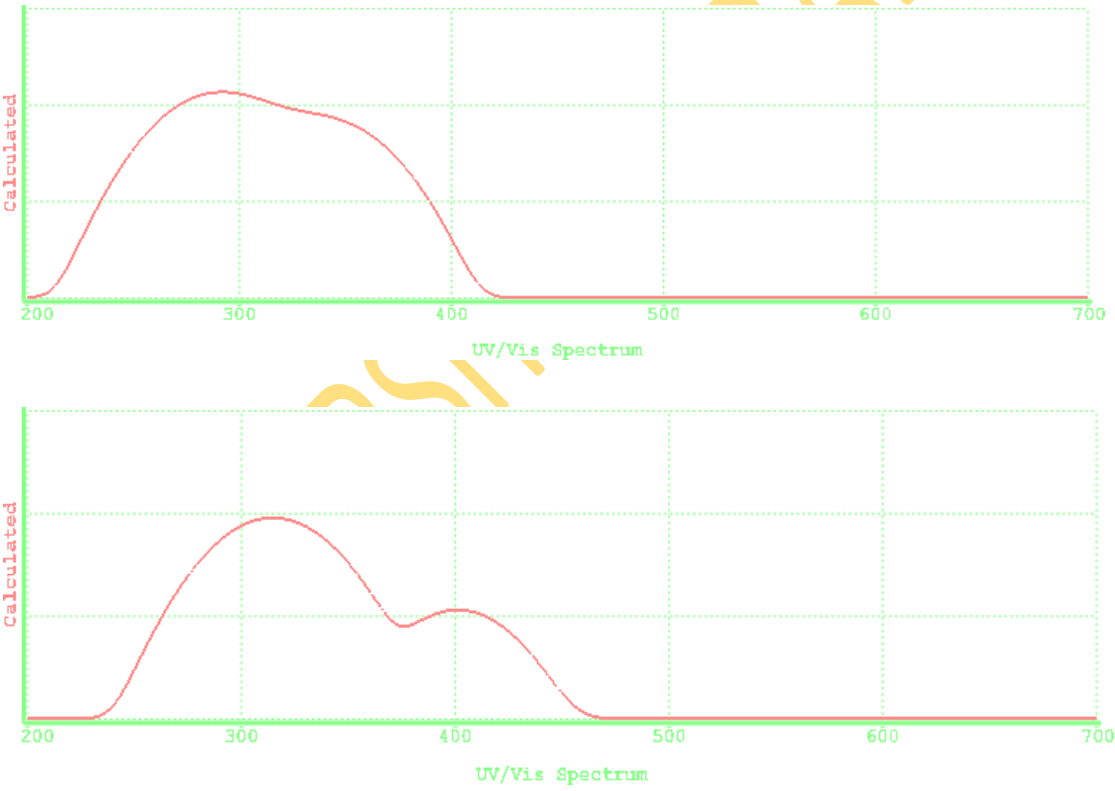

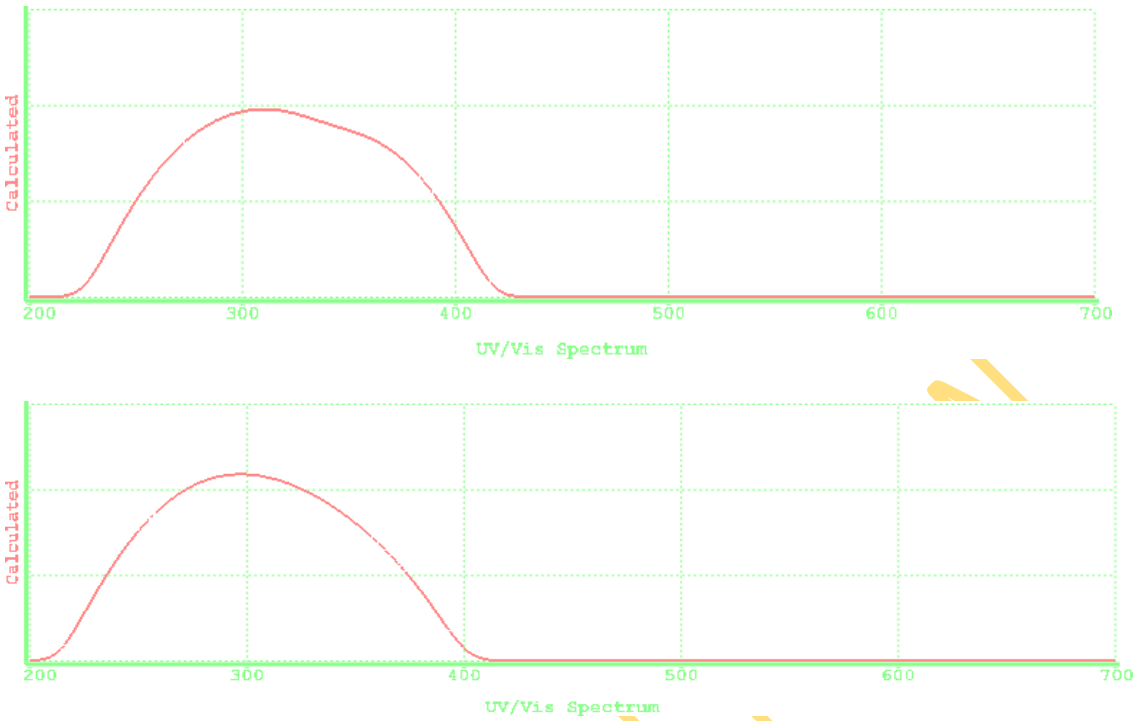

Figure 4.26: UV-visible spectra of Tricarbonyl (1-4-η-5-exo-N-substituted aminopyridino-2-methoxycyclohexa-1,3-diene) iron complexes

LIST OF REFERENCES

Abdulhamid Alsaygh. 2007. Synthesis and characterizations of a new bis(tricarbonyl-iron) compound containing ferrocenethiolate ligand and its trimethylphosphine derivatives. X-ray structure of bis(μ2-ferrocenethiolato) bis(tricarbonyl-iron). *The Arabian Journal for Science and Engineering 32*,2: 163-170.

Abel, E. W. 1963. Structure and reactivities of biscyclopentadienyl. *Quarterly Review* 17: 133-138.

Abrahamsson, M., Jager, M., Kumar, R. J., Osterman, T., Persson, P., Beeker, H. C., Johansson, O. and Hummarstrom, L. 2008. Bistridentate ruthenium (II) polypyridyl-type complexes with microsecond ^{3}MLCT state lifetimes: Sensitizers for rod-like molecular arrays. *Journal of America Chemical Society*130, 46: 15533- 15542.

Abu-Omar, M. M., Loaiza, A. and Hontzeas, N. 2005. Reaction mechanism of mononuclear non-heme iron oxygenases. *Chemistry Review* 105: 2227-2252.

Alexander, B. D. and Dines, T.J. 2004. Ab initio calculations of the structures and vibrational spectra of ethene complexes.*Journalof Physical Chemistry A* 108,1: 146-156.

Altun, A., Shaik, S. and Thiel, W. 2007. What is active the species of cytochrome P450 during camphor hydroxylation? QM/MM studies of different electronic states of compound 1 and of reduced and oxidized iron-oxo intermediates*Journal of America Chemical Society*129: 8978-8987.

Amanda, L. E., Dieter, F. and Thomas, B. R. 2001. Syntheses of Ru-S Clusters with Kinetically Labile Ligands via the Photolysis of $[(cymene)_3Ru3S_2](PF_6)_2$. *Inorganic Chemistry*40:1459-1465.

Amira, S., Spangberg, D., Zelin, V., Probst, M. and Hermansson, K. 2005. Distorted five-fold coordinaionof Car-Parrinello molecular dynamics. *Journalof Physical Chemistry B*109: 14235-14243.

Annie, L., Julia K., Helena, C., Shahera, F., Natalia, M., Claudia, A., Ilan, M. 2001. Addition–β-elimination: a new method for the preparation of organometallic compounds. *Journal of Organometallic Chemistry* 624: 26–33.

Appel, H., Gross, E. K. U. and Burke, K. 2003. Excitations energies in time-dependent density functional theory. *Physical Review Letters* 90: 043005.(pp1-4).

Arcisauskaite, V., Kongsted, J., Hansen, T. and Mikkelsen, K. V. 2009. Charge transfer excitation energies in pyridine-silver complexes studied by a QM/MM method. *Chemical Physics Letters* 470: 285-288.

Atay N. Zeynep and Varnali Tereza, 2002 A Semi empirical study on Metal Ion/Murexide Complexation. *Turkish Journal of Chemistry* 26: 303-309.

Baik, M. H. and Friesner, R, A. 2002. Computing redox potentials in solution: Density functional theory as a tool for rational design of redox agents. *Journalof Physical Chemistry A*106: 7407-7412.

Barckholtz, T.A. and Bursten. E.B. 2000. Density Functional calculations of dinuclear organometallic carbonyl complexes. Part 1; Metal-metal and metal-CO bond energies. *Journalof Organometallic Chemistry*. 596: 212-220.

Bar-Nahum, I., Gupta, A. K., Huber, S. M., Ertem, M. Z., Cramer, C. J. and Tolman, W.B. 2009. Reduction of nitrous oxide to dinitrogen by mixed valent Tricopper-disulfido clusters. *Journalof America Chemical Society.* 131, 8: 2812-2814.

Bassan, A., Borowski, T., Schofield C. J. and Siegbahn, P. E. M. 2006. Ethylene biosynthesis by amino cyclopropane-1-carboxylic acid oxidase: A DFT study. *Chemistry A European Journal* 12: 8835-8846.

Bauernschmitt, R. and Ahlrichs, R. 1996. Treatment of electronic excitations within the adiabatic approximation of time dependent density functional theory. *Chemical Physics Letters* 256: 454-464.

Becke, A.D. 1993. "A new mixing of Hartree-Fock and local density-functional theories". *Journal of Chemical Physics*98,2: 1372–1377.

Bell, C. B., Wong, S.D., Xiao, Y. M., Klinker, E. J., Tenderholt, A. L., Smith, M. C., Rohde, J. U., Que, L., Cramer, S.P. and Solomon, E. I. 2008. A combined NRVS and DFT study of iron(IV)oxide model complexes: A diagnostic method for the elucidation of non-heme iron enzyme intermediates. *Angewandte Chemie International Edition* 47: 9071-9074.

Benitez, D., Tkatchouk, E. and Goddard, W. A. 2009. Conformational analysis of Olefin-Carbene Ruthenium metathesis catalyst. *Organometallics*28: 2643-2648.

Bernasconi, L., Sprik, M. and Hutter, R. 2004. Hartree- Fock exchange in time dependent density functional theory: Application to charge transfer excitations in solvated molecular systems. *Chemical Physics Letters* 394: 141-146.

Berry, J. F., George S. D. and Neese, F. 2008. Electronic structure and spectroscopy of "superoxidized" iron centers in model systems: theoretical and experimental trends. *Physics Chemistry Chemistry Physics* 10: 4361-4374.

Bertsch, G. F., Schnell, A. and Yabana, K. 2001. Electron-vibration coupling in time-dependent density functional theory: Application to benzene. *Journalof Chemical Physics* 115: 4051-4060.

Besley, N. A. and Blundy, A. J. 2006. Electronic excited states of Si(100) and organic molecules adsorbed on Si(100). *Journalof Physical Chemistry B* 110: 1701-1710

Betley, T. A., Wu, Q., Van Voorhis, T. and Nocera, D. G. 2008. Electronic design criteria for O-O bond formation via metal-oxo complexes. *Inorganic Chemistry.* 47: 1849-1861.

Bhattacharyya, S., Stankovich, M. T., Truhlar, D. G. and Gao, J. L. 2007. Combined quantum mechanical and molecular mechanical simulations of one-and two-electron reduction potentials of flavin cofactor in water, medium-chain acyl-CoA dehydrogenase, and cholesterol oxidase. *Journal Physicalof Chemistry A* 111: 5729-5742.

Bingham Richard C., Dewar Michael J.S. and Donald, H. Lo. 1975. Ground states of molecules XXV. MINDO/3. An improved version of the MINDO Semi empirical SCF-MO method. *Journal of American Chemical Society* 97, 6: 1285-1293.

Birch, A. J., Cross, P.E., Lewis, J., White, D. A. and Wild, S. B. 1968. The Chemistry of coordinated ligands Part II. Irontricarbonyl complexes of some cyclohexadienes. *Journalof Chemical SocietyA*42:332-346.

Birke, R. L., Huang, Q., Spataru, T. and Gosser, D. K. 2006. Electroreduction of a series of alkylcobalamins: Mechanism of stepwise reductive cleavage of the Co-C bond. *Journal of American Chemical Society* 128: 1922-1936.

Blumberger, J., Bernasconi, L., Tavernelli, I., Vuilleumier, R. and Sprik, M. 2004. Electronic structure and salvation of copper and silver ions: A theoretical picture of a model aqeous redox reaction. *Journal American of Chemical Society*126: 3928- 3938.

Bouzakaraoui, S., Bouzzine, S.M., Bouachrine, M. and Hamidi, M. 2005. Theoretical Study on the Structure and properties of Polythiophine. *Journal of Molecular. Structure. Theochemistry.* 725: 39-47.

Bouzzine, S.M., Bouzakraoui, S., Bouachrine, M. and Hamidi, M. 2004. Structure and Electronic properties of new materials based on Thiophene and Phenylene. *Physics Chemistry News*19: 110- 116.

Brewer, S. H., Wicaksana, D. and Jon-Paul, M. 2005. Investigation of the electrical and optical properties of iridium oxide by reflectance FTIR spectroscopy and density functional theory calculations.*Journal of Chemical Physics* 313: 25-31.

Brian, F. G., Jack Lewis., Ian E. Ryder and Martyn V. Tivigg. 1976. Preparation and Isomerization of carbonyl (Preparation and Isomerization of carbonyl (η-cyclohepta-1,4-diene (η-cyclohexa-1,3-diene) iron complexes. *Journalof Chemical Society,Dalton Transaction 421-425.*

Bronsted, J.N. 1923. Lowry TM. The electronic theory of valency. IV. The origin of acidity. *Recueil des Travaux Chimiques des Pays-Bas* 42, 718-728.

Brown, C. D., Neidig, M. L., Neibergall, M. B., Lipscomb, J, D. and Solomon, E. I. 2007. VTVH-MCD and DFT studies of Thiolate bonding to $\{FeNO\}^7/\{FeO_2\}^8$ complexes of isopenicillin N synthase. Substrate determination of oxidase versus oxygenase activity in non heme Fe enzymes. *Journal American of Chemical Society* 129: 7427-7437.

Burke, K., Petersilka, M. and Gross, E.K.U. 2002. Recent Advances in Density Functional Methods, edt. P. Fantucci and A. Bencini, *World Scientific, Singapore Vol.* 3: 67-73.

Crabtree Robert H.. 2005. The Organometallic Chemistry of the Transition metal 4th edition. *Wiley Interscience, John Wiley &sons,* ISBN: 0-471-66256-9. Andrei G. Kutateladze (2005). Computational methods in photochemistry. *CRC Press, Taylor&Francis Group.* ISBN: 0-8247-5345-3.

Cape J. L. and Hurst, J. K. 2008. Detection and mechanistic relevance of transient ligand radicals formed during $[Ru(bpy)_2(OH_2)]_2O^{4+}$ catalysed water oxidation.*Journal of American Chemical Society*130: 827-829.

Caramori G. F. and Frenking, G. 2007. The nature of the Ru-NO bond in Rutheniumtetraamine nitrosyl complexes. *Organometallics* 26: 5815-5822.

Carbonniere, P., Ciofini, I., Adamo, C. and Pouchan, C. 2006. Vibrational behavior of tetrahedral d^o oxo-compounds: A theoretical study. *Chemical Physics Letters.* 429: 52-57.

Caricato, M., Mennucci, B., Tomasi, J., Ingrosso, F., Cammi, R., Corni, S. and Scalmani, G. 2006. Formation and relaxation of excited states in solution: A new time dependent density functional theory. *Journalof Chemical Physics.* 124: 124520(1-10).

Casarin, M., Finetti, P., Vittadini, A., Wang, F. and Ziegler, T. 2007. Spin-Orbit relativistic Time dependent density functional calculations of metal and ligand pre-edge XAS intensities of organotitanium complexes: $TiCl_4$,$Ti(\eta^5\text{-}C_5H_5)Cl_3$ and $Ti(\eta^5\text{-}C_5H_5)Cl_2$. *Journalof Physical Chemistry A* 111, 24: 5270-5279.

Casida, M. E., Jamorski, C., Casida, K. L. and Salahub, D. R. 1998. Molecular excitation energies to high-characterization and correction of the Time-dependent local density approximation ionization threshold. *Journal of Chemical Physics* 108: 4439- 4450.

Castro, A., Marques, M. A. L., Romero, A.H., Oliveira, M. J. T. and Rubio, A. 2008. The role of dimensionality on the quenching of spin-orbit effects in the optics of gold nanostructures. *Journal of Chemical Physics* 129: 144110(1-4).

Cave, R. J., Burke, K. and Castener Jr, E. W. 2002. A theoretical investigation of the ground state and excited states of coumarin 151 and coumarin 120. *Journal of Physical ChemistryA* 106: 9294-9305.

Charlot, M. F. and Aukauloo, A. 2007. Highlighting the role of medium in DFT analysis of the photophysical properties of ruthenium (II) polypyridine-type complexes. *Journal Physical of Chemistry A* 111: 11661-11667.

Chatt, J. 1974. Infra- red spectra and structure of Olefin co-ordination compounds. *Advances in Organometallic Chemistry* 12: 12-30.

Chatt, J. and Duncanson L.A. 1953. Olefin co-ordination compounds. Part III. Infra-red spectra and structure. Attempted preparation of acetylene complexes. *Journal of Chemical Society* 2939-2947.

Chaudhari, F. M. and Pauson, P. L. 1966. Metal derivatives of conjugated diene II. Triphenylphosphine derivatives. *Journalof Organometallic Chemistry* 5: 73-78.

Chen, H., Hirao, H., Derat, E., Schlichting, I. and Shaik, S. 2008a. Quantum mechanical/Molecular mechanical study on the mechanisms of heme degradation by the enzyme hemeoxygenase. *Journalof Physical Chemistry B*112, 31: 9490-9500.

Chen, H., Moreau, Y., Derat, E. and Shaik, S. 2008b. Quantum mechanical/molecular mechanical study of mechanisms of heme degradation by the enzyme heme

oxygenase: The strategic function of water cluster.*Journal of American Chemical Society*130, 6: 1953-1965.

Cheng, Q. C. L., Wu, Q. and Van Voorhis, T. 2008. Rydberg energies using excited state density functional theory. *Journal of Chemical Physics* 129: 124112(1-9).

Chiorescu, I., Deubel, D. V., Arion, V. B. and Keppler, B. K. 2008. Influence of Density functionals and basis sets on one bond carbon-carbon NMR spin-spin constants. *Journalof Chemical Theory and Computation*4, 3: 448-456.

Cho, K. B., Hirao, H., Chen, H., Carvajal, M. A., Cohen, S., Dera, E., Thiel, W. and Shaik, S. 2008. Compound I in heme Thiolate enzyme: A comparative QM/MM study. *Journalof Physical ChemistryA* 108, 50: 13128-13138.

Cho, K. B., Carvajal, M. A. and Shaik, S. 2009. First half-reaction mechanism of nitric oxide synthesis: The role of Proton and oxygen couple electron transfer in the reaction by Quantum mechanics/ Molecular mechanics. *Journalof Physical Chemistry B* 113, 1: 336-346.

Christoffersen, R.E. 1989. Basic Principles and Techniques of Molecular Quantum Mechanics. 1st Edition, Springer-Verlag.

Correa, A. and Cavallo, L. 2006. The elusive mechanism of olefin metathesis promoted by (NHC) Ru-based catalyst: A trade between steric, electronic and solvent effects. *Journal of American Chemical Society*128: 13352-13353.

Cotton, F. A. and Wilkinson, G. 1972, Historical Background of Organometallic Chemistry. *Advanced Inorganic Chemistry*, 3rd Edition Interscience, New York, Chapter 22.

Craid, A., Poffenberger, N., Tennent, H. and Wojcicki, A. 1980. Synthesis, characterization and some reactions of organometallic complexes containing bridging dithionite ligand. *Journalof Organometallic Chemistry* 191: 107-121.

Craig D. M. 2001. Integrating Molecular Modeling into Inorganic Chemistry Laboratory. *Journal of Chemical Education* Vol.78, 6: 840-844.

Cramer, C. J. and Truhlar, D. G. 2009. Density functional theory for transition metal and transition metal chemistry. *Physics Chemistry Chemistry Physics* 11: 10757-10816.

---------- 2002. Essentials of Computational Chemistry- Theories and models. *Chichester: John-Wiley & Sons*ISBN: 0-470-09182-7.

Cundari T. R. 2001a. Computational Organometallics. *Marcel Dekker Inc*. ISBN: 0-8247-0478-9.

----------**,** 2001b. Computational Organometallics. Edited by Cundari, T. R. pp 1-6. *Marcel Dekker Inc*. ISBN: 0-8247-0478-9.

De Abreu, H. A., Guimaraes, L. and Duarte, H. A. 2006. Density functional theory study of Iron(III) hydrolysis in aqueous solution. *Journal of Physical Chemistry A* 110: 7713-7718.

De Proft, F, Martin, J. L and Geerlings, P. 1996a. Calculation of molecular electrostatic potentials and fukui functions using density functional. *Chemical Physics Letters* 256: 400-408.

---------- ---------- and ----------1996b. On the performance of density functional methods for describing atomic populations, dipole moments and infrared intensities. *Chemical Physics Letters* 250: 393-401.

Dearing, A. 1988. Computer-aided Molecular Modeling; Research Tool. *Journal of Computer-aided Molecular Design* 2: 179-189.

DeeBeer, G. S., Petrenko, T. and Neese, F. 2008. Prediction of iron K-edge absorption spectra using TD-DFT. *Journalof Physical Chemistry A* 112, 50: 12936-12943.

Della Sala, F. and Gorling, A. (2003). Excitation energies of molecules by time-dependent density functional theory based on effective exact exchange Kohn-Sham-potentials. *International Journalof Quantum Chemistry* 91: 131-138.

Derat, E., Shaik, S., Rovira, C., Vidossich, P. and Alfonso-Prito, M. 2007. The effect of water molecule in the mechanism of formation of compound O Horseradish peroxidase.*Journal of American Chemical Society*129: 6346-6347.

Dewar, M.J.S. and Thiel, W. 1977a. The MNDO Method: Ground states of molecules. *Journal of American Chemical Society* 99: 4899-4907.

----------. Ford, G.P., Mckee, M.L., Rzepa, H.S. and Wade, L.E. 1977b. The Cope rearrangement of MINDO/3 studies of the rearrangement of 1,5-hexadiene and bicyclo[2.2.0] hexane. *Journal of American Chemical Society* 99: 5069-5075.

----------, Zoebisch, E.G. Healey, E.F. and Stewart, J.J.P. 1985. General Quantum Mechanical molecular model. *Journal of American Chemical Society* 107: 3902-3909.

Diego del Rio and Augustin Galindo. 2002. Theoretical Study of the bonding capabilities of 1,4-diaza-1,3-butadiene and cis-1,3-butadiene ligands in cyclopentadienyl Tantalum (V) complexes. *Journal of Organometallic Chemistry* 655, 1: 16-22.

Dominique, G. and Shinichiro, N. 2000. Calculation of the absorption wavelength of dyes using time-dependent density functional theory (TD-DFT) *Dyes and Pigments* 46: 85-92.

Dreuw, A. and Head-Gordon, M. 2005, Single-reference ab initio methods for the calculation of excited states of large molecules. *Chemical Review* 105: 4009-4037.

Eluvathingal D. Jemmis, Mariappan Manoharan, and Pankaz, K. Sharma. 2000. Exohedra η^5 and η^6 Transition-metal organometallic complexes of C_{60} and C_{70}; A theoretical study. *Organometallics* 19, 10: 1879-1887.

Emile, H. Braye and Walter Hubel. 1965. Organometallic complexes XVI. Ferraindeneiron and indenone iron carbonyl complexes. *Journal of Organometallic Chemistry 3: 38-42.*

Eun, J. L., Jin, S. H., Tae-Jeong, K., Youngjin, K., Eun, M. H., Jae, J. L., Kihyung, S. and Dong-Uk, K. 2006. Synthesis and Structural Characterization of Main Group 15 Organometallics R_3M and $R(Ph)_2P(=N\text{-}Ar)$ (M = P, Sb, Bi; R = phenanthrenyl; Ar = 2,6-iPr2-C_6H3). *Bulletin Korean Chemical Society* 26, 12: 1946-1952.

Fan, J., Seth, M., Autschbach, J. and Ziegler, T. 2008. Circular dichroism of trigonal dihedral chromium(III) complexes: A theoretical study based on open-shell time-dependent density functional theory. *Inorganic Chemistry* 47: 11656-11668.

Fisher, E.O. and Werner, H. 1966. Metal π-Complexes. Vol. 1. Elsevier.

Follett, A. D., McNabb, K. A., Peterson, A. A., Scanlon, J. D., Cramer, C. J. and McNeill, K. 2007. Characterisation of Co-C bonding in dichlorovinylcobaloxime complexes. *Inorganic Chemistry* 46: 1645-1654.

Fontanesi, C., Benassi, R., Giovanardi, R., Marcaccio, M., Paolucci, F. and Roffia, S. 2002. *Journal of Molecular Structure, Theochemistry* 612: 277-285.

Forslund, L. E., Rudiger, F. and Kaltsoyannis, N. 2002. Time-dependent density functional theory studies of the electronic absorption spectra of N, N-disubstituted 2, 3-dialkylnyl-1,4-diazabuta-1,3-dienes. *Journalof Chemical Society, Perkin Transaction* 2: 494-501.

Frankland, E. 1848. Zinc alkyl, Edward Frankland, and the beginning of main-group Organometallic Chemistry. *Liebigs Annal. Chemie*. 71, 171. *Organometallics* 20: 2940-2955.

Fronzoni, G., Stener, M., Decleva, P., Wang, F., Ziegler, T., Van Lenthe, E. and Baerends, E. J. 2005. Spin-orbit relativistic time dependent density functional theory calculations for the description of core electron excitations: $TiCl_4$ case study. *Chemical Physics Letters* 416: 56-63.

Geerlings, P., De Proft, F. and Langenaeker, W. 1996. Density functional theory: A source of chemical concept and cost-effective methodology for their calculations.*Advances inQuantum Chemistry*33, 303-329.

Ghosh, A. Tangen, E. Ryeng, H and Taylor, P. R. (2004), Electronic structure of high-spin Iron (IV) complexes. *European Journal of Inorganic Chemistry* 4555-4560.

Gilbert, A. T. B. Besley, N.A. and Gill, P. M. W. 2008. Self- consistent field calculations of excited states using the maximum overlap method. (MOM). *Journalof Physical. ChemistryA* 112: 13164-13172.

Gloria I. C., Claudia A. C., Diego, V. Y. and Jose, H. Z. 2002. Theoretical Study of the interaction energy profile of Cobalt phthalocyanine and 2-mercaptoethanol. Effect of the graphite on the global reactivity. *Journal of Molecular Structure, Theochemistry* 580: 193-200.

Glossman-Mitmic, D. 2009. Computational molecular characterisation of coumarin-102. *Journalof Molecular Structure,Theochemistry* 911: 105-108.

Gorling, A., Trickey, S. B., Gisdakis, P. and Rosch, N. 1999. A critical Assessment of Density Functional Theory with regard to Applications in Organometallic Chemistry. Brown, J. M. and Hofmann P. 1999. Topics in Organometallic Chemistry. *Spring-Verlag, Berlin Heidelberg NY*, ISBN: 3-540-64253-6.

Goswani Biplab, Sougata Pal, Pranab Sarkar, G. Seifert, and Springborg. M. 2006. Theoretical Study of Structural, electronic, and optical properties of Zn_mSe_n clusters. *Physical Reviews B* 73: 205312 (1-10).

Grabo, T., Petersilka, M. and Gross, E. K. U. 2000. Molecular excitation energies from time-dependent density functional theory. *Journalof Molecular Structure Theochemistry* 501: 353-367.

Guillemoles, J. F., Barone, V., Joubert, L. and Adamo, C. 2002. A Theoretical investigation of the ground and excited states of selected ruthenium and osmium polypyrdyl molecular dyes. *Journalof Physical Chemstry A* 106, 46: 11354-11360.

Gund, P., Barry, D. C., Blaney, J. M. and Cohen, N. C. 1988. Guidelines for Publications in Molecular Modeling Related to Medicinal Chemistry. *Journal of Medicinal Chemistry*31: 2230-2234.

Han, W. G., Liu, T., Lovell, T. and Noodleman, L. 2006, Density functional theory study of Fe (IV) d-d optical transition in active-site models of class I ribonucleotide reductase intermediate X with vertical Self Consistent Field methods. *Inorganic Chemistry* 45: 8533-8542.

Han, W. G. and Noodleman, L. 2008a. Structural model studies for the high valent intermediate Q of methane monohydrogenase from broken symmetry density functional calculations. *Inorganica Chimica Acta* 361: 973-986.

Han, W.G and L. Noodleman, L. 2008b, Structural model studies for the peroxo intermediate P and the reaction pathway from P→Q of methane monooxygenase using broken-symmetry density functional calculations. *Inorganic Chemistry* 47: 2975-2986.

Harman, W. H. and Chang, C. J. 2007. N_2O activation and oxidation reactivity from a non heme iron pyrole platform. *Journal of American Chemical Society* 129: 15128-15129.

Harvey Jeremy, N., Rinaldo Poli and Kevin M. Smith. 2003. Understanding the reactivity of transition metal complexes involving multiple spin states. *Coordination Chemistry Review*238: 347-361.

Hazan, C., Kumar, D., de Visser, S. P. and Shaik, S. 2007. A density functional study of the factors that influence the regioselectivity of toluene hydroxylation by cytochrome P450 enzymes. *European Journal of Inorganic Chemistry* 18: 2966-2974.

Hebben, N., Himmel, H. J., Eickerling, G., Herrmann, C., Reiher, M., Herz, V., Presnitz, M. and Scherer, W. 2007. The first open paddlewheel structures in diruthenium chemistry example of intermediate magnetic behaviour low and high spin in Ru^{+2} species. *Chemistry A European Journal* 13: 10078-10095.

Hegedus L. S. 1994. Transition metals in the Synthesis of Complex Organic Molecules. *University Science Books*, Mill Valley, CA

Hehre, W.J., Radon, L., Schleyer, P.R. and Pople J.A. 1986. Ab initio Molecular Orbital Theory. New York.

Hehre. W. J., 2003. A guide to molecular mechanics and molecular orbital calculations in Spartan. Wavefunction Inc. ISBN 1-890661-18-X.

Heikki M. T., Tristram, C., Andrea, A., Chantall, F. and Rene T. B. (2007). Computational modeling of isotropic electron paramagnetic resonance spectra of doublet state main group radicals. *Journal of Organometallic Chemistry* 692: 2705-2715.

Herrmann, C., Neugebauer, J., Presslt, M., Uhlemann, U., Schmitt, M., Rau, S., Popp, J. and Reiher, M. 2007. The first photoexcitation step of ruthenium-based models for artificial photosynthesis highlighted by resonance Raman spectroscopy. *Journal of Physical Chemistry B* 111: 6078-6087.

Hieber, W. Schnh, R. and Fuchs, H. 1943. Metal carbonyls XXXVII. Rhenium halopentacarbonyls their tendency of formation and properties. *Zeischrift fur Anorganische und Allgermeine Chieme* 48: 243-255.

Hileman, J.C. 1965. Preparative Inorganic reactions Vol.1 Wiley-Interscience, N.Y.

Hinchlife, A. 1989. Computational Quantum Chemistry, 1st Edition, John Wiley & Sons Ltd.

Hirao, H., Que, L. and Shaik, S. 2008. A two state reactivity rationale for counterintuitive axial ligand effect on the C—H activation reactivity of non heme FeIV=O oxidant. *Chemistry A European Journal* 14: 1740-1756.

Hirose, K., Meir, Y. and Wingreen, N. S. 2004. Time-dependent density functional theory of excitation energies of closed-shell quantum dots. *Physica E* 22: 486-489.

Hodgson, J. L., Namazian, M., Bottle, S. E. and Coote, M. L. 2007. One electron oxidation and reduction potentials of nitroxide antioxidants: A theoretical study. *Journal of Physical ChemistryA*111: 13595-13605.

Hohenberg, P. and Kohn, W. 1964. Original papers: *Physical Review B* 136: 864-887.

Housecroft, C. E. and Sharpe, A. G. 2008. Inorganic Chemistry (3rd Edition), *Pearson Education Limited*

Hu, Z. and Boyd, R. J. 2000. Assessment of theoretical methods for the study of transition metal carbonyl complexes: $[Cl_2Rh(CO)_2]^-$ and $[Cl_2Rh(CO)]^-$ as case study. *Journal ofChemical Physics* 113: 9393-93102.

Huang, K. W., Han, J. H., Musgrave, C. B. and Fujita, E. 2007. Carbondioxide reduction by pincer rhodium η^2-dihydrogen complexes: Hydrogen-binding modes and mechanistic studies by density functional theory calculations. *Organometallics* 26: 508-513.

Hutinet, M., Cramer, C. J., Gagliardi, L., Moughai Shai, A. R., Bernadinelly, G., Cerny, R. and Nitsche, J. R. 2007. Self-sorting chiral subcomponent rerrangement during crystallization.*Journal of American Chemical Society*129, 28: 8774-8780.

Hyperchem. Hyperchem release 7. 2002. Tools for molecular modeling and computational Chemistry, Hypercube Inc. USA.

Illie G. Dinulescu., Emil G. Georgescu and Margareta Avian. 1977. Investigations in the cyclobutene series XLIII. Diacetylcyclobutadiene irontricarbonyl and 3,6-dimethylpyridazino(4,5-cyclobutadiene irontricarbonyl. *Journalof Organometallic Chemistry 127:193-196.*

Ingold, C.K. 1933. Significance of tautomerism and of the reactions of aromatic compounds in the electronic theory of organic reactions.*Journal of Chemical Society, Dalton Transaction*1120-1127.

----------. 1934. Principle of an electronic theory of organic reactions. *Chemical Review*15, 225-274.

Jackson, T.A., Rhode, J.U., Seo, M. S., Sastri, C. V., Dchont, R., Stubna, A., Ohta, T., Kitagawa, T., Munch, E., Nam, W. and Que, L. 2008. Geometric and Electronic structures of Non heme oxoiron (IV) complexes.*Journal of American Chemical Society*130, 37: 12394-12407.

Jeffrey, S. and Steven, L. B. 2001. Organometallic chemistry at the interface with material science. *Catalysis Today* 66: 3-13.

Jensen F. 2007. Introduction to Computational Chemistry. *Chichester. John-Wiley & Sons. Second Edition* ISBN-10-0-470-01187-4.

Jensen, K. P. and Ryde, U. 2003a. Theoretical prediction of the Co-C bond strength in Cobalamins. *Journalof Physical Chemistry A* 10: 7539-7545.

----------, Ooi, B. L. and Christensen, H. E. M. 2008. Computational Chemistry of Modified [$M_2Fe_3S_4$] and [$M_2Fe_2S_4$] Clusters: Assessment of trends in electronic structure and properties. *Journalof Physical Chemistry A* 112: 12829-12841.

Job, A. and Cassal, A. 1926. Preparation of Chromium Carbonyl through the medium of a Magnesium derivatives. *Comptes rendus chieme* 183: 392-394.

Johnson B. B. and Peticolas, W. L. 1976. The resonant Raman Effect. *Annual Review Physical Chemistry* 27: 465-52.

Jose, V. and Maria, T. C. 1999. The 'acac method' for the synthesis of coordination and organometallic compounds: synthesis of gold complexes. *Coordination Chemistry Review* 193: 1143–1161.

Keally, T.J. and Pauson P.L. 1951. Preparation of dicyclopentadienyl Iron. *Nature* 168: 1039-1044.

Ketterer, N. A., Fan, H. J., Blackmore, K. J., Yang, X. F., Ziller, J. W., Baik M. H. and Heyduk, A. F. 2008. $\pi \rightarrow \pi^*$ Bonding interactions generated by halogen oxidation of ZirconiumIV Redox-Active ligand complexes.*Journal of American Chemical Society*130: 4364-4374.

King, R. B.1966. New organometallic compounds of transition metals. *Inorganic Chemistry*5:2231-2235.

---------- 1967. Organometallic chemistry of transition metals XX. Some reactions of molybdenum and chromium with olefinic and acetylenic compounds. *Inorganic Chemistry* 6: 30-36.

----------.and Bisnette, M. B. 1964. Organometallic chemistry of transition metals VI. Some cycloheptatrienyl derivatives of chromium, molybdenum and cobalt. *Inorganic Chemistry* 3: 787-790.

----------, and ----------**.** 1967. Organometallic chemistry of transition metal XXI. Some pentamethylcyclo-pentadienyl derivatives of various transition metals. *Journalof Organometallic Chemistry* 8: 287-297.

Klinker, E. J., Shaik, S. and. Hirao, L. 2009. A two state reactivity model explains unusual kinetic isotope effect pattern in C-H bond cleavage by non-heme oxoiron(IV) complexes. *Angewandte Chemie International Edition*48: 1291-1291.

Kohn, W and Sham, L.J. 1965. Original papers: *Physical Review*A 140: 133-149.

Koopmans, Tjalling. 1934. "Über die Zuordnung von Wellenfunktionen und Eigenwerten zu den Einzelnen Elektronen Eines Atoms". *Physica* (Elsevier) 1: 104–113.

Kozimor, S. A., Yang, P., Batista, E. R., Boland, K. S., Burns, C. J., Christensen, C., Clark, N.,.Conradson, S. D., Hay, P.J., Lezama, J. S., Martin, R. L., Schwarz, D. E., Wilkerson, M. P. and Wolfsberg, L. E. 2008. Covalency trends in group IV metallocene dichloride. Chloride K-edge X-ray absorption spectroscopy and time dependent density functional theory. *Inorganic Chemistry* 47: 5365-5371.

Krapp, A., Pandey K. K. and Frenking, G. 2007. Transition metal-carbon complexes: A theoretical study.*Journal of American Chemical Society* 129: 7596-7610.

Kritayakornupong, C. 2007. Ab initio QM/MM molecular dynamics simulations of Ru^{+3} in aqueous solution. *Chemical Physics Letters* 441: 226-231.

Kryatov, S. V., Rybak-Akimova, E. V. and Schindler, S. 2005. Kinetics and mechanisms of formation and reactivity of non heme iron oxygen intermediates. *Chemical Review* 105: 2175-2226.

Kunishita, A., Teraoka, J., Scanion, J. D., Matsumoto, T., Suzuki, M., Cramer, C. J. and Itoh, S. 2007. Aromatic hydroxilation reactivity of mononuclear Cu(II) alkylperoxo complex.*Journal of American Chemical Society*129, 23: 7248-7249.

Laine, P. P., Ciofini, I., Ochsenbein, P., Amouyal, E., Adamo, C. and Bedioui, F. 2005. Photochemical processes within compact dyads based on triphenylpyridinium functionalized bypyryl complexes of Ruthenium (II). *ChemistryA European Journal*11: 3711-3727.

----------., Loiseau, F., Campagna, S., Ciofini, I. and Adamo, C. 2006. Conformationally gated photoinduced processes within photosentizer-acceptor dyads based on Osmium (II) complexes with Triarylpyridino-functionalized Terpyridyl ligands: Insight from theoretical analysis. *Inorganic Chemistry* 45: 5538-5551.

Lanci, M. P. and Ruth, J. P. 2006. Oxidation isotope effects upon reversible O_2-binding reactions: Characterizing mononuclear superoxide and peroxide structures.*Journal of American Chemical Society*128, 50: 16006-16007.

----------., Smirnov, V. V., Cramer, C. J., Gauchenova, E. V., Sundermeyer, J. and Roth, J. P. 2007. Isotopic probing of molecular oxygen activation of Copper(I) sites.*Journal of American Chemical Society*129, 47: 14697-14706.

Laura C. H., Gerber, L. A, Watson, S. P, Wei Weng, B. M. and Oleg, V. O. 2007. Bis(methylidene) Complex of Tantalum Supported by a PNP Ligand *Organometallics26:*4866-4868

Lee, C., Yang, W. and Parr, R. G. 1988. Development of the Colle-Salvetti correlation-energy formula into a functional of electron density. *Physical Review B* 37: 785-789.

Leib, R. D., Donald, W. A., O'Brien, J. T., Bush, M.F. and Williams, E. R. 2007. Reduction energy of 1M aqeous RutheniumIII hexaammine in the gas phase: A route towards establishing an absolute electrochemical scale.*Journal of American Chemical Society*129: 7716-7717.

Leigh, G. J. and Fisher, E. O. 1965. The reactions of cycooctadienes with the hexacarbonyls of Group VI transition elements. *Journalof Organometallic Chemistry4: 461-465.*

Lewars, E. 2003. Computational Chemistry-Introduction to the theory and applications of molecular and quantum mechanics. *Kluwer Academy. Publishers:* Norwell, MA, USA.

Lewis, J., Cotton, F. A. P. and Johnson, B. F. G. 1963. Tricarbonyl (cyclooctadiene) complexes of iron, ruthenium and osmium. *Chemistry and Industry (London)* 30-36.

Li, C., Zhang, L., Zhang, C., Hirao, H., Wu, W. and Shaik, S. 2007. Which oxidant is really responsible for sulphur oxidation by cytochrome P450 *Angewandte Chemie International Edition* 46: 8168-8179.

Li, Z. H., Gong, Y., Fan, K. N. and Zhou, M, F. 2008. Is the FeO^-_2 Anion bent or linear? *Journalof Physical Chemistry A* 112: 13641-13649.

Li-ming Yang., Xiao-ping Li., Yi-hong Ding and Chia-chung Sun. 2008. Theoretical Study on a class of organometallic complexes based on all metal Aromatic Ga_3^- through Sandwiching Stabilization. *European Journalof Inorganic Chemistry 12:* 2099-2106.

Liu, F., Cardolaccia, T., Hornstein, B. J., Schoonover, J. R. and Meyer, T, J. 2007. Electrochemical oxidation of water by an adsorbed µ-oxo bridge Ru complex. *Journal of American Chemical Society*129: 2446-2447.

----------, Concepcion, J. J., Jurss, J. W., Cardolaccia, T., Templeton, J. L. and Meyer, T.J. 2008. Mehanisms of water oxidation from the blue dimer to photosystemII. *InorganicChemistry* 47: 1727-1752.

Liu, Z. 2008. Theoretical studies of natural pigments relevant to sensitized solar cells. *Journalof Molecular Structure, Theochemistry* 862: 44-48.

Louis, S. H. 1990. Chromium carbene complexes in the synthesis of molecules of biological interest. *Pure &Applied Chemitry* 62,4: 691-698

Maitra, N. T., Burke, K. and Woodward, C. 2002. Memory in time-dependent density functional theory. *Physical Review Letters*89: 023002(1-4).

Manchot, W. and Manchot, W. J. 1936. Synthesis of metal carbonyl and Organotransition metal carbonyl. *Zeischrift fur Anorganische und Allgermeine Chieme* 26: 385-389.

Manna, M.R., Ichord, H.A. and Sperhn, D.W. 2003. Nuclear Spin Statistics on the Structure of extended aromatics C48N12 Azafullerene. *Chemical Physics Letters* 378: 449-458.

Marcaccio, M., Paolucci, F., Fontanesi, C., Fioravanti, G. and Zanarini, S., 2008. Electrochemistry and Spectroelectrochemistry of polypyridine ligands: A theoretical approach. *Inorganica Chimica Acta.* 360: 1154-1162

Marques, M. A. L. and Gross, E. K. U. 2004. Time dependent density functional theory. *Annual Review Physical Chemistry* 55: 427-455.

Maseras Felix. 1999. Hybrid Quantum mechanics/Molecular mechanics methods in Transition metal chemistry. Topics in Organometallic Chemistry, Vol. 4 edited by Brown, J. M and Hofmann P. Pp 166-189. *Spring-Verlag, Berlin Heidelberg NY*, ISBN: 3-540-64253-6.

Mathew, J., Koga, N. and Suresh, C. H. 2008. C-H bonding activation through α-bond metathesis and agnostic interactions: Deactivation pathway of a Grubbs second-generation catalyst. *Organometallics* 27: 4666-4670.

McCleverty, J. A. 1976. *Organometallic Chemistry Reviews*119: 261-284.

Mclver Jr, J.W. and Kormonicki. 1971. Rapid Geometry optimization for Semi empirical molecular orbital methods. *Chemical Physics Letters* 10: 303-321.

McQuarrie, D.A. 1983. Quantum Chemistry, 1st Edition, University Science Books.

Mehmet Sayim Karacan. 2006. Semi empirical Studies of the electronic structure of Iron-Sulfur proteins model compounds.*Canadian Journal of Analytical Sciences and Spectroscopy* 52, 1: 25-31.

Michael, Cais and Narkis, W. 1965. Organometallic studies. VIIIa. Aminocyclopenta-dienylmanganese tricarbonyl and some related compounds. Application of the Schmidt reaction to metallocenyl ketones. *Journal of Organometallic Chemistry* 3: 188-199.

Mitic, N., Clay, M. D., Saleh, L., Bollinger, J. M. and Solomon, E.I. 2007. Spectroscopic and electronic structure studies of intermediate X in ribonucleotide reductase R2

and two variants: A description of the Fe^{IV}-oxo bond in the FeIII-O-Fe^{IV} dimer. *Journal of American Chemical Society*129: 9049-9065.

Moens, J., Roos, G., Jaque, P., De Proft, F. and Geerlings, P. 2007. Is the Hoveyda-Grubbs complex a vinyllogous fischer- type carbine? Aromaticity controlled activity of ruthenium metathesis catalyst. *Chemistry A European Journal* 13: 9331-9337.

Moeris, J., Jaque, P., DeProft, F. and Geerlings, P. 2008. The study of redox reactions on the basis of conceptual DFT principles: EEM and vertical quantities. *Journal of Physical ChemistryA*112, 26: 6023-6031.

Mond, L., Langer, C. and Quike, F. 1890. "Action of carbonmonoxide on Nickel" *Journal Chemical Society, Dalton Transaction* 57: 749-753.

---------- and ---------. 1891. "On iron carbonyls" *Journalof Chemical Society. Dalton Transaction*59: 1090-1093.

----------, Hirtz, H. and Cowap, M. D. 1910. Some new metal carbonyls. *Journal of Chemical Society, Dalton Transaction* 97: 798-810.

Morell, C., Grand, A. and Toro-Labe, A, 2005. A new dual descriptor for chemical reactivity. *Journalof Physical ChemistryA* 109: 205-212.

Morschel, P., Janikowski, J., Hilt, G. and Frenking, G. 2008. Ligand-Tuned regioselectivity of a cobalt-catalysed Diels-Alder reaction: A theoretical study. *Journal of American Chemical Society*130: 8952-8966.

Muckerman, J. T., Polyansky, D. E., Wada, T., Tanaka, K. and Fujita, E. 2008. Water oxidation by a Ruthenium Complex with non innocent quinine ligands: Possible formation of an O-O bond at a low oxidation state of the metal. *Inorganic Chemistry* 47:1787-1802.

Nam, W. 2007. High-Valent Iron (IV)-Oxo complexes of heme and non-heme ligands in oxygenation reactions. *Accounts Chemical Research* 40: 522-531.

Nazeeruddin, M. K., De Angelis, F., Fantacci, S., Selloni, A., Viscardi, G., Liska, L., Ito, S., Takeru, B. and Gratzel, M. 2005. Combined experimental and DFT-TDDFT computational study of photoelectrochemical cell Ruthenium sensitizers. *Journal of American Chemical Society*127: 16835-16847.

Neamen, D. 2006. An Introduction to semiconductor devices (1st Edition) McGraw-Hill.

Neidig, M. L., Brown, C. D., Light, K. M., Fujimori, D. G., Nolan, E. M., Price, J. C., Barr, E. W., Bollinger, J. M., Krebs, C., Walsh, C. T. and Solomon, E. I. 2007. CD and MCD of CytC3 and Taurine deoxygenase: Role of the facial Triad in α-KG-dependent oxygenases. *Journal of American Chemical Society 1*29: 14224-14231.

Odiaka, T. I. 1980. Synthetic and Mechanistic studies of nucleophilic attack on organic molecules coordinated to metal carbonyls. *Ph. D Thesis*, University of Wales, Cardiff.

----------, and Kane-Maguire L. A. P. 1981. Kinetics of nucleophilic attack on coordinated organic moieties: Addition of pyridines to dienyl cations. *Journal Chemical Society, Dalton Transaction 1162-1168.*

----------, and Williams, P. A. 1981. Kinetics of nucleophilic attack on co-ordinated organic moieties: Addition of toluidine to tricarbonyl (1-5-η-dienyl) iron cations. *Journal Chemical Society, Dalton Transaction 200-204.*

----------, Kane-Maguire, L.A.P., Turgoose, S. and Williams P.A. 1981. Kinetics of Nucleophilic Attack on Co-ordinated Organic moieties. Significance of amine basicity in determining the nucleophilicities of pyridines and anilines towards (1-5-dienyl)Fe(CO_3) Iron. *Journal of Organometallic Chemistry* 188: C5 – C9.

----------, Kane-Maguire, L.A.P, Turgoose, S. and Williams P.A. 1981. Kinetics of Nucleophilic Attack on Co-ordinated Organic moieties. Addition of anilines to tricarbonyl (1-5-dienyl) Iron cations. *Journal of Chemical Society, Dalton Transaction*2489 - 2495.

Odiaka, T. I. 1985. Mechanism of attack on tricarbonyl (cycloheptatrienyl) Tungsten cation by triphenylphosphine. *Inorganica Chimica Acta 103: 9-13.*

----------, and Okogun, J.I. 1985. New tricarbonyl (amido-substituted-1,3-diene) iron complexes. *Journalof Organometallic Chemistry* 288, C30-C32.

----------, and Kane-Maguire. 1985. Mechanisms of addition of primary aromatic amines and cyclohexylamine to tricarbonyl (cycloheptatrienyl) tungsten cation. *Journal of Organometallic Chemistry 284: 35-36.*

----------, 1987. Synthetic and mechanistic studies of the addition of 4-chloroaniline to tricarbonyl (1-5-η-dienyl) iron II cations. *Journalof Organometallic Chemistry 321: 227-235.*

----------, 1988a. Steric and electronic influence on the addition of pyridines to tricarbonyl iron II complexes. *Journalof Organometallic Chemistry 345: 135-141.*

----------, 1988b. Synthetic and Mechanistic Studies of the addition of 2,6-dimethylaniline to tricarbonyl(1-5-η-dienyl) iron(II) complexes. (Dienyl = C_6H_7, 2-$MeOC_6H_7$ or C_7H_9). *Inorganica Chimica Acta* 145: 267-271

----------, Okogun, J.I. and Okorie, D.A. 2007. New Iron Tricarbonyl (cyclohexa-1,3-dienesubstituted) natural products. *Journal of Science Research*, 7, 1: 1-8.

Pandian, S., Hillier, I. H., Vincent, M. A., Burton, N. A., Ashworth, I. W., Nelson, D. J., Percy J. M. and Rinaudo, G. 2009. Prediction of ring formation efficiency via dense ring closing metathesis (RCM) reactions using M06 density functional theory. *Chemical Physics Letters* 476: 37-40.

Park, M. J., Lee, J., Suh, Y., Kim, J. and Nam, W. 2006. Reactivities of mononuclear non- Heme iron intermediates including that iron (III)-hydroxo species.*Journal of American Chemical Society*128, 8: 2630-2634.

Parr R.G and Yang W. 1989. Density Functional theory of atoms and molecules. NY: Oxford University press.

----------, Domnelly, R., Levy, M. and Palke, W. 1978. Electronegativity: The density functional view point. *Journal ofChemical Physics* 68: 3801-3805.

----------, Von Szentpaly, L. and Liu, S. 1999. Electrophilicity index. *Journal of American Chemical Society*121: 1922-1924.

Parthasarathi, R., Subramanian, V., Roy, D. R. and Chattaraj, P.K. 2004. Electrophilicity index as a possible descriptor of biological activity. *Bioorganic and Medicinal Chemistry* 12: 5533-5544.

Patterson, E. V., Cramer C. J. and Truhlar, D. G. 2001. Reductive dechlorination of hexachloroethane in the environment: Mechanistic studies via computational electrochemistry.*Journal of American Chemical Society* 123: 2025-2031.

Pau, M. Y. M., Davis, M. I., Orville, A. M., Lipscomb, J. D. and Solomon, E. I. 2007. Spectroscopic and electronic structure study of the enzyme- substrate complex of

Intradiol deoxygenases: Substrate activaton by a high spin Ferric non heme iron site. *Journal of American Chemical Society* 129: 1944-1958.

Pauson, P. L., Smith, G. H. and Valentine, J. H. 1967. Cycloheptatriene and trpylium metal complexes Part V. 7-endo substituted tricarbonylcycloheptatriene chromiums. *Journalof Chemical Society C 1063-1065.*

Pearson, A. J.andReeS, D.C. 1980. Synthesis of Organic Compounds from Organometallic Compounds.*Tetrahedron Letters* 21: 8927-8943

----------. 1994. Iron compounds in organic synthesis *Academic press*, London. ISBN 0-12-548270.

Peralta, G. A., Seth, M., Zhekova, H. and Ziegler, T. 2008. Magnetic circular dichroism of Phthalocyanine (M= Mg, Zn) and tetraazaporphyrin (M=Mg, Zn, Ni) metal complexes: A computational study based on Time-dependent density functional theory. *Inorganic Chemistry* 47: 4185-4198.

Petersilka, M., Gross, E. K. U. and Burke, K. 2000. Excitations energies from time-dependent density functional theory using exact and approximate functionals. *International Journalof Quantum Chemistry*80: 534-554.

----------, Gossmann, U. J. and Gross, E. K. U. 1996. Excitation energies from time- dependent functional theory. *Physics Review Letters* 76: 1212-1215.

Petrenko, T., Ray, K., Wieghardt, K. E. and Neese, F. 2006. Vibrational markers for the open-shell character of Transition metal Bis-thiolenes: An infra-red resonance, Raman and Quantum chemical study.*Journal of American Chemical Society*128, 13: 4422-4436.

Politzer, Peter and Abu-Awwad, Fakher. 1998. "A comparative analysis of Hartree–Fock and Kohn–Sham orbital energies". *Theoretical Chemistry Accounts: Theory, Computation, and Modeling (Theoretica Chimica Acta)*99,2: 83–87.

Pople J. A. and Nesbet, R. K. 1954. Self-consistent Orbitals for Radicals, *Journal of Chemical Physics*22:571-576.

Popp, B. V., Wendlandt, J. E., Landis, C. R. and Stahl, S. S. 2007. Reaction of molecular oxygen with an NHC-coordinated Pd complex: Computational insights and experimental implications. *Angewandte Chemie International Edition* 46: 601-604.

Praetorius, J. M., Allen, D. P., Wang, R. Y., Webb, J. D., Grein, F., Kennepohl, P. and Crudden, C, M. 2008. N-Heterocyclic carbine complexes of Rh: Reaction with dioxygen without oxidation. *Journal of American Chemical Society*130: 3724-3725.

Pratt D. A. and Van der Donk, W. A. 2005. Theoretical investigations into the intermediacy of chlorinated vinylcobalamins in the reductive dehalogenation of chlorinated ethylenes.*Journal of American Chemical Society* 127: 384-396.

Que, L. 2007. The road to Non-Heme oxoferryls and beyond. *Accounts of Chemical Ressearch*40: 493-500.

Radon, M. and Pierloot, K. 2008. Binding of Co, NO, and O_2 to heme by Density functional and multireference ab initio calculations. *Journal of Physical Chemistry A*112: 11824-11832.

Ray, K., George, S. D., Solomon, E. I., Wieghardt, K. and Neese, F. 2007. Description of the ground state covalencies of bis(dithiolate) transition metal complexes from x-ray absorption spectroscopy and time dependent density functional calculations. *Chemistry A European Journal* 13: 2783-2797.

Reilly, N. M., Reveles, J. U., Johnson, G. E., del Campo, J. M., Khanna, S. N., Koster, A. M. and Castleman, A. W. 2007. Experimental and Theoretical study of the structure and reactivity of $Fe_mO_n^+$ (m=1, 2: n=1-5) *Journalof Physical Chemistry C* 111: 19086-19097.

Ren, J., Kaxiras, E. and Meng, S. 2010. Optical properties of clusters and molecules from real-time time-dependent density functional theory using a self-consistent field. *Molecular Physics* 108, 14: 1829-1844.

Richard C. Bingham, Michael J.S. Dewar and Donald, H. Lo. 1975. Ground states of molecules XXV. MINDO/3. An improved version of the MINDO Semi empirical SCF-MO method. *Journal of American Chemical Society* 97, 6:1285-1293.

Riggs, J.E. and Sun, Y. P. 2000. Optical limiting properties of mono- and multiple functionalized fullerene derivatives.*Journal of Chemical Physics* 112: 4221(1-8).

Rinaldo Poli and Jeremy N. Harvey. 2003. Spin forbidden chemical reactions of transition metal compounds. New ideas and new computational challenges. *Chemical Society Reviews* 32: 1-8**.**

Rinaldo, D., Philipp, D. M., Lippard, S. J. and Friesner, R. A. 2007. Intermediates in dioxygen activation by methane monooxygenase: A QM/MM Study.*Journal of American Chemical Society*129: 3135-3147.

Robert A. Jackson., Mario E.G.Valerio., Marcos A.Couto., dos Santos and Jomar B. Amaral. 2004. Computer modeling of mixed metal fluorides for optical applications. *Journal of Physics Condense Matter* 15: 2523-2532.

Roth, J. P. and Cramer, C. J. 2008. Direct examination of H_2O_2 activation by a Heme peroxidase.*Journal of American Chemical Society*130: 7802-7803,

Roy, R. E. and Hughbanks, T. 2006. Electronic transition in $[Re_6S_8X_6]$, (X= Cl, Br, I): Results from time-dependent density functional theory and solid-state calculations. *Inorganic Chemistry*45: 8273-8282.

Rubio-Pons, O., Luo, Y. and Agren, H. 2006. Effects of conjugation length, electron donor and acceptor strengths on two photon absorption cross sections of asymmetric zinc porphyrin derivatives. *Journalof Chemical Physics*124: 094310 (1-10).

Rung, E. and Gross, E. K. U. 1984. Density- functional theory for time-dependent systems. *Physical Review Letters* 52: 997-1000.

Salassa, L., Garino, C., Salassa, G., Gobetto, R. and Nervi, C. 2008. Mechanism of ligand photodissociation in photoactivable $[Ru(bpy)_2L_2]^{+2}$ complexes: A density functional theory study. *Journal of American Chemical Society* 130: 9590-9597.

Sandeep Nigam, Chiranjib Majumder and Kulshreshtha, S.K. 2006. Theoretical Study aromaticity in Inorganic tetramer clusters. Indian Academy of Sciences. *Journal of Chemical Science* 6: 575-578.

Sanford, M. S., Love, J.A. and Grubbs, R. H. 2001. Mechanism and activity of Ruthenium olefin metathesis catalyst.*Journal of American Chemical Society* 123: 6543-6554.

Sarangi, R Gorelsky, S. I., Basumallick, L., Hwang, H. J., Pratt, R. C., Stack, T. P. D., Lu,Y., Hodgodson, K. O., Hedman, B. and Soloman, E. I. 2008. Spectroscopic and density functional theory studies of the blue-copper site in M121SeM and C112SeC Azurin: Cu-Se versus Cu-S bonding.*Journal of American Chemical Society*130: 3866-3877.

Sato, H., Taniguchi, T., Monde, K., Nishimura, S. I. and Yamagishi, A. 2006. Dramatic effects of d-electron configurations on vibrational circular dichroism spectra of tris(acetylacetonato) metal(III). *Chemical Review Letters* 35: 364-365.

Scalmani, G., Frisch, M. J., Mennucci, B., Tomasi, J., Cammi, R. and Barone, V. 2006. Geometries and properties of excited states in the gas phase and in solution: Theory and application of a time dependent functional theory polarizable continum model. *Journalof Chemical Physics*124: 094107(1-8).

Schipper, P. R. T. Gritsenko, O. V. Van Gisbergen S. J, A and Baerends, E. J. 2000. Molecular calculations of excitation energies and (hyper) polarizability with a statistical average of orbital model exchange-correlation potentials. *Journal of Chemical Physics*112: 1344-1353.

Schro¨ der, D., Souvi, S. O. and Alikhani, E. 2009. Hydrated metal-oxide versus dihydroxide structures of [MO2H2]+ cations with M= Fe, Co and Ni. *Chemical Physics Letters* 470: 162-165.

Schultz, D., Biaso, P. R.,. Shahi, R M., Geoffroy, M., Rissanen, K., Gagliardi, L., Cramer, C. R. and Nitschke, J. R. 2008. *Chemistry A European Journal*14: 7180-7187.

Schultz, N. E., Zhao, Y. and Truhlar, D. G. 2005. Density Functionals for Inorganometallic and Organometallic Chemistry. *Journalof Physical ChemistryA* 109: 11127-11143.

Schwartz, J. K., Wei, P. P., Mitchell, K. H., Fox, B. G. and Solomon, E. I. 2008. Geometry and electronic structure studies of the binuclear non-heme ferrous active site of Toluene-4-monooxygenase: Parallels with methane monooxygenase and insight into the role of the effector proteins in O_2 activation. *Journal of American Chemical Society*130: 7098-7109.

Seah, L. K., Elaine, P. L., Weng, K. L. and Lai, Y. G. 2006. Highly Oxidized Ruthenium Organometallic Compounds. The Synthesis and One-Electron Electrochemical Oxidation of [Cp*RuIVCl_2(S_2CR)] (Cp*). *Organometallics*25:6134-6141.

Shaik, S., Hirao, H. and Kumar, D. 2007. Reactivity of high valent iron-Oxo species in enzymes and synthetic reagents: A tale of many states. *Accounts Chemical Research* 40: 532-542.

----------, Kumar, D. and de Visser, S. P. 2008. A valence bond modeling of trends in hydrogen abstraction barriers and transition states of hydroxylation reactions catalysed by cyctochrome P450 enymes.*Journal of American Chemical Society* 130: 10128-10140.

Sheng, H. L., Quan, Y. H., Peng, X., Ting, B. W., Ian D. W. and Guochen, J. 2005. Synthesis and Characterization of $C_{10}H_{10}$-Bridged Bimetallic Ruthenium Complexes. *Organometallics* 24:769-772.

Shigeyoshi, S., Yu-ya, O. and Hirofumi, S. 2010. Theoretical and computational studies of organometallics reactions: Successful or not? *Theoretical Chemistry Record* 10: 29-45.

Shoji, M. Koizumi, K., Kitagawa, Y., Yamanaka, S., Okumura, M. and Yamaguchi, K. 2007. Theory of chemical bonds in metalloenzymesIV: Hybrid-DFT study of Rieske-type [2Fe- 2S] clusters. *International Journal of Quantum Chemistry* 107: 609-729.

Sieffert, N. and Bu¨ hl, M. 2009. Noncovalent interactions in a Transition metal triphenylphosphine complex: A density functional case study. *Inorganic Chemistry* 48: 4622-4624.

Solomon, E. I., Brunold, T. C., Davis, M. I., Kemsley, J. N., Lee, S. K., Lehnert, N., Neese, F. A. J., Skulan, A.J., Yang Y. S. and Zhou, J. 2000. Geometric and electronic structure/ function correlations in non heme iron enzymes. *Chemical Reviews*100: 235-350.

Spartan'10 V1.1.0. 2011. Tutorial and User's guide. *Wavefunction Inc. Japan.* ISBN 978-1-890661-41-4.

Stefan, K., Bernhard, W., Allison, M. M., Anthony, L. S., Gerard,P. M. and Gerard, K. 2008. Synthesis and reaction chemistry of 4-nitrile-substituted NCN-pincer Pd^{+2} and Pt^{+2} complexes. *Journal of Organometallic Chemistry* 693: 1991-1996.

Stener, M., Nardelli, A. De Francesco, R. and Fronzoni, G. 2007. Optical excitation of gold nanoparticles: A Quantum chemical scalar relativistic time dependent density functional theory study. *Journalof Physical Chemistry C* 111: 11862-11871.

----------.,----------. and Fronzoni, G. 2008a. Efficient realization of the Fock- space coupled-cluster method with connected triple excitations. *Chemical Physics Letters* 462: 358-362.

----------**,** ----------, and ----------2008b. Spin-orbit effects in the photoabsorption of WAu_{12} and $MoAu_{12}$: a relativistic time dependent density functional theory study. *Journalof Chemical Physics*128: 134307(1-9)..

Stewart, J.J.P. 1989. Optimization of parameters for Semi empirical methods: The MNDO-PM3 method. *Journal of Computational Chemistry*10, 2: 209-220.

Stewart, I. C., Benitez, D., O'Leary, D. J., Tkatchouk, E., Day, M. W., Goddard, W. A. and Grubbs, R. H. 2009. Conformations of N-Heterocyclic carbine ligands in Ruthenium complexes relevant to olefin metathesis.*Journal of American Chemical Society* 131: 1931-1938

Stratmann, R. E., Scuseria, G, E. and Frisch, M. J. 1998. An efficient implementation of Time-dependent density functional theory for the calculation of excitation energies of large molecules. *Journalof Chemical Physics* 109: 8218-8224.

Strickland, N. and Harvey, J. N. 2007. Spin Forbidden ligand binding to the Ferrous Heme group: Ab initio and DFT. *Journal of Physical Chemistry B* 111: 4567-4573.

Strohmeier, W. and Bigorgne, M. 1965. New triphenylphosphine metal complexes. *Journal of Organometallic Chemistry* 5: 341-345.

Sun, Q., Reddy, M., Marquez, P., Jena, C., Gonzalez, M. and Wang, Q. 2007. Theoretical study on Gold-coated iron oxide nanostructure: Magnetism and Bioselectivity for amino acids. *Journalof Physical Chemistry C* 111: 4159-4163.

Szabo, A. and Ostlund, N.S. 1982. Modern Quantum Chemistry. *Introduction to Advanced Electronic Structure Theory*. 1st Edition, McGraw Hill Publishing Co.

Tao, J.M. and Vignale, G. 2006. Time-dependent density functional theory beyond the local-density approximation. *Physical Review Letters* 97: 036403(1-4).

Tateyama, Y., Blumberger, J., Sprik, M. and Tavernelli, I. 2005. Density functional molecular dynamics study of the redox reactions of two anionic aqueous transition metal complexes. *Journalof Chemical Physics* 122: 234505(1-8).

Thomas, E. B. and Javier, A. C. 2004. Photolysis of diruthenium hexacarbonyl tetrahedrane compounds in Nujol glass matrices. *Journalof Organometallic Chemistry*689: 947–2951.

Thomas, K. S., John, L. H., Christopher, R. Z., Geun-Bae, Y. and Morten, S. 1996. Synthesis and Structure of the Ruthenium(II) Complexes. DNA Cleavage by an Organometallic dppz Complex (bipy).*Inorganic Chemistry*35:4383-4390.

Thompson, M. 2007. The evolution of organometallic complexes in organic light emitting devices. *Mrs Bulletin* 32, 9: 694-699.

Torker, S., Merki, D. and Chen, P. 2008. Gas-Phase thermochemistry of Ruthenium carbine metathesis catalyst.*Journal of American Chemical Society* 130: 4808-4818.

Uudsemaa, M. and Tamm, T. 2003. Density functional theory calculations of aqueous redox potentials of fourth period transition metals. *Journalof Physical. Chemistry A* 107: 9997-10003.

Uwe, H.F. 1996. Synthesis of novel liquid crystalline organometallic polymers. *Pure & Applied Chemistry* 68, 2: 309-312.

Van Leeuwen, R. 2001. Key concepts in time dependent functional theory. *International Journalof Modern Physics B* 15: 1969-2024.

Walter, A. H. 1989. Electronic Structure and properties of Solids. *Dover Publications.* ISBN 0-486-66021-4.

Wang, D. Q., Zheng, J. J., Shaik, S. and Thiel, W. 2008. Quantum and Molecular Mechanical study of the first proton transfer in the catalytic cycle of cytochrome P450 cam and its mutant D251N. *Journalof Physical Chemistry B* 112, 16: 5126-5138.

Wang, Y., Kumar, D., Yang, C. L., Han, K. L. and Shaik, S. 2007. Theoretical study of N-demethylation of substituted N,N-dimethylanilines by cytochrome P450: The mechanistic significance of kinetic isotope effect profiles. *Journalof Physical Chemitry B* 111, 26: 7700-7710.

Wanli, K., Xiaoyan, W., Jianbi, H. 2009. Synthesis, crystal structure and biological activities of four novel tetranuclear di-organotin(IV)carboxylates. *Journal of Organometallic Chemistry* 694: 2402-2408.

Webster, C. E. 2007. Computational insights into degenerate ethylene exchange with a Grubbs-type catalyst.*Journal of American Chemical Society* 129: 7490-7491.

Wilkinson, G., Rosenblum, M., Whiting, M.C., and Woodward, R. B. 1952. The Structure of Iron bis-cyclopentadienyl. *Journal of America Chemical Society* 74: 2125-2126.

Woffgang, A. Hermann, Carl Kruger, Richard Gooddard and Ivan Bernal. 1977. Transition metal methylene, A carbonyl analogous ligand, Crystal structure of μ-methylene-bis-(carbonyl-η^5-cyclopentadienylRhodium). *Journalof Organometallic Chemistry 140: 73-89.*

Yan Ping, W., Wen Fa, X. Bin, L. and Wen Lian, L. 2007. Synthesis, Characterization, photoluminescence and electroluminescence properties of new 1,3,4-oxadiazole-containing rhenium(I) complex. *Chinese Chemical Letters* 18: 1501-1504.

Yang, X. Y., Wang, Y. C., Geng, Z. Y. and Liu,Z. Y. 2006. Theoretical study of the reactivity of 4d transition metal ions with N_2O. *Chemical Physics Letters* 430: 265-270.

Yoshizawa, K., Ohta, T., Yamabe, T. and Hoffmann, R. 1997. Dioxygen cleavage and methane activation on diiron enzyme model: A theoretical study. *Journal of American Chemical Society* 119: 12311-12321.

Young, D. 2001. Computational Chemistry; A practical guide for applying techniques to Real world problems. *New York. John-Wiley &Sons.* ISBN: 0-471-33368-9.

Zhao, Y. and Truhlar, D. G. 2009. Benchmark energies data in a model system for Grubbs II metathesis catalysis and their use for development, assessment and

validation of electronic structure methods. *Journalof Chemical Theory and Computation*5, 2: 324-333.

Ziese, W. C. 1831. Of the effect between platinum chloride and substance of the resulting new. *Annual Review of Physical Chemistry* 97, 4: 497-541.

PUBLICATIONS

(i) Odiaka, T.I, **Akinyele, O.F** and Adejoro, I.A, (2011) Synthesis and Characterisation of New pyridino -1-4-η- Cyclohexa-1,3-diene) derivatives of Irontricarbonyl Complexes. *E. Journal of Chemistry 8(3), 960-965*

(ii) Adejoro, I.A, Odiaka, T.I and **Akinyele, O.F.** (2010). Structure, Electronic and Thermodynamic properties of New pyridino-1-4-η-Cyclohexa-1,3-diene)

derivatives of Iron Tricarbonyl Complexes – A Theoretical Approach. *European Journal. of Science Research* 47, 2:230-240.

(iii) Adejoro, I.A, Odiaka, T.I and **Akinyele, O.F.** (2011) Semi-Empirical (PM3) Studies of New Pyridino-1-4-η-2-methoxycyclohexa-1,3-diene Iron Tricarbonyl Complexes. *Inorganic Chemistry: An Indian Journal, Trade Sci. Inc.Vol. 6(1).*

(iv) Adejoro I. A, Odiaka T.I and **Akinyele O.F.** (2012) Molecular Modeling and Computational Studies Of Dimethylpyridino-1,4-η-2-methoxycyclohexa-1,3-diene Iron tricarbonyl Complexes. *Asian Journal Chemical Research (AJRC)*, 5, 1: 146-152.

(v) Odiaka, T.I, Adejoro, I.A and **Akinyele, O.F.** (2012)Semi-Empirical (PM3) Studies of Novel Aminopyridino-1- 4-η-Cyclohexa-1,3-diene Iron tricarbonyl Complexes. *American Journal of Science and Industrial (AJSIR)* 3, 1: 1-13.

(vi) Adejoro I. A, Odiaka T.I and **Akinyele O.F.**(2013) Structure and Electronic properties of Aminopyridino-1-4-η–2-methoxycyclohexa-1,3-diene Irontri-carbonyl complexes- A Semi Empirical PM3 Approach. *Asian Journal of Research in Chemistry. (AJRC)*, 6, 11: 1034-1039.

(vii) Adejoro, I.A, Odiaka, T.I and **Akinyele, O.F.** (2014) Density Functional Theory and Reactivity Parameters of Dimethylpyridino-1-4-η-cyclohexa-1,3-diene irontricarbonyl complexes. *Journal of Natural Science Research*4, 1: 38-45.